

https://dspace.org/

Targeted transcriptional silencing of hepatitis B virus using designer epigenome modifiers expressed from in vitro transcribed mRNA

Singh, Prashika

2025

University of the Witwatersrand, Johannesburg

https://hdl.handle.net/10539/48455

Singh, Prashika. (2024). Targeted transcriptional silencing of hepatitis B virus using designer epigenome modifiers expressed from in vitro transcribed mRNA [PhD thesis, University of the Witwatersrand, Johannesburg]. WIReDSpace. https://hdl.handle.net/10539/48455

Downloaded from a DSpace repository. https://dspace.org/

Targeted transcriptional silencing of hepatitis B virus using designer epigenome modifiers expressed from in vitro transcribed mRNA

Prashika Singh

Thesis submitted to the Faculty of Health Sciences, University of the Witwatersrand, in fulfilment of the requirements for the degree of

Doctor of Philosophy in Medicine

15 January 2025

Johannesburg

Declaration

I, Prashika Singh (student number: 671465) declare that this thesis is my own work. It is being submitted for the degree of Doctor of Philosophy in Medicine at University of the Witwatersrand, Johannesburg. It has not been submitted before for any degree or examination at this or any other University.



……....……

15 day of January 2025

Dedication

To my family and Raveena Singh, my late sister. Thank you for your unconditional love and support throughout this journey.

Publications and presentations

Publications

Ely, A., Singh, P., Smith, T.S. and Arbuthnot, P., 2021. In vitro transcribed mRNA for expression of designer nucleases: Advantages as a novel therapeutic for the management of chronic HBV infection. *Advanced drug delivery reviews*, *168*, pp.134-146.

Smith, T., Singh, P., Chmielewski, K.O., Bloom, K., Cathomen, T., Arbuthnot, P. and Ely, A., 2021. Improved Specificity and Safety of Anti-Hepatitis B Virus TALENs Using Obligate Heterodimeric Fok I Nuclease Domains. *Viruses*, *13*(7), p.1344

Singh, P., Kairuz, D., Arbuthnot, P. and Bloom, K., 2021. Silencing hepatitis B virus covalently closed circular DNA: The potential of an epigenetic therapy approach. *World Journal of Gastroenterology*, *27*(23), p.3182

Kairuz, D., Singh, P., Smith, T., Arbuthnot, P., Ely, A. and Bloom, K., 2022. Synthetic mRNA gene therapies and hepatotropic non-viral vectors for the treatment of chronic HBV infections. In *Messenger RNA Therapeutics* (pp. 157-179). Cham: Springer International Publishing

Jacobs, R., Singh, P., Smith, T., Arbuthnot, P. and Maepa, M.B., 2022. Prospects of viral vector-mediated delivery of sequences encoding anti-HBV designer endonucleases. *Gene Therapy*, pp.1-8

Singh, P., Smith, T., Arbuthnot, P. and Ely, A., 2024. 14 In Vitro RNA Transcription. *Handbook of Molecular Biotechnology*, p.137- 151

Conferences

Singh. P, Bloom, K., Cathomen, T, Claudio, Arbuthnot. P., Ely. A (2019), Targeted transcriptional silencing of hepatitis B virus using designer epigenome modifiers expressed from in vitro transcribed mRNA, International Centre for Genetic Engineering and Biotechnology (ICGEB), 16-19 September, Cape Town, South Africa.

Abstract

Approximately two-thirds of the world's population has been exposed to the hepatitis B virus (HBV), the causative agent of hepatitis B, with sub-Saharan Africa experiencing a high prevalence, where up to 8% of the population are chronic carriers. The persistence of HBV infection is largely due to the stable replicative intermediate, covalently closed circular DNA (cccDNA), which current treatments do not effectively target or eliminate. Consequently, a reliable cure for chronic hepatitis B (CHB) remains unavailable. Gene editing technologies, such as Clustered Regularly Interspaced Short Palindromic Repeats/CRISPR-associated protein (CRISPR/Cas), Transcription Activator-Like Effector Nucleases (TALENs), and Zinc Finger Nucleases (ZFNs), can directly target cccDNA and offer the potential to eliminate this reservoir. However, these methods are limited by the risk of off-target effects, including chromosomal deletions and translocations. In contrast, emerging epigenome editing technologies provide safer alternatives. Designer epigenome modifiers (DEMs) offer a less genotoxic option by modifying cccDNA epigenetically. DEMs, comprising DNA methyltransferase (DNMT) and Kruppel-associated box (KRAB) repressor domains along with a Transcription Activator-Like Effector-DNA binding domain (TALE-DBD) were designed to target the HBV *surface* (*S*), *core* (*C*), and *polymerase* (*P*) open reading frames (ORFs). Control DEMs lack a KRAB domain and contain catalytically inactive DNMT. Given the strategic positioning of CpG islands in the HBV genome, these regions make the viral genome an ideal target for DNA methylation. To improve the efficacy of already existing DEMs, this study evaluated the use of mRNA-based platforms (mRNA-based vectors, pmRNA-pA and pT7-(AG)) for expressing anti-HBV DEMs for the first time, allowing for targeted silencing of the *S*, *C*, and *P* ORFs of HBV *in vitro*. Sequences encoding the DEMs were cloned into an expression vector specifically designed for in vitro transcription of mRNA. In vitro transcribed anti-HBV DEM-encoding mRNA were transfected into liver-derived Huh7 and HEK 293T cells. Markers of viral replication, including HBV surface antigen (HBsAg) and viral *surface* and pregenomic RNA (pgRNA) and stimulation of interferon response genes were assessed. Bisulphite sequencing was used to confirm the methylation of HBV DNA, and 3-(4,5-Dimethylthiazol-2-yl)-2,5-diphenyltetrazolium bromide (MTT) assays were conducted to assess the toxicity of the synthesized DEM RNA. The pT7-(AG) vector, featuring more stable regulatory sequences, a longer poly-A tract, and multiple termination codons, proved to be more effective than the original platform. DEMs expressed

from this platform achieved a significant reduction in HBsAg levels, particularly with the complete substitution of uridine nucleotides with pseudouridine, incorporation of CleanCap® AG, and removal of dsRNA. HBsAg levels were reduced by 21-41 %, and up to 50-90 % reduction was observed with double transfection. Additionally, viral *surface* transcript levels decreased by 42-70 %, while pregenomic transcript levels decreased by 62-72 % correlating with increased trend in methylation at all three targeted CpG islands. There was no evidence of immune stimulation or metabolic toxicity, indicating that the observed transcriptional activity resulted from DEM activity and suggest that DEMs are safe. Furthermore, the SL and PL DEMs exhibited the greatest transcriptional silencing. This proof-of-concept study demonstrates that optimising mRNA stability, half-life, and immunogenicity can significantly enhance the efficacy of DEMs. However, further in vivo characterisation of these DEMs, along with an assessment of their duration of action at both on-target and off-target activities, is required. Nevertheless, targeted epigenome silencing of HBV through the use of epigenome editors expressed as in vitro transcribed mRNA represents a promising therapeutic approach for modulating viral replication and potentially treating CHB.

Acknowledgments

I would like to express my sincere gratitude to my supervisors, Prof. Abdullah Ely and Prof. Patrick Arbuthnot. Their unwavering encouragement, guidance, and commitment to my development have been invaluable throughout my postgraduate studies. I truly appreciate their support and patience, which have greatly contributed to my growth during this journey.

I am immensely grateful to the members of the Antiviral Gene Therapy Research Unit for their willingness to assist and for creating a supportive, joyful, and encouraging work environment. A special thanks to Ms. Tiffany Shenay Smith for her encouragement and assistance throughout my research. I would also like to thank Ms Ridhwaanah Jacobs for her support during this journey.

I would like to extend my gratitude to the following individuals for providing the necessary materials for the completion of my research: Dr. Kristie Bloom for supplying the DEM plasmids, Prof. Abdullah Ely for the pT7(AG) RNA expression vector, and Dylan Kairuz for the pT7-Luc 2 plasmid. Ms. Tiffany Shenay Smith for the assistance with the cloning of pmRNA-GFP vector.

I wish to extend my heartfelt gratitude to my family for their unwavering support and encouragement throughout my journey. Their continuous love, prayers, and patience have been invaluable, without which the completion of this work would not have been possible. I would also like to give special thanks to my beloved late sister, Raveena Singh, whose continued support brought me strength, laughter, and the motivation to pursue and complete my studies

I would like to extend my gratitude to the National Research Foundation (NRF) of South Africa, the Poliomyelitis Research Foundation (PRF), the Antiviral Gene Therapy Research Unit/South African Medical Research Council, and the Wits Health Consortium for their financial assistance.

Most importantly, all glory, praise, and honour go to our Heavenly Father, Lord and Savior Jesus Christ for His grace, strength, and never-ending joy, as well as for the faith to accomplish my endeavours and milestones in life.

Table of Contents

Declaration ii

Dedication iii

Publications and presentations iv

Abstract v

Acknowledgments vii

Table of Contents viii

List of Figures xiv

List of Tables xviii

List of abbreviations xix

1. Introduction 1

1.1 Hepatitis B virus epidemiology 1

1.2 Viral genotypes and transmission 2

1.3 HBV virion and genome organisation 3

1.3.1 Viral replication 4

1.4 Available Treatment for HBV 7

1.4.1 First line treatment 7

1.4.2 Current and emerging strategies for HBV treatment 8

1.5 cccDNA: viral reservoir 9

1.5.1 Direct targeting of cccDNA 10

1.6 Epigenetics: potential for therapeutic application 11

1.6.1 HBV genome: ideal target for DNA methylation 14

1.6.2 DNA methylation of HBV 17

1.7 Potential of epigenome editing 17

1.7.1 Effector domains 19

1.7.2 Programmable DBDs 19
1.7.3 Epigenome modifiers targeting HBV 21
1.8 Therapeutic potential of designer epigenome modifiers (DEMs) platform 22
1.9 Applications of mRNA Technology 23
1.10 Essential structural elements required for functional IVTed mRNA 25
1.10.1 ORF: Coding region 25
1.10.2 Poly(A) tail 26
1.10.3 Untranslated regions (UTRs) 27
1.10.4 5' Cap structure 28
1.10.5 Co-transcriptional capping 29
1.10.6 Post-transcriptional capping 32
1.11 Strategies to enhance mRNA stability, protein translation, and minimise immunogenicity 34
1.11.1 Immunogenicity of IVTed mRNA 34
1.11.2 Chemical modification of mRNA 35
1.11.3 Purification of mRNA 38
1.12 Potential of anti-HBV DEM-based mRNA therapeutic 38
1.13 Aims and objectives 41
Chapter 2 42
2. Methods and Materials 42
2.1 Construction of an RNA expression platform (pmRNA) encoding transgene sequences 42
2.1.1 Construction of anti-HBV DEM mRNA expression vectors 42
2.1.2 Construction of pmRNA-GFP reporter plasmid for optimisation studies 47
2.1.3 Construction of pmRNA vectors expressing active anti-HBV DEMs lacking KRAB domain49

Table of Contents

2.2 *In Vitro* Synthesis of mRNA from DNA templates 51
2.2.1 Production of in vitro transcribed therapeutic and reporter mRNA 51
2.2.2 Post-transcriptional capping of IVTed mRNA 51
2.2.3 Removal of dsRNA by cellulose purification 52
2.3 Characterisation of poly(A) tail length in IVTed mRNA using 3' RACE 53
2.3.1 Analysis of poly(A) tail length in IVTed mRNA following introduction into cultured cells 54
2.4 Characterisation of the anti-DEM mRNA in culture mammalian cells 54
2.4.1 Evaluation of Anti-HBV DEM mRNA *in vitro* 54
2.4.2 Detection of Anti-HBV DEM using immunofluorescence staining 55
2.4.3 Evaluation of IVTed reporter mRNA using a luciferase assay 56
2.4.4 Evaluation of toxicity of anti-HBV DEMs in cultured cells 56
2.5 Construction of mRNA expression plasmid pT7-(AG) DEM 4×S 57
2.5.1 Design of pT7-(AG) RNA expression platform 57
2.5.2 Production of IVTed therapeutic and reporter mRNA 66
2.6 Characterisation of the DEM mRNA expressed from pT7(AG)-DEM 4×S *in vitro* 66
2.6.1 Evaluation of Anti-HBV DEM mRNA silencing *in vitro* 66
2.6.2 Detection of Anti-HBV DEM mRNA 67
2.6.3 Evaluation of toxicity of anti-HBV DEMs expressed from pT7(AG)-DEM 4×S 67
2.6.4 Quantitative reverse transcriptase PCR (qRT-PCR) of HBV viral transcripts 67
2.6.5 qRT-PCR of innate response to DEM-encoding mRNA 68
2.7 Bisulphite sequencing 70
2.8 Data analysis and programs 70
3. Results 71
3.1 Generation of DEM mRNA produced from RNA expression vector 71

3.1.1 Construction of pmRNA-pA expression vector encoding anti-HBV DEMs 71

3.1.2 mRNA synthesis of DEM-encoded DNA 77

3.2 IVT Optimisation of anti-HBV DEM mRNA 81

3.2.1 Improved characteristics of ARCA-capped IVTed mRNA 81

3.2.2 Characterisation of anti-HBV DEM mRNA expressed from pmRNA-pA vector 83

3.3 Post-transcriptional capping of IVTed GFP and anti-HBV DEM mRNA 87

3.3.1 Enhanced translation of IVTed GFP and anti-HBV DEM mRNA using post-transcriptional capping strategies 87

3.3.2 Expression of IVTed dDEM mRNA when post-transcriptionally capped 89

3.3.3 Expression of active anti-HBV DEM-encoded IVTed mRNA in cultured cells 92

3.4 Analysis of the functional elements present in pmRNA expression vector and IVTed mRNA 96

3.4.1 Complete functional elements required for pmRNA DEM plasmid expression 96

3.4.2 Characterisation of anti-HBVDEM plasmids *in vitro* 98

3.4.3 Confirmation of the poly (A) tail in IVTed DEM mRNA 103

3.5 Influence of IVT methods, modified nucleotides, Cap analogue structures, and dsRNA removal on mRNA efficacy 107

3.5.1 Enhanced reporter mRNA efficacy 107

3.5.2 Transcriptional repression of HBsAg secretion by anti-HBV DEM mRNA 111

3.6 Utilisation of second mRNA expression vector: pT7-(AG) 113

3.6.1 Generation of pT7(AG)-DEM 4× S constructs 114

3.7 Characterisation of pT7(AG)-DEM 4×S plasmids *in vitro* 116

3.7.1 Expression of anti-HBV DEM-encoding plasmids in cultured cells 116

3.7.2 Plasmid DNA expressing anti-HBV DEM from the pT7(AG)-DEM 4× S vector shows no cytotoxicity 118

3.7.3 Anti-HBV DEM mRNA produced from the pT7-DEM 4× AG vector effectively mediates the expression 120

3.7.4 Immunohistochemical detection of HA-tag from active DEM mRNA expressed from the pT7(AG)-DEM 4×S vector 122

3.8 Anti-HBV DEM mRNA expressed from the pT7(AG)-DEM 4×S vector effectively mediates transcriptional silencing of HBV 124

3.8.1 Active DEM mRNA mediates transcriptional silencing of HBV viral surface proteins 124

3.8.2 Transcriptional silencing of HBV transcription mediated by anti-HBV DEM mRNA produced from the pT7(AG)-DEM 4×S vector 127

3.8.3 Targeted methylation of HBV CpG islands induced by DEMs 129

3.8.4 Anti-HBV DEMs does not exhibit cellular-mediated cytotoxicity 134

3.8.5 Lack of innate immune stimulation mediated by anti-HBV DEM mRNA expressed from the pT7(AG)-DEM 4×S vector 136

4. Discussion 138

4.1 Epigenome editing as an alternative to current therapeutic approaches for HBV 138

4.2 Application of RNA expression platforms for the expression of anti-HBV epigenome modifiers 139

4.3 Expression of DEM mRNA from the pmRNA platform 139

4.4 Functional DEM mRNA expressed from pT7 (AG) RNA expression platform 142

4.4.1 Expression of active anti-HBV DEMs mRNA *in vitro* 143

4.4.2 Transcriptional silencing of HBV surface protein and viral transcripts 144

4.5 Safety of using transcriptional repressor DEMs expressed as mRNA 147

4.6 Future work 148

4.6.1 Target specificity and safety of epigenome editors 149

4.7 Therapeutic benefit of expressing DEMs from IVTed mRNA 150

4.8 Conclusion 151

5. 5. Appendix 153

5.1 Gel electrophoresis 154

5.2 Extraction of DNA fragments from agarose gel 155

5.3 Preparation and transformation of chemically competent *E. coli* 155

5.4 Large-scale plasmid preparation 156

5.5 In vitro transcription protocols 157

5.5.1 RiboMAX^{TM} Large Scale RNA Production System (Promega, WI, USA)Table ... 157

5.5.2 Transcript T7 High Yield Transcription Kit (ThermoScientific, CA, USA) 158

5.5.3 New England Biolabs (NEB) individual IVT components (New England Biolabs, NJ, USA) 158

5.6 Nucleic acid extraction protocols 159

5.6.1 RNA extraction from monolayer cells 159

5.6.2 DNA extraction from monolayer cells 160

5.7 Cell culture: maintenance and propagation of mammalian cells 161

5.8 Assessment of HBsAg using ELISA 162

5.9 mRNA Platforms for Expressing Transgene Sequences 167

5.9.1 GFP reporter mRNA expression vector 167

5.9.2 Active pmRNA-DEMΔKRAB plasmids 170

5.9.3 Active pT7(AG)-DEMΔKRAB 4×S plasmids 178

5.10 Ethic Clearance 191

References 192

List of Figures

Figure 1.1: HBV replication 6
Figure 1.2: DNA Methylation of Cytosine. 13
Figure 1.3:Schematic representation of the ORFs in the HBV genome with predicted CpG islands. 16
Figure 1.4:Overview of epigenome editing. 18
Figure 1.5:Representative scheme of in vitro transcribed (IVTed) mRNA. 24
Figure 1.6: Schematic representation of co-transcriptionally capped mRNA cap structures. 31
Figure 1.7: Schematic representation of mRNA cap structures produced post-transcriptionally. 33
Figure 1.8: Chemical structures of modified nucleotides. 37
Figure 1.9: Schematic representation of active and inactive DEMs. 40
Figure 2.1: A schematic illustrating the cloning strategy used to generate active and inactive pmRNA-DEM plasmids. 46
Figure 2.2: Schematic illustrating the cloning strategy used to generate pmRNA-GFP. 48
Figure 2.3: A schematic illustrating the cloning strategy used to generate active pmRNA-DEMΔKRAB plasmids. 50
Figure 2.4: Design of the ECS-Fragment for pT7-(AG) Cloning. 59
Figure 2.5: A schematic illustrating subcloning strategy of pT7(AG)-ECS 4×S. 61
Figure 2.6: A schematic illustrating the cloning strategy used to generate active pT7(AG)-DEM 4×S and pT7(AG)-DEMΔKRAB 4×S plasmids. 65
Figure 3.1: Confirmation of active pmRNA-DEM DNA by enzymatic digestion. 73
Figure 3.2: Confirmation of KRAB domain in active pmRNA-DEM plasmids by enzymatic digestion. 74
Figure 3.3: Confirmation of inactive pmRNA-dDEM DNA by enzymatic digestion. 75
Figure 3.4: Restriction enzyme digestion confirming the absence of KRAB domain in inactive pmRNA-dDEM constructs. 76
Figure 3.5: Linearisation and IVT of anti-HBV DEMs *in vitro*. 78
Figure 3.6: Assessment of IVTed DEM mRNA expressed from pmRNA expression vector in cultured cells. 80
Figure 3.7: Linearisation and IVT of reporter mRNA *in vitro*. 82

Figure 3.8: Comparison of Cap 0 and ARCA capping strategies and purification techniques for IVTed reporter mRNA. 84
Figure 3.9: *In vitro* assessment of cap-independent translation of IVTed FLuc reporter mRNA. 86
Figure 3.10:Comparison of Cap 0 and Cap 1 post-transcriptional capping strategies for reporter mRNA. 88
Figure 3.11: Immunofluorescence detection of IVTed active and control DEM mRNA *in vitro*. 91
Figure 3.12: Linearisation and IVT of active pmRNA-DEMΔKRAB plasmids. 93
Figure 3.13: Evaluation of expression and functionality of post-transcriptionally capped Cap0 DEMs lacking the KRAB domain. 95
Figure 3.14:Confirmation of TALE-DBD and poly (T) track in pmRNA-DEM expression plasmids. 97
Figure 3.15: Immunohistochemical detection of HA-tag expression from pmRNA-DEM plasmid DNA in active and inactive DEMs..... 100
Figure 3.16: Plasmid DNA encoding anti-HBV DEMs achieve transcriptional repression without cellular toxicity..... 102
Figure 3.17: Analysis of the poly (A) tail in IVTed mRNA. 106
Figure 3.18: Effects of modified nucleotides, purification, and capping strategies on IVTed mRNA. 110
Figure 3.19: Effects of modified nucleotides, purification, and capping on IVTed DEM mRNA. 112
Figure 3.20: Confirmation of active pT7(AG)-DEM 4×S plasmid DNA by enzymatic digestion. 115
Figure 3.21:Immunofluorescence detection of pT7(AG)-DEM 4×S plasmid DNA *in vitro*. 117
Figure 3.22: Anti-HBV DEM DNA expressed from the second RNA expression vector. 119
Figure 3.23:Linearisation and IVT of pT7(AG)-DEM 4×S and reporter pT7-mCherry encoding plasmids. 121
Figure 3.24: Immunofluorescence Detection of Active DEM mRNA in Huh7 Cells. 123
Figure 3.25: Transcriptional silencing of HBsAg by anti-HBV DEM mRNA expressed from the pT7(AG)-DEM 4×S vector. 126
Figure 3.26: Assessment of anti-HBV DEM mRNA-mediated silencing of HBV viral transcripts *in vitro*. 128

Figure 3.27: Potential methylation patterns in HBV CpG Islands I-III following DEM transfection in cultured cells. 133
Figure 3.28: Assessment of toxicity associated with anti-HBV DEM mRNA. 135
Figure 3.29: Assessment of interferon response stimulation by anti-HBV DEM-encoding mRNA in cultured cells. 137
Figure 5.1: Plasmids maps of pCMV-dDEM and pCMV-DEM under the control of a CMV promoter. 163
Figure 5.2: Restriction enzyme digestion of pmRNA-pA backbone. 164
Figure 5.3: Restriction enzyme digestion of CMV inactive and active DEMs to excise the TALE-encoding domain. 165
Figure 5.4: Restriction enzyme digestion of CMV inactive and active DEMs to excise the effector-encoding domains. 166
Figure 5.5: Restriction enzyme digestion of pCMV-eGFP -encoding plasmid. 168
Figure 5.6: Confirmation of GFP reporter mRNA expression vector by enzymatic digestion... 169
Figure 5.7: Restriction enzyme digestion of pVAX-CMV TALEN-encoding plasmids..... 171
Figure 5.8: Confirmation of active pmRNA-DEMΔKRAB DNA by enzymatic digestion. 172
Figure 5.9: Restriction enzyme digestion of pUC57-ECS -encoding plasmid with *Nde*I and *Esp*3I. 173
Figure 5.10: Restriction enzyme digestion of pUC57-ECS -encoding plasmid with *Nde*I and *Esp*3I. 174
Figure 5.11: Restriction enzyme digestion of pT7(AG)-ECS 4×S-encoding plasmid. 175
Figure 5.12: Restriction enzyme digestion of active pmRNA-DEMs. 176
Figure 5.13: Restriction enzyme digestion of active pmRNA-DEMs to excise the TALE-DNMT-encoding sequences. 177
Figure 5.14: Restriction enzyme digestion of active pmRNA-DEMΔKRAB to excise transgenes. 179
Figure 5.15: Confirmation of active pT7-DEMΔKRAB AG 4× DNA by enzymatic digestion. 180
Figure 5.16: Sequencing confirmation of TALE-DBD sequences in Anti-HBV DEMs. 183
Figure 5.17: Sequencing confirmation of DNMT3A sequences in anti-HBV DEMs. 185
Figure 5.18: Sequencing confirmation of DNMT3L sequences in anti-HBV DEMs. 187
Figure 5.19: Immunofluorescence detection of pT7(AG)-DEMΔKRAB 4×S mRNA. 188

Figure 5.20: IVT of DEM produced from pT7-DEM 4× AG vector and assessment of transcriptional repression of HBsAg *in vitro*. 189

List of Tables

Table 1.1:Global geographic distribution of HBV genotypes with corresponding CpG islands including the 3 conventional and novel CpG islands..... 15
Table 1.2: Comparison of DNA binding domains, Zinc Fingers, TALEs and CRISPR for epigenome editing. 20
Table 2.1: Post-transcriptional capping protocol for producing Cap 0 and Cap 1 mRNA 52
Table 2.2: Primer Sequences used to amplify HBV surface and pgRNA transcripts by RT-qPCR 68
Table 2.3: Primer sequences used to amplify IFN-β and IFN- inducible genes 69
Table 5.1: Description of plasmids used in this study 153
Table 5.2 : IVT reaction setup with RiboMAXTM Large Scale RNA Production System reaction set up 157
Table 5.3 : IVT reaction setup with Transcript T7 High Yield Transcription Kit 158
Table 5.4: IVT reaction setup with NEB IVT components, TriLink Buffer and CleanCap AG . 158
Table 5.5: Composition of 10× TriLink CleanCap® AG IVT buffer 159
Table 5.6: Amino Acid Repeat-Variable Di-Residues (RVDs) of S, C, and P TALE-DBDs Responsible for Single Nucleotide Recognition (Bloom et al., 2013)..... 181
Table 5.7: RT-qPCR results for HPRT Gene amplification in mock and DEM-transfected Huh7 cells using Luna® Universal One-Step Reagent (without reverse transcriptase)..... 190

List of abbreviations

ATF	-	Artificial transcription factor (ATF)
Bp	-	Base pair
BSA	-	Bovine serum albumin
Cas9	-	CRISPR associated 9
cccDNA	-	Covalently closed circular DNA
CHB	-	Chronic HBV infection
CMV	-	Cytomegalovirus
CRISPR	-	Clustered regularly interspaced short palindromic repeats
CpGs	-	CpG dinucleotides
DSB	-	Double-stranded breaks
ddH_2O	-	Double distilled water
dsRNA	-	Double-stranded RNA
DAPI	-	4',6-diamidino-2-phenylindole
DEM	-	Designer epigenome modifier
dDEM	-	Dead (inactive) designer epigenome modifier
DMEM	-	Dulbecco's Modified Eagle's Medium
DMSO	-	Dimethyl sulphoxide
DBD	-	DNA binding domain
DNMTs	-	DNA-methyltransferases
E. coli	-	*Escherichia coli*
EDTA	-	Ethylene diamine tetra-acetic acid
eGFP	-	Enhanced green fluorescent protein
ELISA	-	Enzyme Linked Immunosorbent assay
FBS	-	Foetal bovine serum
FITC	-	Fluorescein isothiocyanate
FLuc	-	Firefly luciferase
HA	-	Haemagglutinin epitope
Huh7	-	Human hepatoma 7

List of Abbreviations

HBcAg	-	Hepatitis B core antigen
HBV	-	Hepatitis B virus
HBeAg	-	Hepatitis B e antigen
HBx	-	Hepatitis B virus X protein
HCC	-	Hepatocellular carcinoma
HDI	-	Hydrodynamic injection
IFIT 1	-	Interferon-induced proteins with tetratricopeptide repeats 1
IFN	-	Interferon
IFN-α	-	Interferon alpha
IFN-β	-	Interferon beta
IRES	-	Internal ribosome entry site
IVT	-	In vitro transcription
IVTed	-	In vitro transcribed
KRAB	-	Krüppel-associated box
LiCl	-	Lithium chloride
mRNA	-	messenger RNA
MDA5	-	Melanoma differentiation-associated protein 5
m1A	-	N1-methyladenosine
m6A	-	N6-methyladenosine
5moU	-	5-Methoxyuridine (5moU),
m1ψ	-	N1-methylpseudouridine
m5U	-	5-Methyluridine
MTT	-	3-(4,5-Dimethylthiazol-2-yl)-2,5-diphenytetrazolium bromide
NAs	-	Nucleos(t)ide analogues
NLS	-	Nuclear localisation signal
NLRs	-	Nucleotide oligomerisation domain (NOD)-like receptors
Nm	-	Nanometres
NTCP	-	Sodium taurocholate co-transporting polypeptide
ORF	-	Open Reading Frame

List of Abbreviations

OAS 1	-	Oligoadenylate synthetase 1
PABPs	-	Poly (A) binding proteins
PBS	-	Phosphate buffered saline
PCR	-	Polymerase chain reaction
PKR	-	Double stranded RNA-dependent protein kinase
pgRNA	-	Pregenomic RNA
PRRs	-	Pattern recognition receptors
PTMs	-	Post-transcriptional modifications
qPCR	-	Quantitative PCR
rcDNA	-	Relaxed circular DNA
RIG-I	-	Retinoic acid-inducible gene I
RLRs	-	Retinoic acid-inducible gene-I-like (RIG-I-like) receptors
rpm	-	Revolutions per minute
RT-qPCR	-	Reverse transcriptase quantitative PCR
ssRNA	-	Single-stranded RNA
TALE	-	Transcription activator-like effector
TALEN	-	Transcription activator-like effector nuclease
TLRs	-	Toll-like receptors
UTR	-	Untranslated region
VCE	-	Vaccinia Capping Enzyme
VPE	-	Viral particle equivalents
ZF	-	Zinc Finger
ZFN	-	Zinc Finger Nuclease

List of symbols

3', 5'	-	Three prime, five prime
A	-	Alpha
B	-	Beta
Δ	-	Delta
Ψ	-	Pseudouridine

Chapter 1

1. Introduction

1.1 Hepatitis B: the virus, the disease and the epidemiology

The hepatitis B virus (HBV) was discovered in the 1960s, and it soon became one of the first human hepatitis viruses to be well characterised at a molecular level (Blumberg et al., 1967). HBV belongs to the *Hepadnaviridae* family and is a small, enveloped DNA virus with strong liver tropism and species-specificity (Levrero et al., 2009, Guo et al., 2023). This highly transmissible virus possesses a unique genomic organisation and has evolved a successful replication mechanism that has allowed for indefinite persistence of the virus in the livers of infected individuals (Zhou and Holmes, 2007). HBV infection of hepatocytes results in liver inflammation and can be either acute or chronic (Marion and Robinson, 1983). Acute infection generally occurs after initial exposure and may last up to six months with an estimated 90%–95% of individuals clearing the infection completely without the requirement for treatment (Mani and Andrisani, 2019). However, individuals who are unable to clear the virus after six months are diagnosed as having a chronic infection. Chronically infected individuals can be asymptomatic and can serve as carriers further contributing to virus transmission (Kasianchuk et al., 2023). Persistent immune-mediated clearance of infected cells during chronic HBV infection (CHB) leads to liver damage which in turn may lead to hepatocellular carcinoma (HCC) and/or cirrhosis (Chen and Tian, 2019).

HBV continues to be a major global cause of mortality, with a prevalence of 3.2% worldwide as of 2022 and an estimated 257.5 million people infected (WHO, 2022). Approximately 14% of these individuals are diagnosed and only 8% are treated (WHO, 2022). Chronicity is influenced by multiple viral factors and is caused as result of the stable covalently closed circular DNA (cccDNA), which resides indefinitely within infected hepatocytes (Sung et al., 2012, Péneau et al., 2022). This cccDNA serves as a template for viral replication and transcription, leading to the production of new virions and contributing to the maintenance of a persistent viral reservoir. Additionally, the inability of the host immune system to clear the infection is the primary cause of chronicity, as the virus remains in the individual indefinitely. This contributes further to the

persistence of the infection through the maintenance of a stable viral reservoir. CHB continues to cause significant mortality and morbidity globally, with an estimated 250–300 million chronic carriers contributing to approximately 880,000 deaths annually (Hu et al., 2019). Additionally, infants infected with HBV during the perinatal period (approximately 90%) and in individuals who are immunocompromised are highly likely to develop CHB (Long et al., 2022). CHB significantly increases the risk of developing HCC and cirrhosis (Sung et al., 2021, Llovet et al., 2016). HBV is highly endemic in sub-Saharan Africa and Asia, in these areas the seroprevalence of HBsAg is above 8% of the population (Amponsah-Dacosta, 2021) and progression to chronicity is common in these regions with high rates of cirrhosis and HCC. In contrast, HBV is moderately endemic in the Mediterranean Basin and Eastern Europe with a prevalence ranging from 2-8%. Meanwhile, North Africa and Western Europe are considered to have low endemicity (Nguyen et al., 2020). In regions with a high prevalence of HBV, particularly sub-Saharan Africa and Southeast Asia, HCC is among the most common cancers (Amponsah-Dacosta, 2021). Liver cirrhosis is a major risk factor for HCC development, and the prognosis for HCC is poor, with a 5-year survival rate of approximately 18% (Draper, 2020). It has been reported that untreated individuals with HBV-induced cirrhosis face a liver-related mortality rate of 49.86 per 1,000 person-years, which is significantly higher than the 11.39 per 1,000 person-years for those receiving treatment (Makuza et al., 2024). Additionally, recent studies have reported a 5-year cumulative incidence of hepatocellular carcinoma (HCC) at 22.9% (Guo et al., 2024).

1.2 Viral genotypes and transmission

HBV replicates through an RNA intermediate via reverse transcription. The lack of proofreading ability of the viral DNA polymerase predisposes HBV to mutations leading to a relatively high mutation rate of 10% compared to other viruses (Mimms, 1995, Caligiuri et al., 2016). Based on the high variability of HBV sequences and nucleotide divergence of 7.5-8 %, 10 genotypes have been identified (A to J) which are further subdivided into multiple subgenotypes with a DNA divergence between 4 to 7.5% (Kramvis, 2014). HBV genotypes are distributed geographically, and this distribution significantly influences clinical outcomes, with the severity of the disease varying according to the specific genotype present. Specifically, genotypes C and A are associated with more severe cirrhosis and hepatocellular carcinoma (HCC) (Yuen et al., 2008, Kumar et al., 2005, Rajoriya et al., 2017).

HBV is primarily transmitted through exposure to infected bodily fluids and blood, which occurs through both vertical and horizontal transmission routes. Vertical transmission occurs when an infected mother passes the virus to her newborn through contaminated bodily secretions or blood (Borgia et al., 2012). In contrast, horizontal transmission involves the spread of the virus between individuals through physical contact or contact with infected bodily fluids. In highly endemic regions, such as Southeast Asia, the virus is commonly acquired early in childhood or perinatally, while in Africa, horizontal transmission primarily occurs during childhood (Borgia et al., 2012, Keane et al., 2016). The spread of the virus in these regions is exacerbated by socioeconomic factors, insufficient disinfection of medical equipment, and the use of contaminated blood or blood components (Gnyawali et al., 2022, Mohamud et al., 2024, Sauerbrei, 2014). An HBV vaccine has been available since 1982 and has a 95% efficacy rate. and has been universally implemented to reduce infection rates and new cases globally. It has proven highly effective in preventing initial HBV infections, offering over 95% protection to infants, children, and young adults, and achieving seroprotection rates of 98-100% in children and 90-95% in adults (Van Den Ende et al., 2017, Dasgupta et al., 2020). This widespread vaccination has also contributed to lower liver cancer rates(Dasgupta et al., 2020, Romano' and Zanetti, 2022, Schillie and Murphy, 2013) . However, since it is a prophylactic vaccine, it does not provide therapeutic benefits for those already infected with HBV or impact established chronic hepatitis B (CHB) infections (Sheena et al., 2022). Additionally, 5-10% of immunocompetent adults may not reach protective antibody levels, highlighting the need for improved vaccination strategies, particularly in high-transmission areas (Romano' and Zanetti, 2022, Schillie and Murphy, 2013)

1.3 HBV virion and genome organisation

The infectious HBV particle, known as a 'Dane particle,' consists of an outer lipid bilayer that surrounds a nucleocapsid. The nucleocapsid itself is composed of hepatitis B core antigen (HBcAg) organised in an icosahedral structure, and it contains the viral polymerase and a partially double-stranded viral genome known as relaxed circular DNA (rcDNA). Embedded in the lipid bilayer are hepatitis B surface antigens (HBsAg), which include small (S), middle (M), and large (L) surface proteins (Dane et al., 1970, Nassal, 2015). rcDNA is comprised of a short plus strand and a long minus strand. The minus strand serves as a template for the viral

polymerase, which synthesises the plus strand of DNA. Meanwhile, the plus DNA strand is utilised for transcription of viral mRNA (Nassal, 2015).

The 3.2 kb viral genome of HBV is intricately arranged as all genes are encoded within the four overlapping open reading frames (ORFs) namely surface (*S*), polymerase (*P*), core (*C*) and (*X*). The viral genome encodes for the expression of five viral transcripts (Seeger and Mason, 2000). These transcripts encode seven proteins, namely five structural proteins consisting of the three forms of HBsAg (S, M and L), HBc, hepatitis B e antigen (HBeAg) and two non-structural proteins polymerase , and X protein (HBx) (Lamontagne et al., 2016). The *S* ORF, which can be divided into the S, pre-S1 and pre-S2 regions, encodes the 3 surface envelope antigens. The *C* ORF encodes the core and precore proteins. Core is translated from the pgRNA and assembles into the nucleocapsid. Precore is translated from the precore mRNA and is processed to yield HBeAg (Seeger and Mason, 2015). Whereas the *P* ORF encodes the polymerase protein which is responsible for the reverse transcription of pgRNA and *X* ORF encodes the HBx protein (Seeger and Mason, 2015). Transcriptional control of the viral genome is highly regulated involving four distinct promoters (pS1, pS2, pC, pX), two enhancing elements (enhancer I and enhancer II) and other regulatory elements (Seeger and Mason, 2000). The highly condensed multifunctional nature of the genome results in the majority of the sequence encoding for more than one functional element (McNaughton et al., 2019) contributing to the high mortality.

1.3.1 Viral replication

Infection begins when HBV, encoding pre-S1 and pre-S2 proteins, attaches to the host cell by binding to heparan sulfate proteoglycans and glypican 5 (GPC5) (Verrier et al., 2016). The virus then binds to the sodium taurocholate cotransporter polypeptide (NTCP) on hepatocytes and interacts with the epidermal growth factor receptor (EGFR) to mediate viral entry into the cell(Yan et al., 2012, Iwamoto et al., 2019). Following entry, the viral nucleocapsid is released and transported to the nucleus. Once in the nucleus, the nucleocapsid disintegrates to release the core proteins (HBcAg) and rcDNA (Gallucci and Kann, 2017). Once in the nucleus, rcDNA undergoes processing and is repaired to form cccDNA using host DNA repair machinery (Schreiner and Nassal, 2017). Repair of rcDNA requires the simultaneous removal of the viral polymerase covalently attached to the 5′ end of the minus strand DNA (Delius et al., 1983) and a short RNA oligomer at the 5′ end of the plus strand. The RNA oligomer, which served as a

primer for plus-strand DNA synthesis is removed to facilitate ligation of the two strands. Following this, the two DNA strands undergo covalent ligation to form the cccDNA (Chuang et al., 2022). cccDNA associates with histone and non-histone proteins producing a compact stable minichromosome that primarily functions as a transcriptional template for all viral RNA and consequently is essential for protein production and viral replication (Nassal, 2015). Three subgenomic RNAs (preS1 mRNA, preS2/S mRNA and HBx mRNA) and two genomic RNA (pregenomic RNA (pgRNA) and precore RNA (pcRNA)) are transcripts encoded by cccDNA (Levrero et al., 2009) and in the cytoplasm are translated into viral proteins including envelope proteins, core proteins and polymerase.

Envelope proteins and core packaging proteins are synthesised from preS1, preS2 and HBcAg mRNAs. Envelope proteins are necessary for the formation of the viral envelope, while core packaging proteins facilitate the packaging of nascent viral DNA into the capsid (Nassal, 2015). pgRNA operates as a bicistronic mRNA, allowing for the translation of core protein and viral polymerase. The translation of polymerase initiates a signal that starts the encapsidation process. This process causes the reverse transcription of the minus strand producing the function as a template for plus-strand synthesis (Delius et al., 1983). This results in a mature nucleocapsid containing the rcDNA genome. Mature nucleocapsids are enveloped to form HBV virions which secreted from the hepatocytes via secretory pathways (Soussan et al., 2000). Alternatively, some nucleocapsids are transported to the nucleus replenishing the cccDNA pool (Beck and Nassal, 2007). In this way, the cccDNA reservoir is maintained even in the absence of detectable viraemia over long periods of time (Blondot et al., 2016), leading to the stable maintenance of cccDNA reservoir in the nucleus of the infected hepatocytes (Figure 1.1).

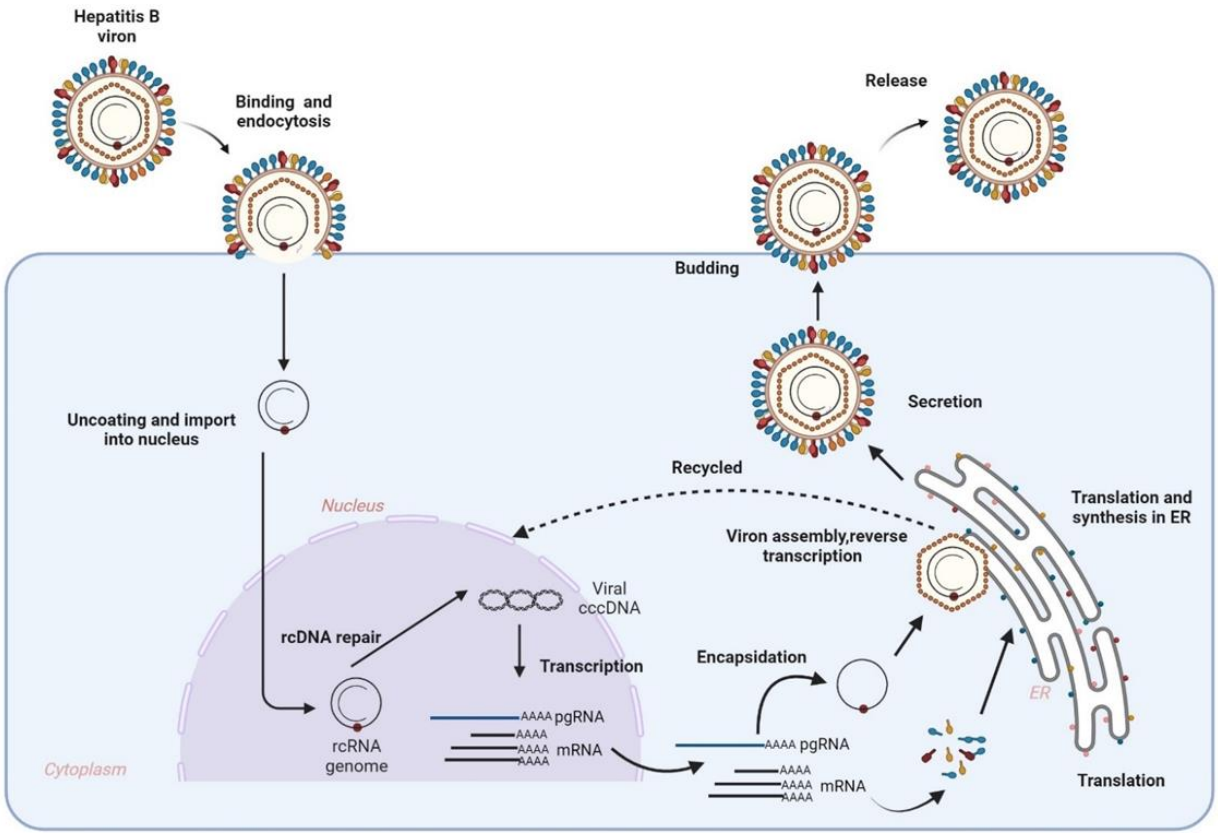

Figure 1.1: HBV replication. HBV attaches to the host cell by binding to the NTCP, mediating viral entry into the cell. Following entry, the viral nucleocapsid is released and transported to the nucleus, where it disintegrates to rcDNA. Once in the nucleus, rcDNA undergoes processing and is repaired to form cccDNA. cccDNA serves as the viral template for the transcription of subgenomic RNAs and pgRNA, which are transported to the cytoplasm. In the cytoplasm, these RNAs are translated into viral proteins, including envelope proteins, core proteins, and polymerase. The translation of polymerase initiates a process of encapsidation, which involves reverse transcription of the minus strand to generate the plus strand, leading to the formation of a mature nucleocapsid containing progeny DNA (rcDNA). The nucleocapsid then binds to the endoplasmic reticulum, acquiring an envelope with surface proteins. Finally, the nucleocapsid can either be secreted or re-enter the nucleus to produce additional cccDNA (Adapted from (Wei and Ploss, 2020).

1.4 Available Treatment for HBV

1.4.1 First line treatment

Approved licensed therapies for management of CHB consists of immunomodulating agents and nucleos(t)ide analogues (NAs). Immune modulators derived from interferon (IFN) alpha (standard IFN-α and pegylated IFN-α) epigenetically control minichromosome cccDNA and modulate host antiviral immune response (Belloni et al., 2012) removing infected hepatocytes. Treatment has been shown to be effective in approximately 20% of patients limiting its usefulness (Gish et al., 2015). Five oral NAs, comprising lamivudine, entecavir, telbivudine, tenofovir and adefovir dipivoxil potently block the viral reverse transcriptase thereby suppressing replication (Trépo et al., 2014). NA treatment does not eliminate cccDNA and has no effect on integrated viral sequences which are associated with continued HBsAg expression and HBV-related carcinogenicity (Lok et al., 2017). Therefore necessitating life-long treatment which is complicated by drug-toxicity and the emergence of drug resistant viruses (Zoulim, 2011). Managing HBV in patients co-infected with HIV is more complex because of accelerated HBV replication, delayed HBeAg seroconversion, and a higher risk of CHB, which adversely affects survival outcomes (Maponga et al., 2020). In South Africa, HIV-positive individuals receive antiretroviral therapy (ART), typically including tenofovir disoproxil fumarate (TDF) with lamivudine or emtricitabine, which are effective against HBV (Hamers et al., 2013). This facilitates simultaneous treatment of both infections and reduces complications. However, HBV mono-infected patients often lack comparable integrated antiviral therapy, leading to worse disease progression and treatment outcomes, as eligibility is determined by clinical staging and guidelines (Sonderup et al., 2020). Additionally, co-infected patients may sometimes receive only HBV monotherapy, increasing the risk of developing HBV-resistant mutants (Selabe et al., 2007). NAs along with PEGylated IFN-α comprise first line treatment of HBV and has shown success when used as a combination therapy (Liver, 2017). Presently there are no approved therapies that reliably silence or eliminate cccDNA from chronic carriers (Fanning et al., 2019). The failure of these therapies to completely eliminate cccDNA highlights the requirement for novel therapeutic approaches to treat CHB infections.

1.4.2 Current and emerging strategies for HBV treatment

Considering the limitations of current antiviral therapies, along with mortality rates, new infections, and the percentage of individuals chronically infected, the most feasible goal is a functional cure. A functional cure is defined as having undetectable HBV DNA levels with a sustained loss of HBsAg in the serum following the discontinuation of therapy (Zeisel et al., 2015). Given this, emphasis has been placed on the development of a broad spectrum of therapies targeting critical points in the HBV replication cycle. Some of these therapies are in preclinical and early clinical trials, aiming to provide effective alternatives for those infected (Lee et al., 2020).

The treatment of HBV infection involves several therapeutic approaches, each targeting different stages of the virus' lifecycle. One primary strategy is the use of direct-acting antiviral therapies. These include entry inhibitors, such as Bulevirtide (Hepcludex) and Myrcludex B, which block the NTCP receptor to prevent the virus from entering hepatocytes (Yan et al., 2012); capsid assembly inhibitors, including ZM-H1505R (Canocapavir), disrupt the viral capsid formation inhibiting the encapsidation of pgRNA thereby impairing the formation of cccDNA (Schinazi et al., 2018, Berke et al., 2017, Parikh et al., 2023). Additionally, secretion inhibitors, such as REP 2139, block viral assembly by targeting viral proteins essential for assembling new virions and prevents envelopment of the virus (Schinazi et al., 2018, Fanning et al., 2019, Bazinet et al., 2020). Reverse transcriptase including lamivudine and polymerase inhibitors, such as nucleos(t)ide analogs, function by suppressing viral DNA synthesis (Lai et al., 2017)

In addition to these methods, targeting HBV gene expression presents another therapeutic approach. Post-transcriptional control inhibitors, such as RNA interference (RNAi) molecules (Morrissey et al., 2005, Ely et al., 2008), antisense oligonucleotides (ASOs) (Maepa et al., 2015), and locked nucleic acids (LNA) (Javanbakht et al., 2018), work by directly binding to HBV mRNA to suppress its translation or induce its degradation. Another significant strategy involves immune modulation, which aims to enhance the host’s immune responses using therapies that target Toll-like receptors (TLRs) and immune checkpoint molecules like programmed cell death protein 1 (PD-1) and PD ligand 1 (PD-L1) (Ma et al., 2018, Fisicaro et al., 2010). Additionally, efforts to target the cccDNA reservoir include gene editing technologies like zinc finger nucleases (ZFNs)(Cradick et al., 2010), transcription activator-like effector nucleases (TALENs)

(Bloom et al., 2013, Smith et al., 2021), and the clustered regularly interspaced short palindromic repeats/CRISPR-associated proteins (CRISPR/Cas) system (Schiwon et al., 2018), which disrupt cccDNA by causing targeted mutagenesis at specific HBV genome sequences. Epigenetic therapies harness the target specificity of gene editing technologies to modify the cccDNA and repress HBV gene expression without altering the DNA sequence (Zhao et al., 2013, Bloom et al., 2019). Combining these various antiviral and immune modulatory strategies may enhance treatment efficacy and move closer to achieving functional cure for chronic HBV infection. However, challenges remain, particularly in managing the cccDNA reservoir, which continues to present as a major obstacle.

1.5 cccDNA: viral reservoir

HBV cccDNA is maintained in quiescent hepatocytes without affecting viability and functions as a viral template for transcription of pgRNA and subgenomic RNAs. This replication intermediate is inherently stable in infected hepatocytes, persisting for years. This stability is attributed to its half-life, which contributes to the persistence of CHB (Laras et al., 2006). The half-life of cccDNA is estimated to be around 40 days (Ko et al., 2018) which is consistent with studies in ducks and woodchucks which indicate 30 to 50 days (Addison et al., 2002). The viral genome maintains its cccDNA copy number using two mechanisms. The first and main method is the infection and re-infection of hepatocytes (Beck and Nassal, 2007). The second mechanism involves conversion of rcDNA to cccDNA via the intracellular conversion pathway after transportation to the nucleus (Nassal, 2015). While various mechanisms contribute to the maintenance of the cccDNA reservoir, reactivation of cccDNA in infected hepatocytes upon discontinuation of antiviral treatment or under conditions of low immunity indirectly contributes to its preservation (Palmore et al., 2009).

Several mechanisms contribute to the elimination of cccDNA, including clearance of infected hepatocytes through T cell-mediated apoptosis, loss or dilution of cccDNA during mitosis, and treatment with antivirals such IFNs (Naully et al., 2024, Addison et al., 2002, Lucifora et al., 2014). However, T cell-mediated apoptosis may not be a feasible strategy because it requires the continuous turnover of a significant proportion of both infected and uninfected hepatocytes (Phillips et al., 2010). Additionally, cccDNA persists during mitosis and is distributed to progeny hepatocytes, even though it lacks a nuclear retention signal and an origin of replication,

preventing it from replicating independently (Lucifora and Protzer, 2016). Studies have shown that as few as 1.5 copies of cccDNA per cell are sufficient to maintain a chronic infection (Laras et al., 2006), which can persist indefinitely despite undetectable levels of HBsAg in the blood (Rehermann et al., 1996). Current therapies can reduce but not completely eliminate the persistent viral cccDNA reservoir, necessitating lifelong treatment. In response to this, there is renewed interest in sequence-specific technologies, such as gene and epigenome editing. These approaches have the potential to directly target, eliminate, or silence the cccDNA reservoir by inducing mutations within the HBV genome or silencing HBV transcription and replication, which is likely to impair viral fitness. These therapies provide a promising strategy for overcoming the limitations of existing treatments.

1.5.1 Direct targeting of cccDNA

Sequence-specific gene targeting has been achieved using various approaches. Notably, significant advancements have been made in targeting HBV using RNA interference (RNAi), artificial nucleases, and, more recently, base and prime editing technologies (Smekalova et al., 2024). RNAi exploits the endogenous microRNA (miRNA) pathway to modulate and silence transcription, ultimately affecting target protein coding genes. However it is limited by potential off-target effects and toxicity due to the interference and oversaturation of the endogenous miRNA pathway (Jackson et al., 2006, Grimm et al., 2006). Artificial nucleases are able to target anywhere in the genome, including regulatory elements and non-coding genes, and facilitate target mutagenesis which is achieved through to use of the error-prone non-homologous end joining DNA repair pathway. Similar to RNAi, nuclease-mediated gene editing is associated with off-target activity, which can result in unintended alterations to DNA and lead to genetic changes. Additionally, this technology often struggles with the effective targeting of biallelic genes, which can increase the frequency of chromosomal deletions and truncations. Such structural changes can disrupt gene function(Amabile et al., 2016). Furthermore, *Hepadnaviruses* depend on double stranded breaks (DSBs) in the host genome and the cellular repair machinery to integrate their viral genomes. Nuclease-mediated mutagenesis, which introduces DSBs, can therefore potentially influence viral integration. The induction of DSBs increases the risk of chromosomal translocations, which can lead to further genomic instability (Feitelson and Lee, 2007, Kosicki et al., 2018). Although these technologies are widely used in research and hold great potential, their

limitations highlight the need for a safer and more effective approach to targeting the HBV genome. Epigenome engineering offers a safer alternative by combining the ability to selectively induce sequence specific gene silencing without alteration to the DNA sequence (Mlambo et al., 2018).

1.6 Epigenetics: potential for therapeutic application

The term epigenetics, meaning "beyond genetics", was coined in 1942 and describes the reversible or heritable changes in chromosomes that affects the phenotype without alteration to the genomic DNA (Waddington, 1942). This highly regulated process which may be inherited between cell generations is crucial for gene expression, cell behaviour and function (Waddington, 1942). Epigenetic changes influence whether a gene is transcribed or repressed by modifying gene expression through post-transcriptional modifications (PTMs) (Wu and Morris, 2001). PTMs involve the direct addition or removal of chemical marks on DNA or histone protein tails, which affect the recruitment of transcriptional machinery and regulatory molecules(Andrews et al., 2016). The organisation of DNA and histones into chromatin, also known as the 'epigenome,' is essential for gene regulation. Chromatin primarily exists in two states namely heterochromatin and euchromatin. Heterochromatin comprises highly condensed chromatin, which makes the DNA inaccessible to the transcriptional machinery and is associated with gene silencing. In contrast, euchromatin consists of more loosely organised chromatin, making DNA more accessible and facilitating active transcription (Morrison and Thakur, 2021). DNA methylation is a commonly studied epigenetic modification and is crucial for regulating gene expression (Jaenisch and Bird, 2003).

Within mammalian cells, methylation predominantly occurs in CpG dinucleotides (CpGs) which are unequally dispersed within the genome and found as clusters termed CpG islands which on average can be 1 kb long (Bird, 1987). DNA methylation is an important epigenetic modification and is facilitated by DNA-methyltransferases (DNMTs) (Okano et al., 1999). A family of DNMTs comprised of DNMT1, DNMT3A, DNMT3B and DNMT3L is responsible for DNA methylation by facilitating the transfer of a methyl group from donor S-adenosyl-L-methionine to the fifth carbon atom of the cytosine forming a 5-methylcytosine (5meC) and is associated with transcriptional silencing (Jones, 2012) (Figure 1.2). DNMT3A and DNMT3B are crucial for *de novo* DNA methylation during development and are capable of methylating unmethylated and

hemimethylated DNA (Jeltsch and Jurkowska, 2014), while DNMT1 has a high affinity for and methylates hemimethylated DNA. Additionally, DNMT1 is required for the maintenance of DNA methylation pattern during replication acquired on the new DNA strand thereby maintaining pre-existing epigenetic marks (Vandiver et al., 2015). Catalytically inactive Dnmt3-like (Dnmt3L) protein is required to enhance the methyltransferase activities of Dnmt3 proteins by binding to their catalytic domains, making it instrumental for initiating methylation (Jeltsch and Jurkowska, 2014). Methylation of DNA by DNMTs blocks binding of transcription factors to promoters or recruits methyl-CpG binding domain (MBD) proteins and cofactors such as histone deacetylases (HDACs), histone methyltransferases (HTMs), and chromatin remodellers forming a repressive transcription complex responsible for the closed repressive chromatin state resulting in transcriptional gene repression (Klose and Bird, 2006).

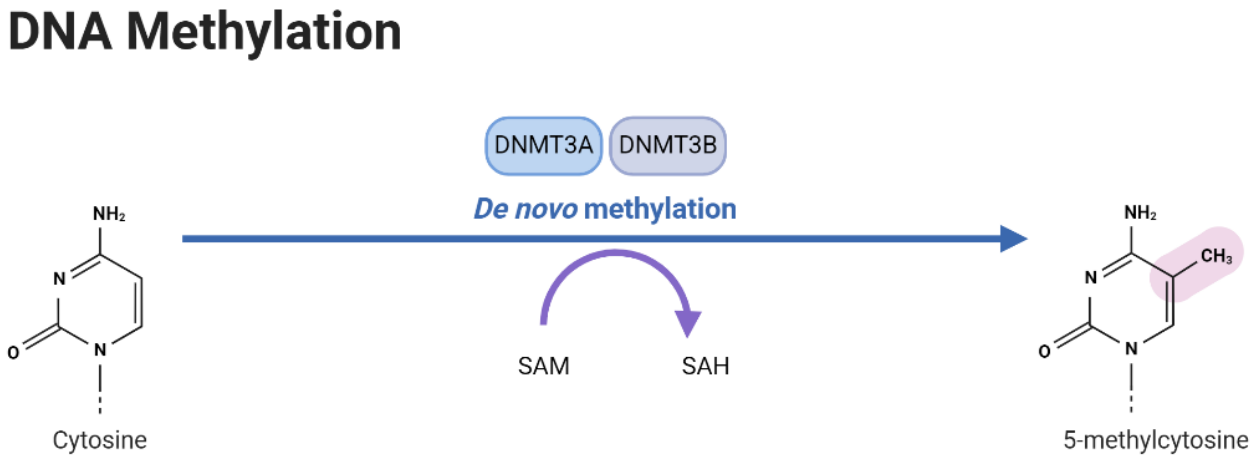

Figure 1.2: DNA Methylation of Cytosine. DNA methylation involves the covalent transfer of a methyl group to the carbon 5 position of the cytosine ring. DNA methyltransferase enzymes (DNMTs) catalyse this reaction by transferring a methyl group (CH_3) from the donor S-adenosyl-L-methionine (SAM), resulting in the formation of 5-methylcytosine (5meC) and S-adenosyl-L-homocysteine (SAH). This process is a crucial epigenetic mechanism that influences gene expression.

1.6.1 HBV genome: ideal target for DNA methylation

cccDNA persists in the nucleus as a stable minichromosome associated with host cellular histone and non-histone proteins (Nassal, 2015). This episomal minichromosome is under the regulation of several host transcription factors chromatin-modifying enzymes, host repair enzymes and viral proteins (Singh et al., 2021). As a hepatotropic virus, cccDNA contains binding sites for liver-specific and ubiquitous transcription factors (Quasdorff and Protzer, 2010). All these factors play an intricate role in the epigenetic regulation, synthesis, stabilisation and transcription of viral cccDNA. cccDNA contains three to six predicted CpG islands (Table 1.1), with conventional CpG islands (I, II, III) observed in the majority of HBV genotypes, while novel CpG islands (IV, V) tend to vary among these genotypes. Among the ten genotypes of HBV (A-J), genotypes C, F, G, H and J contain two CpG islands while genotypes of A, B, D, E contain three CpG islands (Zhang et al., 2013). Novel CpG islands IV is found within genotypes A, B, C, D, H and F but is seldom in genotypes G, H, and I (Table 1.1). The first CpG island (CpG I) overlaps the ATG start site of the small HBsAg gene, CpG II overlaps the enhancer I and II, *HBx* gene promoter and the core promoter. CpG III spans the ATG start site of *polymerase* gene and the Sp1 promoter (Figure 1.3) (Vivekanandan et al., 2008, Kaur et al., 2010). CpG islands are positioned strategically in regulatory domains within the genome making these CpG islands ideal target sites for DNA methylation (Jain et al., 2015). This implies that epigenetic modifications of the HBV genome by DNA methylation may influence viral replication and persistence of infection thereby making it a potential novel approach to target HBV (Jain et al., 2015, Kim et al., 2011).

Table 1.1:Global geographic distribution of HBV genotypes with corresponding CpG islands including the 3 conventional and novel CpG islands (Nguyen et al., 2020, Chen et al., 2018)

Genotype	**Country**	**CpG islands**			
		1	**2**	**3**	**Novel**
A	India, Sub-Saharan Africa, Western Africa, Northwest Europe, North America	✓	✓	✓	IV, VI
B	Asia, Greenland, Northern Canada	✓	✓	✓	IV, V, VI
C	Asia, Australia	−	✓	✓	IV, V, VI
D	Europe, Africa, India, Mediterranean countries	✓	✓	✓	IV, V
E	West African	✓	✓	✓	IV
F	South and central America	−	✓	✓	V, IV
G	France, Italy ,United Kingdom Germany, America	−	✓	✓	−
H	Central America	−	✓	✓	IV, V
I	Vietnam	✓	✓	✓	−
J	Japan	−	✓	✓	−

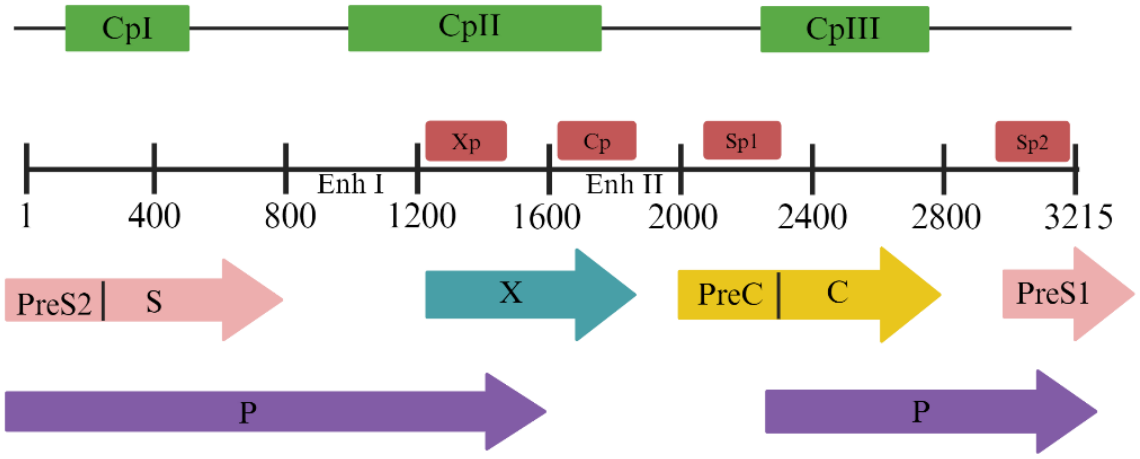

Figure 1.3: Schematic representation of the ORFs in the HBV genome with predicted CpG islands. Representation of HBV in the linear configuration with the *S*, *C*, *P* and *X* ORFs, the main regulatory elements, and enhancers I and II, the four promoters, pre-S1, pre-S2 and X promoters and the basic core promoter (BCP) and the three predicted CpG islands (CpG I, II and III). The positions of the CpG islands are indicated in the above genome. Nucleotide numbering is based on the *Eco*RI restriction site as position 1 (Adapted from (Hong et al., 2017)).

1.6.2 DNA methylation of HBV

Epigenetic modification of the HBV genome by methylation influences transcriptional regulation of viral mRNA and replication (Kim et al., 2011). CpG islands and the rate of methylation on cccDNA vary across different genotypes and are associated with viral transcriptional repression (Kaur et al., 2010).

Methylation of CpG II and III is highly conserved among different genotypes and is associated with lower levels of HBsAg and viraemia(Vivekanandan et al., 2008, Jain et al., 2015, Zhang et al., 2014). Additionally, hypermethylation of CpG II correlates with reduced levels of HBsAg and HBeAg(Vivekanandan et al., 2008, Guo et al., 2009). In contrast, methylation of CpG I appears to be rare and varies among genotypes (Zhang et al., 2014). HBeAg-negative patients who test negative for HBsAg but have persistent HBV DNA in the liver have significantly greater methylation of CpG II (Guo et al., 2009). Subsequent studies validated these results and further demonstrated a lower frequency of methylation of CpG I, while other studies confirmed an association between CpG I methylation and HBV replication(Vivekanandan et al., 2008, Jain et al., 2015). Furthermore, the state of disease progression impacts the methylation of CpG islands, with higher levels of HBV cccDNA methylation in CpG II and III observed in HCC tissues compared to cirrhotic and infected tissues(Vivekanandan et al., 2008, Guo et al., 2009, Jain et al., 2015). Since cccDNA function depends on its epigenetic modification, suppression through these mechanisms is a feasible strategy for treating CHB (Hong et al., 2017).

1.7 Potential of epigenome editing

Epigenome editing exploits the epigenetic enzymes of DNMTs, histone lysine methyltransferases (KMTs), histone acetyltransferases (HATs), demethylases and chromatin-remodelling complexes for the precise *de novo* placement or removal of epigenetic marks at specific target sites to facilitate or inhibit gene expression. Epigenome modifiers use epigenetic effector domains, which could constitute several epigenetic enzymes for targeted epigenome editing, fused to a programmable DNA binding domain (DBD) engineered to target any endogenous DNA sequence (Kungulovski and Jeltsch, 2016, Gilbert et al., 2014) (Figure 1.4). The novelty of epigenome modifiers lies in their ability to achieve targeted transcriptional repression or activation of gene expression with potentially long-lasting effects depending on type of effector domain utilised

(Stolzenburg et al., 2016, Kungulovski and Jeltsch, 2016). The efficacy of epigenome editing is dependent on both the epigenetic effector and DBDs. Epigenome editing offers targeted regulation of gene expression by inhibiting both alleles of a gene, making it a powerful tool for precise epigenetic control. One significant advantage is that certain epigenetic marks can be inherited, which reduces the need for repeated administrations (Van Der Gun et al., 2013). Furthermore, epigenome editing generally results in fewer adverse effects compared to nucleases, as it does not alter the host DNA sequence and the modifications can be reversible (Gilbert et al., 2014). Additionally, once established, the modified chromatin is stably maintained by the cell's endogenous machinery during cell division, ensuring long-term effects (Goell and Hilton, 2021).

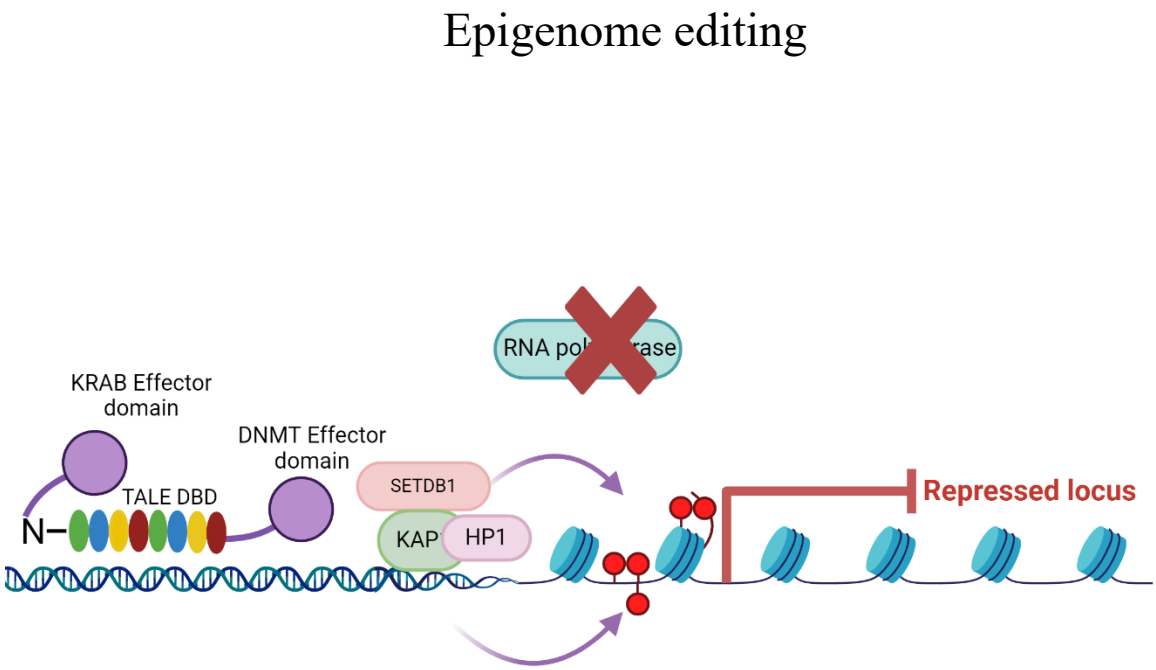

Figure 1.4:Overview of epigenome editing. Epigenome modifier platforms typically consist of a DNA binding domain (DBD) fused to effector domains such as DNMTs or the KRAB domain. The DBD allows for precise targeting of specific genomic sequences. The KRAB domain facilitates the recruitment of heterochromatin-forming complexes and co-repressors, while the DNMT domain catalyzes DNA methylation. This modification leads to changes in DNA conformation, resulting in a closed, condensed state that prevents transcription factors and RNA polymerase binding thereby inhibiting transcription. Thus, epigenome modifiers can regulate gene expression by altering chromatin structure.

1.7.1 Effector domains

Epigenome-modifying effectors are composed of domains of epigenetic enzymes involved in PTMs of DNA and histone proteins and can be classified as transcriptional repressors or activators. Transcriptional repressors trigger gene silencing by mediating recruitment of heterochromatin forming complexes that elicit steric hindrance, preventing the binding of transcription factors and RNA polymerase binding and elongation (Klose and Bird, 2006). The most commonly used repressors domains have been sourced from DNMTs, the Krüppel-associated box (KRAB) domain, KMTs, histone lysine demethylases (KDMs), and HDACs while Mxi1 and the mSin interaction domain (SID) are less commonly used (Singh et al., 2021). Transcriptional activators induce activation of genes and consists of the herpes simplex virus protein VP16 and the p65 subunit of the human NF-κB complex (Liu et al., 2001). Epigenome-modifying enzymes can be further subdivided based on how they function, catalytically active effectors such as DNMTs, have enzymatic activity while scaffolding effectors such as VP16 are catalytically inactive and function by triggering recruitment of cofactors (Hall and Struhl, 2002).

1.7.2 Programmable DBDs

Most epigenome-modifying enzymes with the exception of a few enzymes such as PR/SET Domain 9 (Prdm9) do not have a DBD and hence lack genome sequence-binding specificity. Rather, their target specificity is reliant on the various recruited transcription factors with which they form complexes with to control gene expression. Hundreds to thousands of transcription factors bind multiple target sequences and therefore control of gene expression is difficult to regulate (de Groote et al., 2012). Therefore, epigenetic modifiers employ programmable DBDs to guide the epigenetic effector to target DNA sequences increasing sequence specificity of gene activation or repression. Commonly used DBDs include ZFPs, TALEs and dCRISPR/Cas (Table 1.2), the use of these DBDs have been reported to induce transcriptional activation and repression (Zhao et al., 2013, Mlambo et al., 2018, Gilbert et al., 2014).

Selecting programmable DBDs offers unique advantages and disadvantages related to off-target and on-target effects, specificity, ease of use, and cost (Table 1.2). The same is true for the selection of the epigenetic effector domain as heritability of silencing and temporal stability are crucial considerations (Kungulovski et al., 2015, Kungulovski and Jeltsch, 2016). Nonetheless,

sequence-specific gene silencing with the use of epigenome modifiers provides a substitute to the conventional methods of nuclease mediated therapies and gene repression using RNAi.

Table 1.2: Comparison of DNA binding domains, Zinc Fingers, TALEs and CRISPR for epigenome editing.

	Zinc fingers	**TALEs**	**CRISPR/dCas**
Type of recognition	Protein-DNA	Protein-DNA	RNA-DNA
Components	Zinc finger domain,	TALE repeats	sgRNAs and Cas 9
Target site restriction	G-rich regions	Starts with T and ends with A	Requirement of PAM sequence at the end of each target site
Off-target	High	Low	Variable to high
Multiplexing	Difficult	Difficult	Possible
Customisability	Low	Low	Easy
Target length	9-36 bp	30-40 bp	20-22 bp
Cloning	Necessary	Necessary	Not Necessary
Target specificity	Low	High	High
Affordability	High, resource and time consuming	Affordable but time consuming	Affordable and rapid
Major advantage	Small size facilitating easy packaging.	High specificity recognising 1 bp	To target a new sequence, the only sgRNA needs to be redesigned
Major limitation	Requirement of a linker sequence for fusion pf modules.	Redesign TALE sequence for new target and difficulty binding methylated DNA	Use of Cas protein (large protein) making packaging and delivery difficult. Stability of sgRNA

1.7.3 Epigenome modifiers targeting HBV

The first epigenome modifier was generated by joining six ZF-DBDs fused to a KRAB repression domain. This epigenome modifier targeted viral X or enhancer I (EnhI) sequences achieving gene silencing of HBV. Significant repression of *HBx* gene transcription was achieved in both reporter cell line and Hep3B cell line harbouring integrated HBV DNA, although cellular growth arrest was observed (Zhao et al., 2013). Building on this, Luo *et al*., using a similar approach designed an artificial transcription factor (ATF) targeting a different sequence within EnhI. In this study authors reported improved inhibition of viral transcription and replication of HBc, HBx, HBeAg protein, and viral progeny in HepG2.2.15 cells and HBV transgenic mice, without affecting cell growth or inducing observable toxicity (Luo et al., 2018). These initial studies showed the antiviral potential of epigenome modifiers. Substituting the repressor domain with a DNMT to achieve targeted methylation of viral DNA was initially reported in a study that fused C-terminal region of the DNMT3A to a six-finger ZF (XPDnmt3aC). The XPDnmt3aC targeted the overlapping region between the *HBx* promoter and CpG II. Evaluations in HepG2 cells and HBV transgenic mice achieved *de novo* methylation and led to a significant decrease in viral particle production and reduced the expression of viral replication markers (Core mRNA, HBsAg and HBx proteins) (Xirong et al., 2014).

Furthermore, targeted epigenetic editing of HBV has recently been reported with use of engineered TALEs in conjunction with the KRAB repressor domain (rTALEs) (Bloom et al., 2019). rTALEs, SPL and SPR targeted the *S* ORF and was evaluated in both in vitro and in vivo models. Significant inhibition of viral replication, mRNA, HBsAg and circulating viral particle equivalents (VPEs) was observed without toxicity; furthermore, increased methylation of intrahepatic HBV DNA at CpG island II was achieved. The specificity of the rTALEs was improved by inclusion of a liver-specific mouse modified murine transthyretin receptor (MTTR) promoter. Despite overwhelming application of CRISPR/Cas utilised as a nuclease, studies using CRISPR interference or deactivated Cas9 fusions platforms for epigenome editing of HBV have been yet to be demonstrated (Larson et al., 2013). DNMT domains fused to dCas9 DNA has shown great promise in other disease models (Whittaker et al., 2023, Nuñez et al., 2021). Given the success in these studies, targeted epigenome silencing of HBV represents a therapeutic means by which to modulate viral replication which can be used as a potential treatment for CHB.

1.8 Therapeutic potential of designer epigenome modifiers (DEMs) platform

Mlambo *et al.*. established a novel platform called the Designer Epigenome Modifier (DEM), which combines the effector domains KRAB and DNMT (specifically DNMT3a and DNMT3L) with the TALE DNA-binding domain (TALE-DBD) to target the HIV *CCR*5 or *CXCR*4 genes (Mlambo et al., 2018). These genes are crucial for the early stages of HIV infection, with both *CCR5* and *CXCR4* being a coreceptor essential for viral entry into cells. DEMs were able to achieve robust and sustained repression of these genes. In a short-term study, both CCR5 transcript and protein levels were reduced, and CXCR4 receptors in T lymphocytes were effectively silenced. This repression increased over time and was maintained throughout the 18-day investigation, proving resistant to cell division and metabolic activation.

The study also demonstrated target specificity, with enhanced methylation occurring at on-target sites and negligible off-target methylation caused by DEMs. In contrast, control constructs lacking the KRAB domain and containing a catalytically inactive DNMT3A domain, referred to as inactive DEMs (dead DEMs/dDEMs), did not achieve any repression, this effect was also observed with constructs which had the KRAB domain excluded (DMT) highlighting the efficacy of the all-in-one architecture of DEMs for targeted gene silencing. Additionally, Mlambo *et al*., utilised DEMs expressed as in vitro transcribed (IVTed) mRNA to target a GFP reporter gene, which resulted in significantly greater repression compared to DNA-based constructs. This significant improvement in silencing of the GFP gene highlights the considerable potential of using mRNA-expressed therapeutics (Mlambo et al., 2018).

The success of IVTed mRNA in this study highlights the potential of mRNA-based platforms. This versatile platform has been utilised in various therapies, such as immunotherapy, cell reprogramming, CAR T-cell therapy, regenerative medicine, and gene editing, demonstrating its effectiveness across multiple fields (Qin et al., 2022). Due to renewed interest and advances, IVTed mRNA platforms have shown remarkable potential not only in gene silencing but also in developing therapeutic interventions.

1.9 Applications of mRNA Technology

Several critical discoveries have led to improved efficacy, stability, and immunogenicity of mRNA since its discovery, resulting in the establishment of synthetic mRNA as a viable technology/platform (Brenner et al., 1961, Jirikowski et al., 1992). More recently, the emergence of Severe Acute Respiratory Syndrome Coronavirus 2 virus (SARS-CoV-2) at the end of 2019 has led to the accelerated development and FDA approval of the first two mRNA-based vaccines, BNT162b2 (BioNTech) and mRNA-1273 (Moderna) (Polack et al., 2020, Baden et al., 2021).

IVTed mRNA offers several significant advantages over DNA and protein substitution for intracellular gene expression. One major benefit is that mRNA-based therapeutics generally present a better safety profile compared to DNA, as there is a lower risk of integration into the host genome, thereby reducing the likelihood of carcinogenesis and mutagenesis (Schlaeger et al., 2015, Wu et al., 2022). Additionally, mRNA does not require a nuclear localisation sequence since it does not need to enter the nucleus to be functional; this makes it effective in both mitotic and non-mitotic cells (Zhong et al., 2018) . Furthermore, because mRNA is transported directly to the cytoplasm, it can be translated into protein more rapidly than DNA. Moreover, mRNA can be administered repeatedly via intravenous injection, facilitating easier and more flexible dosing (Zhong et al., 2018). IVTed mRNA can be manufactured in a cell-free system, which is both scalable and cost-effective, allowing for easy standardisation (Meng et al., 2017). Finally, the immunogenicity of mRNA can be modulated through chemical modifications and purification, which enhances its stability and expression, as discussed in detail later in the thesis.

Synthetic mRNA can be produced through IVT, an enzymatic reaction that uses bacteriophage RNA polymerase T7, SP6 or T3 to catalyse the synthesis of RNA from the corresponding DNA template (Milligan and Uhlenbeck, 1989, Melton et al., 1984, Dunn et al., 1972). The DNA template to be transcribed requires a 5' untranslated region (UTR), an open reading frame (ORF) encoding the sequence of interest, a 3' UTR and a poly (T) track. These elements along with 5' cap structure constitutes the structural elements of a functional mRNA (Ely et al., 2021, Zhong et al., 2018) (Figure 1.5). The reaction takes a few hours, and a 5’ cap analogue can be included during IVT or added enzymatically afterward. This process can generate milligrams of mRNA in a single reaction (Baronti et al., 2018). The resulting mRNA produced resembles fully processed

mature mRNA molecules found in eukaryotic cells (Ely et al., 2021, Zhong et al., 2018) (Figure 1.5).

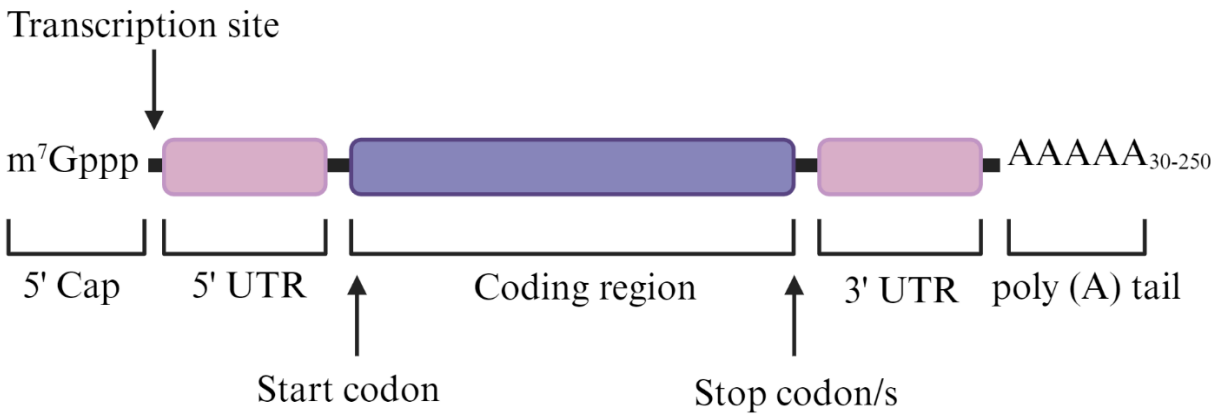

Figure 1.5: Representative scheme of in vitro transcribed (IVTed) mRNA. The general structure of IVTed mRNA consists of the essential elements, 5' cap, 5' untranslated region (UTR), open reading frame (ORF) encoding the sequence to be transcribed, 3' UTR and a poly (A) tail sequence. The mRNA also contains start and stop codons that are crucial for the initiation and termination of translation (Adapted from (Zhang et al., 2023))

1.10 Essential structural elements required for functional IVTed mRNA

1.10.1 ORF: Coding region

Eukaryotic genes consist of multiple introns and exons. Introns are removed during the intricate and complicated process of splicing to generate a complete mRNA which can be used for protein translation. In IVT, the ORF encodes the sequence of interest to be translated. The ORF is situated between the two UTRs and consists of a continuous sequence of codons. It typically begins with the start codon AUG (Sieber et al., 2018) and ends with a stop codon, which can be UAA, UAG, or UGA. A single stop codon, or a combination of these, can be incorporated at the end of the ORF (Xia, 2021).

Translation is initiated at the start codon and is terminated by the stop codon/s. The ORF is generally codon optimised to enhance protein expression and improve translational efficiency. Codon optimisation involves using codons recognised by abundant tRNAs. The selection of codons for optimisation is based on their association with the availability and frequency of tRNAs. Replacing rare codons with more frequent synonymous codons can influence translation elongation rates and mRNA secondary structure, thereby affecting mRNA stability, post-transcriptional regulation, translation efficiency, and protein folding (Pop et al., 2014, Yu et al., 2015, Gaspar et al., 2013). While codon optimisation can be beneficial, it may sometimes have detrimental effects. This is because it can disrupt natural codon usage patterns, which are optimised to regulate co-translational processes and the speed of translation (Pop et al., 2014, Yu et al., 2015). Rare codons play a crucial role in forming mRNA secondary structures and regulating translation elongation rates (Gaspar et al., 2013). Replacing these rare codons might affect mRNA regulation and stability, as well as alter protein folding as rare codons are associated with slower translation elongation, which is required to allow for important interactions with chaperone proteins. Therefore, although codon optimisation can enhance mRNA stability and improve protein expression, careful consideration is required to avoid potential adverse effects on the protein produced.

1.10.2 Poly(A) tail

mRNA contains a poly(A) tail, which consists of a sequence of repeating adenine residues at the 3' end, and is characteristic of mature mRNA, facilitating translation and stability. This sequence is responsible for ensuring nuclear export, recruitment of translation initiation factors and improves the half-life of mRNA (Jalkanen et al., 2014). The poly(A) tail contains crucial binding sites for poly (A) binding proteins (PABPs). Binding of PABPs to the poly(A) tail results in the recruitment of the large scaffold protein complex eIF4G which is comprised of eIF4A (RNA helicase) and eIF4E (cap-binding protein) increasing the affinity for mRNA cap (Gallie, 1998). The synergistic effect of the poly(A) tail and cap of mRNA circularise the mRNA by forming a cap/PABP/eIF4E-eIF4G-PABP-poly(A) complex. This closed loop structure improves binding and recycling of ribosomes and protect mRNA from degradation (Gallie, 1998, Newbury, 2006). A sufficiently long poly(A) tail is necessary for circularisation of the mRNA as physical interactions between the poly(A) tail and the cap is required to maintain mRNA stability (Lima et al., 2017). The length of the poly(A) tail influences mRNA half-life, stability, and subsequent protein translation. A tail length of approximately 120 nucleotides is considered optimal (Holtkamp et al., 2006, Park et al., 2016) and a minimum length of 30 nucleotides is required for mRNA stability (Lima et al., 2017), whereas shortening of the poly(A) sequence initiates RNA degradation. Once, the poly(A) sequence has shortened to less than 12 nucleotides, mRNA degradation occurs through de-capping enzymes, 5’-3’ exonucleases and de-adenylating enzymes occurring in the P-body sites in the cytoplasm (Newbury, 2006).

The poly(A) tail can be incorporated co-transcriptionally or post-transcriptionally. Co-transcriptional incorporation involves the inclusion of a poly(A) sequence into the design of DNA template or can be added post-transcriptionally through enzymatic polyadenylation, whereby incorporation or extension of tail sequence to the 3' end occurs using poly(A)-polymerase. Enzymatic polyadenylation is variable and leads to the generation of a mixture of polyadenylated mRNA with varying lengths (Holtkamp et al., 2006). Furthermore, enzymatic polyadenylation, while effective, adds an extra step to the manufacturing process, thereby increases the overall cost and complexity of large-scale production. Synthetic mRNA with a known homogeneous poly(A) tail length can be produced by encoding a poly(A) tract in the DNA template. However, DNA templates containing these poly(A) tract sequences have been

reported to have stability issues (Grier et al., 2016). To address this instability problem, segmented poly(A)-tails have been recently explored. This approach involves introducing a short linker within the poly(A) track to enhance stability (Trepotec et al., 2019). Overall, DNA template encoding a poly(A) track is the preferred approach to generate mRNA with a well-defined poly(A) tail length.

1.10.3 Untranslated regions (UTRs)

UTRs are non-coding elements located at the 5' and 3' ends of synthetic mRNA, flanking the coding region and thereby mimicking mature eukaryotic mRNA. The length, sequence, and secondary structures of UTRs are critical for regulating mRNA translation. UTRs are involved in mRNA transport from the nucleus to the cytosol (Asrani et al., 2018), inhibition of decapping and degradation, assembly of the translational machinery (Leppek et al., 2018), the regulation of translation (Suknuntha et al., 2018), and enhancement of mRNA stability (Asrani et al., 2018). The 5' UTR comprises the Kozak sequence (GCCGCCRCCATGG) located immediately upstream of the translation start site and crucial in the initiation of translation of the ORF (Kozak, 1986). The length of the 5'-UTR is a critical parameter because it contains binding sites for regulatory proteins and is essential for cap-dependent translation, which is common in most organisms. This process relies on the protein preinitiation complex, which scans the 5'-UTR until it finds the AUG start codon. The recognition of this codon initiates the formation of the 80S initiation complex, where the 60S ribosomal subunit joins the 40S subunit, and protein synthesis begins (Hinnebusch and Lorsch, 2012). Alternatively, 5' UTRs containing internal ribosome entry site (IRES) elements allow for cap-independent translation initiation (Huez et al., 1998).

The 3' UTR, located immediately after the stop codon, includes several regulatory elements such as microRNA response elements (MREs), which inhibit translation or stimulate mRNA degradation, iron-responsive elements (IREs), and adenylate-uridylate (AU)-rich elements (AREs). These elements impact mRNA stability, degradation, and translation by influencing how the mRNA is processed and degraded. AREs, in particular, act as decay signals within the 3' UTR, promoting the removal of the poly(A) tail and leading to rapid mRNA decay and reduced protein production (Ryan et al., 2018, Klausner et al., 1993, Chen and Shyu, 1995). Replacing ARE sequences in the 3' UTR can increase mRNA half-life, while UTRs enriched with CG sequences often exhibit enhanced stability and translation efficiency (Suknuntha et al., 2018,

Sergeeva et al., 2016). UTR sequences derived from human α- and β-globin genes naturally confer higher levels of stability and translation, making them frequently used to enhance the stability and translation of IVTed mRNA. Additionally, arranging two human β-globin 3' UTRs in a head-to-tail orientation further improves the stability and translation efficiency of synthetic mRNA (Holtkamp et al., 2006, Adibzadeh et al., 2019).

1.10.4 5' Cap structure

Eukaryotic mRNAs feature a 5' cap structure, which is essential for their function. Bacteriophage RNA polymerases, however, do not naturally produce capped transcripts. Therefore, to mimic eukaryotic mRNA functionality, IVTed mRNA must be capped. This capping can be achieved either enzymatically or by including a cap analogue in the reaction (Furuichi, 2014). The 5' cap plays several crucial roles, it facilitates ribosome recognition and recruitment, initiates translation, protects mRNA from degradation by preventing 5' to 3' exonuclease activity, stabilises mRNA by blocking its recognition by the innate immune system, and is involved in nuclear export (Evdokimova et al., 2001, Gingras et al., 1999, Gonatopoulos-Pournatzis and Cowling, 2014, Schoenberg, 2011). This cap structure is a modified nucleoside, N7-methylguanosine (m7G), linked to the first nucleotide of the RNA via a reverse 5' to 5' triphosphate bond, referred to as Cap 0 (m7GpppN), which is the simplest form (Furuichi, 2014). Synthetic mRNA is capped either co-transcriptionally during IVT or post-transcriptionally through enzymatic reactions (Henderson et al., 2021, Martin and Moss, 1975) (Figure 1.6). In mammals, mRNA undergoes 2'-O-methylation at the 2' position of the ribose ring of the first or second nucleotide, resulting in three cap conformations: Cap 0 (m7GpppN), Cap 1 (m7GpppNm, with methylation on the first adjacent nucleotide), and Cap 2 (m7GpppNmNm, with methylation on the first two nucleotides) (Figure 1.6). While Cap 0 is sufficient for initiating translation, Cap 1 and Cap 2 have been shown to enhance protein production (Furuichi, 2014, Sikorski et al., 2020).

1.10.5 Co-transcriptional capping

Co-transcriptional capping involves the incorporation of cap analogue (m7GpppG) during IVT allowing capping and IVT to occur in a single reaction. During IVT, RNA polymerases initiate transcription with a guanosine, thus first-generation cap (m7GpppG) competes with GTP, which acts as the initiator nucleotide to be included as the first nucleotide in the new transcript. This produces both capped and uncapped mRNA, with a 5' triphosphate, resulting in variable capping efficiency and reproducibility (Henderson et al., 2021, Kocmik et al., 2018). The 5' triphosphate of uncapped mRNA stimulates the immune response producing unwanted effects. Additionally, use of the m7GpppG cap analogue can produce reverse capped mRNA as both guanosine residues of the Cap (m7GpppG) have a 3'-OH group and RNA polymerisation may start from either guanosine residue of this cap analogue. This can yield up to half of the mRNA accommodating the cap structure in the undesired direction which inhibits the mRNA recognition by eIF4e and binding with the cap binding complex, subsequently resulting in poor translation. Additionally, the presence of a reverse cap appears to exert an inhibitory effect on the translation process (Ely et al., 2021, Kocmik et al., 2018).

To address the limitations of earlier cap structure, second-generation cap analogues known as Anti-Reverse Cap Analogues (ARCAs) were developed. These analogues are modified at the 3'-OH group of the m7GpppG structure, replacing it with either a 3'-O-methyl group (m7(3'-O-methyl)GpppG) or a 3'-deoxy group (m7(3'-deoxy)GpppG) (Stepinski et al., 2001) (Figure 1.6). This modification prevents the elongation of the transcript at the 3'-O-methyl or 3'-deoxy group, thus avoiding the incorporation of the ARCA analogue in the reverse orientation (Stepinski et al., 2001). Despite this advancement, ARCA cap analogues are limited to producing only Cap 0 mRNA. Additionally, because ARCA lacks the 2'-O-methylation found in Cap 1 and Cap 2, the stability of ARCA mRNA is reduced compared to mRNA with 2'-O-methylation, making it more susceptible to degradation by exonucleases (Kocmik et al., 2018, Picard-Jean et al., 2018).

TriLink Biotechnologies uses third-generation cap analogues, known as CleanCap®, which mimic the natural Cap 1 and Cap 2 structures. These CleanCap® analogues facilitate the co-transcriptional incorporation of the Cap 1 structure during IVT(Henderson et al., 2021). CleanCap® analogues are trinucleotides, in contrast to the dinucleotide analogues used in the first and second generations. CleanCap® analogues, such as CleanCap® AG and CleanCap®

AU, feature 2'-O-methylation on the first nucleotide. The 'AG' and 'AU' descriptors refer to the specific nucleotides incorporated into the mRNA following the cap structure. These cap structures significantly enhance capping efficiency, achieving 90–99% compared to the 60–80% efficiency observed with conventional co-transcriptional capping methods, and also exhibit reduced immune stimulation (Henderson et al., 2021, Vlatkovic et al., 2022). CleanCap® trinucleotide cap analogues may introduce chemical or structural modifications that can affect RNA polymerase binding to the DNA template, potentially reducing transcription efficiency. To overcome this, a modified T7 promoter is required in the DNA template to optimise RNA polymerase binding and ensure efficient incorporation of the cap analogues during IVT. This modified promoter is specifically designed to recognise the trinucleotide cap sequence minimizing interference with RNA polymerase binding to the cap analogue sequence (Henderson et al., 2021). Co-transcriptional capping is favoured as it reduces the number of steps in the manufacturing of IVTed mRNA, decreases purification steps, manufacturing time and loss of IVTed mRNA and is easily scalable for large scale production.

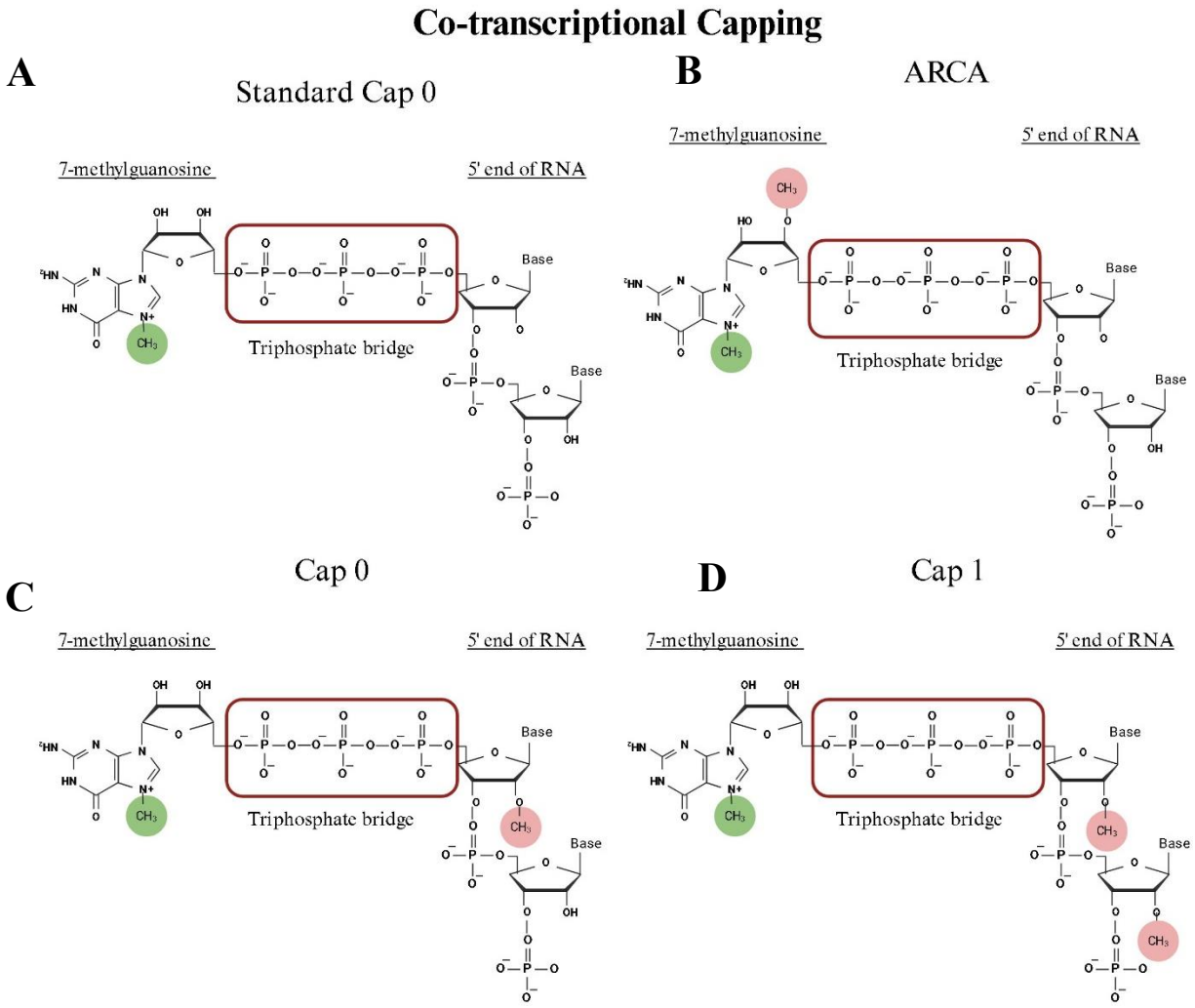

Figure 1.6: Schematic representation of co-transcriptionally capped mRNA cap structures. Chemical structures of mRNA produced co-transcriptionally during IVT transcription. (A) Standard Cap 0 structure represented by 7-methylguanosine connected to RNA by triphosphate bridge (indicated in red) facilitating translation initiation. (B) ARCA Cap characterised by the inclusion of a 3'-OH group on N7-methylguanosine, enhancing the mRNA's resistance to degradation. (C) Cap 1 mRNA characterised by addition of the 2'-O-methylation of the 2' position of the ribose ring of the first nucleotide (D) Cap 2 mRNA characterised by 2'-O-methylation of the 2' position at the ribose of the second nucleotide. Cap 1 and Cap 2 increase mRNA stability, improves translation efficiency and evade the innate immune response. Differences between the cap structures are highlighted in pink (Adapted from (Singh et al., 2024))

1.10.6 Post-transcriptional capping

Enzymatic capping is the second method used to incorporate a cap analogue into synthetic mRNA, and it involves adding the cap structure post-transcriptionally. This process involves first performing IVT in a single reaction. Following IVT, a separate enzymatic reaction is performed to further modify the nascent mRNA. This is done using Vaccinia Capping Enzyme (VCE) to add the Cap 0 structure. The VCE constitutes 5′-triphosphatase (TPase), guanylyltransferase (GTase) and methyltransferase (Mtase) activities (Kyrieleis et al., 2014) and is responsible of all three steps in the synthesis of capped IVTed mRNA (m7GpppRNA). Initially, a m7G cap is added to the 5' end of the IVTed mRNA by the VCE, resulting in Cap 0 mRNA(Martin and Moss, 1975). This Cap 0 structure features an unmodified ribose at the 2'-O position of the first nucleotide. A separate enzyme, 2'-O-methyltransferase is required to convert Cap 0 mRNA to Cap 1 mRNA (Figure 1.7). The 2'-O-methyltransferase enzyme recognises the Cap 0 structure, binds to the mRNA, and facilitates the transfer of a methyl group from S-adenosyl methionine (SAM), which acts as the methyl donor to the 2'-O position of the ribose sugar of the first nucleotide, producing the Cap 1 mRNA(Kyrieleis et al., 2014). A limitation of enzymatic capping is the requirement of IVTed and purified RNA before a separate enzymatic reaction is performed to add the cap which increases the risk of mRNA loss and raises the cost due to additional purification steps. However, the advantage of post-transcriptional enzymatic capping is that it can achieve nearly 100% capping efficiency (Xu et al., 2020).

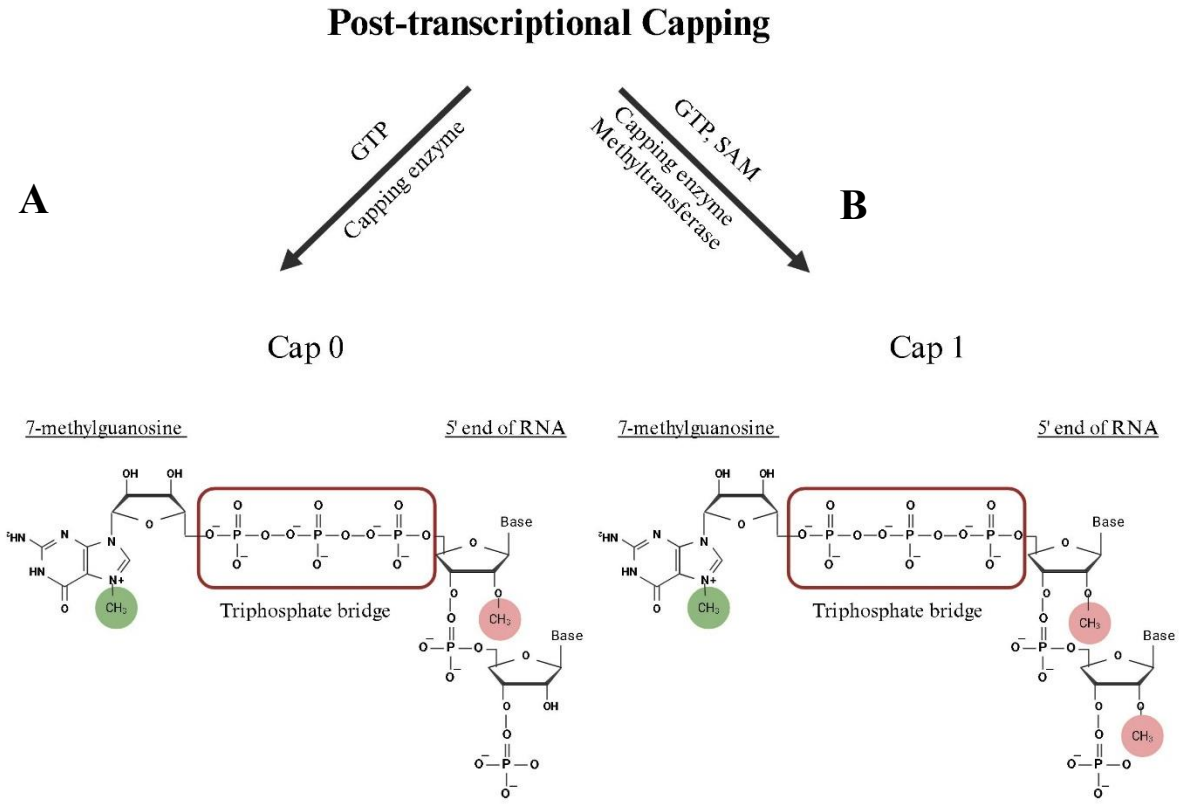

Figure 1.7: Schematic representation of mRNA cap structures produced post-transcriptionally. (A-B) Chemical structures of mRNA Cap 0 and Cap 1 produced post-transcriptionally using the Vaccinia Capping System and 2′-O-Methyltransferase. (A) IVT mRNA, Vaccinia capping enzyme, and GTP are required to produce Cap 0 mRNA. During the capping process, a single phosphate is removed from the first nucleotide of the mRNA, allowing GTP to be added, followed by methylation to form Cap 0. (B) IVT mRNA Cap 0, 2′-O-Methyltransferase, and S-adenosylmethionine (SAM) are required to produce Cap 1 mRNA. The 2′-O-Methyltransferase transfers a methyl group from SAM to the 2′-O of the ribose ring of the first nucleotide, resulting in the formation of Cap 1 mRNA (Adapted from (Singh et al., 2024))

.

1.11 Strategies to enhance mRNA stability, protein translation, and minimise immunogenicity

1.11.1 Immunogenicity of IVTed mRNA

Synthetic mRNA is inherently immune-stimulatory, triggering various innate immune pathways that lead to the production of inflammatory cytokines and inhibition of translation. Host-encoded pattern recognition receptors (PRRs) on antigen-presenting cells and other immune cells, recognise exogenous mRNA, leading to innate immune activation and inhibition of protein expression (Lee et al., 2019). PRRs are classified into endosomal and cytoplasmic. Endosomal PRRs primarily comprise Toll-like receptors (TLRs), transmembrane proteins found on the endosomal compartment or on plasma membrane of immune cells. Viral RNAs and IVTed mRNAs activate several TLRs (He et al., 2011). Cytoplasmic PRRs also known as cytoplasmic RNA sensors consist of retinoic acid-inducible gene-I-like (RIG-I-like) receptors (RLRs), melanoma differentiation-associated protein 5 (MDA5), nucleotide oligomerisation domain (NOD)-like receptors (NLRs), double stranded RNA-dependent protein kinase (PKR), oligoadenylate synthetase (OAS) receptors, and laboratory of genetics and physiology 2 (LGP2; also known as DHX58) (Chan and Jin, 2022). Non-self-molecules including synthetic mRNA are recognised by PRRs based on the molecular structures rather than any specific sequence of the nucleic acids or proteins. Ligand-bound PRRs induce type I interferons (IFN-α or IFN-β) and nuclear factor kappa B (NF-κB) signalling pathways, which modulate and direct both innate and adaptive immunity (Nelson et al., 2020).

1.11.1.1 Endosomal PRRs

TLRs are expressed on immune cells such as dendritic cells and macrophages. Of the ten known TLRs, four recognise nucleic acids, TLR7 and TLR8 recognise single-stranded RNA (ssRNA), TLR3 recognises double-stranded RNA (dsRNA), and TLR9 recognises unmethylated CpG DNA (He et al., 2011). More specifically, TLR8 responses to GU-rich ssRNA and to RNA degradation by-products whereas TLR7 has shown to be activated by AU-rich RNA strands (Forsbach et al., 2008). Activation of TLRs by RNA induces an intracellular signalling cascade resulting in the type I interferon production and pro-inflammatory cytokines (Fang et al., 2022). Upon secretion of interferons (IFNs), other inflammatory cytokines RNA degrading enzymes

such as OAS and RNase L and a variety of interferon stimulated genes (ISGs) are upregulated which inhibits translation and promotes RNA degradation (Fang et al., 2022, Anderson et al., 2011).

1.11.1.2 Cytoplasmic PRRs

RLRs, which include RIG-I and MDA5, detect dsRNAs and atypical RNA lacking a 5' cap or poly(A) sequence in the cytoplasm. This detection initiates a downstream signalling cascade involving kinases, adaptors, and transcription factors, ultimately leading to the activation of IFN. RIG-I and MDA5 are able to distinguish between self RNA and non-self RNA (Chan and Jin, 2022, Kato et al., 2008) and have substrate specificity. RIG-I detects dsRNA with minimal lengths of ~20 base pairs (bp) and these include 5′-diphosphate (5′-pp) or triphosphate (5′-ppp) dsRNA while MDA5 senses longer dsRNA molecules (normally >1000 bp) (Kato et al., 2008). NLRs are involved in regulating caspase-1 production, which is responsible for apoptosis. NLRs consists of NOD2 and NLRP3. NOD2 is crucial in sensing ssRNA whereas NLRP3 senses dsRNA resulting in the activation of IFN-I synthesis and production of proinflammatory cytokines (Kanneganti et al., 2006). Binding of IFN-I to IFN receptors of surrounding and activated cells results in the production of ISGF-3 that triggers the transcription of more than 300 ISGs, OASs, RNA-specific adenosine deaminase (ADAR), and PKR. PKR binding to dsRNAs or ssRNA containing an exposed 5′-triphosphate, leads to the activation of NF-κB-mediated apoptosis. Activation of OAS by binding to dsRNA activates RNase L and activated RNase L leads to degradation of cellular RNAs, additionally it causes global translational arrest (Nallagatla and Bevilacqua, 2008, Gil et al., 1999).

1.11.2 Chemical modification of mRNA

The reduced stability and high immunogenicity of IVTed mRNA impede its long-term therapeutic use. To address these issues and enhance translation efficacy, incorporating modified nucleosides into IVT mRNA is a widely utilised strategy. This approach improves stability, inhibits immunogenicity, and prevents degradation and clearance. Naturally RNA undergoes several types of post-transcriptional modification with hundreds of modified nucleotides identified to date. The innate immune system is complex with several receptors involved in the recognition of IVTed mRNA and modified nucleotides inhibit recognition by these receptors

(Nallagatla and Bevilacqua, 2008). By mimicking endogenous RNA modified nucleotides prevent the activation of immune system improving translation efficacy of IVT mRNA (Karikó et al., 2008). These modifications include, pseudouridine (ψ), N1-methylpseudouridine (m1ψ), 5-methoxyuridine (5moU), 5-methyluridine (m5U), 2-thiouridine (s2U), 5-methylcytidine (m5C), N1-methyladenosine (m1A) and N6-methyladenosine (m6A) (Figure 1.8). During IVT, native nucleotides are replaced with the corresponding modified nucleotide. Native nucleotides can be partially substituted however this produces heterogeneous mRNA populations, thus for therapeutic purposes substitution of 100% of the native nucleotide has become standard practice.

Use of ψ, s2U, m1ψ, 5moU and m5U is able to suppress TLR immune signalling effectively by hindering recognition (Karikó et al., 2005). Moreover, ψ, m1ψ, and s2U have been shown to limit PKR recognition and substitution of uridine with ψ protects RNA from inducing OAS and RNase L-mediated RNA cleavage (Nallagatla and Bevilacqua, 2008, Anderson et al., 2011). Use of ψ and its methylated analogue m1ψ significantly reduces immune and increase translation significantly in vitro and in vivo facilitating up to a ninefold increase in mRNA translation. Additionally, a 13-fold increase in translation was observed with m1ψ compared to other modified nucleotides (Andries et al., 2015, Anderson et al., 2011). dsRNA, a byproduct that occurs during the IVT reaction, is highly immunogenic and reported to be reduced when using ψ, m1ψ, or m5C, thereby improving the RNA purity (Mu et al., 2018). Incorporation of modified nucleotides is suggested to inhibit production of other immunogenic byproducts of IVT reactions besides dsRNA.

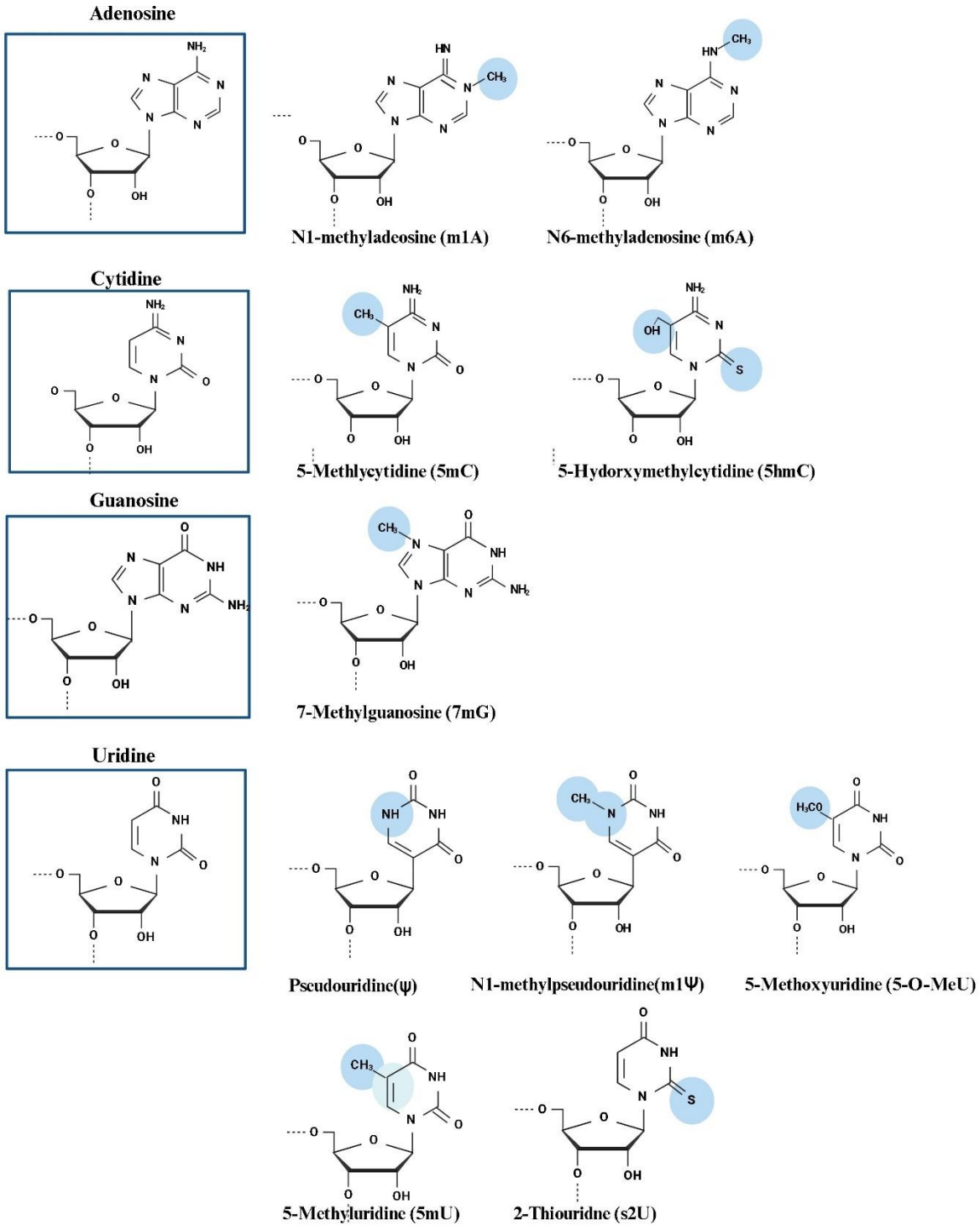

Figure 1.8: Chemical structures of modified nucleotides. Modified nucleotides commonly used during in vitro transcription (IVT) of mRNA. The chemical groups that differ from four cognate nucleotides are highlighted in blue (Adapted from (Singh et al., 2024)).

1.11.3 Purification of mRNA

After IVT, purification of the produced mRNA is necessary for the complete removal of contaminants. Besides the removal of unincorporated nucleotides (NTPs), enzymes, and buffer components, important sources of impurity include aberrant mRNAs such as short, aborted RNAs and dsRNA by-products. These impurities are highly immunostimulatory and can reduce translational efficiency, necessitating purification to produce high-quality mRNA(Milligan et al., 1987, Karikó et al., 2011). Laboratory-based purification methods such as phenol/chloroform, lithium chloride (LiCl), alcohol based precipitation, and silica columns can efficiently remove free NTPs, and other small contaminants but do not allow for the removal of truncated RNA fragments, dsRNA, or DNA (Milligan et al., 1987, Karikó et al., 2011, Baiersdörfer et al., 2019). Chromatography-based techniques have proven to be effective at removal of these impurities. Tangential flow ultrafiltration and crossflow filtration have emerged as additional purification methods that can be used in conjunction with chromatography. Removal of impurities using these techniques decreases IVTed mRNA immunogenicity and enhances stability and translation of mRNA (Edelmann et al., 2014, Baiersdörfer et al., 2019, Karikó et al., 2011).

1.12 Potential of anti-HBV DEM-based mRNA therapeutic

Epigenome modifiers used to silence HBV have mainly focused on the use of ZF-DBDs (Zhao et al., 2013, Luo et al., 2018, Xirong et al., 2014) and only recently TALE-DBDs have been used to target HBV. TALE-DBDs have several advantages over the use of ZF-DBDs (Table 1.2) increasing their application. While CRISPR-DBDs (have been extensively used in various diseases and models, their application in HBV gene therapy have been limited. Additionally, previous epigenome modifiers targeting HBV have predominantly utilised a single repressor domain, such as KRAB or DNMT. Based on the observed enhanced efficacy of epigenome modifiers (DEMs) when combining KRAB and DNMT domains, DEMs targeting HBV using TALE-DBD were developed. These TALE domains, repurposed from existing nuclease technologies and targeting the *S*, *C*, and *P* (ORFs), are fused to both KRAB and active DNMT (DNMT3a and DNMT3L) or mutant DNMT domains were also generated (Figure1.9). To create the dDEMs the KRAB domain was removed, as mutating this domain does not eliminate its ability to recruit heterochromatin-forming complexes (Murphy et al., 2016). In contrast a single amino acid mutation within the catalytic site of the DNMT3A domain is sufficient to abolish its

activity (Mlambo et al., 2018). DEMs function by depositing specific epigenetic marks on DNA, primarily through methylation, which leads to transcriptional repression of regulatory regions by recruiting heterochromatin-forming complexes. This allows for precise targeting of the epigenome. Furthermore, the KRAB domain recruits heterochromatin-forming complexes, resulting in the condensation of DNA and making it inaccessible to transcription factors and DNA polymerase. An anti-HBV S DEM expressed from plasmid DNA was able to show reduced serum concentration of HBsAg by 90%, intrahepatic viral RNA by 98% and circulating viral particle equivalents (VPEs) by 76% in vivo. A concomitant 8-fold increase in methylation of CpG II was also observed (unpublished work by Dr Kristie Bloom). To further improve the transcriptional repression of existing anti-HBV DEMs, this research assessed the feasibility of expressing DEMs targeting HBV from the mRNA platform.

Transcriptional repressors function by binding to target DNA sequences, which prevents the recruitment of transcription machinery and blocks the binding of RNA polymerases and activators. This inhibition alters DNA conformation, making it less accessible and leading to reduced transcription and viral load (Payankaulam et al., 2010, Lewis, 1996). However, the prolonged translation of epigenome modifiers from DNA constructs can lead to nonspecific off-target effects, posing a significant challenge for therapeutic applications. Transient expression of epigenome modifiers from IVTed mRNA addresses this issue (Sahin et al., 2014). Since IVTed mRNA is present only for a short duration, it minimises the risk of nonspecific off-target effects. This transient expression enables faster protein production, more precise epigenome editing, and easy scalability. Although IVTed mRNA encoding epigenome modifiers has shown potential in transcriptional repression and in generating mouse models (Nuñez et al., 2021, Horii et al., 2020), its therapeutic application targeting HBV has been limited. Therefore, this thesis explores the benefits of using IVTed mRNA for expressing epigenome modifiers, particularly for HBV therapy.

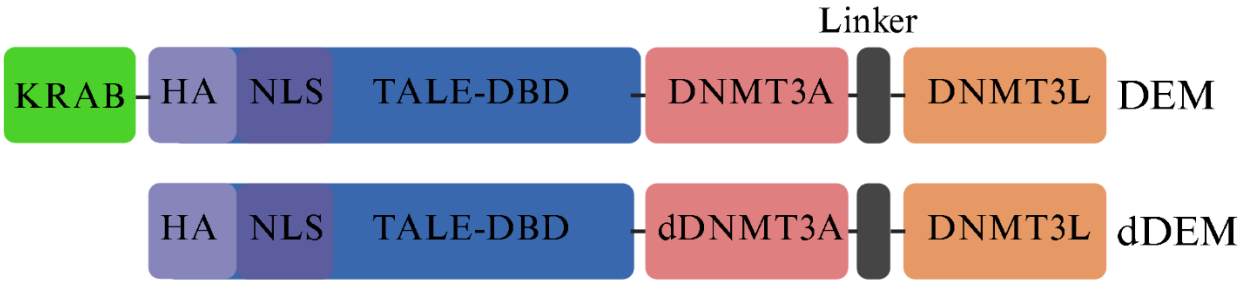

Figure 1.9: Schematic representation of active and inactive DEMs. Structure of active and control DEMs constructs depicting a TALE DNA-binding domain comprising hemagglutinin tag (HA), nuclear location signal (NLS) fused to active DNMT and KRAB domains (top) or fused to inactive DNMT domain(bottom). The DNMT domain is composed of catalytically active (DNMT3A) or mutant (dDNMT3A) linked to DNMT3L which enhances the catalytic activity of the DNMTs (Modified and adapted from (Mlambo et al., 2018)).

1.13 Aims and objectives

Current treatments do not impact nor completely remove the cccDNA reservoir responsible for the persistence of HBV. Gene editing technologies target cccDNA directly and offer the possibility of eliminating this reservoir. However, a major concern with the use of designer nucleases is the potential for off-target cleavage resulting in genotoxicity. Altering or modifying cccDNA epigenetically by *de novo* methylation using DEMs is a safer and less genotoxic alternative to designer nucleases.

The research aimed to evaluate anti-HBV DEMs expressed from mRNA platform to achieve permanent silencing of viral gene expression. This involved using a DEM consisting of repressor domains (KRAB and DNMT) combined with the TALE-DBD to facilitate targeted methylation of HBV CpG islands and the formation of heterochromatin complexes at the *S*, *C*, and *P* ORFs.

Objectives of this study were:

1. Generation of anti-HBV DEM mRNA expressing vectors
2. In vitro transcription of active and dead DEM mRNA
3. In vitro assessment of anti-HBV DEM RNA
4. Formulation of anti-HBV RNA DEM into liposomes and hepatotropic delivery in vivo
5. Assessment and evaluation of lipoplexed DEM RNA safety in mice
6. In vivo assessment of anti-HBV DEM efficacy
7. On- and off-target methylation analysis using MassArray technology and RNA sequencing

Chapter 2

2. Methods and Materials

2.1 Construction of an RNA expression platform (pmRNA) encoding transgene sequences

2.1.1 Construction of anti-HBV DEM mRNA expression vectors

Existing anti-HBV DNA DEMs utilise site-specific TALE-DBDs, repurposed from existing TALEN technology due to their high target specificity (Bloom et al., 2013). These DEMs target the *S*, *C*, and *P* ORFs of HBV fused to different epigenome effector domains, producing both control(dead) and active pCMV-DEMs (pCMV-dDEM and pCMV-DEM). Active DNA DEMs consist of TALE-DBD, KRAB and DNMT (DNMT3A + DNMT3L) domains, while inactive control DNA dDEMs consist of TALE-DBD and dDNMT (mutant DNMT3A + DNMT3L) (Figure 1.9). All the plasmids used in this study is described in (Appendix Table 5.1). All constructs were under the control of a CMV promoter (unpublished work by Dr Kristie Bloom). The TALE DBDs were designed as left and right pair monomers, with the right monomer (denoted as R) binding to the antisense strand and the left monomer (denoted as L) binding to the sense strand of designated target sequence (Bloom et al., 2013). The DEM mRNA expression plasmids were adapted from these CMV-driven DEM vectors. To generate active and inactive anti-HBV DEM mRNA expression vectors, the various DEM sequences were cloned into a pmRNA vector (pmRNA-pA), (Figure 2.1). This RNA expression vector contains a T7 promoter, 5' UTR (with Kozak sequence) and 3' UTR (with poly (A) tract). These are all the essential elements required for IVT and intracellular translation.

The six active and inactive pCMV-DEMs plasmids were first, individually double digested with *Xba*I and *Bam*HI in the first set of separate reactions yielding a 2643 bp fragment representing the KRAB and TALE domain-encoding sequences for the active DEMs and a 2352 bp fragment representing the TALE domain-encoding sequence for the inactive dDEMs. In a second separate set of reactions, the inactive and active pCMV-DEMs plasmids were individually double digested with *Bam*HI and *Apa*I to excise the active and inactive DNMT and dDNMT domain-

encoding sequences yielding a 1642 bp fragment each. In a third reaction, pmRNA-pA was doubled digested with *Xba*I and *Apa*I to allow for ligation of inserts, producing 3737 bp fragment representing the RNA backbone. The digestion reactions were set up as follows, 1 µg of plasmid DNA, 1× buffer, 1 U of each respective enzyme, made to a total volume of 20 µl using double distilled water (ddH_2O) and incubated at 37 °C for 2 hours. Digestion reactions were resolved on a 1 % agarose gel containing ethidium bromide (0.5 µg/ml) (Appendix 5.1) and imaged using Omega Fluor™ Gel Documentation System (Gel Company Inc., CA, USA). The expected bands were excised from the agarose gel and purified using the Qiagen MinElute Gel Extraction kit according to the manufacturer's instructions (Qiagen, Hilden, Germany) (Appendix 5.2). The backbone DNA was treated with alkaline phosphatase to remove 5' phosphates, 1 U of FastAP thermosensitive alkaline phosphatase (Thermo Scientific, CA, USA) according to the manufacturer's instructions and incubated at 37 °C for 30 minutes.

The KRAB and TALE domain-encoding sequences along with the active DNMT domain-encoding sequence were subsequently ligated into pmRNA-pA in a 3-way ligation reaction producing the active pmRNA-DEMs. Whereas the TALE-encoding and inactive dDNMT domain-encoding sequences were ligated into pmRNA-pA in a 3-way ligation reaction producing inactive pmRNA-dDEMs. Ligation reactions were set up as follows, 1× ligation buffer, 2 U of T4 DNA ligase (Thermo Scientific, CA, USA) and ddH_2O to a final volume of 20 µl and was incubated at 16 °C overnight. The ligation mixes for each respective active and inactive DEMs were used to transform 100 µl of competent bacteria (Appendix 5.3) and were plated on Luria-Bertani agar plates containing ampicillin (100 µg/ml). Single colonies were selected and inoculated in Luria-Bertani medium supplemented with ampicillin (100 µg/ml), and cultures were incubated overnight at 37 °C. Plasmid DNA was extracted from bacterial cultures using EconoSpin™ All-in-One Spin Columns according to the manufacturer's instructions (Epoch Life Sciences, MO, USA). The plasmids were screened using restriction digestion with *Xba*I and *Bam*HI to confirm the KRAB and TALE domain-encoding sequences in the case of the active DEMs and only the TALE domain-encoding sequence in the case of the inactive pmRNA-DEMs. Restriction digestion using *Bam*HI and *Apa*I was used to confirm presence of either the active or inactive DNMT domain-encoding sequence. Restriction digestion with *Xba*I and *Nhe*I was used to confirm the presence of KRAB domain in the active pmRNA-DEMs. Positive clones for the respective active pmRNA-DEM and inactive pmRNA-dDEM were prepared using the QIAGEN

Plasmid Maxi Kit (Qiagen, Hilden, Germany) according to the manufacturer's instructions (Appendix 5.4). Correct plasmids are hereafter referred to as active DEM (pmRNA -SR, -SL, -CR, -CL, -PR and -PL DEM) or inactive dDEM (pmRNA -SR, -SL, -CR, -CL, -PR and -PL dDEM) plasmids. The pCMV-VAX TALEN and pmRNA-DEM plasmids were digested with *Bgl*I to confirm correct TALE-DBDs. Confirmation of poly(A) track in active DNA pmRNA-DEMs was validated by standard Sanger sequencing (Inqaba Biotec, Pretoria, South Africa).

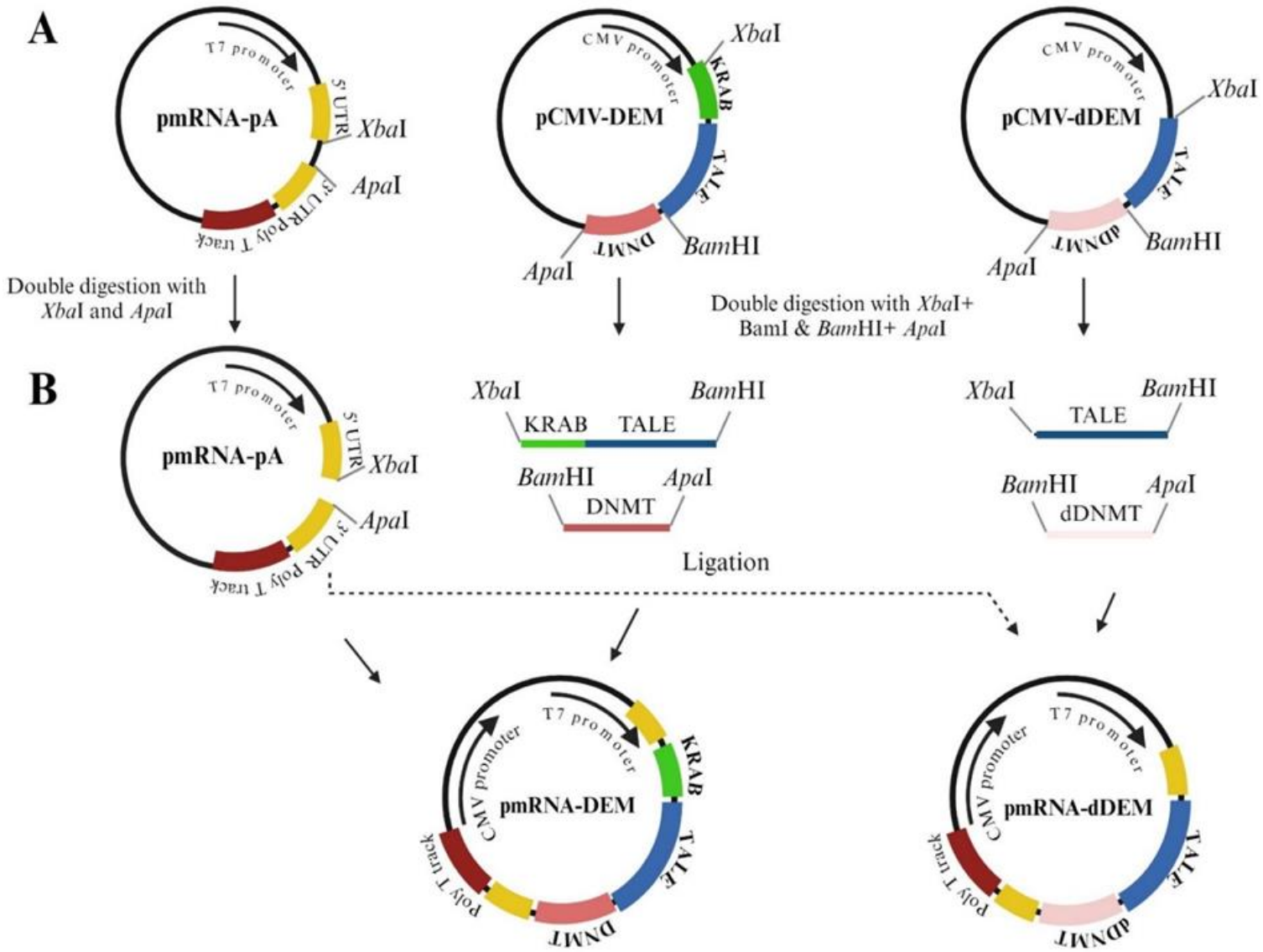
A
T7 promoter
pmRNA-pA
5' UTR
XbaI
ApaI
3' UTR Poly T track
CMV promoter
pCMV-DEM
XbaI
KRAB
TALE
DNMT
ApaI
BamHI
CMV promoter
pCMV-dDEM
XbaI
TALE
dDNMT
ApaI
BamHI
Double digestion with XbaI and ApaI
Double digestion with XbaI+ BamI & BamHI+ ApaI
B
T7 promoter
pmRNA-pA
5' UTR
XbaI
ApaI
3' UTR Poly T track
XbaI
BamHI
KRAB
TALE
BamHI
ApaI
DNMT
XbaI
BamHI
TALE
BamHI
ApaI
dDNMT
Ligation
T7 promoter
CMV promoter
pmRNA-DEM
KRAB
TALE
DNMT
Poly T track
T7 promoter
CMV promoter
pmRNA-dDEM
TALE
dDNMT
Poly T track

Figure 2.1: A schematic illustrating the cloning strategy used to generate active and inactive pmRNA-DEM plasmids. (A) Restriction digestion; the pmRNA-pA vector was digested with *Xba*I and *Apa*I to generate compatible ends for the ligation of the transgene sequences. In a second reaction active and inactive pCMV-DEM plasmids (pCMV-dDEM and pCMV-DEM) were individually double digested with *Xba*I and *Bam*HI to produce a fragment containing the KRAB and TALE domain-encoding sequences for active DEMs, and TALE domain-encoding fragment for the inactive dDEMs. In a third reaction, pCMV-DEM plasmids were double digested with *Bam*HI and *Apa*I to yield fragments containing the active DNMT and dDNMT domains. (B) Ligation, the KRAB and TALE domains along with active DNMT domains were ligated into pmRNA-pA to generate active pmRNA-DEMs, while the TALE and inactive dDNMT domains were ligated into pmRNA-pA to produce inactive pmRNA-dDEM

2.1.2 Construction of pmRNA-GFP reporter plasmid for optimisation studies

The pCMV-GFP plasmid was double digested with *Xba*I and *Apa*I to remove the eGFP-encoding sequence. The digestion reaction was set up as follows, 1 µg of plasmid DNA, 1× buffer, 1 U each respective enzyme, made to a total volume of 20 µl using ddH_2O and incubated at 37 °C for 2 hours. The digestion reaction was resolved on a 1 % agarose gel containing ethidium bromide (0.5 µg/ml) (Appendix 5.1) and imaged using Omega Fluor™ Gel Documentation System (Gel Company Inc., CA, USA). The expected fragment size of 727 bp was excised, purified using the Qiagen MinElute Gel Extraction kit (Qiagen, Hilden, Germany) (Appendix 5.2) and ligated into the pmRNA-pA expression vector digested with *Xba*I and *Apa*I (Section 2.1.1). The ligation mixes were used to transform 100 µl of competent cells (Appendix 5.3), and the transformed bacteria were plated on Luria-Bertani agar plates containing ampicillin (100 µg/ml) and incubated overnight at 37 °C. Single colonies were selected and inoculated in Luria-Bertani medium supplemented with ampicillin (100 µg/ml), and were incubated overnight at 37 °C. Plasmid DNA was extracted from bacterial cultures using EconoSpin™ All-in-One Spin Columns (Epoch Life Sciences, MO, USA) according to the manufacturer's instructions. The plasmid DNA was screened by enzyme restriction digestion with *Alw*44l and *Ava*II, and positive clone was prepared using the QIAGEN Plasmid Maxi Kit (Qiagen, Hilden, Germany) according to the manufacturer's instructions (Appendix 5.4). The correct plasmid is hereafter referred to as pmRNA-eGFP (Figure 2.2).

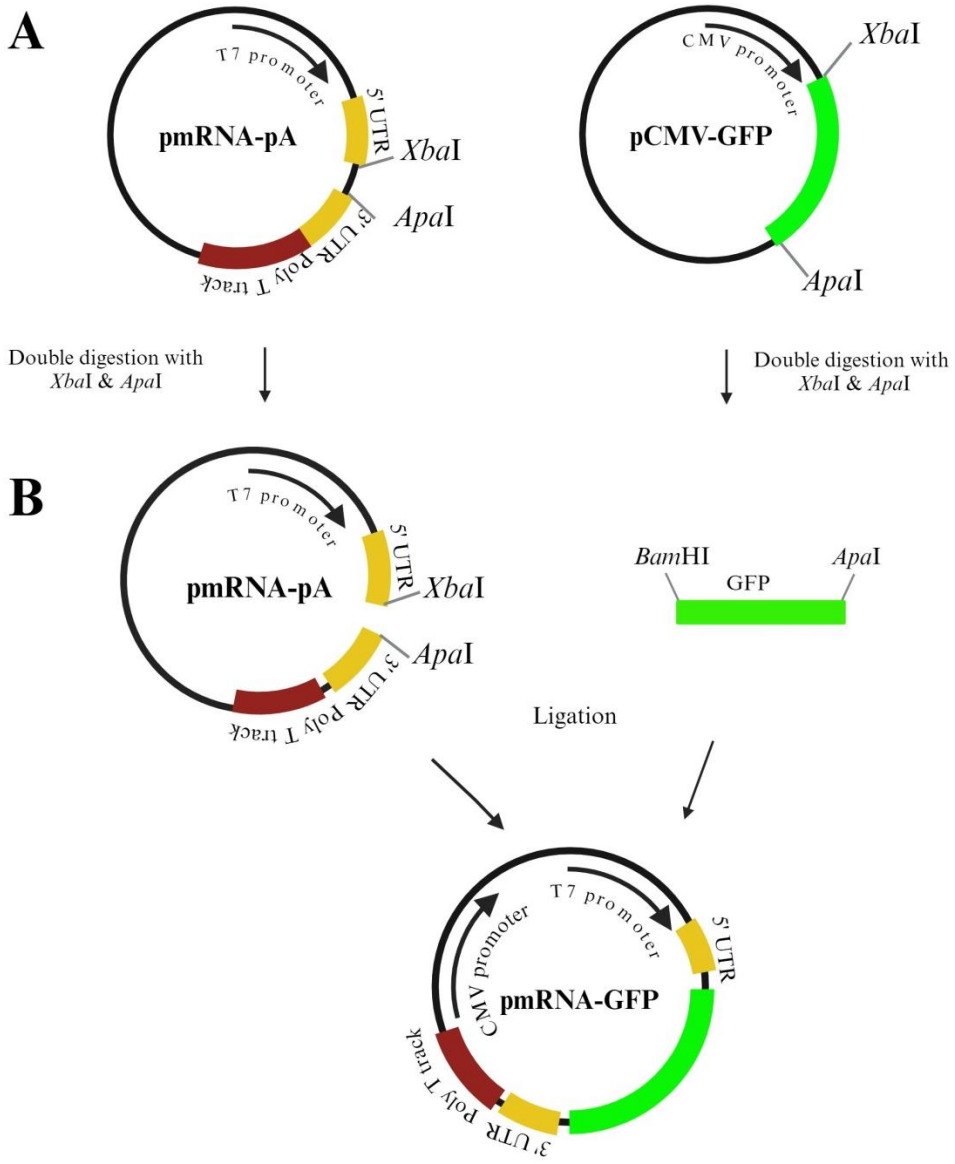

Figure 2.2: Schematic illustrating the cloning strategy used to generate pmRNA-GFP. (A) Restriction digestion; in the first reaction, the pmRNA-pA vector was double-digested with *Xba*I and *Apa*I to generate compatible ends for the ligation of the eGFP transgene. Simultaneously, in a second reaction pCMV-eGFP plasmid was double-digested with *Xba*I and *Apa*I, resulting in the excision of a fragment containing the eGFP-encoding sequence. (B) Ligation; the eGFP fragment was ligated into the prepared pmRNA-pA producing pmRNA-eGFP plasmid.

2.1.3 Construction of pmRNA vectors expressing active anti-HBV DEMs lacking KRAB domain

Active pmRNA-DEMs without the KRAB domain sequence was generated and termed pmRNA-DEMΔKRAB (pmRNA- SR, CR and PL DEMΔKRAB) (Figure 2.3). pVAX-CMV-SR, -CR and -PL TALENs were double digested with *Xba*I and *Bam*HI to excise the TALE sequence without the KRAB domain-encoding sequence. The digestion reaction was set up as follows, 1 µg of plasmid DNA, 1× buffer, 1 U each respective enzyme, made to a total volume of 20 µl using ddH_2O and incubated at 37 °C for 2 hours. The restriction digestion reactions were resolved on a 1 % agarose gel containing ethidium bromide (0.5 µg/ml). The expected fragment size of 2346 bp representing the TALE sequence was extracted, purified using the Qiagen MinElute Gel Extraction kit (Qiagen, Hilden, Germany) (Appendix 5.2) and ligated into the pmRNA-pA backbone (Section 2.1.1) in a three-way ligation reaction along with the active DNMT domain-encoding purified sequence (Section 2.1.1). The ligation mixes were used to transform 100 µl of competent cells (Appendix 5.3) and plated on Luria-Bertani agar plates containing ampicillin (100µg/ml) and incubated overnight at 37 °C. Single colonies were selected and inoculated in Luria-Bertani medium supplemented with ampicillin (100 µg/ml), cultures were incubated overnight at 37 °C. Plasmid DNA was extracted from bacterial cultures using EconoSpin™ All-in-One Spin Columns (Epoch Life Sciences, MO, USA) according to the manufacturer's instructions. The plasmids DNA were screened by enzyme restriction digestion. Double digestion using *Xba*I & *Bam*HI was used to confirm TALE domain-encoding sequences while digestion with *Bam*HI & *Apa*I was used to confirm presence of active DNMT domain-encoding sequence and digestion with *Xba*I and *Nhe*I was used to confirm the absence of KRAB domain. Positive clones were prepared using the QIAGEN Plasmid Maxi Kit (Qiagen, Hilden, Germany) according to the manufacturer's instructions (Appendix 5.4).

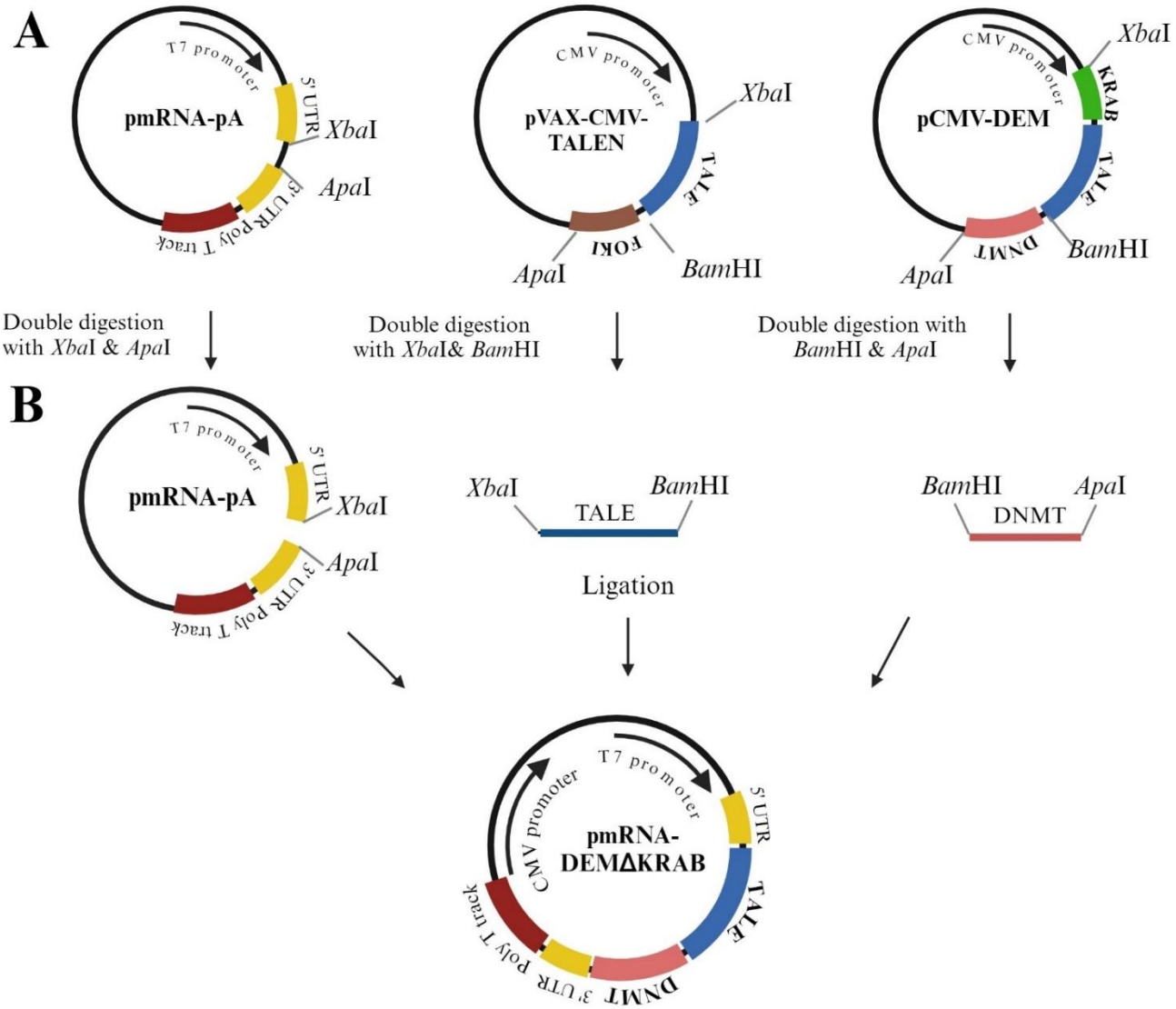

Figure 2.3: A schematic illustrating the cloning strategy used to generate active pmRNA-DEMΔKRAB plasmids. (A) Restriction digestion; in the first reaction, the pmRNA-pA vector was double digested with *Xba*I and *Apa*I to generate compatible ends for the insertion of the transgene sequences. In a second reaction inactive pVAX-CMV-TALENs was double digested with *Xba*I and *Bam*HI to produce a fragment containing the TALE domain sequences. In a third reaction, active pCMV-DEM plasmids were digested with *Bam*HI and *Apa*I to yield a fragment containing the active DNMT B) Ligation; the transgene fragments were ligated into the prepared pmRNA-pA backbone, producing pmRNA-DEMΔKRAB.

2.2 In Vitro Synthesis of mRNA from DNA templates

2.2.1 Production of in vitro transcribed therapeutic and reporter mRNA

In preparation for IVT, 25 ug of active and inactive pmRNA-DEMs, active pmRNA-DEMsΔKRAB and pmRNA-eGFP DNA templates were linearised with 25U of *Bbs*I enzyme (New England Biolabs, NJ, USA) and 1× buffer and ddH_2O to a final volume of 200 µl and reactions were incubated overnight at 37 °C. Linearised DNA templates were purified using either phenol:chloroform or sodium acetate (NaOAc) precipitation. Purified DNA template concentration was confirmed with N80 Nanophotometer Spectrophotometer (Implen, CA, USA) and linearisation was confirmed on a 1 % agarose gel (Appendix 5.1). IVT reactions were performed using RiboMAX^{TM} Large Scale RNA Production System (Promega, WI, USA) (Appendix, Table 5.2) or TranscriptAid T7 High Yield Transcription Kit (Thermofisher Scientific, MA, USA) Appendix, Table 5.3) according to the manufacturer's instructions or New England Biolabs (NEB) individual IVT components (Appendix, Table 5.4) along with TriLink buffer (Appendix, Table 5.5). IVT reactions were incubated for 2 hours at 37 °C followed by DNase treatment at 37 °C for 15 minutes to remove residual template DNA. IVT reactions were co-transcriptionally capped with Promega Ribo m7G cap analogue (standard Cap 0), Ambion anti-reverse cap analogue (ARCA Cap 0) (New England Biolabs, NJ, USA) or TriLink CleanCap® AG (TriLink Biotechnologies, CA, USA) according to the manufacturer's instructions. For production of modified mRNAs, 100% pseudouridine (ψ) (TriLink Biotechnologies, CA, USA) was incorporated to reaction according to protocol. For polyadenylated RNA, 1× *E. coli* Poly (A) Polymerase reaction buffer, 2 µl ATP (10 mM) and 1 µl *E. coli* Poly (A) Polymerase (Thermo Scientific, CA, USA) was used. The reaction was incubated at 37 °C for 30 minutes and LiCL was used to purify and precipitate the RNA.

2.2.2 Post-transcriptional capping of IVTed mRNA

Vaccinia Capping Enzyme System (New England Biolabs, NJ, USA) was used for post-transcriptional enzymatic capping of mRNA according to the manufacturer's instructions. The capping reaction was set up using the components listed in Table 2.1. The enzymatic capping reaction was incubated at 37 °C for 30 minutes to generate Cap 0 mRNA or incubated for 1 hour

to generate Cap 1 mRNA. The synthesised mRNA was purified using NaOAc or LiCL precipitation (Appendix 5.5).

Table 2.1: Post-transcriptional capping protocol for producing Cap 0 and Cap 1 mRNA

Components	Final Volume (Cap 0)	Final Volume (Cap 1)
Denatured RNA reaction	15 µl	14 µl
10× Capping buffer	2 µl	2 µl
GTP (10 Mm)	1 µl	1 µl
SAM (2 mM)	1 µl	1 µl
Vaccinia Capping Enzyme (10 U/µl)	1 µl	1 µl
mRNA 2'-O-Methylatreansefrase (50 U/µl)	-	1 µl
Total volume	**20 µl**	**20 µl**

2.2.3 Removal of dsRNA by cellulose purification

Cellulose chromatography-based purification of synthesised RNA was carried out according to the protocol described by Baiersdörfer et al (2019) (Baiersdörfer et al., 2019). Briefly, 0.2 g of cellulose (Sigma-Aldrich, MO, USA) was washed with 1 ml of chromatography buffer (Appendix5.5) by shaking the cellulose slurry at 250 rpm room for 10 minutes at room temperature. Approximately, 700 µl of the cellulose slurry was transferred to a 0.22 µm ultracentrifuge spin column (Sigma-Aldrich, MO, USA) and centrifuged for 1 minute at 14 000 ×g. The flow-through was discarded and 500 µl of chromatography buffer was added to the column and incubated for 5 minutes at room temperature with shaking at 250 rpm. This was followed by centrifugation of the column for 1 minute at 14 000 ×g and the flow-through was discarded. One hundred and fifty micrograms of capped RNA was mixed with 500 µl of chromatography buffer, added to the column and incubated for 30 minutes at room temperature with shaking at 250 rpm. After the incubation, the column was centrifuged for 1 minute at 14 000 ×g and flow-through containing purified RNA was collected. To ensure majority of dsRNA was removed the above process was repeated. LiCL purification of the cellulose purified RNA was used to precipitate the RNA. RNA was quantified by spectrophotometry using the N80

Nanophotometer Spectrophotometer (Implen, CA, USA). RNA integrity was assessed using denaturing formaldehyde gel electrophoresis (Appendix 5.1).

2.3 Characterisation of poly(A) tail length in IVTed mRNA using 3' RACE

The presence of the poly (A) tail of IVTed mRNA was verified using a 3' RACE (Rapid Amplification of cDNA Ends) kit (Sigma-Aldrich, MO, USA). Initially, first strand cDNA synthesis was performed, approximately 1 µg of total extracted RNA or 50 ng of IVTed mRNA and ddH_2O was made up to a final volume of 11 µl. This was followed by the addition of 1 µl of the adapter primer (10 µM). This is an oligo-dT adapter primer that binds the poly (A) tail region on mRNA. All heating steps were carried out in Bio-Rad T100™ Thermal Cycler. The reaction mixture was gently mixed, centrifuged and heated at 70 °C for 10 minutes and cooled on ice for 1 min. To the reaction mixture, 2 µl of 10× PCR buffer, 2 µl of $MgCl_2$ (25 mM), 2 µl of dNTPs (10 mM) and 1 µl of 0.1 M DTT was added gently, mixed, centrifuged, and heated at 42 °C for 5 minutes. Reaction mixture was removed and 1 µl of SuperScript™ II RT added and heated to 42 °C for 50 minutes. Reaction was terminated by incubating the sample at 70 °C for 15 minutes, this was followed by addition of 1 µl of RNase H and was incubated for 20 min at 37 °C. The cDNA was then amplified by using a gene-specific DEM primer (5’ GCTTGCTGCCCCTGAGAGAGTA 3’).

The DEM specific forward primer designed to bind to the end of the DNMT3L domain before the poly(T) track and was used in conjunction with the abridged universal amplification reverse primer (AUAP). The AUAP binds to the extended cDNA to amplify in the 3' direction. The PCR reaction was prepared as follows: 12.5 µl of Taq DNA polymerase 2× Master Mix (Ampliqon, Aarhus, Denmark), 10 pmol each of forward and reverse primers, 2 µl template DNA and ddH_2O made up to a final volume of 20 µl. PCR was carried out in Bio-Rad T100™ Thermal Cycler and cycling conditions were as follows: initial denaturation at 95 °C for 2 minutes; 39 cycles of 95 °C for 15 seconds, annealing at 60 °C for 15 seconds, and extension at 72 °C for 15 seconds followed by a final elongation at 72 °C for 5 minutes and final step cooling to 4 °C. The PCR amplicons were resolved on a 1 % agarose gel containing ethidium bromide (0.5 µg/ml) (Appendix 5.1) and imaged using Omega Fluor™ Gel Documentation System (Gel Company Inc., CA, USA). PCR amplicons was purified using Qiagen MinElute Gel Extraction kit

according to the manufacturer's instructions (Qiagen, Hilden, Germany) (Appendix 5.2) and sequenced (Inqaba Biotech, South Africa).

2.3.1 Analysis of poly(A) tail length in IVTed mRNA following introduction into cultured cells

DEM mRNA was IVTed using TranscriptAid T7 High Yield Transcription Kit (Thermofisher Scientific, MA, USA) (Appendix, Table 5.2) and co-transcriptionally capped by Vaccina capping system (New England Biolabs, NJ, USA) to incorporate Cap 0 according to the manufacturer's instructions (Table 2.1). Huh7 cells were seeded twenty-four before transfection at a confluency of 70% in 6-well plate (Greiner Bio-One, Frickenhausen, Germany). Approximately 2000 ng of SR DEM mRNA was transfected using Lipofectamine™ MessengerMAX™. Three-hours after transfection, total RNA was extracted using TRIzol reagent (Appendix 5.6.1) and 3' RACE Kit (Sigma-Aldrich, MO, USA) was performed.

2.4 Characterisation of the anti-DEM mRNA in culture mammalian cells

In this study, liver-derived human hepatoma cell line Huh7, the kidney-derived human embryonic kidney cell line HEK293T, and HepG2, which is a liver cancer-derived cell line from hepatocellular carcinoma were utilised (Appendix 5.7). The HepG2.hNTCP cells are engineered to express the human NTCP receptor, while the HepG2.2.15 cells contain a stable, greater-than-genome-length HBV integrant integrated into their genome. Cells were seeded twenty-hour prior to transfection. For plasmid DNA transfections, Lipofectamine™ 3000 (Thermo Scientific, CA, USA) was used according to manufacturer's instructions and for IVTed mRNA Lipofectamine™ MessengerMAX™ (Thermo Scientific, CA, USA) was used using 1:1 ratio according to manufacturer's instructions. Transfection reactions were incubated at 37°C with 5% CO_2 for the duration of the experiment. Cells transfected with reporter GFP DNA or IVTed GFP mRNA were used to evaluate transfection efficiency. All reactions were conducted in triplicate.

2.4.1 Evaluation of Anti-HBV DEM mRNA in vitro

Huh7 cells were initially transfected with 70 ng pCH-9/3091 replication-competent plasmid DNA (Table 5.1) and this was followed by transfection of 430 ng IVTed DEM mRNA or a

control mRNA (Firefly luciferase (FLuc) mRNA). Twenty-four hours post transfection, enzyme-linked immunosorbent assay (ELISA) was conducted on supernatant of transfected cells using the Monolisa™ HBs Ag ULTRA kit (Bio-Rad, CA, USA) according to manufacturer's instructions (Appendix 5.8).

2.4.2 Detection of Anti-HBV DEM using immunofluorescence staining

For RNA experiments, Huh7 cells were transfected with 200 ng of each individual IVTed DEM mRNA and FLuc mRNA. For DNA experiments, 200 ng of each plasmid expressing various DEMs or pUC118, which served as a negative control, was transfected. Protein expression of anti-HBV DEM-encoding mRNA and plasmid DNA was determined within Huh 7 cells by immunofluorescence detection of HA tag *in vitro*. Transfection efficiency and assessment of expression of HA tag was assessed after three hours for RNA transfections and forty-eight hours for DNA transfections by analysis of GFP using EVOS FL fluorescence microscope (Thermo Fischer Scientific, CA, USA).

2.4.2.1 Immunofluorescence staining

Growth media was discarded from transfected cells and were washed with 100 µl of 1× phosphate buffered saline (PBS) (Sigma-Aldrich, MO, USA). Cells were subsequently fixed in 100 µl of chilled methanol at room temperature for 15 minutes. The methanol was discarded, and cells were washed twice with 100 µl of 1× PBS and thereafter incubated with 100 µl of 0.1% Triton-X (Sigma-Aldrich, MO, USA) in bovine serum albumin (BSA) for 10 minutes at room temperature. Triton-X was discarded, and the cells washed twice with 100 µl of 1× PBS. To block the cells, 100 µl of 1% BSA (Roche Applied Science, Mannheim, Germany) was added and incubated at room temperature for 1 hour in a humidity chamber. Thereafter, BSA was removed and thirty microlitres of mouse anti-HA primary antibody (Sigma-Aldrich, MO, USA), diluted 1:350 in 1% BSA was added to each well and incubated in a humidity chamber for a further 1 hour at room temperature. Subsequently the cells were washed twice with 200 µl of 1× PBS and incubated with 30 µl fluorescently labelled (Alexa Fluor 488) goat anti-mouse secondary antibody (Sigma-Aldrich, MO, USA), diluted 1:350 in 1% BSA and incubated in the dark for 40 minutes at room temperature. Secondary antibody was removed, and cells were subsequently washed with twice with 100 µl of 1× PBS and stained with 100 µl of 1× 4, 6-

diamidine-2-phenylindole chloride (DAPI), diluted 1:1000 in × PBS for 5 minutes at room temperature. Subsequently, cells were washed twice with 100 µl of 1× PBS. FITC and DAPI filters were used to image and detect signal from the cells using an EVOS FL fluorescence microscope (Thermo Scientific, CA, USA).

2.4.3 Evaluation of IVTed reporter mRNA using a luciferase assay

Huh7 cells were transfected with 200 ng of IRES-FLuc mRNA or Luc2 mRNA co-transcriptionally capped with TriLink CleanCap® AG or post-transcriptionally capped with VCE. TriLink FLuc mRNA served as a positive control, GFP mRNA transfected cells served as the negative control. Luciferase assay was assessed twenty-four hours after transfection. Luciferase® Reporter Assay System kit (Promega, WI, USA) was used to quantify luciferase expression. Cell culture media was removed from transfected cells, and 65 µl of 1× passive lysis buffer was added each well and gently rocked at room temperature for 15 minutes. After incubation, 50 µl Luciferase Assay Reagent (LARII) was mixed with 10 µl of lysed cells in Corning® 96-well white polystyrene plate (Corning incorporated, NY, USA). Luminescence readings was measured using GloMax® Explorer Microplate reader (Promega, WI, USA)

2.4.4 Evaluation of toxicity of anti-HBV DEMs in cultured cells

For RNA experiments, Huh7 cells were transfected with 150 ng of each individual mRNA or FLuc-encoding mRNA which served as a mock transfection. Cell viability was assessed twenty-four hours after mRNA transfection. For DNA experiments, Huh7 cells were co-transfected with 50 ng pCH-9/3091 replication-competent plasmid DNA and 150 ng of each plasmid expressing various DEMs or pUC118, which served as a negative control. Cell viability was assessed forty-eight hours after transfection. Cells receiving no DEM mRNA or DEM DNA were used as the untransfected control and cells receiving 25% DMSO served as positive control.

2.4.4.1 Cell viability assessment using the MTT Assay

Cell viability was determined using a methyl-thiazolyl-tetrazolium (MTT) assay. Thirty minutes before the addition of MTT solution, 25 µl of media was removed and replaced with 25 µl of dimethyl sulphoxide (DMSO) in the positive control and incubated at 37 °C. After the thirty minute incubation, 20 µl of MTT solution (5 mg/mL) in 1× PBS was added to each well, mixed

and incubated for one hour at 37 °C. Cell growth medium was gently aspirated, and the purple formazan by-product was re-suspended in 200 µl of DMSO by aspirating up and down gently and incubated at room temperature for approximately 5 minutes before measuring the optical density of the samples at 570 and 650 nm using the iMark™ Microplate Reader (Bio-Rad, CA, USA).

2.5 Construction of mRNA expression plasmid pT7-(AG) DEM 4×S

2.5.1 Design of pT7-(AG) RNA expression platform

The pT7-(AG) vector has several aspects that have been changed from the pmRNA expression platform such as inclusion of a more stable regulatory 5' and 3' UTRs, 120 poly (T) track and inclusion of four stop codons at the end of the DEM transgene. Four micrograms of pT7-(AG) backbone were double digested with *Nde*I and *Esp*3I with 4 U of each respective enzymes, 1× rCutSmart™ buffer and ddH_2O to a final volume of 80 µl and incubated overnight at 37 °C. The digestion reaction was subsequently resolved on a 1 % agarose gel containing ethidium bromide (0.5 µg/ml) (Appendix 5.1). The pT7-(AG) backbone represented by the 3133 bp fragment was excised from the gel and purified using the MinElute™ Gel Extraction Kit (Qiagen, Hilden, Germany) according to the manufacturer's instructions (Appendix 5.2). The concentration and purity were assessed by spectrophotometry. The backbone DNA was treated with alkaline phosphatase to remove 5' phosphates, 1 U of FastAP thermosensitive alkaline phosphatase (Thermo Scientific, CA, USA) was added and incubated at 37 °C for 30 minutes according to the manufacturer's instructions.

2.5.1.1 Design of the insert sequence

The insert sequence (ECS-fragment) was designed to include (i) the 5' UTR of pT7-(AG) with a *Nde*I restriction site upstream to allow for convenient cloning of the insert fragment into the pT7-(AG) backbone, (ii) *Xho*I, *Apa*I, *Bam*HI restriction sites, that will be used for the insertion of DEM-encoding sequences, and (iii) 4 consecutive stop codons. The 3' end of the ECS-fragment was designed to include the type IIs restriction enzyme site *Bsa*I downstream of the *Bam*HI. The *Bsa*I site was included so that digestion with *Bsa*I would generate an overhang complementary to the *Esp*3I overhang in the pT7-(AG) backbone (Figure 2.4). The ECS-fragment was synthesised and cloned into pUC57 mini plasmid (GenScript, NJ, USA). Approximately, 4 µg of pUC57-

ECS plasmid DNA was double digested with *Nde*I and *Bsa*I with 4 U of each respective enzymes, 1× buffer and ddH_2O to a final volume of 80 µl and incubated overnight at 37 °C. The digestion reaction was resolved on a 1 % agarose gel containing ethidium bromide (0.5 µg/ml). The ECS-fragment represented by the 497 bp fragment was excised from the agarose gel and purified using the MinElute™ Gel Extraction Kit (Qiagen, Hilden, Germany) (Appendix 5.2). The concentration and purity of the extracted DNA was assessed by N80 Nanophotometer Spectrophotometer (Implen, CA, USA).

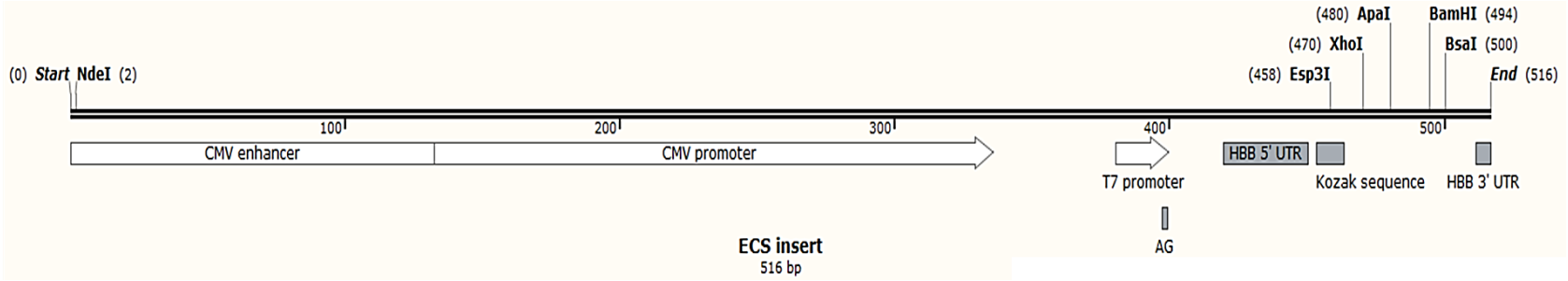

Figure 2.4: Design of the ECS-Fragment for pT7-(AG) Cloning. The ECS-fragment was engineered with several key features: A 5' UTR and an *Nde*I site for easy insertion into the pT7-(AG) backbone, multiple restriction sites (*Xho*I, *Apa*I, *Bam*HI) for integrating DEM-encoding sequences, 4 consecutive stop codons and a *Bsa*I site downstream of *Bam*HI to generate an overhang complementary to the *Esp*3I overhang in the pT7-(AG) vector.

2.5.1.2 Subcloning of pT7(AG)-ECS 4×S plasmid

Construction of pT7(AG)-ECS 4×S is illustrated in Figure 2.5. The ECS-fragment was subcloned into AP treated pT7-(AG) backbone. Ligation reactions were used to transform chemically competent *E. coli* (Thermo Scientific, CA, USA) and plated on 1× ampicillin plates. Single colonies were selected and inoculated in Luria-Bertani media supplemented with 100 µg/ml ampicillin and cultured at 37°C in a shaking incubator overnight (Appendix 5.3). Plasmid DNA was extracted from bacterial cultures using Econospin™ All-in-One Mini Spin Columns (Epoch Life Science, TX, USA) according to the manufacturer's instructions. The purified plasmids were screened by restriction enzyme digestion. Positive clones were selected and prepared on a large scale using the QIAGEN Plasmid Maxi Kit (Qiagen, Hilden, Germany) according to the manufacturer's instructions (Appendix 5.4). pT7(AG)-ECS 4×S was double digested with *Apa*I and *Ava*II, *Ban*II and *Xho*I, *Bgl*I and *Xho*I, and *Nde*I and *Xho*I to confirm the correct plasmid. The pT7(AG)-ECS 4×S plasmid serves as the mRNA expression backbone and contains the necessary restriction sites for cloning DEM transgene sequences.

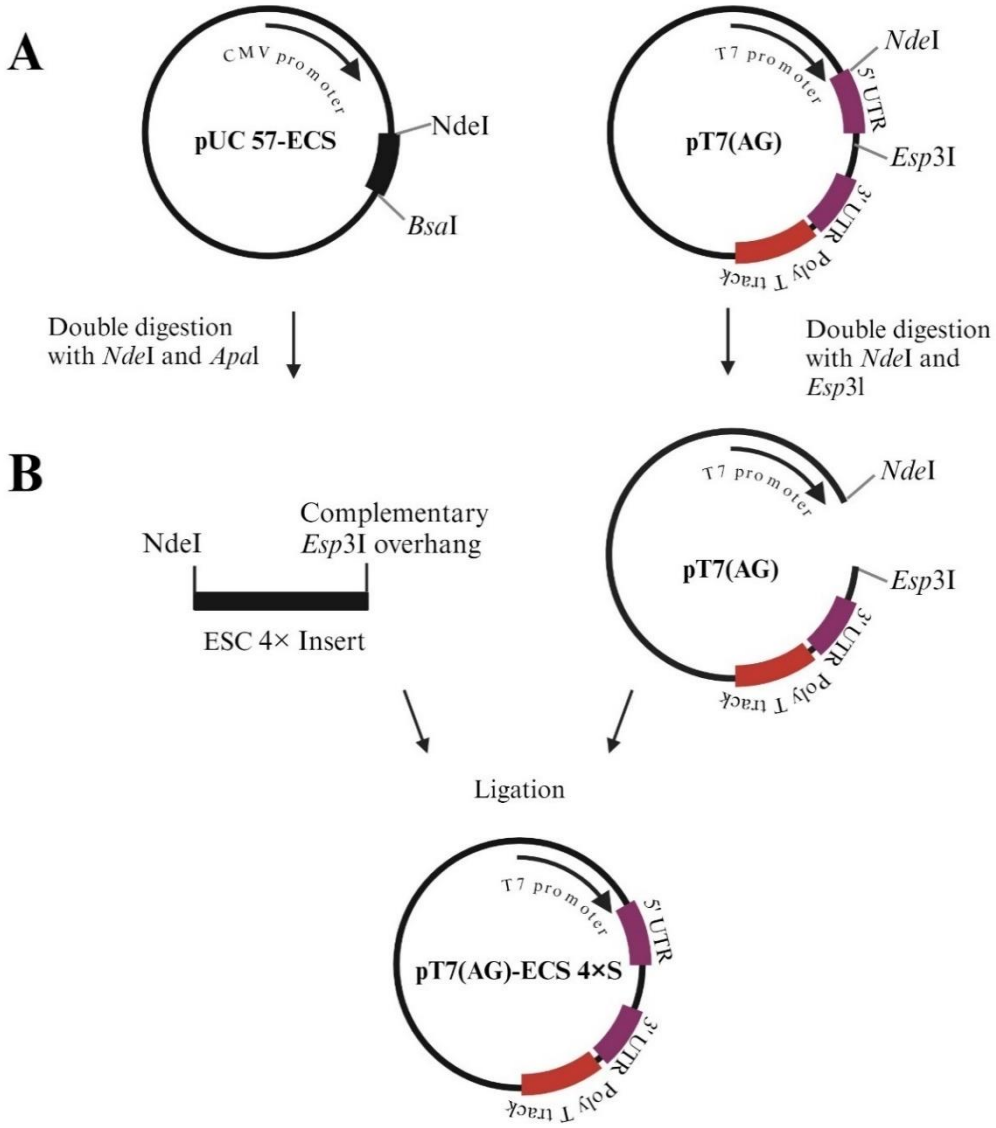

Figure 2.5: A schematic illustrating subcloning strategy of pT7(AG)-ECS 4×S. (A) Restriction digestion; in the first reaction, the pT7-(AG) backbone was double digested with *Nde*I and *Bsa*I to generate compatible ends for insertion of transgene sequence. In the second reaction, the pUC57-ESC was double digested with *Nde*I and *Esp*3I to yield ESC-insert fragment containing complementary end to pT7-(AG) backbone. (B) Ligation; The ECS-insert fragment was ligated into the prepared pT7-(AG) backbone, resulting in the formation of the pT7(AG)-ECS 4×S plasmid.

2.5.1.3 Construction of pT7(AG)-DEM 4×S plasmids

pT7(AG)-ECS 4×S was double digested with *Esp*3I and *Apa*I. The digestion reaction was set up as follows, 1 µg of plasmid DNA, 1× buffer, 1 U each respective enzyme, made to a total volume of 20 µl using ddH_2O and incubated at 37 °C for 2 hours. The digestion reaction was subsequently resolved on a 1 % agarose gel containing ethidium bromide (0.5 µg/ml) (Appendix 5.1). The pT7(AG)-ECS 4×S backbone represented by the 3610 bp fragment was excised from the gel and purified using the MinElute™ Gel Extraction Kit (Qiagen, Hilden, Germany) (Appendix 5.2). The recovered backbone DNA was alkaline phosphatase treated according to the manufacturer's instructions. The pmRNA-SR, SL, -CR, -CL, -PR and -PL DEM plasmids were double digested with *Nco*I and *Xho*I and this excised a 680 bp consisting of the HA-KRAB-TALE (TALE 362 bp)-encoded sequence. Since the *Xho*l restriction site is within the TALE-DBD, a section of the TALE is approximately 362 bp is excised along with HA-KRAB when double digested with *Nco*I and *Xho*I. The remaining TALE-DNMT sequence was excised by double digestion with *Xho*I and *Apa*I and yields a 3640 bp fragment. The digestion reactions were resolved on an agarose gel, excised and gel purified using the MinElute™ Gel Extraction Kit (Qiagen, Hilden, Germany) (Appendix 5.2). The purified inserts (HA-KRAB-TALE and TALE-DNMT) were cloned into pT7(AG)-ECS 4×S producing pT7(AG)-SR, -SL, -CR, -CL, -PR and -PL DEM 4×S (Figure 2.6). Positive clones were selected based on screening with *Ban*II, *Pvu*II and *Xba*I and *Nhe*I to confirm the correct plasmids and prepared on large scale (Appendix 5.5).

2.5.1.4 Construction of pT7(AG)-DEMΔKRAB 4×S plasmids

Active pT7(AG)-DEM 4×S vectors without the KRAB domain sequence were generated and termed pT7(AG)- SR, -SL and -PL DEMΔKRAB 4×S plasmids (Figure 2.6). pT7(AG)-ECS 4×S was double digested with *Esp*3I and *Apa*I and served as the backbone and used for a three-way-ligation. pmRNA -SR, -SL and -PL DEMΔKRAB plasmids were double digested with *Nco*I and *Xho*I to excise HA eiptope-TALE-encoded sequences without the KRAB domain. Active pmRNA-DEMs were digest with *Xho*I and *Apa*I to extract remaining TALE sequence and DNMT domain-encoding sequence. The digestion reaction was set up as follows, 1 µg of plasmid DNA, 1× buffer, 1 U each respective enzyme, made to a total volume of 20 µl using ddH_2O and incubated at 37 °C for 2 hours. The restriction digestion reactions were resolved on a

1 % agarose gel containing ethidium bromide (0.5 µg/ml) (Appendix 5.1). The expected band size of 380 bp for the HA-TALE (TALE 362bp)-encoded sequence, 3640 bp for remaining TALE-DNMT-encoded sequence, sequences were extracted and purified using the Qiagen MinElute Gel Extraction kit (Qiagen, Hilden, Germany) (Appendix 5.2) and ligated into pT7(AG)-ECS 4×S in a three-way ligation. Positive clones were selected based on screening by restriction digestion using *Ban*II, *Pvu*II and *Xba*I and *Nhe*I to confirm the plasmids and prepared on large scale using the QIAGEN Plasmid Maxi Kit (Qiagen, Hilden, Germany) according to the manufacturer's instructions (Appendix 5.4).

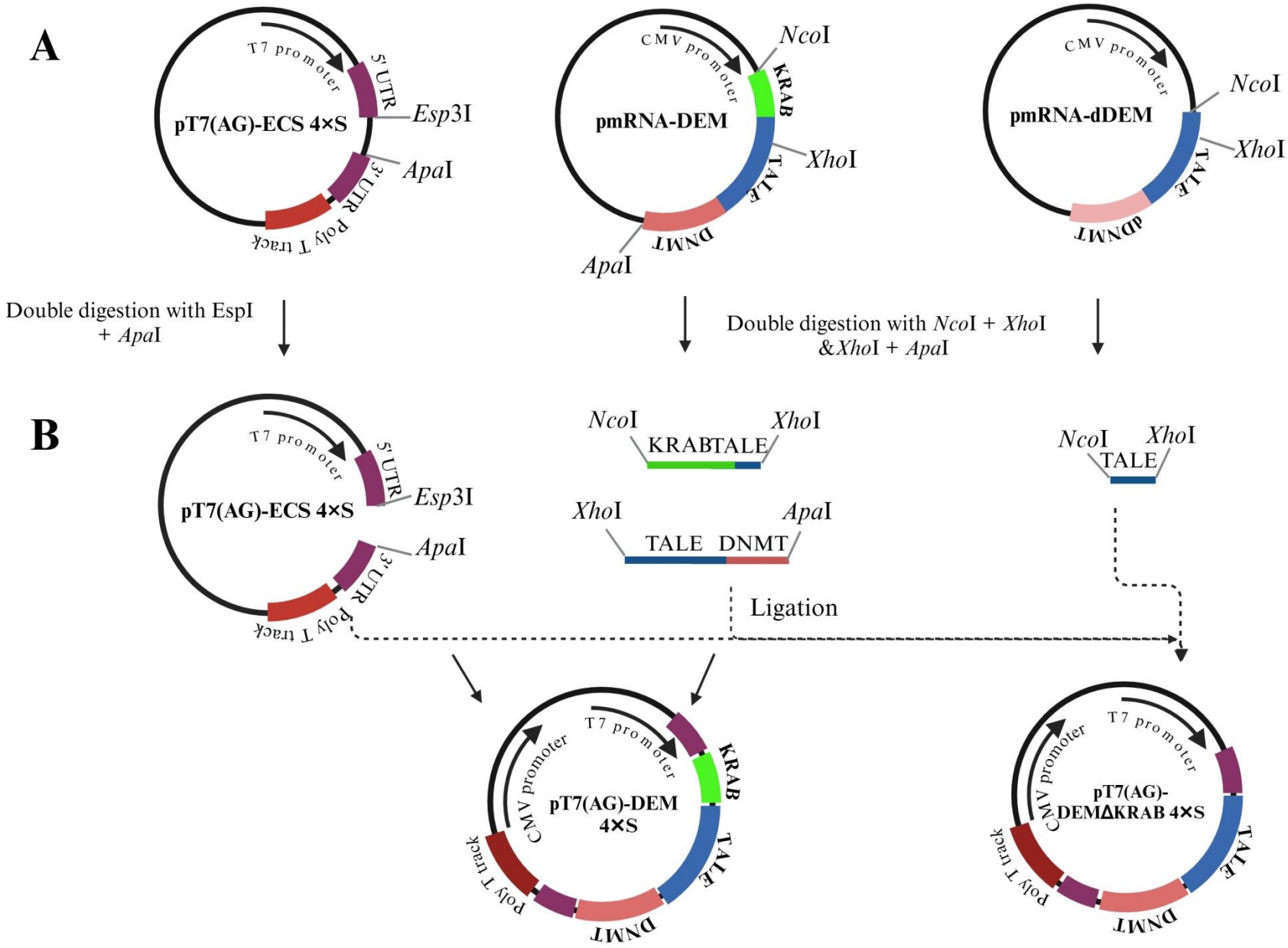
A
T7 promoter
5' UTR
pT7(AG)-ECS 4×S
Esp3I
ApaI
3' UTR
Poly T track
CMV promoter
NcoI
KRAB
pmRNA-DEM
XhoI
TALE
DNMT
ApaI
CMV promoter
pmRNA-dDEM
NcoI
XhoI
TALE
dDNMT
Double digestion with EspI + ApaI
Double digestion with NcoI + XhoI &XhoI + ApaI
B
T7 promoter
5' UTR
pT7(AG)-ECS 4×S
Esp3I
ApaI
3' UTR
Poly T track
NcoI
XhoI
KRABTALE
XhoI
ApaI
TALE DNMT
NcoI
XhoI
TALE
Ligation
CMV promoter
T7 promoter
KRAB
pT7(AG)-DEM 4×S
TALE
DNMT
Poly T track
CMV promoter
T7 promoter
pT7(AG)-DEMΔKRAB 4×S
TALE
DNMT
Poly T track

Figure 2.6: A schematic illustrating the cloning strategy used to generate active pT7(AG)-DEM 4×S and pT7(AG)-DEMΔKRAB 4×S plasmids. (A) Restriction digestion; in the first reaction, pT7(AG)-ECS 4×S was double digested with *Esp*3I and *Apa*I to generate compatible ends for the insertion of the transgene sequences. *Esp*3I generates an overhang complementary to the *Nco*I overhang. In second reaction, pmRNA-DEM plasmids were double digested with *Nco*I and *Xho*I to excise the fragment consisting of the HA-KRAB-TALE (TALE 362 bp)-encoded sequence. In a third reaction, the pmRNA-DEM plasmids were also double digested with *Xho*I and *Apa*I and yields a fragment containing the remaining TALE-DNMT-encoding sequences. In a fourth reaction, pmRNA-DEMΔKRAB plasmids were double digested with *Nco*I and *Xho*I to excise TALE-encoded sequences without the KRAB domain. (B) Ligation; the transgene fragments HA-KRAB-TALE (TALE 362 bp) and TALE-DNMT-encoding sequences were ligated into pT7-ECS AG 4× generating pT7(AG)-DEM 4×S plasmids. While pT7(AG)-DEMΔKRAB 4×S plasmids were generated by ligating the HA epitope-TALE-encoded sequences without the KRAB domain and active TALE-DNMT-encoding (extracted from pmRNA-DEM) into pT7(AG)-ECS 4.

2.5.2 Production of IVTed therapeutic and reporter mRNA

In preparation for IVT, active pT7(AG)-DEM 4×S and pT7-(AG) DEMΔKRAB 4× S DNA templates were digested with 10 U of *Bbs*I (New England Biolabs, NJ, USA) per 10 µg of plasmid DNA, 1×Buffer and ddH_2O to a final volume of 50 µl, the linearisation reactions were incubated overnight at 37 °C. While pT7-mCherry reporter plasmid was digested with *Bsa*I. Linearisation of templates was confirmed on a 1 % agarose gel (Appendix 5.1).

IVT reactions were performed with New England Biolabs (NEB) individual IVT components along with TriLink buffer (Appendix 5.5, Table 5.4 and Table 5.5). IVT reactions were incubated for 2 hours at 37 °C followed by DNase treatment at 37 °C for 15 minutes to remove residual template DNA. IVT reactions were co-transcriptionally capped with TriLink CleanCap® AG (TriLink Biotechnologies, CA, USA) according to the manufacturer's instructions (Table 2.1). For production of modified mRNAs, 100% substitution of uridine with pseudouridine (ψ), 5-methoxyuridine (5moU) or N1-Methyl-Pseudouridine (m1ψ) (TriLink Biotechnologies, CA, USA) was incorporated to reaction according to protocol. After IVT, mRNA was cellulose-purified as described in Section 2.2.3.

2.6 Characterisation of the DEM mRNA expressed from pT7(AG)-DEM 4×S in vitro

2.6.1 Evaluation of Anti-HBV DEM mRNA silencing in vitro

Prior to seeding Huh7 cells, rat tail collagen I (Appendix 5.7) was used to coat the CellStar® plates (Greiner Bio-One, Frickenhausen, Germany). For single mRNA transfection experiments, Huh7 cells were initially transfected with 70 ng of pCH-9/3091 replication-competent plasmid DNA, followed by transfection with 430 ng of either IVT DEM mRNA or FLuc mRNA as a control. For double mRNA transfection experiments, cells were first transfected with 70 ng of pCH-9/3091 plasmid DNA, then 430 ng of IVT DEM mRNA or FLuc mRNA. Six hours later, a second mRNA transfection with the same RNA was performed. HBsAg levels were assessed at twenty-four and forty-eight hours after transfection. HBsAg levels were measured using the Monolisa™ HBs Ag ULTRA kit (Bio-Rad, CA, USA) according to the manufacturer's instructions (Appendix 5.8).

2.6.2 Detection of Anti-HBV DEM mRNA

Huh7 transfections were performed as described in Section 2.4.2, using mCherry mRNA as a negative control to assess transfection efficiency. For the detection of HA-tag, immunofluorescence staining of IVT DEM mRNA expressed from the pT7-(AG) platform was conducted as outlined in Section 2.4.2.1. This staining utilised a rabbit polyclonal anti-HA (Sigma-Aldrich, MO, USA) (diluted 1:250) and goat anti-rabbit labelled (Alexa Fluor 488) secondary antibody (Sigma-Aldrich, MO, USA), (diluted 1:250), following the procedure detailed in Section 2.4.2.1.

2.6.3 Evaluation of toxicity of anti-HBV DEMs expressed from pT7(AG)-DEM 4×S

Transfections of Huh7 cells with Anti-HBV DEM plasmid DNA or IVT DEM mRNA from the pT7(AG)-DEM 4×S platform were performed (after double transfection) and evaluated as described in Section 2.4.4.

2.6.4 Quantitative reverse transcriptase PCR (qRT-PCR) of HBV viral transcripts

Huh7 cells were initially transfected with 115 ng of pCH-9/3091 replication-competent plasmid DNA, followed by transfection with 885 ng of either IVT DEM mRNA or TriLink FLuc mRNA as a control. Six hours later, a second mRNA transfection with the same RNA was performed. Total RNA was extracted from cells, twenty-four hours after the second mRNA transfection using TRIzol® Reagent (Thermo Scientific, CA, USA) according to the manufacturer's instructions (Appendix 5.6.1). To remove contaminating DNA, extracted RNA samples were treated with 15 U of DNase I and 1× DNase buffer and incubated at 37 °C for an hour. Following incubation, RNA was precipitated using 500 µl chilled 100% ethanol and incubated at -20 ℃ for one hour. RNA was centrifuged at 12 000 ×g for 15 minutes at 4 ℃ and supernatant was discarded. RNA pellets were washed with 500 µl of 70% ethanol and centrifuged again at 12 000 ×g for 10 minutes at 4 ℃. Total RNA was resuspended in RNase free H_2O and concentration and purify of the RNA samples were measured by spectrophotometry at wavelength of 260 nm.

Total RNA was reverse transcribed and amplified using Luna® Universal One-Step RT-qPCR master mix kit (New England Biolabs Inc., MA, US). Each reaction contained 500 ng of total RNA, 0.4 µM of forward and reverse primer each, 1× Luna Universal One-Step Reaction mix,

1× Luna WarmStart RT enzyme mix and nuclease-free H_2O to a final volume of 10 µl. Primer sets used for amplification consisted of housekeeping gene *hypoxanthine guanine phosphoribosyltransferase (HRPT*), HBs and BCP (Table 2.2). RT-qPCR was carried out in CFX96 Touch™ Real-Time PCR Detection System (Bio-Rad, CA, USA) using the following conditions: reverse transcription at 55 °C for 10 minutes followed by initial denaturation cycle at 94 °C for 1 minute, followed by 40 cycles of denaturation at 95 °C for 30 seconds, annealing at 55 °C for 30 seconds and extension at 60 °C for 30 seconds. *surface* and *pregenomic* (*pgRNA*) mRNA were quantified relative to HRPT. Melting curve analysis confirmed the specificity of the amplicons and relative change in expression between the DEM transfected samples and mock samples were determined using delta Ct method (Livak and Schmittgen, 2001).

Table 2.2: Primer Sequences used to amplify HBV surface and pgRNA transcripts by RT-qPCR

Gene	**Primer name**	**Primer Sequence (5′-3′)**
BCP	BCP-forward	ACCACCAAATGCCCCTAT
	BCP-reverse	TTCTGCGACGCGGCGA
HBs	HBs-forward	GCCAAAATTCGCAGTCC
	HBs-reverse	ACGGGCAACATACCTT
HRPT	HRPT -forward	AGTCAACCAACACATCCTATC
	HRPT-reverse	GCATTATTAGCGTGCTGTCTT

2.6.5 qRT-PCR of innate response to DEM-encoding mRNA

To determine whether DEM-encoding mRNA triggers an innate immune response *in vitro*, analysis of IFN-β and IFN-inducible genes, *2', 5'-oligoadenylate synthetase 1* (*OAS1*) and *Interferon-induced proteins with tetratricopeptide repeats I* (*IFIT I*) was assessed by qRT-PCR. HEK293 T cells were transfected with 1200 ng of each respective DEM-encoding mRNA, untransfected (mock), Polyinosinic:polycytidylic acid (Poly I:C) (Sigma-Aldrich, MO, USA) served as a positive control for induction of IFN genes. Twenty-four hours post-transfection,

total RNA was extracted from the Hek293 cells using TRIzol™ reagent (Thermo Scientific, CA, USA) as described in (Appendix 5.6.1) and DNase treated as described in Section 2.6.4.

RT-qPCR was performed on total RNA extracted from HEK293 cells using Luna® Universal One- Step RT-qPCR kit (New England Biolabs Inc., MA, USA) described in Section 2.6.4. For quantification of IFN-β and IFN-related genes, primer sets used for *IFN-β*, *OAS1* and *IFIT1* and housekeeping gene *HRPT* (Table 2.3). RT-qPCR was carried out in CFX96 Touch™ Real-Time PCR Detection System (Bio-Rad, CA, USA) using the following thermocycling conditions: reverse transcription at 55 °C for 10 minutes followed by initial denaturation cycle at 94 °C for 1 minute, followed by 40 cycles of denaturation at 95 °C for 60 seconds, annealing at 55 °C for 30 seconds and extension at 60 °C for 60 seconds. Melting curve analysis confirmed the specificity of the amplicons. IFN-β and IFN related gene expression was relativised to HRPT, and change in expression between the DEM transfected samples and mock samples were determined using delta Ct method (Livak and Schmittgen, 2001).

Table 2.3: Primer sequences used to amplify IFN-β and IFN- inducible genes

Gene	Primer name	Primer Sequence (5′-3′)
IFN-β	IFN-β-forward	TCCAAATTGCTCTCCTGTTGTGCT
	IFN-β-reverse	CCACAGGAGCTTCTGACACTGAAAA
OAS1	OAS1- forward	CGAGGGAGCATGAAAACACATTT
	OAS1-reverse	GCAGAGTTGCTGGTAGTTTATGAC
MXA	MXA-forward	CTGGTGCTGAAACTGAAGAAAC
	MXA-reverse	ATCTCAATCTCGTAGTCCTGGTA
IFIT	IFIT-forward	CCCTGAAGCTTCAGGATGAAGG
	IFIT-reverse	AGAAGTGGGTGTTTCCTGCAAG
HRPT	HRPT-forward	TGACACTGGCAAAACAATGCA
	HRPT-reverse	GGTCCTTTTCACCAGCAAGCT

2.7 Bisulphite sequencing

Transfections were carried out as described in section 2.6.1 with FLuc mRNA, SL DEM mRNA and PL DEM mRNA. Twenty-hour hours after transfection total DNA were extracted from cells (Appendix 5.6.2). Bisulphite conversion and Sanger sequencing of extracted DNA was used to confirm methylation status of three CpG islands (Inqaba Biotec, Pretoria, South Africa). Bisulphite specific primer sequences were designed to target the sense and anti-sense strands of DNA targeting the three CpG islands.

2.8 Data analysis and programs

For data analysis, the mean (n=3) and the standard error of the mean (SEM) were calculated. Statistical significance was determined using a two-tailed paired Student's t-test, with p-values < 0.05 considered significant. Graphs were generated using GraphPad Prism 4.0 (GraphPad Software Inc., CA, USA). Figures were created with BioRender.com, and plasmid maps and simulated gels were produced using SnapGene® software (GSL Biotech; available at snapgene.com).

Chapter 3

3. Results

3.1 Generation of DEM mRNA produced from RNA expression vector

3.1.1 Construction of pmRNA-pA expression vector encoding anti-HBV DEMs

To enhance the transcriptional silencing of existing anti-HBV DEMs expressed as DNA, this study utilised an mRNA expression vector to express DEMs for the first time, to enable sequence-specific transcriptional repression of HBV. Established DEM-based technology is a pioneering platform that was generated to regulate expression by specific modification of the epigenome (Mlambo et al., 2018). This platform was adapted for the development of DEMs targeting HBV, site-specific TALE-DBD were repurposed from existing TALEN technology (Bloom et al., 2013) due to their high target specificity to target *S*, *C*, *P* ORFs of the virus (unpublished work) (Appendix, Figure 5.1).

Six active pmRNA-DEM plasmids (pmRNA-SR, -SL, -CR, -CL, -PR, and -PL DEM) and six inactive pmRNA-dDEM (pmRNA-SR, -SL, -CR, -CL, -PR, and -PL dDEM) plasmids were generated. The pmRNA-pA vector underwent double digestion with *Xba*I and *Apa*I yielding a fragment of a 3737 bp backbone fragment (Appendix, Figure 5.2). In separate reactions, plasmids expressing pCMV-DEMs were digested with *Xba*I and *Bam*HI, yielding fragments 2352 bp and 2643 bp and corresponding to the TALE domain for inactive dDEMs and the KRAB and TALE domain sequences for active DEMs (Appendix, Figure 5.3). Additionally, digestion with *Xba*I and *Apa*I excised 1642 bp fragments encoding DNMT domains from both active and inactive DEM constructs (Appendix, Figure 5.4), which were ligated into the pmRNA-pA backbone (Figure 3.1 - 3.2). Restriction digestion with *Bam*HI and *Apa*I verified the presence of DNMT domain sequences, while *Xba*I and *Bam*HI confirmed the KRAB and TALE domains in active DEMs. *Xba*I and *Nhe*I screening further confirmed the presence or absence of the KRAB domain in these constructs. All clones exhibited the expected banding patterns (Figure 3.1 - 3.2). The constructed plasmids, pmRNA-DEM and pmRNA-dDEM, are schematically represented in Chapter 2, Figure 2.1. The plasmids have a total size of 8022 bp and 7731 bp, respectively. Both

plasmids contain a CMV promoter/enhancer driving protein expression, a T7 promoter for mRNA synthesis, and an HA sequence followed by an SV40 nuclear localization signal. Both plasmids contain necessary sequence elements for IVT and intracellular translation, including a 5' UTR with Kozak sequence, 3' UTR, poly(T) tract, and a *Bbs*I restriction site for plasmid linearisation.

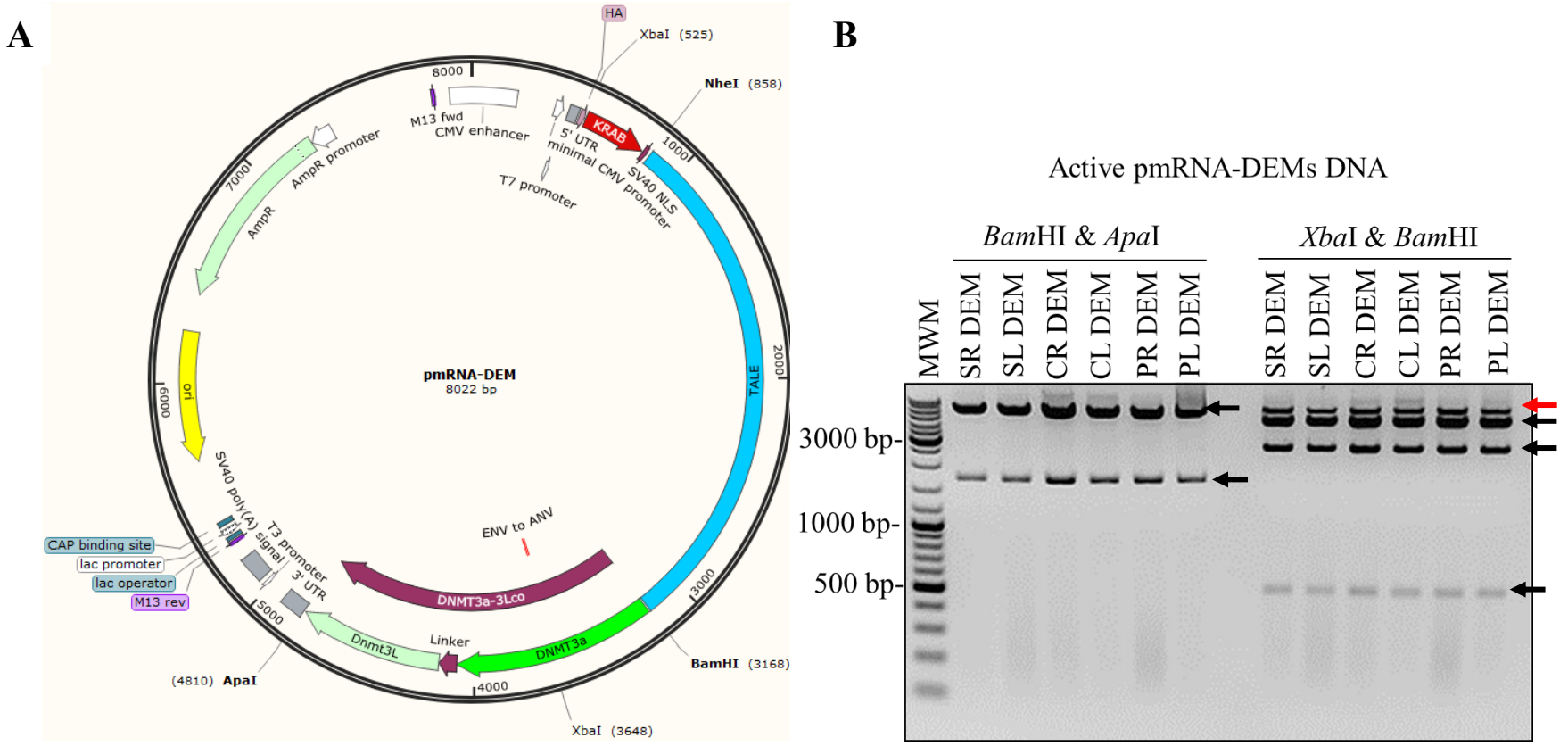

Figure 3.1: Confirmation of active pmRNA-DEM DNA by enzymatic digestion. (**A**) Active pmRNA DEMs were generated by cloning KRAB and TALE domain-encoding sequences along with DNMT domain-encoding sequences into an mRNA expression vector (pmRNA-CMV-pA). (**B**) Digestion with *Bam*HI and *Apa*I, produced bands of 6380 bp and 1642bp confirming the presence of DNMT-encoding domains indicated by the arrows. While restriction digestion of active pmRNA-DEMs constructs with *Xba*I and *Bam*HI yielded bands of 4899 bp, 2643 bp and 480 bp confirming the presence of the KRAB and TALE-encoding domains. indicated by the arrows. Undigested DNA is represented by the top band, indicated by the red arrow. Lane 1: MWM, Molecular weight marker (O'GeneRuler DNA Ladder Mix, 100 bp to 10 000 bp).

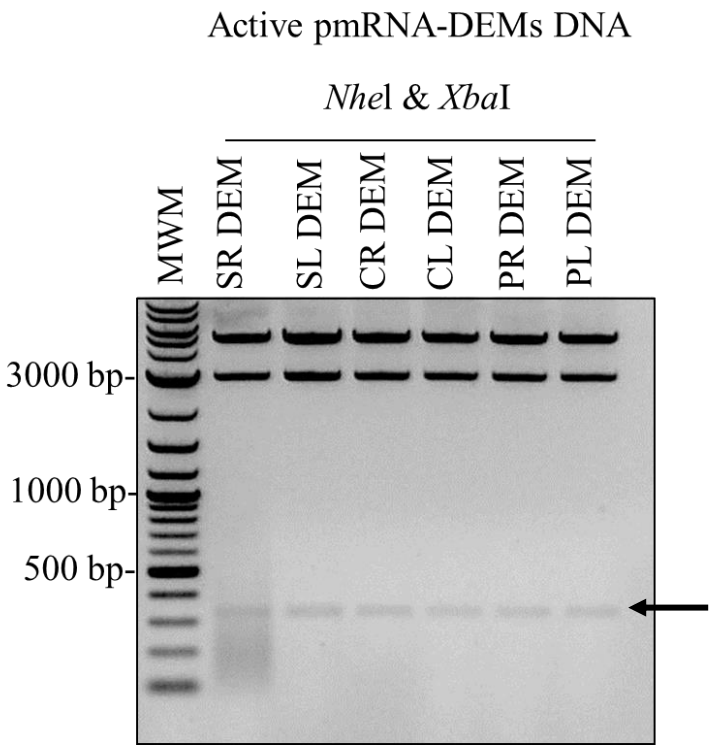

Figure 3.2: Confirmation of KRAB domain in active pmRNA-DEM plasmids by enzymatic digestion. Active pmRNA-DEMs were double digested with *Nhe*I and *Xba*I, yielded bands of 4899 bp, 2790 bp and a 333 bp, with the 333 bp band confirming the presence of the KRAB domain indicated by the arrow. Lane 1: MWM, Molecular weight marker (O'GeneRuler DNA Ladder Mix, 100 bp to 10 000 bp).

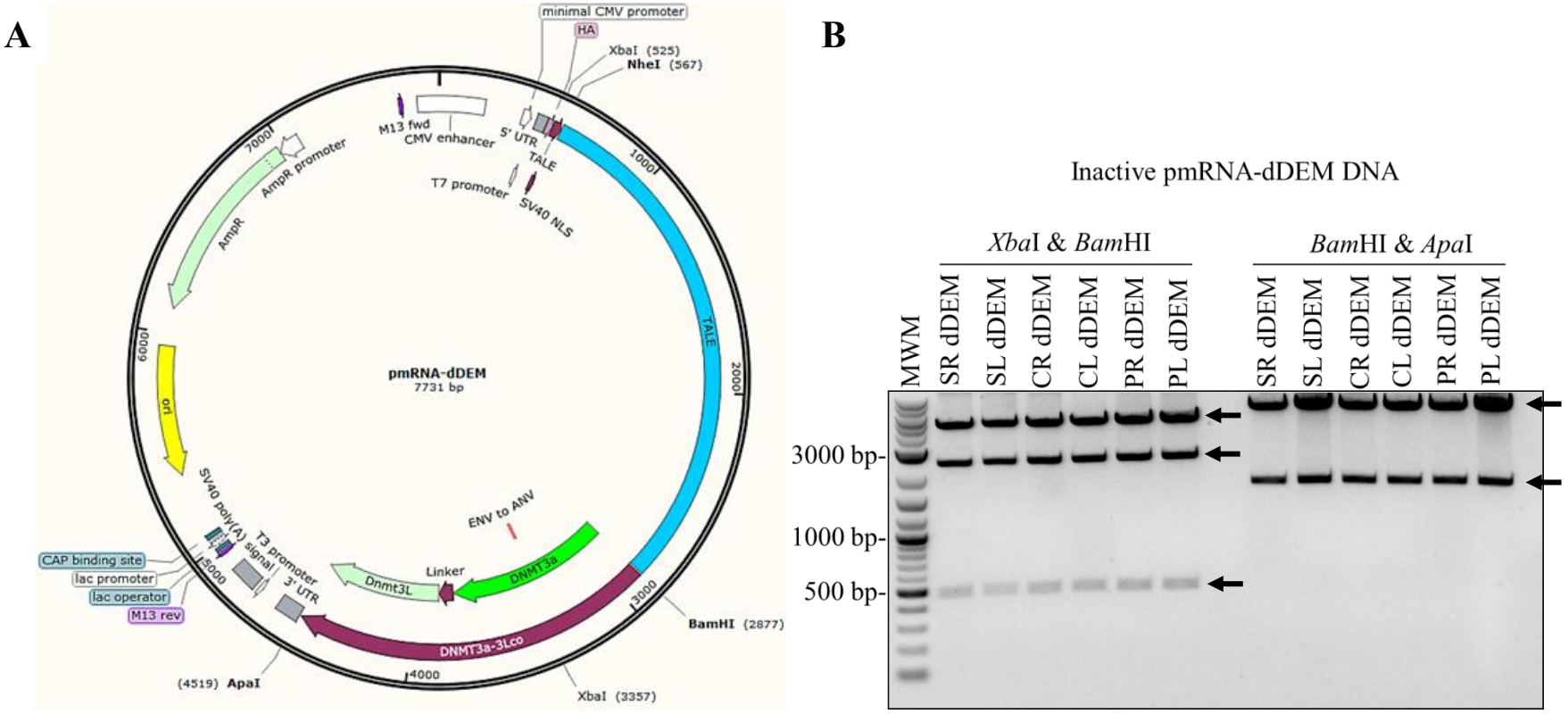

Figure 3.3: Confirmation of inactive pmRNA-dDEM DNA by enzymatic digestion. (**A**) Inactive pmRNA-DEMs constructs were generated by cloning TALE domain-encoding sequences along with dDNMT domain-encoding sequences into an mRNA expression vector (pmRNA-pA). (**B**) Restriction digestion of inactive pmRNA-DEMs constructs with *Xba*I and *Bam*HI yielded bands of 4899 bp, 2352 bp and 480 bp confirming the presence of the TALE -encoding domains.While digestion with *Bam*HI and *Apa*I, produced bands of 6089 bp and 1642bp confirming the presence of dDNMT-encoding domains (indicated by arrows). Lane 1: MWM, Molecular weight marker (O'GeneRuler DNA Ladder Mix, 100 bp to 10 000 bp).

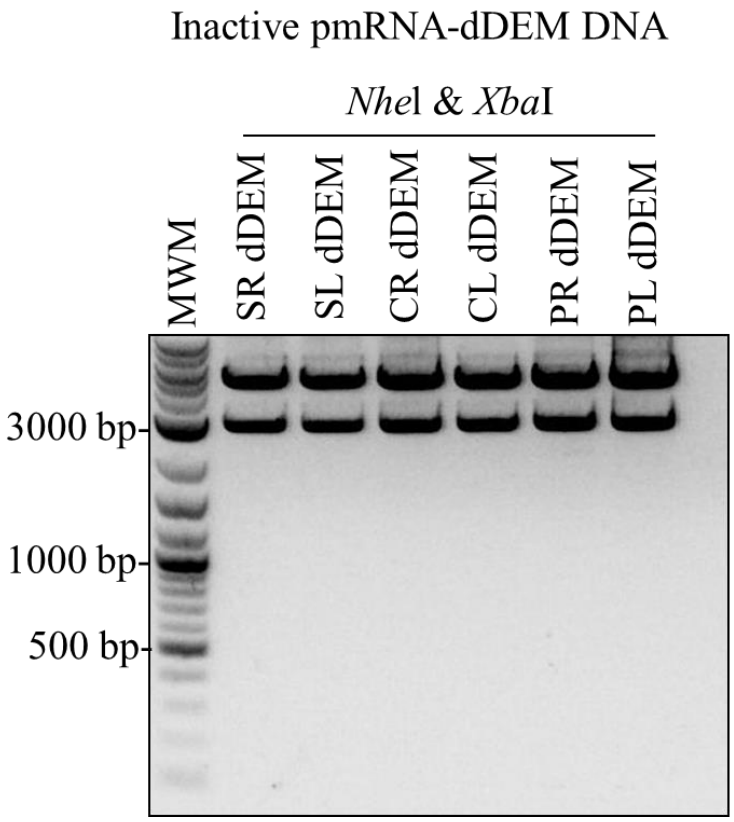

Figure 3.4: Restriction enzyme digestion confirming the absence of KRAB domain in inactive pmRNA-dDEM constructs. Active pmRNA-DEMs were double digested with *Nhe*I and *Xba*I, yielded bands of 4899 bp, 2790 bp and a 42 bp (off-agarose gel), with the lack of a 333 bp band confirming absence of KRAB domain in pmRNA-dDEM DNA constructs. Lane 1: MWM, Molecular weight marker (O'GeneRuler DNA Ladder Mix).

3.1.2 mRNA synthesis of DEM-encoded DNA

Prior to IVT, plasmid templates require linearisation. This step is pivotal for transcription efficacy, as incomplete linearisation of the template could produce a heterogeneous population of mRNA transcripts. Both active anti-HBV DEMs and control dDEMs were completely linearised as indicated by the single bands for each respective DEM on 1% agarose gel (Figure 3.5 A, B). The linearised DNA templates were initially purified using phenol: chloroform. Initial IVT reactions were performed using the RiboM RiboMAX^{TM} Large Scale RNA Production System with Promega Ribo m7G cap analogue (standard Cap 0). IVTed RNA was recovered through phenol:chloroform extraction and precipitated with ethanol. Formaldehyde agarose gel electrophoresis confirmed that a single IVTed mRNA product was obtained for each respective active DEM at 4267 bp and inactive dDEMs at 3974 bp. This result indicates that the IVT mRNA was of the correct size, though some slight smearing was observed, suggesting minor RNA degradation (Figure 3.5 C, D).

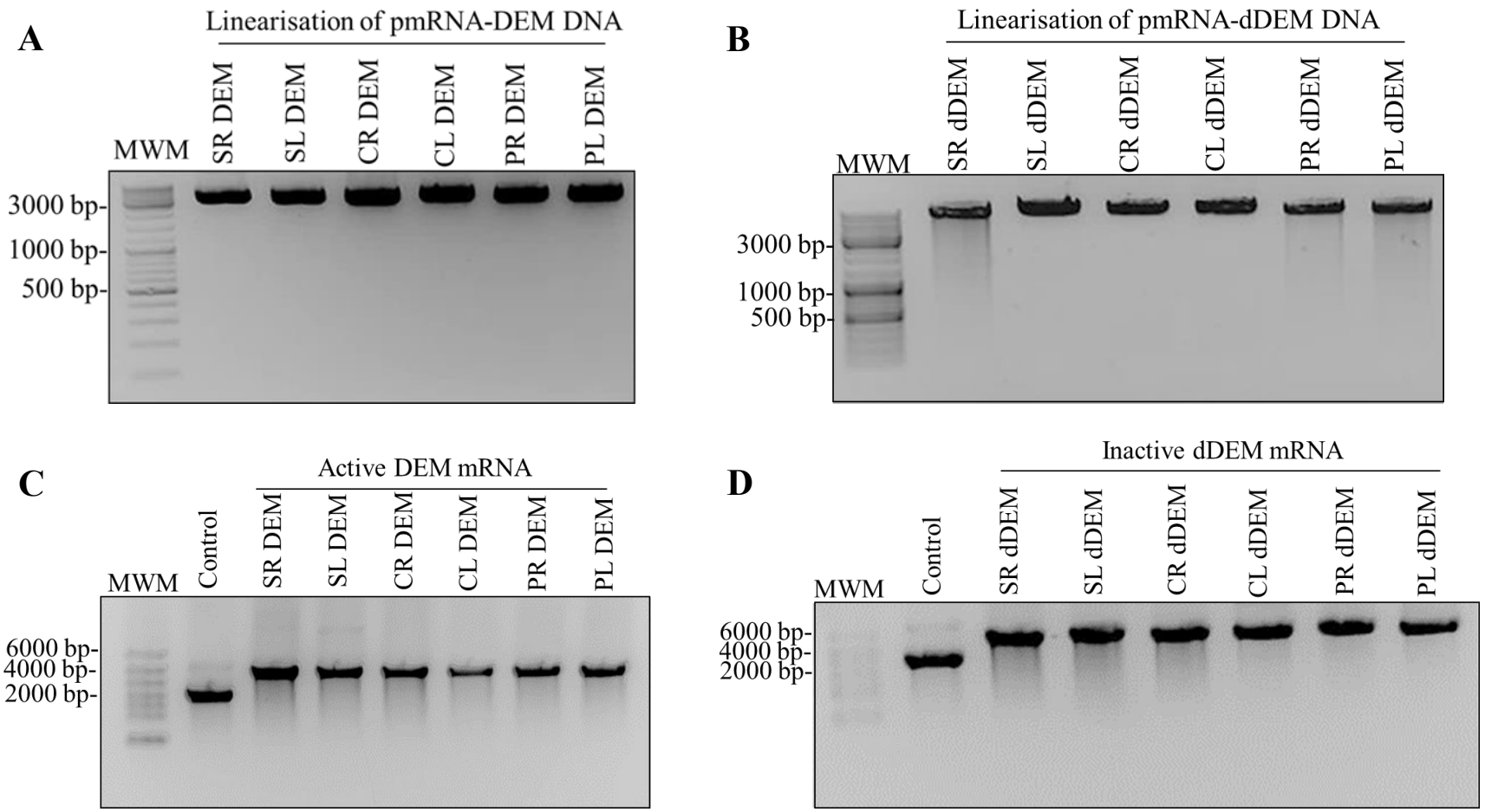

Figure 3.5: Linearisation and IVT of anti-HBV DEMs *in vitro*. (**A-B**) Linearisation of active and inactive pmRNA-DEM DNA templates by *Bbs*I restriction digestion, (**A**) active DEMs and (**B**) control inactive dDEMs. Lane 1: Molecular weight marker (MWM), O'GeneRuler DNA Ladder Mix. (**C-D**) IVT of active and inactive DEMs using RiboM RiboMAX^{TM} Large Scale RNA Production System with Promega Ribo m7G cap analogue, (**C**) active DEMs (4267 bp) and (**D**) control dDEMs (3974 bp). Lane 1: MWM, RiboRuler HR RNA ladder and Lane 2 positive control mRNA.

The feasibility of expressing DEMs from mRNA expression vector was assessed in liver-derived Huh7 cells. Cells were co-transfected with individual active or inactive anti-HBV DEM-encoded mRNA, and HBV replication competent pCH-9/3091 plasmid. This greater-than-genome-length plasmid simulates HBV replication once transfecte d (Nassal, 1992). Twenty-four hours after transfection, culture medium was collected and HBsAg concentration was measured. Control SR, SL, CR, CL, PR and PL dDEM mRNA exhibited no silencing of HBsAg secretion (Figure 3.6 A) as expected, as these mRNA encoded sequences have a mutation within the catalytic domain of DNMTs and lack a KRAB domain and therefore function as mock transfections. However, active anti-HBV SR, SL, CR, CL, PR and PL DEM mRNA also did not exhibit statistically significant repression of HBsAg expression (Figure 3.6 A). The lack of significant silencing of HBsAg expression by SR and SL DEMs was unexpected, especially since these DEMs target the *S* ORF responsible for producing HBsAg proteins. Additionally, previously unpublished work by Dr Kristie Bloom demonstrated significant repression with S DEMs DNA.

Since no reduction was observed, expression of the DEM mRNA was evaluated *in vitro*. Both active and inactive control DEMs have an HA-epitope located at the N-terminus of each TALE-DBD that function as a tag for immunohistochemical detection. Therefore, Huh7 cells were individually transfected with few active DEM-encoded mRNA consisting of either SR, CR and PR DEM mRNA or with TriLink FLuc mRNA which served as a mock transfection. Detection of expression was assessed three hours after transfection by fluorescence microscopy. Results show no detection of HA-tag in cells transfected with the mock evident by the lack of distinct green fluorescence. This was expected as TriLink FLuc mRNA does not contain an HA-tag (Figure 3. 6 B). The anti-HBV DEMs was comparable to mock transfected cells, indicating no expressed of anti-HBV DEMs. Background fluorescence can be observed in all transfected cells including the mock transfected cells and does not represent expression and is likely a result of the assay.

In summary, the results reveal that while IVT of active and control DEM mRNA was produced at the expected sizes, however lack of functionality and expression of the IVTed DEMs in Huh7 cells emphasised the requirement for optimisation of the IVT process.

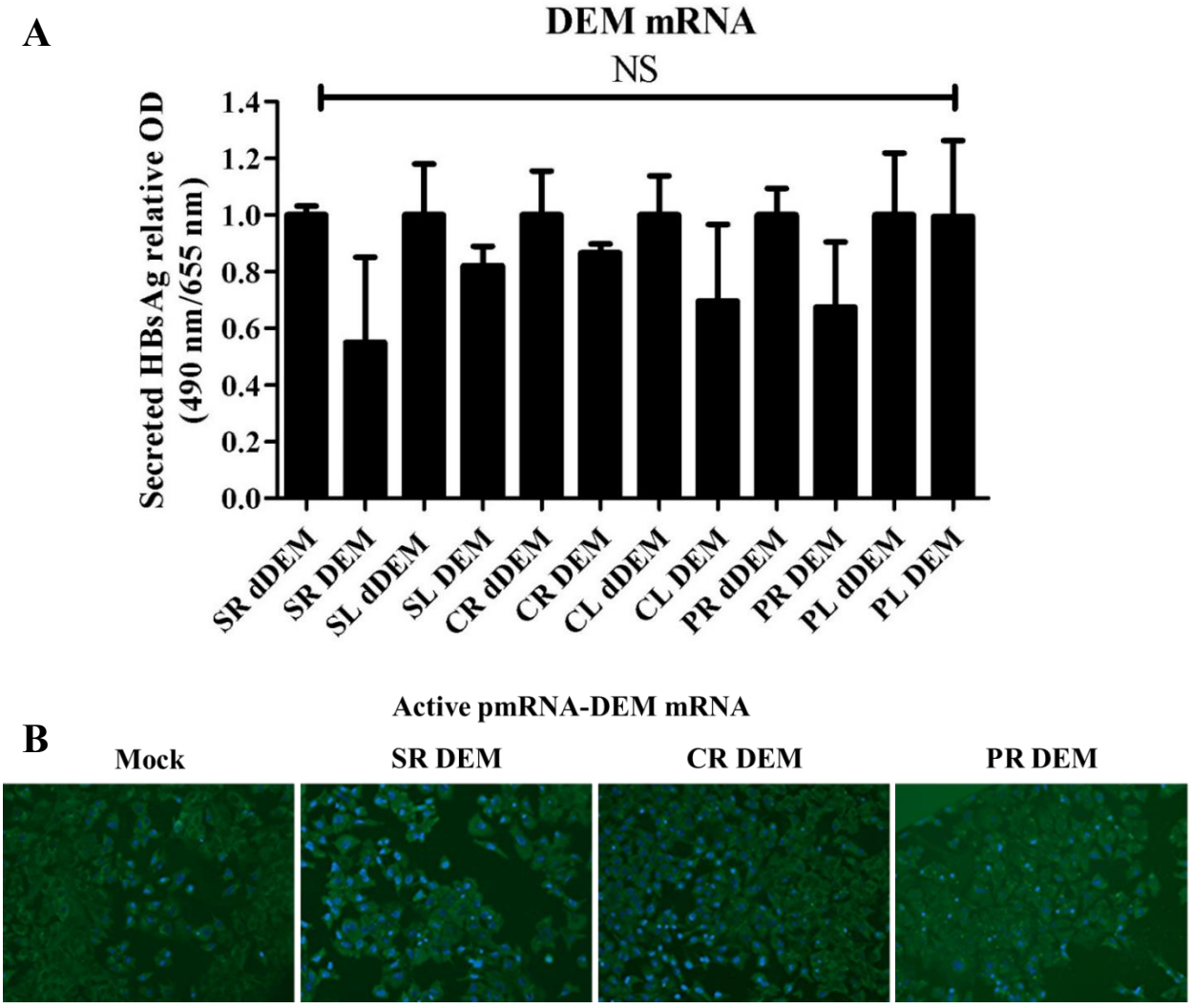

Figure 3.6: Assessment of IVTed DEM mRNA expressed from pmRNA expression vector in cultured cells. (**A**) Assessment of transcriptional silencing of HBsAg levels was assessed twenty-four hours after transfection of Huh7 cells. Cells were individually transfected with active and inactive DEM mRNA and pCH-9/3091 plasmid DNA. Active DEM was normalised against its corresponding inactive DEM mRNA controls. All transfections were performed in triplicate (n = 3), NS represents non-significant. (**B**) Immunofluorescence staining of Huh7 cells transfected with FLuc mRNA (mock transfection) and individual active DEM mRNA was performed to examine expression of HA-tag *in vitro.* A mouse anti-HA primary antibody, along with a fluorescently labelled goat anti-mouse secondary antibody, was used to detect the HA tag

(green), while the nuclei were stained with DAPI (blue). Fluorescence microscopy was used to visualise cells at 20× magnification.

3.2 IVT Optimisation of anti-HBV DEM mRNA

3.2.1 Improved characteristics of ARCA-capped IVTed mRNA

Various optimisation strategies can be employed to produce highly functional IVTed mRNA. These modifications include but are not restricted to utilisation of alternative cap structures, modified nucleotides, and incorporation of UTR sequence elements from highly expressed mRNA. All are aimed at enhancing mRNA half-life, stability and translation rate, thereby enhancing protein translation efficiency while mitigating innate immune activation. To optimise IVT, a plasmid expressing the eGFP transgene was generated to facilitate the evaluation of IVT-produced mRNA in cultured cells, as the GFP reporter mRNA allows for easier assessment (Appendix 5.9.1, Figure 5.6).

To establish highly functional IVT mRNA, purification methods for linearised DNA templates and IVTed mRNA was changed from phenol: chloroform to sodium acetate for DNA templates, while LiCl precipitation was used for the recovery of IVTed mRNA. LiCl precipitation has been shown to be more efficient in eliminating small RNAs and DNA impurities (Nagalakshmi et al., 2008). pmRNA-GFP template DNA was linearised with *Bbs*I digestion. Template DNA was purified using sodium acetate and results show a single band indicating complete digestion (Figure 3.7 A). To verify whether the method of IVT was producing functional mRNA, GFP transgene was IVTed using RiboMAX^{TM} Large Scale RNA Production System and co-transcriptionally capped with Promega Ribo m7G cap analogue (standard Cap 0) (Figure 3.7 B) or capped with Ambion ARCA Cap 0 analogue (Figure 3.7 C). ARCA Cap 0 ensures exclusive cap incorporation in the correct orientation as the standard cap 0 structure can be incorporated in reverse orientation producing non-functional mRNA. GFP mRNA was precipitated using either phenol extraction followed by ethanol precipitation or LiCl.

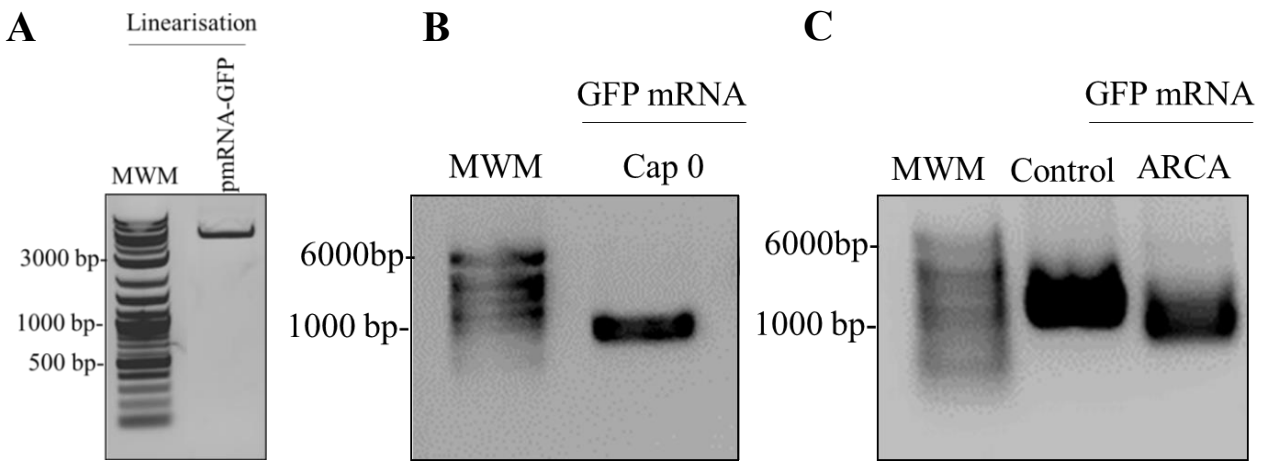

Figure 3.7: Linearisation and IVT of reporter mRNA *in vitro*. (**A**) Linearisation of pmRNA-GFP DNA template (3737 bp) by *Bbs*I restriction digestion overnight, Lane 1: Molecular weight marker (MWM), O'GeneRuler DNA Ladder Mix. (**B-C**) GFP (967 bp) was IVTed using RiboMAX^{TM} Large Scale RNA Production System and co-transcriptionally capped with Promega Ribo m7G cap analogue (standard Cap 0) (**B**) or capped with Ambion ARCA Cap 0 analogue (**C**). Lane 1: MWM, RiboRuler HR RNA ladder and Lane 2 positive control mRNA.

3.2.2 Characterisation of anti-HBV DEM mRNA expressed from pmRNA-pA vector

The reporter mRNA was transfected in three different liver-derived cell lines (HepG2.2.15, HepG2.hNTCP and Huh7 cells) and expression was evaluated using fluorescence microscopy (Figure 3.8). TriLink GFP mRNA was used as a positive control as it is commercially produced (Figure 3.8 A). The results indicate eGFP expression was minimal when co-transcriptionally capped with Promega Ribo m7G cap (standard cap 0) analogue (Figure 3.8 B), while improved expression was observed with mRNA capped with ARCA Cap 0 analogue (Figure 3.8 C). eGFP ARCA capped mRNA was further enhanced with LiCl precipitation (Figure 3.8 D**)**, although it remained significantly lower compared to the expression achieved with commercially produced TriLink GFP mRNA (Figure 3.8 A). Furthermore, cell lines typically challenging to transfect (HepG2.215 and HepG2.hNTCP cells) were successfully transfected particularly with control TriLink GFP mRNA demonstrating effectiveness of mRNA-based technology. Poor conditions or low viability of Huh7 cells could be responsible for low expression of GFP mRNA observed (Figure 3.8 C, D).

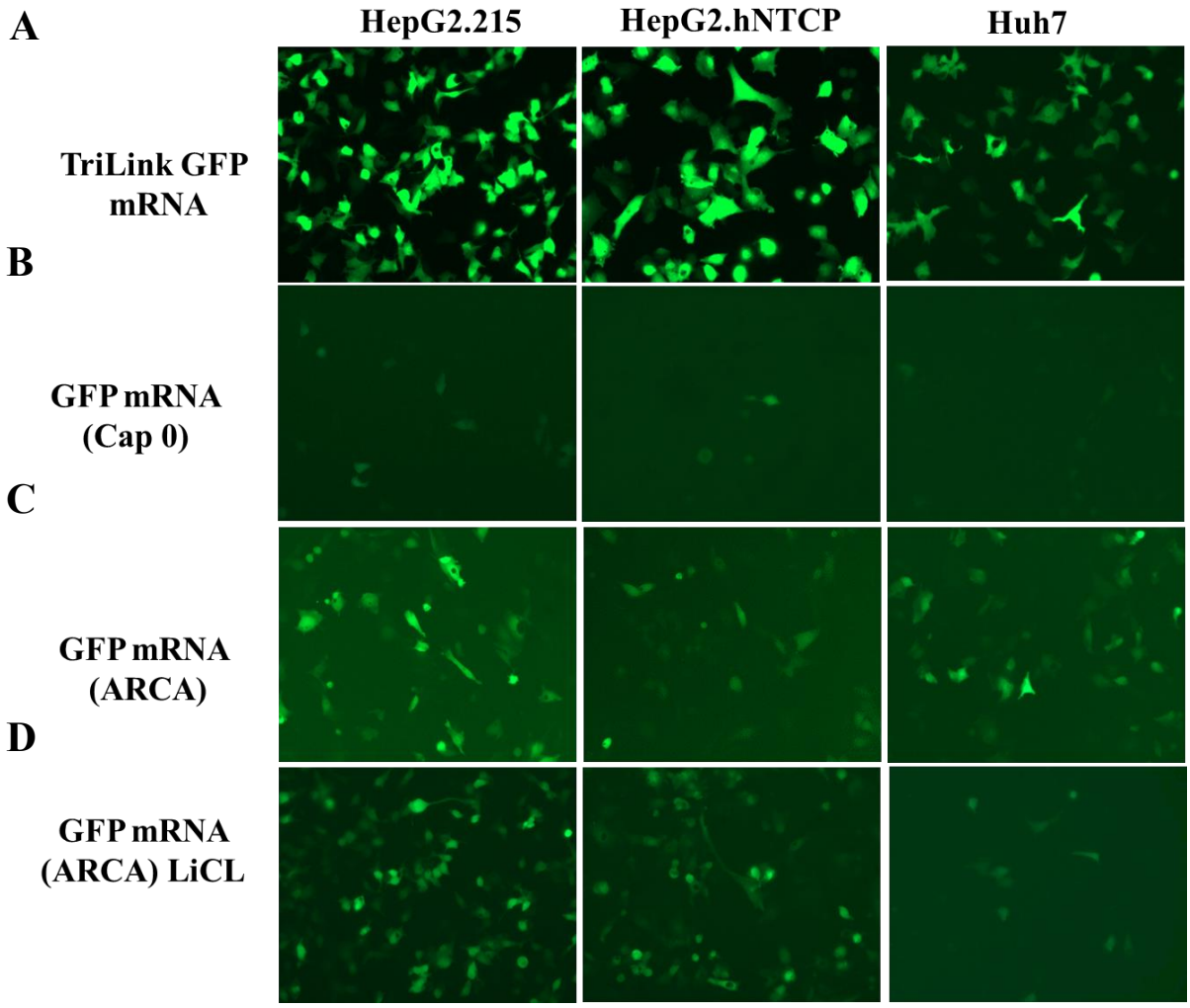

Figure 3.8: Comparison of Cap 0 and ARCA capping strategies and purification techniques for IVTed reporter mRNA. (**A-D**) Expression of reporter mRNA in different cell lines. Liver-derived cells were transfected with IVTed GFP mRNA, and expression was evaluated by GFP fluorescence. (**A**)Trilink GFP mRNA positive control mRNA. (**B**) Reporter mRNA was IVTed using RiboMAX^{TM} Large Scale RNA Production System and co-transcriptionally capped with Promega Ribo m7G cap analogue (standard Cap 0) and purified using phenol extraction. (**C-D**) Reporter mRNA was IVTed using the IVTed RiboMAX^{TM} Large Scale RNA Production System and co-transcriptionally capped with ARCA analogue and purified by (**C**) phenol extraction and ethanol precipitation or (**D**) LiCl precipitation alone. Fluorescence microscopy was used to visualise cells.

The expression of GFP using ARCA Cap, highlighted the importance of the 5' cap for functional mRNA production. Despite the presence of GFP-positive cells, overall expression was low, indicating that IVT required further optimisation. To assess the effectiveness of the IVT method for RNA synthesis, a second reporter, the T7-VEE-FLuc IRES plasmid was utilised. This plasmid encodes firefly luciferase and employs an internal ribosomal entry site (IRES) for cap-independent translation by allowing direct ribosomal binding at the IRES sequence (Godet et al., 2019). Luciferase activity was measured to quantitatively evaluate IVT efficiency. The T7-VEE-FLuc IRES plasmid was transcribed using the RiboMAX™ Large Scale RNA Production Systems-T7 (Figure 3.9 A), and Huh7 cells were transfected with TriLink GFP mRNA (negative control), TriLink FLuc mRNA (positive control), and IRES-FLuc mRNA. Luciferase activity was measured twenty-four hours after transfection and results showed luciferase expression was approximately 10.5 times higher in cells transfected with TriLink FLuc-mRNA compared to those with IRES FLuc-encoded mRNA (Figure 3.9 B). These results suggest that the RiboMAX™ Large Scale RNA Production Systems-T7 kit produces suboptimal RNA corroborating GFP expression results.

In conclusion, purification and 5' cap analogue structure is essential for functional IVTed mRNA along with the method of IVT. Indicating an alternative means of IVT is required.

.

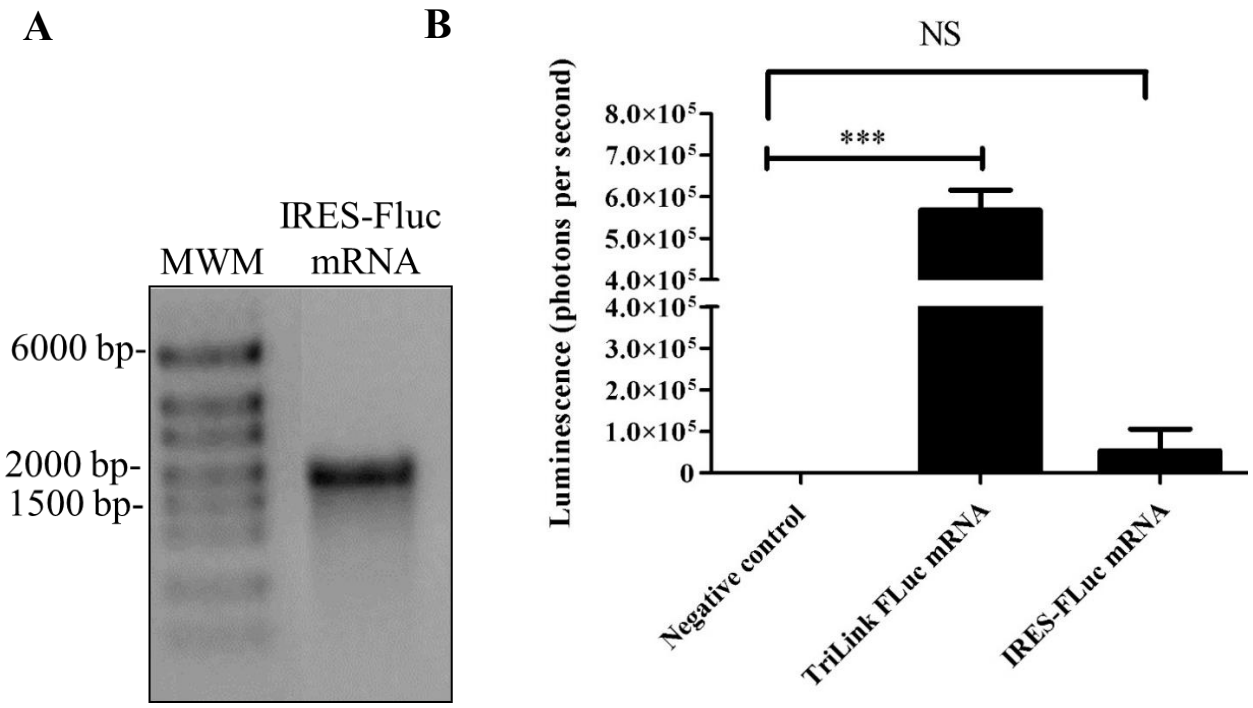

Figure 3.9: In vitro assessment of cap-independent translation of IVTed FLuc reporter mRNA. (**A**) IRES-FLuc mRNA was IVTed using RiboMAX^{TM} Large Scale RNA Production System. Lane 1: MWM, RiboRuler HR RNA ladder. (**B**) Luminescence readings were obtained from Huh7 cells transfected with TriLink-FLuc mRNA, IRES-FLuc mRNA, and a negative control GFP mRNA twenty-four hours after transfection. Results were normalised to the negative control. All transfections were performed in triplicate (n = 3). Statistical significance is indicated by ***, which corresponds to $p < 0.001$, NS represents non-significant results.

3.3 Post-transcriptional capping of IVTed GFP and anti-HBV DEM mRNA

3.3.1 Enhanced translation of IVTed GFP and anti-HBV DEM mRNA using post-transcriptional capping strategies

While IVTed mRNA with the Cap 0 is sufficient to initiate translation, in mammalian cells, mRNA undergoes further post-transcriptional modifications like 2′-O-methylation at position 2′ of ribose ring of the first nucleotide (Cap 1), and sometimes of the second nucleotide (Cap 2). The 2′-O-methylation in mRNA not only enhances the translation efficiency of IVT mRNA [26], but also prevents activation of the innate immune system [26]. TranscriptAid T7 High Yield Transcription Kit in conjunction with the Vaccinia Capping System was used to IVT and post-transcriptionally cap GFP- and anti-HBV DEM-encoding mRNA.

The Vaccinia Capping System has showed 90-100% capping efficiency compared to co-transcriptional capping using the standard Cap 0 and ARCA analogues (Xu et al., 2020, Henderson et al., 2021). The pmRNA-GFP template was IVTed, and the resultant mRNA capped post-transcriptionally (Cap 0 and Cap 1) using the Vaccinia Capping System (Figure 3.10 A). Huh7 cells were transfected with the IVTed capped mRNA and GFP expression was evaluated twenty-four hours after transfection. Results showed a significant improvement in expression of GFP mRNA with either Cap 0 or Cap 1 compared to expression observed with ARCA capped GFP mRNA (Figure 3.10 B). Results observed indicate expression levels nearly comparable to those observed with the TriLink GFP positive control. Results overall indicate an increase in the production of functional mRNA evident by the enhanced GFP expression. Unless stated otherwise, Cap 0 mRNA produced post-transcriptionally using the Vaccinia Capping System was used in further studies.

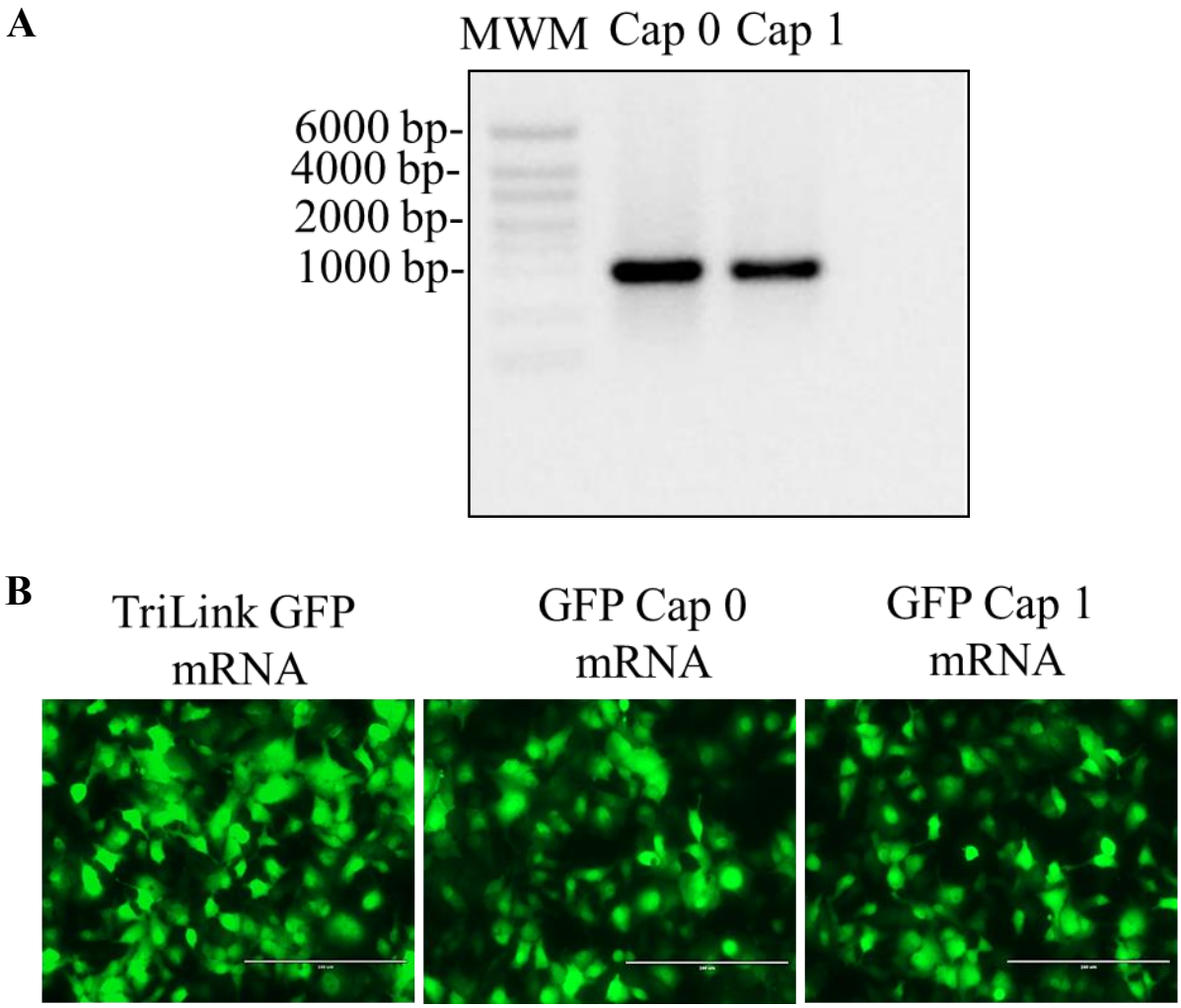

Figure 3.10:Comparison of Cap 0 and Cap 1 post-transcriptional capping strategies for reporter mRNA. (**A**) pmRNA-GFP reporter was IVTed using T7 High Yield Transcription Kit and post-transcriptionally capped with Cap 0 or Cap 1 using the Vaccina Capping System, producing GFP mRNA of 967 bp in size. (**B**) GFP expression by capped mRNA. Expression was assessed in Huh7 cells twenty-four hours after transfection with IVTed Cap 0 or Cap 1 GFP mRNA, along with TriLink GFP mRNA. Fluorescence microscopy was used to visualise cells.

3.3.2 Expression of IVTed dDEM mRNA when post-transcriptionally capped

Due to the significant improvement in the expression of GFP IVTed mRNA, active and inactive pmRNA-SR, -SL, -CR, -CL, -PR, and -PL DEMs were IVTed using TranscriptAid T7 High Yield Transcription Kit and co-transcriptionally capped with Vaccinia Capping System (Cap 0). Huh7 cells were transfected with either DEM mRNA individually or with TriLink FLuc mRNA which served as a mock transfection. TriLink GFP mRNA was used to assess transfection efficiency. Detection of HA-tag was assessed three hours after transfection. Fluorescence microscopy confirmed successful transfection evidenced by GFP expression after three hours. Results show detection of HA-tag in cells transfected with the control dDEMs (Figure 3.11 A). Results show detection in the cytoplasm and nucleus evident by the green fluorescence. Detection of the HA-tag in the cytoplasm was not unexpected as mRNA localises in the cytoplasm to be translated into protein. This protein is transported into the nucleus such as in the case of DEMs to carried out its function and therefore detection of HA expression in the nucleus was expected. In contrast, active DEM-encoded mRNA was comparable to the mock treated cells (Figure 3.11 B). Mock transfected cells, have mRNA that lack the HA-tag and therefore protein will simply not be detected. Furthermore, some background staining can be observed with the active DEMs and mock transfected cells.

Overall, the results indicate, TranscriptAid T7 High Yield Transcription Kit used in conjunction with the Vaccinia Capping System significantly improved IVTed mRNA evident by enhanced GFP protein expression and expression of HA-epitope of dDEM-encoded mRNA. The lack of expression from the active DEM-encoding mRNA could be attributable to the design of the transgene rather than IVT. This is mostly like due to the presence of the KRAB domain which present in the active DEMs, and not in the control dDEMs.

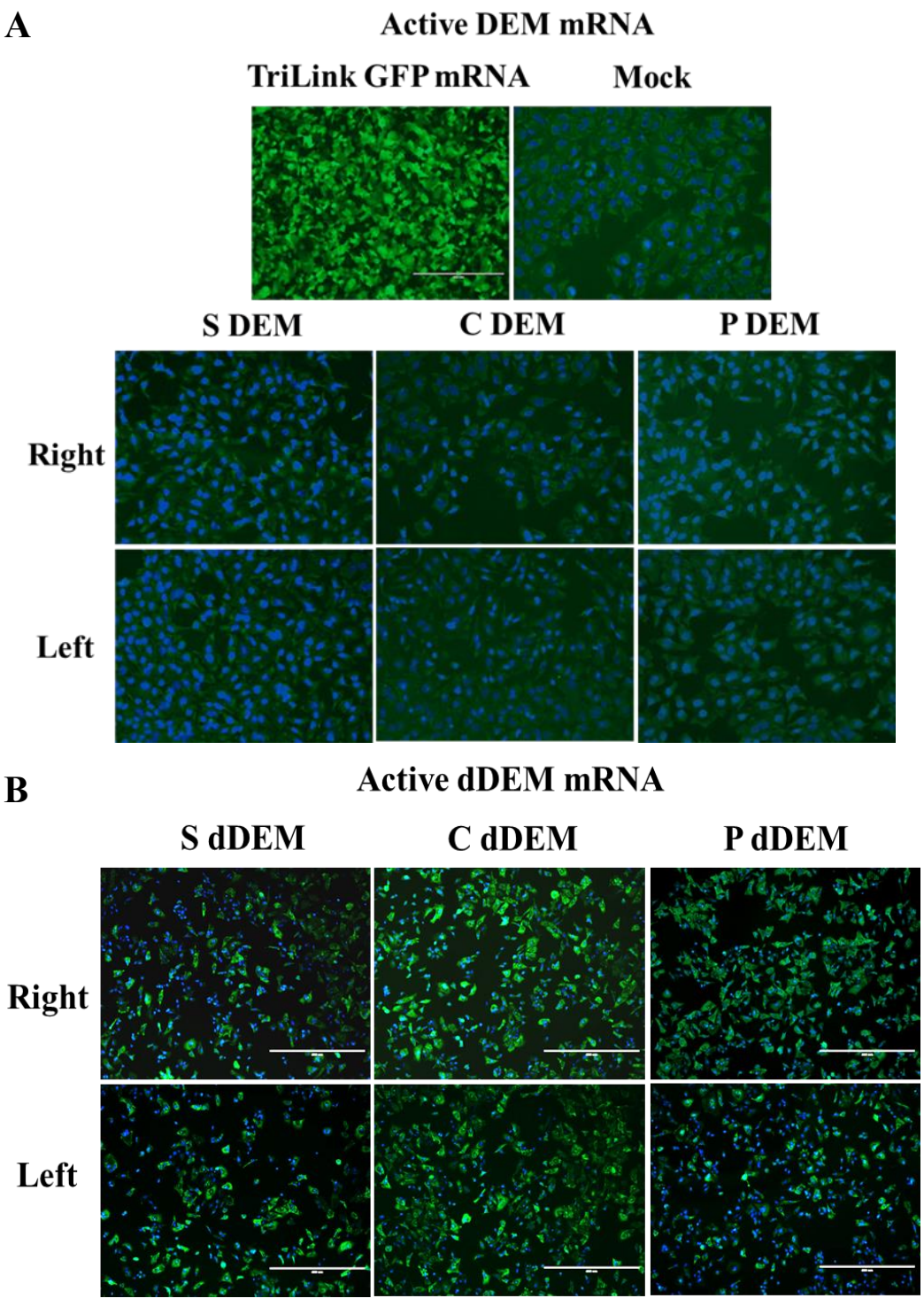
A
Active DEM mRNA
TriLink GFP mRNA
Mock
S DEM
C DEM
P DEM
Right
Left
B
Active dDEM mRNA
S dDEM
C dDEM
P dDEM
Right
Left

Figure 3.11: Immunofluorescence detection of IVTed active and control DEM mRNA *in vitro*. GFP DNA expression was assessed to indicate transfection efficiency. Immunofluorescence staining of Huh7 cells transfected with FLuc mRNA (mock transfection) and individual active and inactive DEM mRNA was performed to examine expression of HA-tag *in vitro*. (**A**) Active DEMs (**B**) inactive dDEMs. A mouse anti-HA primary antibody, along with a fluorescently labelled goat anti-mouse secondary antibody, was used to detect the HA tag (green), while the nuclei were stained with DAPI (blue). Fluorescence microscopy was used to visualise cells at 20× magnification.

3.3.3 Expression of active anti-HBV DEM-encoded IVTed mRNA in cultured cells

The difference between the active and inactive DEM-encoding plasmids is the presence of a single amino acid change in the DNMT3A domain and the lack of a KRAB domain sequence upstream of the TALE-DBD sequence in the inactive dDEM controls (Figure 1.9). The presence of KRAB domain sequence downstream of the HA-tag in the active pmRNA-DEM mRNA most likely could be affecting the folding of the HA-tag when IVTed thereby impairing detection of the HA-tag (Figure 3.11 A). As a result, re-cloning of the active pmRNA DEMs was performed to excise the KRAB domain sequence to further evaluate this hypothesis (Appendix 5.9.2, Figure 5.8). Active pmRNA-SR, -CR and -PL DEMΔKRAB plasmids were generated (Appendix 5.9.2, Figure 5.8) and linearised by *Bbs*I restriction digestion, producing a single band that indicates complete linearisation (Figure 3.12 A). Active DEMs without the KRAB domain was IVTed using TranscriptAid T7 High Yield Transcription Kit and co-transcriptionally capped using the Vaccina Capping System (Cap 0) (Figure 3.12 B).

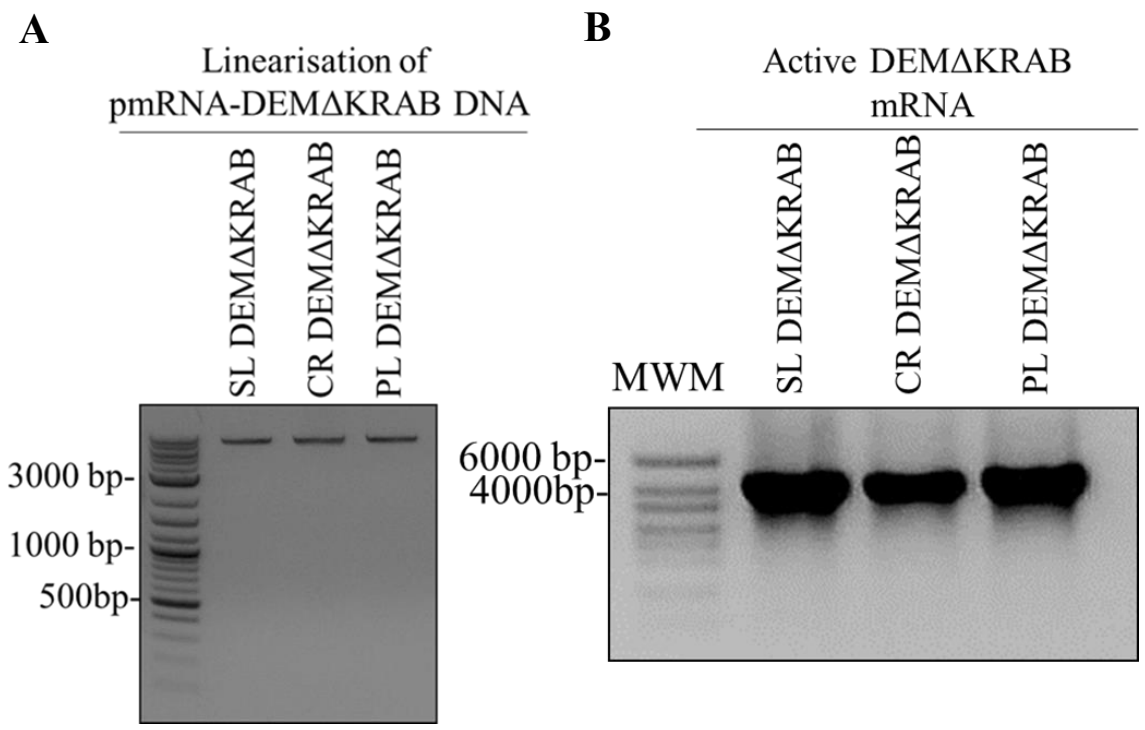

Figure 3.12: Linearisation and IVT of active pmRNA-DEMΔKRAB plasmids. (**A**). Linearisation of pmRNA- SR, -CR, and -PL DEMΔKRAB plasmids (each approximately 7731 bp) was achieved through overnight digestion with *Bbs*I, resulting in a single linearised band, as shown. (**B**). pmRNA- SR, -CR, and -PL DEMΔKRAB were IVTed using the T7 High Yield Transcription Kit and post-transcriptionally capped with the Vaccinia Capping System, resulting in Cap 0 mRNA (each approximately 3974 bp), as indicated by the single band.

Huh7 cells were individually transfected with SR, CR and PL DEMΔKRAB mRNA, TriLink FLuc mRNA (mock) and TriLink GFP mRNA. Immunofluorescence detection of the HA-epitope was performed three hours after transfection. Strong green immunofluorescence was observed, indicating the detection of the HA tag in the cytoplasm and nucleus of cells transfected with active DEMΔKRAB mRNA. In contrast, mock-treated cells showed no HA tag expression, as expected (Figure 3.13 A). These results were unexpected but demonstrated that removal of the KRAB domain restored detection of the HA-tag thus, verifying the hypothesis that the presence, in particular the location, of the KRAB domain in active DEMs influences detection of the HA-tag. Based on the detection of expressed DEM mRNA in vitro for the first time, assessment of anti-HBV DEMΔKRAB transcriptional silencing of viral HBsAg was performed. Huh7 cells were initially transfected with HBV replication-competent cells followed by transfection of individual SR, CR or PL DEMΔKRAB mRNA, TriLink FLuc mRNA served as a mock transfection. Assessment of HBsAg expression at twenty-four hours after transfection revealed no significant difference between the mock and DEMΔKRAB mRNA transfected cells (Figure 13.B). Indicating no silencing of the HBsAg was achieved by the active DEMs without the KRAB domain. This result was unexpected and contrary to the good expression of the DEMΔKRAB mRNA observed in Huh7 cells (Figure 13.A).

These results support the notion that the DNMT domain alone may not be sufficient for gene silencing. Additionally, it could indicate that another functional element necessary for the IVT of mRNA is influencing the production of functional mRNA.

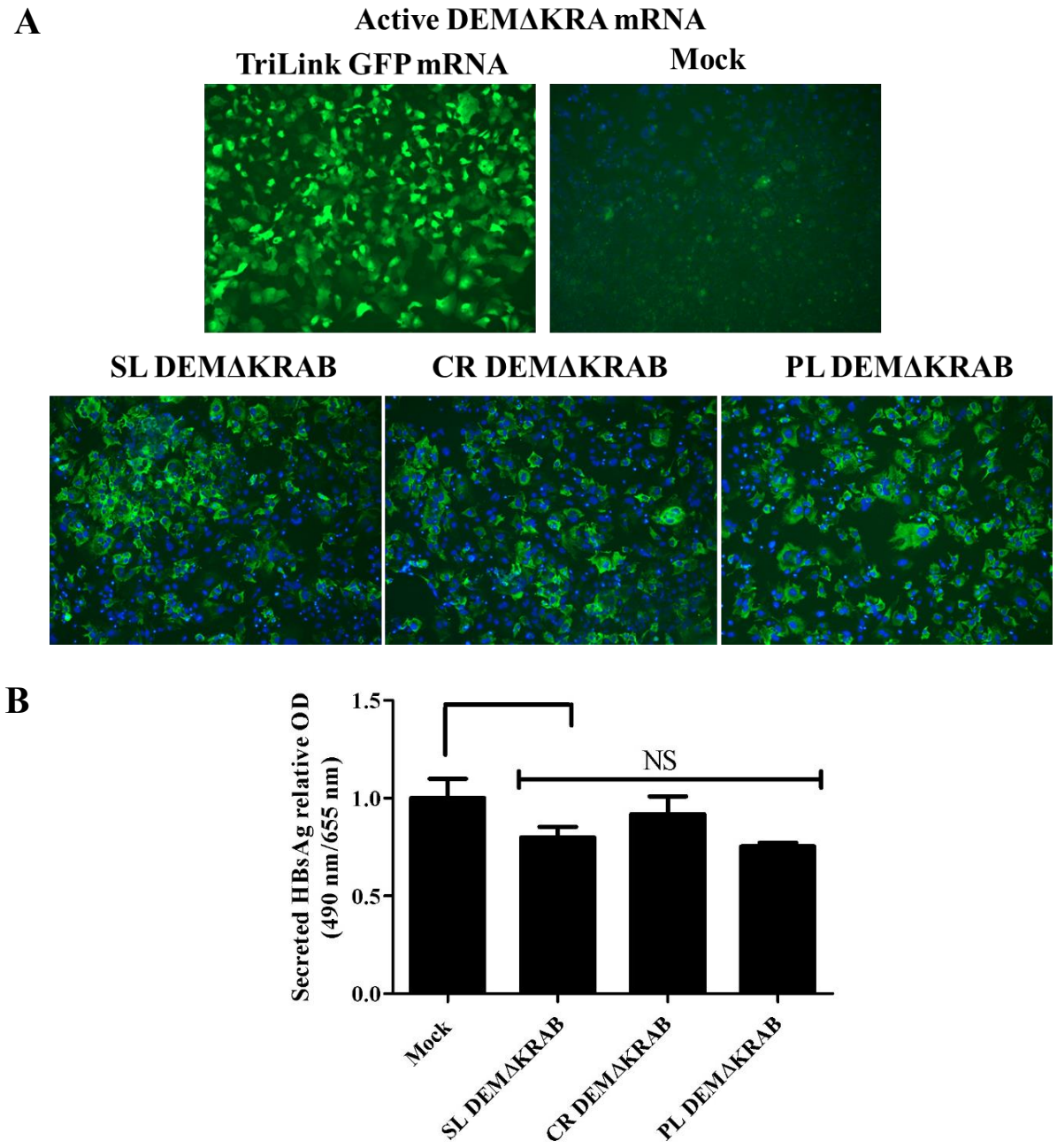

Figure 3.13: Evaluation of expression and functionality of post-transcriptionally capped Cap0 DEMs lacking the KRAB domain. (**A**) Immunofluorescence staining of Huh7 cells transfected with FLuc mRNA (mock transfection) and individual active DEMΔKRAB mRNA was performed to examine expression of HA-tag. In parallel, cells were transfected with TriLink GFP mRNA to determine transfection efficiency. Fluorescence microscopy was used to visualise cells at 20× magnification. (**B**) Huh7 cells were transfected with pCH-9/3091 replication competent plasmid followed by transfection of active DEMΔKRAB mRNA. Transcriptional

silencing of HBsAg levels was assessed twenty-four hours after transfection. All transfections were performed in triplicate (n = 3). NS represents non-significant.

3.4 Analysis of the functional elements present in pmRNA expression vector and IVTed mRNA

3.4.1 Complete functional elements required for pmRNA DEM plasmid expression

Systematic evaluation of several parameters including TALE sequence and poly(A) track of the DNA template was undertaken. *BglI* digestion of the TALE sequences extracted from the active pmRNA-DEMs (Figure 3.14 B) demonstrated the same expected banding pattern as TALE sequences from the original pVAX-CMV TALENs (Figure 3.14 A) confirming the TALE sequences are correct, therefore lack of functionality is not due to the DBD. Since the poly (A) tail of IVTed mRNA is dependent on the length of the poly(A) tract contained in the plasmid DNA, to confirm if the SR DEM plasmid contains the expected 52 adenine residues, the plasmid was sequenced (Figure 3.14 C). Results show the presence of 52 adenine residues constituting the intact poly(A) track.

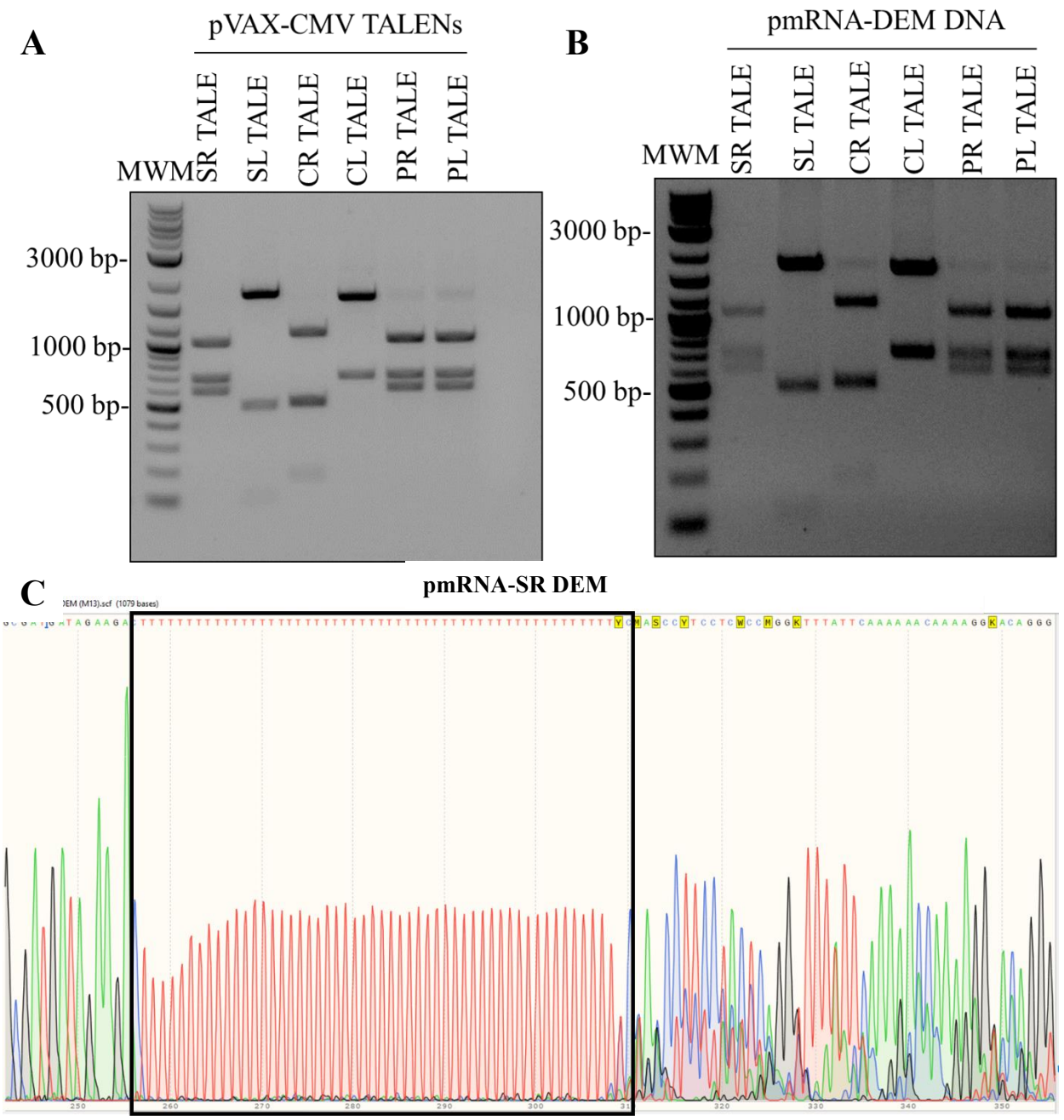

Figure 3.14:Confirmation of TALE-DBD and poly(A) track in pmRNA-DEM expression plasmids. (**A**) TALE-DBD domains were digested from (A) pVAX-CMV TALENs, the original vector from which the DBDs were obtained, and (**B**) active pmRNA-DEMs. The TALE-DBDs were digested with *BgI*I, a comparison of the banding patterns confirmed the presence of the correct DBDs, as indicated by the banding pattern produced by the digested plasmid in (**A**). (**C**) Active pmRNA-SR DEM was sequenced using the universal primer M13 to confirm the

presence of the poly(A) track. The chromatogram of pmRNA-SR DEM shows the presence of a 52-nucleotide poly(A) track.

3.4.2 Characterisation of anti-HBVDEM plasmids in vitro

3.4.2.1 Expression of anti-HBVDEM plasmids in liver-derived cells

The pmRNA-DEM plasmids were constructed to contain both T7 promoter for RNA synthesis and a CMV promoter for the assessment of the plasmid DNA before IVT. Initially, Huh7 cells were transiently transfected with individual plasmid DNA expressing the active with and without the KRAB domain and inactive DEMs. Transfection with the pUC118 plasmid served as the mock transfection. In parallel a pmRNA-GFP transfection was used to evaluate transfection efficacy. Forty-eight hours after transfection, immunofluorescence detection of the HA epitope revealed strong expression of both the inactive DEMs and the active DEMΔKRAB plasmids in the nucleus and expression in the cytoplasm (Figure 3.15 A, C). Expression of DEM plasmid DNA in the nucleus is not unexpected, as once DNA is transcribed within the cell, the DEM RNA is translated in the cytoplasm before being transported into the nucleus to elicit its function. Detection of protein expression in the nucleus of DEM plasmid DNA transfected cells suggests that these active DEMs were successfully translated and transported to the nucleus. These observations made with inactive DEM and active DEMΔKRAB expressed from DNA is consistent with observations made with DEM mRNA equivalents. Detection of HA-tag was observed in cells transfected with active DEM- encoding plasmids, albeit much lower compared to the inactive dDEM plasmid (Figure 3.15 B). This was an unexpected result as its mRNA equivalents were unable to show detection of HA-tag regardless of purification method, cap structure, and method of IVT.

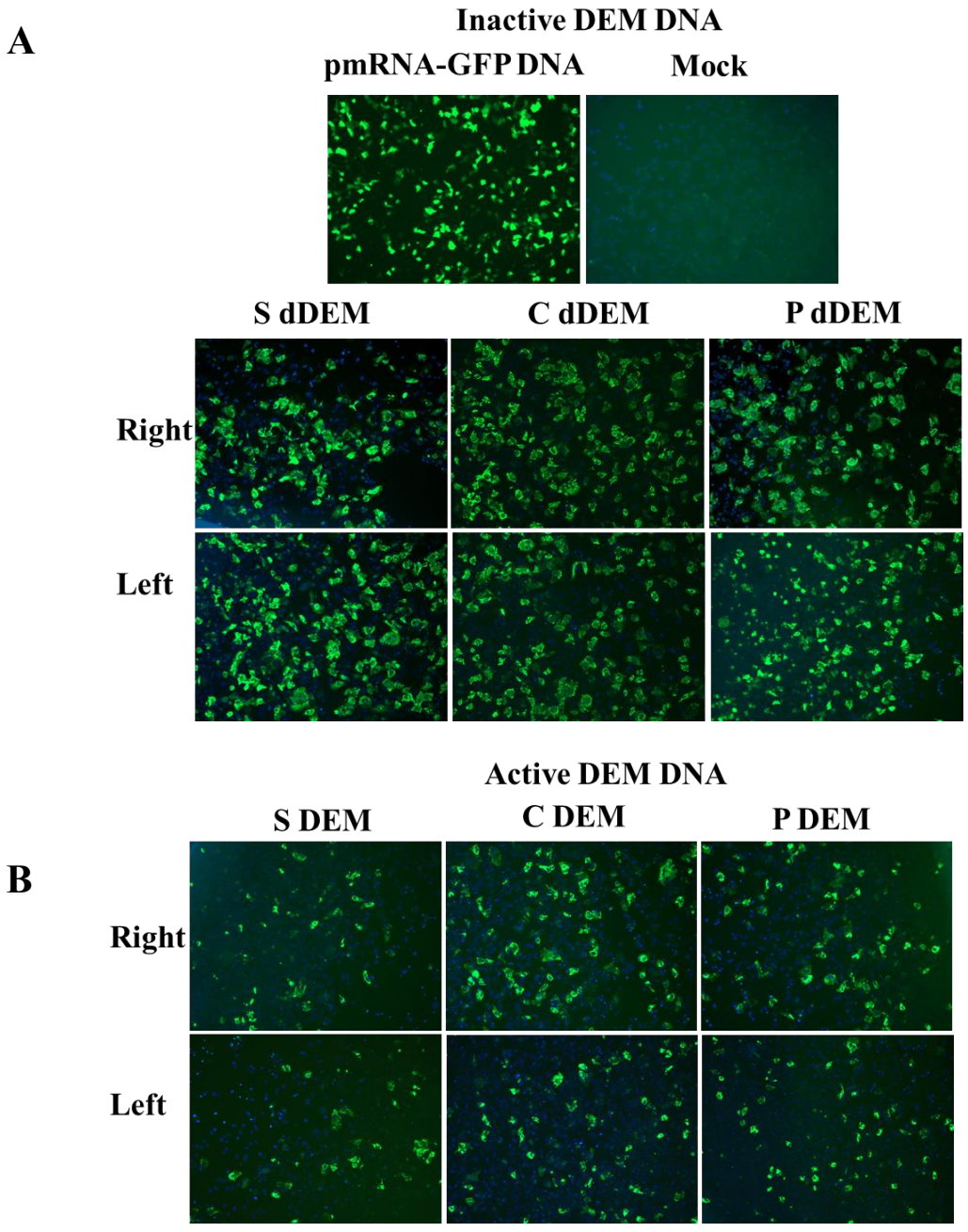
A
Inactive DEM DNA
pmRNA-GFP DNA
Mock
S dDEM
C dDEM
P dDEM
Right
Left
B
Active DEM DNA
S DEM
C DEM
P DEM
Right
Left

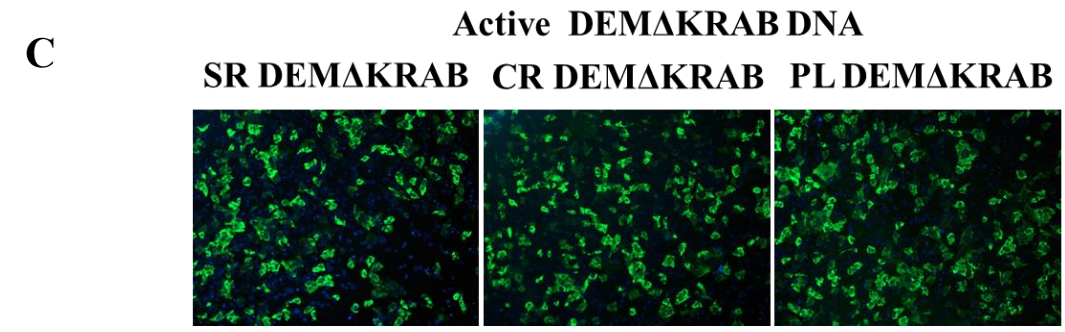

Figure 3.15: Immunohistochemical detection of HA-tag expression from pmRNA-DEM plasmid DNA in active and inactive DEMs. (**A-C**) GFP DNA expression was assessed to indicate transfection efficiency. Immunofluorescence staining of Huh7 cells transfected with FLuc mRNA (mock transfection), (**A**) inactive pmRNA-DEM, (**B**) active pmRNA-DEM, and (**C**) active pmRNA-DEMΔKRAB plasmids was performed to evaluate HA-tag expression. Cells were examined 48 hours post-transfection. Detection was achieved using a mouse anti-HA primary antibody and a fluorescently labelled goat anti-mouse secondary antibody (green), with nuclei stained by DAPI (blue). Fluorescence microscopy was conducted at 20× magnification.

3.4.2.2 Transcriptional silencing of HBsAg mediated by anti-HBV DEM-encoding plasmid DNA without inducing toxicity

Anti-HBV active DEMs (pmRNA-DEMs) with and without the KRAB domain (pmRNA-DEMΔKRAB) plasmids or pUC118 which served a mock control were individually co-transfected with HBV replication-competent pCH-9/3091 plasmid into Huh7 cells to confirm functionality of anti-HBV DEMs. Significant transcriptional silencing of viral HBsAg was observed active DEMs with KRAB domain, PR and PL DEMs, showing approximately 48% and 41% reduction. The SR and SL DEMs achieved 24% and 36% reduction, while CR and CL DEMs caused 36% and 22% reduction **(**Figure 3.16 A**)**. These results suggest active DEM with the KRAB domain, in particular C and P DEMs are causing repression over a long distance since these DEMs do not directly target the *S* ORF responsible for the production of HBsAg. The P DEMs targets enhancer I while C DEMs are in close proximity to preS1 promoter. This indicates that the pre-S1 and pre-S2 promoters are being silenced, as they are responsible for translation of L, M, S viral protein making up the surface HBsAg. Results also suggest that possible methylation of CpG II and CpG III could be occurring based on the location of the CpG islands. Furthermore, targeting of enhancer I has demonstrated reduction in HBsAg in other studies (Zhao et al., 2013, Luo et al., 2018). Interestingly, no reduction in HBsAg was observed with the active plasmid DEMs without the KRAB domain (Figure 3.16 B) collaborating what was observed with its mRNA equivalents**.** Reduction of HBsAg levels was due to the function of the DEMs and not a result of cellular toxicity as there was no difference in cell viability between all active anti-HBV DEM transfected cells and the untransfected cells (Figure 3.16 C, D).

Overall, the results indicate that the pmRNA-pA plasmid with the cloned active DEM transgene sequences with the KRAB domain can be expressed and effectively cause targeted transcriptional repression of HBV replication, without negatively affecting cell viability.

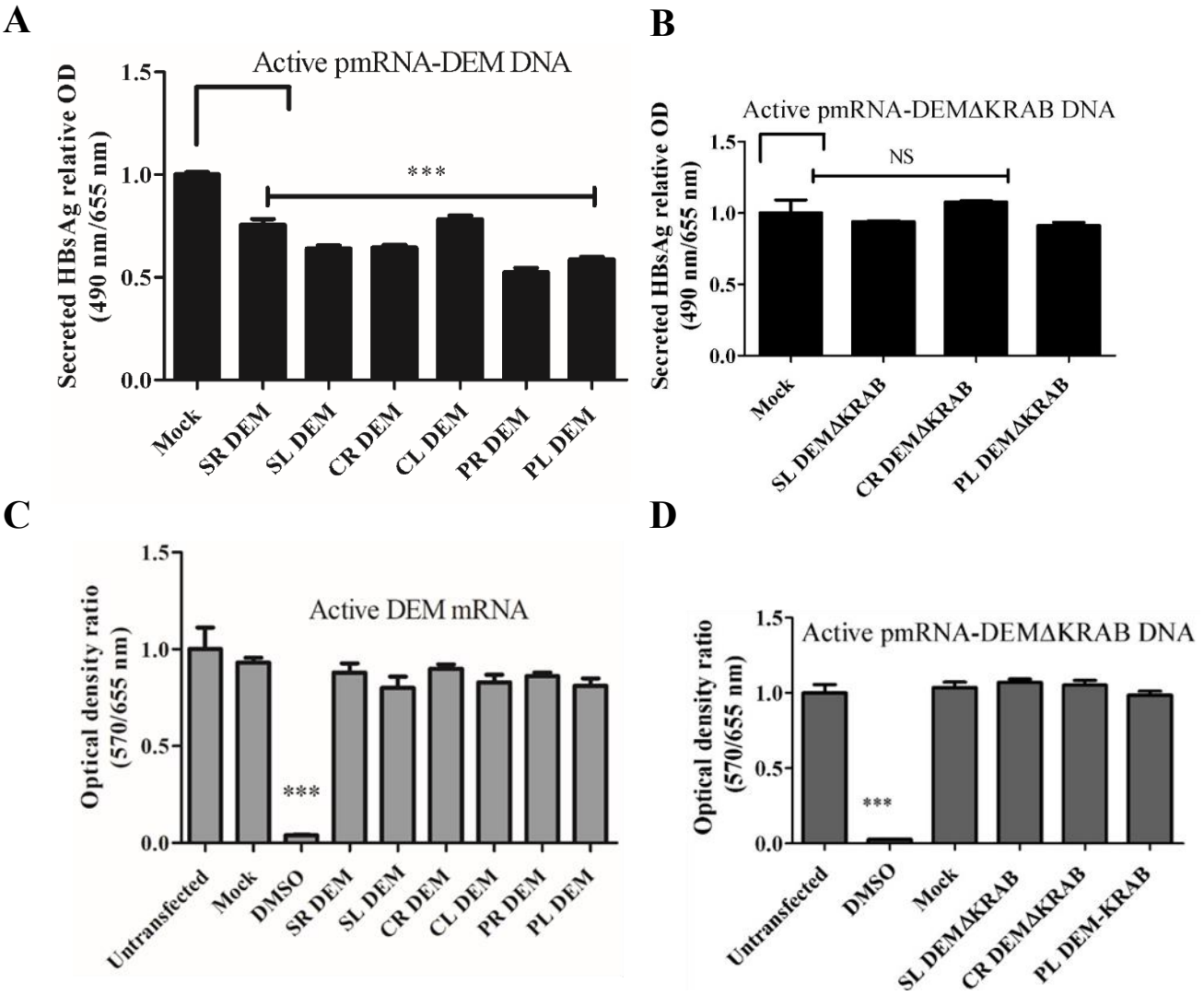

Figure 3.16: Plasmid DNA encoding anti-HBV DEMs achieve transcriptional repression without cellular toxicity. (**A-B**) The efficacy of active pmRNA-DEMs and pmRNA-DEMΔKRAB DNA was evaluated in Huh7 cells co-transfected with the HBV replication-competent pCH-9/3091 plasmid. HBsAg levels were assessed 48 hours post-transfection. (**C-D**) To evaluate the potential toxicity associated with active pmRNA-DEMs and pmRNA-DEMΔKRAB, an MTT assay was conducted 48 hours after mRNA transfection. DMSO served as the positive control, while untransfected cells acted as the negative control. All transfections were performed in triplicate (n = 3), and data were normalised to the untransfected control. Statistical significance is indicated by ***, corresponding to $p < 0.001$; NS represents non-significant results.

3.4.3 Confirmation of the poly (A) tail in IVTed DEM mRNA

Since the poly (T) tract was intact within the DEM plasmids before IVT, shortening of the poly (A) tail on the mRNA was assessed by 3' RACE. Shortening of the poly (A) tail would affect the stability and half-life of mRNA. This methodology allows for accurate determination of the sequence of the 3' end of mRNA transcripts. Active SR DEM was IVTed using TranscriptAid T7 High Yield Transcription Kit and co-transcriptionally capped using the Vaccina Capping System. IVTed SR DEM mRNA was converted to cDNA using an oligo-dT adapter primer which binds the poly (A) tail region on mRNA. This is followed by RNA template degradation by RNase H activity of the reverse transcriptase. Thereafter, amplification was performed using a DEM specific forward primer and abridged universal amplification reverse primer (AUAP). The AUAP primer binds the homologous region of the oligo-dT adapter primer that was used for first strand cDNA synthesis (Figure 3.17 A). Results show a single band at the 223 bp indicating amplification of the poly (A) tail (Figure 3.17 B). The DEM forward primer binds at the end of the 3' of the DNMT3L which is located upstream of the poly (A) track and amplifies through to the poly (A) tail. Therefore, the total size of the PCR includes the 52 adenine residues (Figure 3.17 B). The PCR products were excised and sequenced. Sequencing results show the presence of stretch of adenine (A) residues at the end of the sequence confirming presence and length of the poly-A tail (Figure 3.17 C). Length was 60 adenine residues because mRNA was polyadenylated which was carried out before 3' RACE on IVTed mRNA.

After confirming the presence of a poly(A)tail on the mRNA, IVTed SR DEM RNA was transfected into Huh7 cells to determine whether the tail length is shortened upon introduction into the cellular environment. Total RNA was extracted and reverse transcribed and amplified as previously described. Additionally, alongside SR DEM cDNA, pmRNA-SR DEM DNA was amplified using DEM specific forward primer (Figure 3.17 D) and pA reverse primer that is designed to bind downstream of the poly (A) track (Figure 3.13E). This control compares the amplified plasmid DNA with the cDNA to determine whether the poly(A) tail of the mRNA is shortened or maintained after transfection. Results shows amplicon sizes of the SR DEM cDNA at the expected 223 bp, while for the pmRNA-SR DEM DNA at 243 bp and a higher top band indicated by the arrow which could be a result of the addition of too much pDNA. Since this fragment is large it affects its migration and therefore is seen at the top of the agarose gel.

pmRNA-SR DEM DNA has a slightly larger amplicon size compared to cDNA, which is expected since it binds immediately downstream of the poly(A) track in the plasmid DNA. Therefore, this degradation is not affecting the stability of SR DEM mRNA, additionally a minimum poly(A) tail length of 30 adenine residues is required for mRNA synthesis.

Results overall show the transgene sequences in the plasmid DNA are functional evident by the silencing of viral surface antigen by all pmRNA-DEM DNA. Furthermore, intact poly(A) track was confirmed in the plasmid before IVT. Additionally, the poly(A) was confirmed to be present in IVTed mRNA, as well as after the RNA is transfected into cells. This indicates other factors could be affecting the stability and even translatability of the IVT mRNA.

A

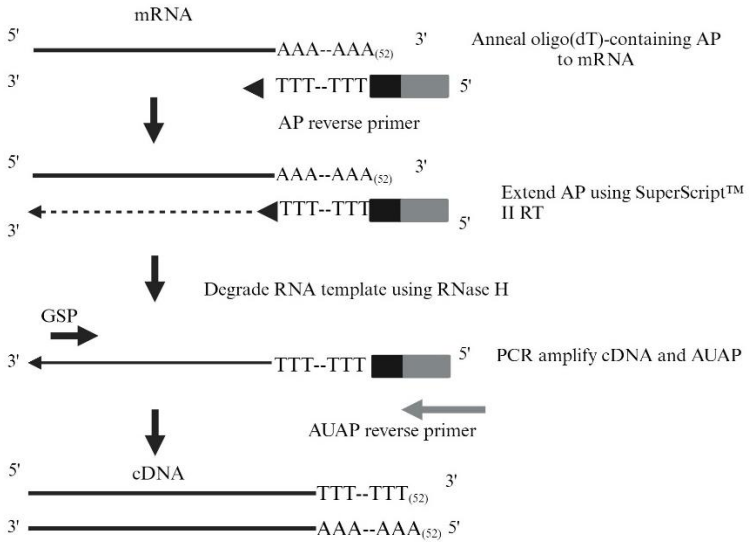
mRNA
5'
AAA--AAA(52)
3'
Anneal oligo(dT)-containing AP to mRNA
3'
TTT--TTT
5'
AP reverse primer
Extend AP using SuperScript™ II RT
Degrade RNA template using RNase H
GSP
PCR amplify cDNA and AUAP
AUAP reverse primer
cDNA
TTT--TTT(52)
AAA--AAA(52)

B

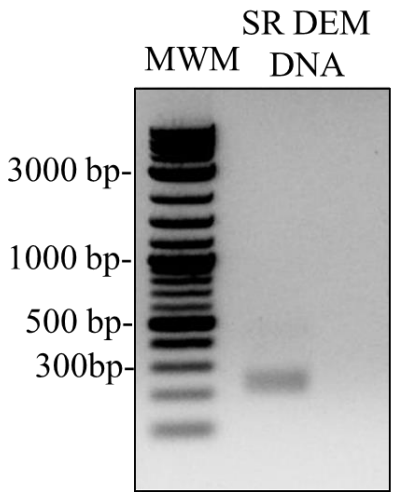
SR DEM
MWM
DNA
3000 bp-
1000 bp-
500 bp-
300bp-

C

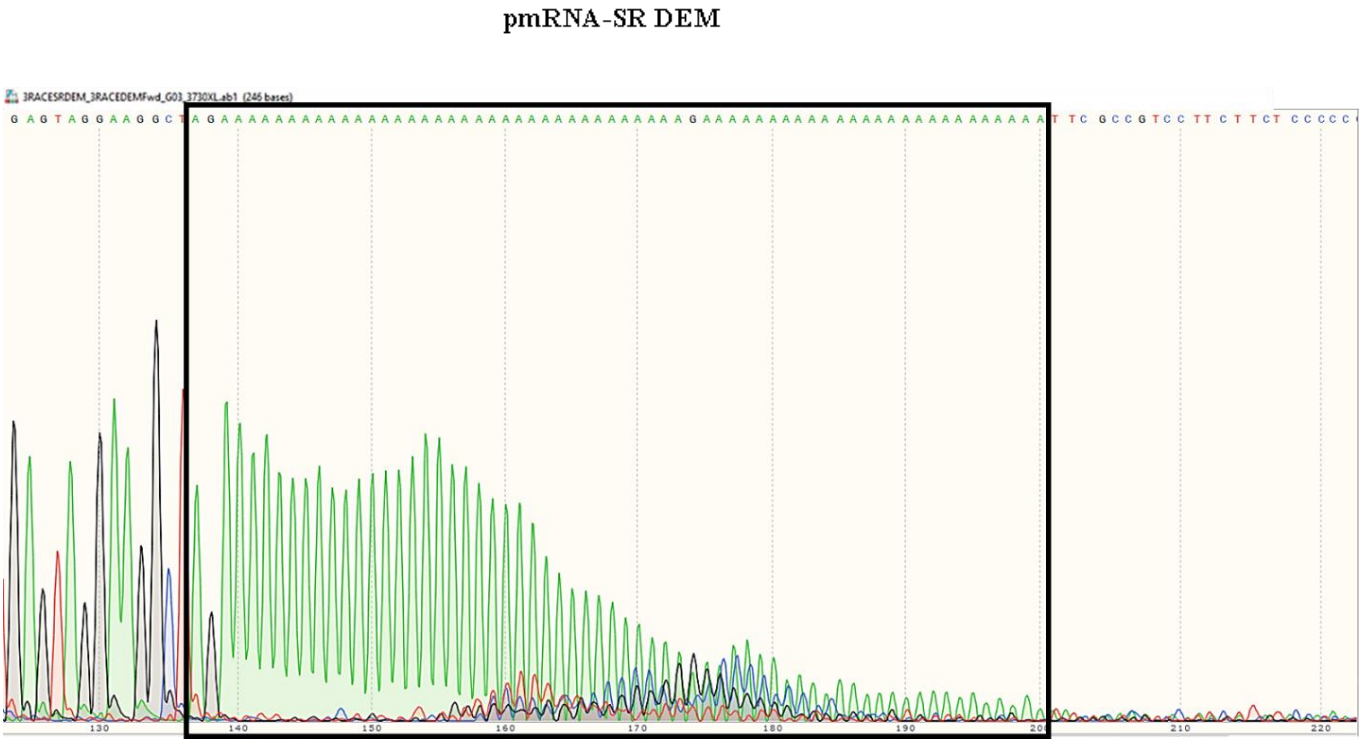
pmRNA-SR DEM
3RACESRDEM_3RACEDEMFwd_G03_3730XL.ab1 (246 bases)

D

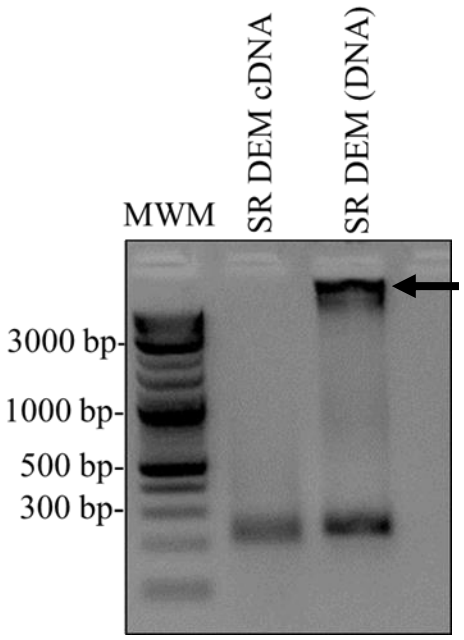

Figure 3.17: Analysis of the poly (A) tail in IVTed mRNA. (**A**) 3' RACE schematic, the adapter primer (AP) binds at the mRNA poly(A) tail on mRNA and is extended by reverse transcription to produce the first strand of cDNA. RNase H activity removes the original mRNA template. The cDNA is then amplified directly using a DEM-specific primer and the abridged universal amplification primer (AUAP) which is homologous to the AP sequence used in the initial cDNA synthesis. (**B**) PCR amplification of cDNA using DEM and poly (A) track specific primers. (**C**) Sequencing of cDNA to confirm the length of the 3' poly (A) track after IVT. (**D**) IVTed SR DEM mRNA was transfected into Huh7 cells and total RNA extracted and converted to cDNA using 3' RACE. PCR was performed on SR cDNA and SR DEM plasmid DNA.

3.5 Influence of IVT methods, modified nucleotides, Cap analogue structures, and dsRNA removal on mRNA efficacy

3.5.1 Enhanced reporter mRNA efficacy

A limitation of using IVTed mRNA is its potential to stimulate the innate immune response. Unmodified IVTed mRNA can induce an immune response that inhibits the expression of the mRNA. This effect is reduced when modified nucleotides are incorporated into the mRNA. The use of modified nucleotides not only inhibits immune recognition, prevents degradation and clearance, and increases translation efficiency, but it has also been shown to reduce the formation of dsRNA byproducts during IVT (Karikó et al., 2008). dsRNA produced during IVT is highly immunogenic and can trigger a strong immune response, leading to the production of pro-inflammatory cytokines impacting the stability and translation of mRNA. To circumvent immune stimulation by IVTed mRNA, the modified nucleotide pseudouridine (ψ) was incorporated during the transcription process. Additionally, to optimisation the IVT protocol further, the IVT reactions was performed using NEB individual components instead of the TranscriptAid T7 High Yield Transcription Kit as different IVT conditions have been shown to improve the quality of mRNA (Popova et al., 2024). TriLink IVT buffer was in conjunction with TriLink CleanCap® AG (Cap 1) as studies have demonstrated enhanced production of mRNA with TriLink CleanCap® AG cap analogue. After IVT, cellulose-based chromatography was employed to further ensure the removal of dsRNA contaminants.

Two mRNA reporters were initially used to assess if the various modifications improve quality and translation of mRNA. pmRNA-GFP was linearised by *Bbs*I restriction digestion (Figure 3.7 A) while pT7-Luc 2, a second RNA expression platform expressing firefly luciferase (FLuc), was linearised by *Bsa*I restriction digestion (Figure 3.18 A). Both vectors were completely linearised as evident by the single bands. IVTed GFP-mRNA and Luc2-mRNA were either post-transcriptionally capped using Vaccinia Capping System (Cap 0) or co-transcriptionally IVTed with TriLink CleanCap® AG (Cap 1). IVTed mRNA was subjected to cellulose-based chromatography for removal of dsRNA (Figure 3.18 B-C). Cellulose-treated GFP and Luc2 mRNA were transfected in Huh7 cells to analyse the influence of various modifications on protein expression. Twenty-hours after transfection, expression of GFP mRNA was assessed by

fluorescence imaging while luciferase assay used to evaluate Luc2 mRNA expression. Fluorescence imaging demonstrated enhanced improvement in GFP expression when cellulosed purified compared to non-cellulose purified mRNA (Figure 3.18 C), and this effect was further improved when mRNA was co-transcriptionally capped with TriLink CleanCap® AG (Figure 3.18 C). These observations were further validated with quantitative results from luciferase assay which showed higher expression of Luc2-mRNA using CleanCap® AG compared to Vaccinia-capped Luc 2 mRNA (Figure 3.18 E). The quantitative results demonstrate significantly higher expression of TriLink FLuc mRNA compared to in-house produced FLuc mRNA, even after optimised IVT and purification. This difference is attributed to the high purity of TriLink FLuc mRNA, which results from extensive chromatographic purification, thus validating the importance of well-optimised processes for producing effective IVTed mRNA.

In summary the results reveal incorporation of modified nucleotides, cellulose purification and co-transcriptional capping of IVT mRNA led to increased protein expression and therefore was included for further DEM mRNA experiments.

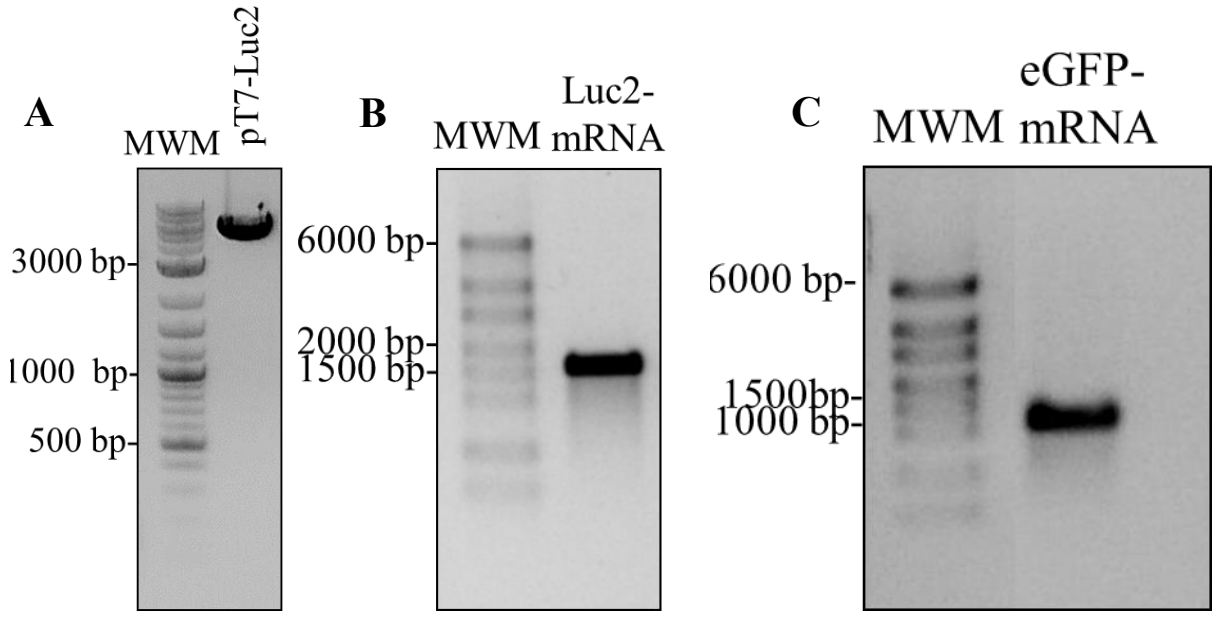
A
MWM
pT7-Luc2
3000 bp-
1000 bp-
500 bp-
B
Luc2-
MWM mRNA
6000 bp-
2000 bp-
1500 bp-
C
eGFP-
MWM mRNA
6000 bp-
1500bp-
1000 bp-

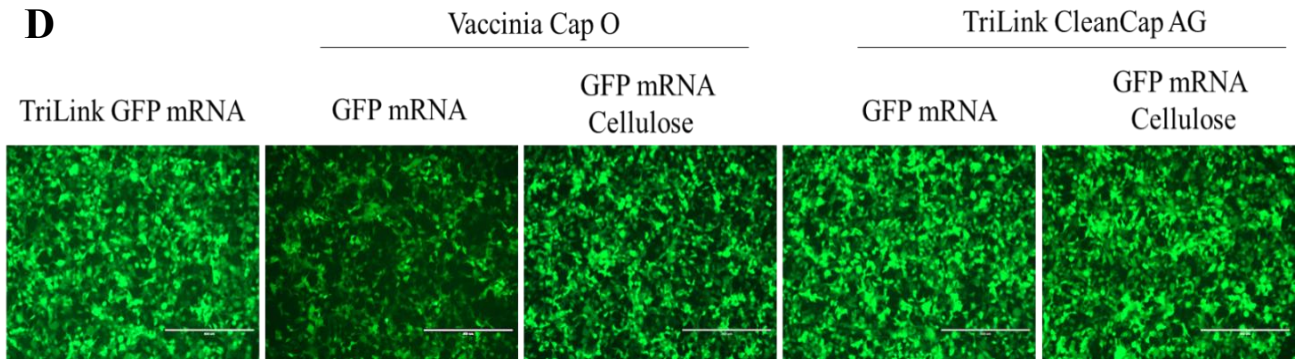
D
Vaccinia Cap O
TriLink CleanCap AG
TriLink GFP mRNA
GFP mRNA
GFP mRNA
Cellulose
GFP mRNA
GFP mRNA
Cellulose

E

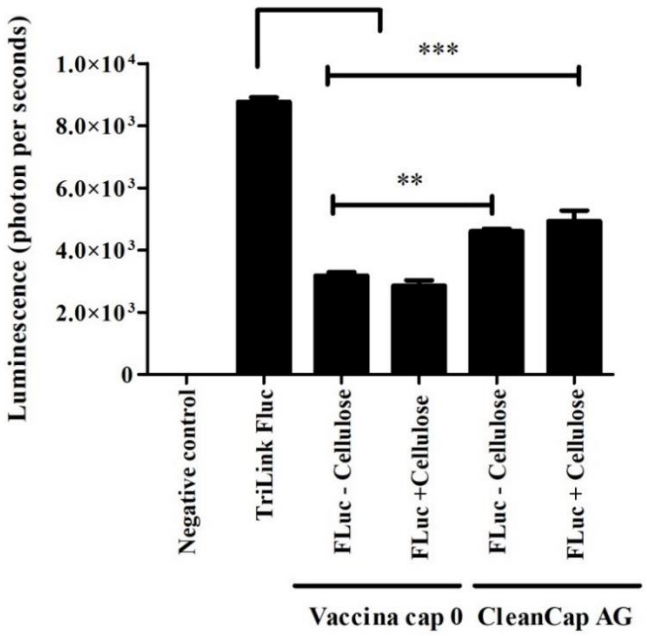

Figure 3.18: Effects of modified nucleotides, purification, and capping strategies on IVTed mRNA. (**A**) pT7-Luc2 was linearised with *Bbs*I overnight prior to IVT. (**B-C**) pmRNA-GFP and pT7-Luc2 mRNA was IVTed using 100% ψ and NEB individual IVT components. The mRNA was either post-transcriptionally capped (Cap 0) using the Vaccinia Capping System or co-transcriptionally capped with TriLink CleanCap® AG and subsequently purified using cellulose. (**D**) Analysis of GFP expression, GFP-mRNA variants, including Vaccinia-capped, Vaccinia-capped and cellulose-purified, CleanCap® AG, and CleanCap AG cellulose-purified mRNA, were transfected into Huh7 cells. GFP expression was assessed twenty-four hours after transfection to evaluate the effect of different capping and purification methods (**E**) Luminescence from Huh7 cells transfected with TriLink-FLuc mRNA, Luc2-mRNA variants Vaccinia-capped, Vaccinia-capped and cellulose-purified, CleanCap® AG, and CleanCap AG cellulose-purified, and a negative control mRNA was measured twenty-four hours post-transfection. Statistical significance is indicated by *** ($p < 0.001$).

3.5.2 Transcriptional repression of HBsAg secretion by anti-HBV DEM mRNA

Based on the preceding results achieved with reporter mRNA, active pmRNA-DEMs were IVTed using NEB individual components for IVT, TriLink buffer, complete substitution of uridine with ψ and RNA was co-transcriptionally capped with TriLink CleanCap AG (Figure 3.19 A). Following IVT of DEM mRNA, RNA was cellulosed purified. To evaluate the efficacy of IVTed DEM-mRNA on transcriptional silencing of viral replication, Huh7 cells were initially transfected with an HBV replication competent pCH-9/3091 plasmid, this was followed by transfection of each respective individual SR, SL, CR, CL, PR and PL DEM mRNA or Luc2-encoded mRNA which served as the mock transfection. Twenty-four hours after transfection supernatants of HBsAg levels was assessed using ELISA.

Results show HBsAg was significantly reduced compared to mock-treated cells for the first time when IVTed anti-HBV DEMs were used (Figure 3.19 B). Statistically significant silencing of 8%, 11% and 23 % was achieved with CR, CL and PL DEM-encoding mRNA. The lack of repression by the S DEMs was unexpected as anti-HBV S DEM expressed from plasmid DNA was able to show reduced serum concentration of HBsAg by 90%. The reduced HBsAg by previously discussed CR, CL and PR-encoding mRNA suggests that these DEMs are silencing the preS1 and preS2 promoters inhibiting the production of viral surface protein. Results also suggests that possible methylation of CpG II and CpG III could be occurring. This is because the P DEM targets the *P* ORF and enhance I, this region overlaps with CpG II, while the *C* DEM targets the *C* ORF, which is situated close to the Sp1 promoter and overlaps with CpG III. The reduced HBsAg secretion observed was not due to cytotoxicity as demonstrated by no difference in cell viability of cells transfected with DEM mRNA and untransfected cells (Figure 3.19 C).

In conclusion, IVT with NEB components, modified nucleotide ψ, TriLink CleanCap® AG, and cellulose-based purification improved DEM protein expression by reducing mRNA immunogenicity and increasing stability. DEM expressed from mRNA was able to achieve transcriptional repression of HBV; however, its expression was significantly lower compared to its DNA counterparts. Furthermore, the TriLink FLuc mRNA enhanced expression compared to Luc2 mRNA indicates that further optimisation of the IVT process is necessary to enhance efficacy of in house IVTed mRNA.

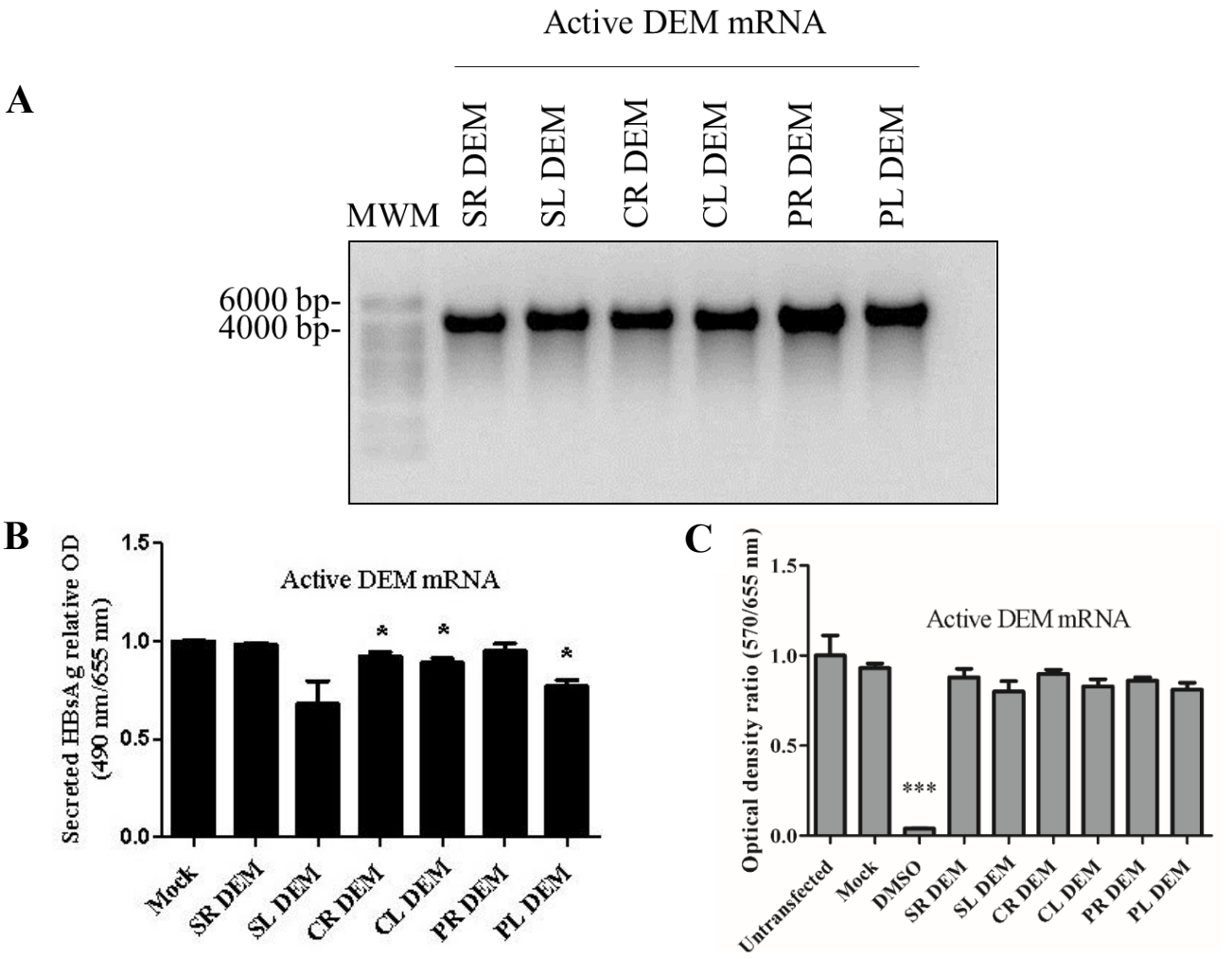

Figure 3.19: Effects of modified nucleotides, purification, and capping on IVTed DEM mRNA. (**A**) pmRNA-DEMs were IVTed with 100% ψ substitution and using NEB individual IVT components. The mRNA was co-transcriptionally capped with TriLink CleanCap® AG and subsequently purified using cellulose purification (**B)** Effects of IVTed DEM mRNA on HBsAg expression was evaluated after twenty-four hours after transfection into Huh7 cells. (**C**) To assess potential DEM mRNA cytotoxicity, an MTT assay was conducted twenty-four hours after transfection of mRNA. DMSO served as the positive control while untransfected cells acted as the negative control. All transfections were performed in triplicate (n = 3), and data were normalised to the untransfected control. Statistical significance is represented by, * indicates $p < 0.05$ and ***indicates $p < 0.001$.

3.6 Utilisation of second mRNA expression vector: pT7-(AG)

The limited transcriptional silencing of DEM mRNA expressed from the pmRNA expression vector suggests that this vector may be inefficient for expressing more complex transgene sequences. In contrast, simpler transgene reporter sequences like GFP were effectively expressed from the same pmRNA expression cassette. This indicates that while less complex sequences can be successfully expressed, more complex transgenes like DEM face challenges. Notably, the DEM DNA counterparts were functional and successfully reduced HBsAg levels, highlighting the functionality of the therapeutic potential of DEMs. As a result, a second mRNA expression vector termed pT7-(AG) was employed. The pT7-(AG) expression vector was used to encode several transgene mRNA sequences producing favourable results regardless of the specific sequence employed (unpublished work by Dr Kristie Bloom). Structurally the pT7-(AG) plasmid differs from the pmRNA in several aspects, as it contains different (i) regulatory 5' and 3' UTRs sequences, (ii) poly A tract of 120 bases and (iii) inclusion of four stop codons downstream of the transgene. Based on this, active DEM and DEMΔKRAB transgenes were cloned into the pT7-(AG) plasmid. The pT7-(AG) plasmid was designed in such a way as to allow any transgene sequence can be cloned into the mRNA expression plasmid however, this required a fragment sequence to be designed with the relevant restriction enzyme sites to be subcloned into pT7-(AG) plasmid for downstream cloning.

The ECS-fragment was designed with the same 5' UTR sequence as pT7-(AG) and included an upstream *Nde*I restriction site for convenient cloning. It is also designed to contain *XhoI*, *Apa*l, and *Bam*HI sites for inserting HA-tag and DEM transgene sequences, followed by four stop codons and *Bsa*I type IIS sites downstream to generate complementary overhangs for *Esp*3I overhang present in the pT7-(AG) backbone (Chapter 2, Figure 2.4). The ECS-fragment was synthesised by GenScript in a pUC57 mini plasmid, termed pUC57-ECS (Appendix, Figure 5.9). After double digestion with *Nde*I and *Bsa*I, the pUC57-ECS plasmid yielded an insert of 498 bp (Appendix, Figure 5.10), while the pT7-(AG) plasmid produced a 3133 bp fragment for ligation of insert (Appendix, Figure 5.11). The ECS-fragment was then subcloned into the pT7-(AG) backbone, generating the pT7(AG)-ECS 4×S plasmid. Screening with *Apa*I, *Ava*II, *Bam*HI, *Xho*I, *Bgl*I, and *Nde*I confirmed successful subcloning with the expected banding patterns (Appendix, Figure 5.11 A)

3.6.1 Generation of pT7(AG)-DEM 4× S constructs

The pT7(AG)-ECS 4×S plasmid, containing the necessary restriction sites for cloning DEM transgene sequences, served as the final destination backbone. After double digestion with *Esp*3I and *Apa*l, the plasmid yielded a 3610 bp backbone fragment (Appendix, Figure 5.11 B). In separate reactions, six active pmRNA-SR, -SL, -CR, -CL, -PR and -PL DEM plasmids double digested with *Nco*I and *Xho*l yielded 680 bp band corresponding to HA-KRAB with a short section of the TALE HA-KRAB-TALE (TALE 362 bp) (Appendix, Figure 5.12). While digestion with *Xba*I and *Apa*I excised 3640 bp band corresponding to TALE-DNMT-encoding sequences (Appendix, Figure 5.13), which were ligated into the pT7(AG)-ECS 4×S plasmid. This produced pT7(AG)-DEM 4×S plasmids (pT7(AG)-SR, -SL, -CR, -CL, -PR and -PL DEM 4×S) (Figure 3.20). Screening with *Nco*I, *Xho*I, *Nhe*I, and *Xba*I confirmed successful cloning with expected banding patterns achieved with all six DEMs (Figure 3.20). Active SR, SL and PL DEM without the KRAB domain expression from pT7-(AG) was generated and termed pT7(AG)-DEMΔKRAB 4×S (pT7(AG)-SR, -SL, and -PL DEMΔ KRAB4×S) (Appendix 5.9.3, Figure 5.14).

The constructed plasmids, pT7(AG)-DEM 4×S and pT7(AG)-DEMΔKRAB 4×S plasmids are schematically represented in Chapter 2, Figure 2.6. The plasmids have a total size of 7930 bp and 7725 bp, respectively. Similar to the pmRNA expression plasmids, both plasmids contain a CMV promoter/enhancer driving protein expression, a T7 promoter for mRNA synthesis, and an HA sequence followed by an SV40 nuclear localization signal. Both plasmids contain necessary sequence elements for IVT and intracellular translation, including a 5' UTR with Kozak sequence, 3' UTR, poly(A) tract, four stop codons after transgene sequence and a *Bbs*I restriction site for plasmid linearisation. The constructed pT7(AG)-DEM 4×S plasmids were sequenced to ensure the transgene sequences were present and did not contain any mutated sequences (Appendix Table 5.6, Figure 5.16- S1.18).

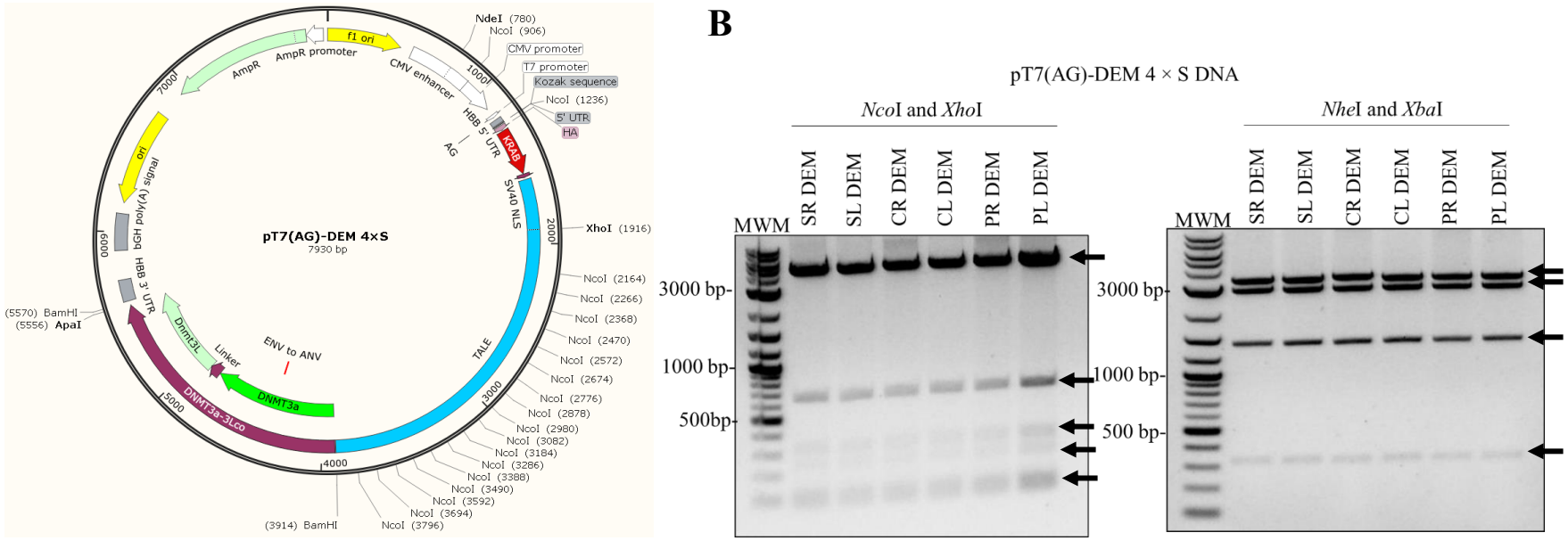

Figure 3.20: Confirmation of active pT7(AG)-DEM 4×S plasmid DNA by enzymatic digestion. (**A**) Active pT7(AG)-DEM 4×S plasmids were constructed by inserting KRAB and TALE domain-encoding sequences, along with DNMT domain-encoding sequences, into the pT7(AG)-ECS 4×S RNA expression vector. (**B**) Restriction digestion of active pT7(AG)-DEM 4×S plasmids with *Nco*I and *XhoI* produced expected bands of 5040 bp, 680 bp, 330 bp, 248 bp, and 102 bp (indicated by arrows). While digestion with *Nhe*I and *Xba*I yielded bands of 3336 bp, 2790 bp, 1471 bp, and 333 bp, with the 333 bp band confirming the presence of the KRAB domain. Lane 1 shows the molecular weight marker (O'GeneRuler DNA Ladder Mix).

3.7 Characterisation of pT7(AG)-DEM 4×S plasmids in vitro

3.7.1 Expression of anti-HBV DEM-encoding plasmids in cultured cells

Initially, pT7(AG)-DEM 4×S plasmid DNA expression, anti-HBV efficacy and cytotoxicity was assessed in cultured liver-derived Huh7 cells before IVT of DEMs. To evaluate pT7(AG)-DEM 4×S constructs with and without the KRAB domain expression, Huh7 cells were transiently transfected with plasmid DNA consisting of either pT7(AG)-SR, -SL, -CR, -CL, -PR and -PL DEM 4×S or pT7(AG)-SR, -SL and -PL DEMΔKRAB 4×S plasmids as well as reporter plasmids pT7-mCherry which served as the negative control(mock). Additionally, pT7-mCherry also served to assess transfection efficiency, mCherry expression indicated good DNA transfection efficiency (Figure 3.21). Expression was observed in both the cytoplasm, with the majority in the nucleus of cells transfected with anti-HBV DEM DNA with (Figure 3.21 A) and without KRAB domain (Figure 3.21 B) compared to the mock (pT7-mCherry) transfected cells. These results align with observations made with anti-HBV DEMs expressed in pmRNA-pA vectors (Figure 3.15 A, B).

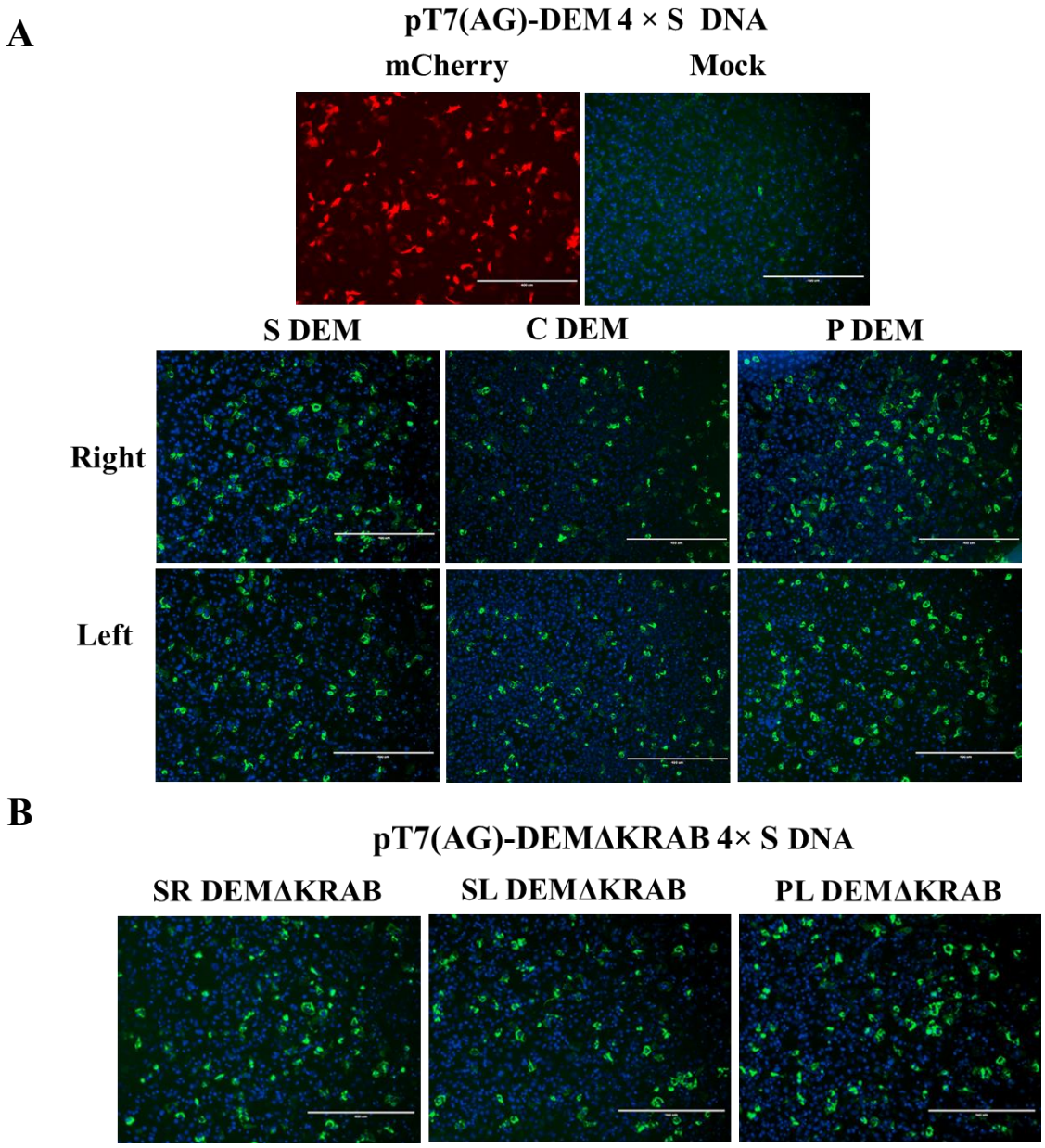

Figure 3.21:Immunofluorescence detection of pT7(AG)-DEM 4×S plasmid DNA *in vitro*. Immunofluorescence staining of Huh7 cells transfected with pT7-mCherry DNA (mock transfection) and individual active DEM DNA with or without KRAB domain was performed to examine expression of HA-epitope *in vitro*. (**A**) pT7(AG)-DEM 4×S (**B**) pT7(AG)-DEMΔKRAB 4×S. In parallel, cells were transfected with pT7-mCherry served to determine transfection efficiency. A mouse anti-HA primary antibody in conjunction with a fluorescently labelled goat anti-mouse secondary antibody was used for detection of HA-tag (green), while the nuclei were

stained with DAPI (blue). Fluorescence microscopy was used to visualise cells at 20× magnification.

3.7.2 Plasmid DNA expressing anti-HBV DEM from the pT7(AG)-DEM 4× S vector shows no cytotoxicity

Before evaluating efficacy of DEMs at transcriptionally silencing viral surface antigen, a marker of HBV replication, an MTT assay was preformed to assess whether DEM expressed from DNA induces any cytotoxic changes within cells after transfection. Huh7 cells were co-transfected with individual pT7(AG)-SR, -SL, -CR, -CL, -PR and -PL DEM 4×S plasmid DNA and with pCH-9/3091, and the results showed no significant difference in cell viability between untransfected, mock-transfected, and DEM plasmid -transfected cells, indicating no cytotoxicity was induced (Figure 3.22 A). When assessing transcriptional repression, a significant reduction in HBsAg expression mediated by pT7(AG)-SR, -SL, -CR, -CL, -PR, and -PL was observed, with decreases of 44%, 74%, 69%, 56%, 46%, and 80%, respectively. (Figure 3.22 B). Notably, SL and PL DEMs showed the most substantial reduction in surface antigen concentrations, and it is most likely these DEMs are silencing the key regulatory elements such as pre-S1 and pre-S2 promoters, enhancer I and could be causing methylation of CpG islands, inhibiting the production of viral surface protein. These findings suggest that pT7(AG)-DEM 4×S plasmid DNA, particularly pT7(AG)- SL and PL DEMs, are effective in silencing HBV surface proteins, and the observed reductions are not due to cytotoxic effects.

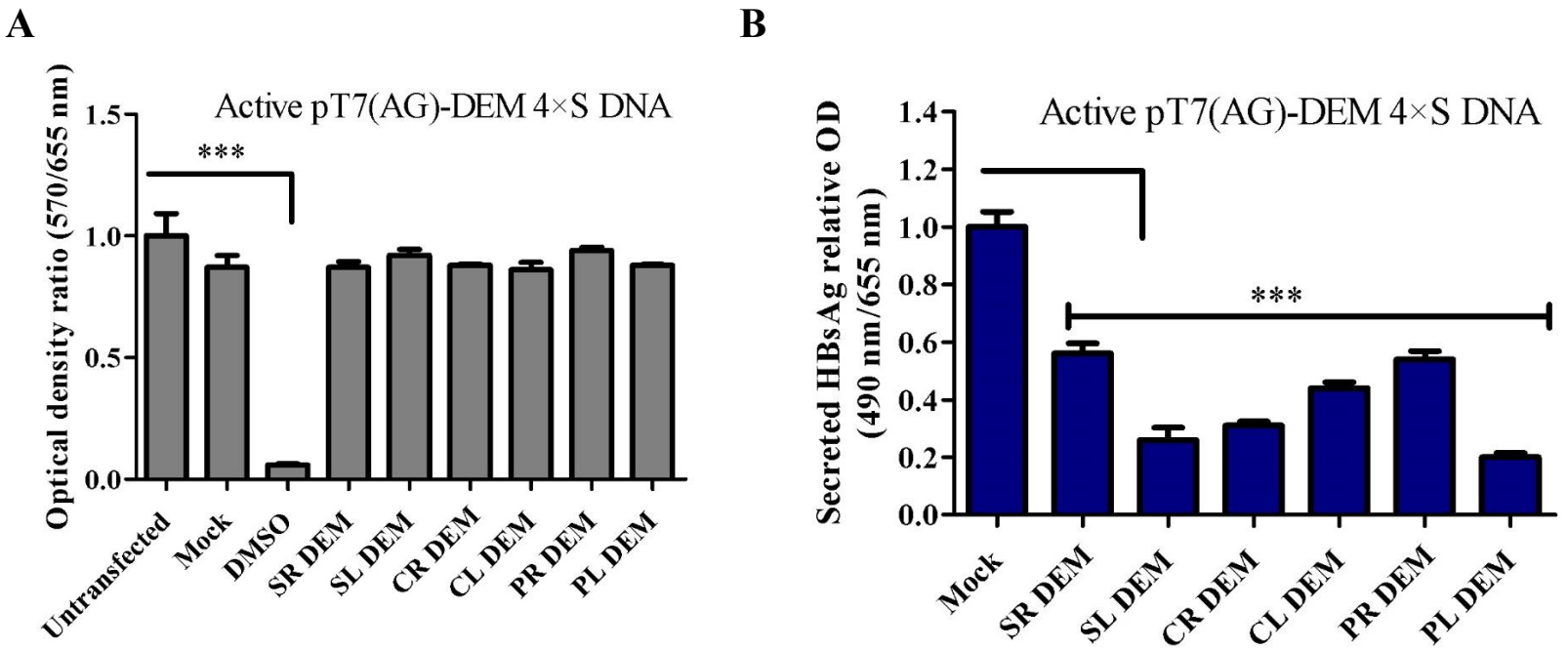

Figure 3.22: Anti-HBV DEM DNA expressed from the second RNA expression vector. Huh7 cells were co-transfected with the pCH-9/3091 replication-competent plasmid and pT7(AG)-DEM 4×S plasmids. (**A**) An MTT assay was performed, with DMSO serving as the positive control; data were normalised to the untransfected control. (**B**) An ELISA demonstrated that DEM-encoding plasmids mediated a significant reduction in viral surface HBsAg after transfection. Both assays were performed forty-eight hours after transfection in triplicate, and error bars indicate the SEM (n=3). Statistical significance is indicated as follows: ** $p<0.01$; *** $p<0.001$.

3.7.3 Anti-HBV DEM mRNA produced from the pT7-DEM 4× AG vector effectively mediates the expression

Active pT7(AG)-DEM 4×S plasmids (Figure 3.23 A) were linearised by *Bbs*I restriction digestion, while pT7-mCherry (Figure 3.23 B) was linearised by *Bsa*I restriction digestion. DNA templates linearised using *Bbs*I were highly efficient as complete linearisation occurred as indicative by the presence of a single band for each respective DEM DNA template (Figure 3.23 A). Whereas linearisation-using *Bsa*I was less efficient as some smearing of the pT7-mCherry DNA can be observed nonetheless a single band is present (Figure 3.23 B).

Anti-HBV pT7(AG)-DEM 4×S (Figure 3.23 C) and reporter-encoding plasmids (pmRN-eGFP, pT7-Luc2, and pT7-mCherry) (Figure 3.23 D) were IVTed using NEB individual components with TriLink AG buffer, 100% modified nucleotides were incorporated using ψ. All transcribed RNA were co-transcriptionally capped using TriLink CleanCap® AG, purified using cellulose-based chromatography after IVT ensuring removal of contaminating dsRNA, and recovered using LiCl precipitation. Agarose gel electrophoresis indicates single IVTed mRNA products were obtained for each respective active DEM, Luc2 and eGFP–encoding mRNA indicating successful IVT at the expected sizes. While two additional bands can be seen with the mCherry mRNA indicating poor IVT however, the main prominent band is present at the correct size of 708 bp (Figure 3.23 D).

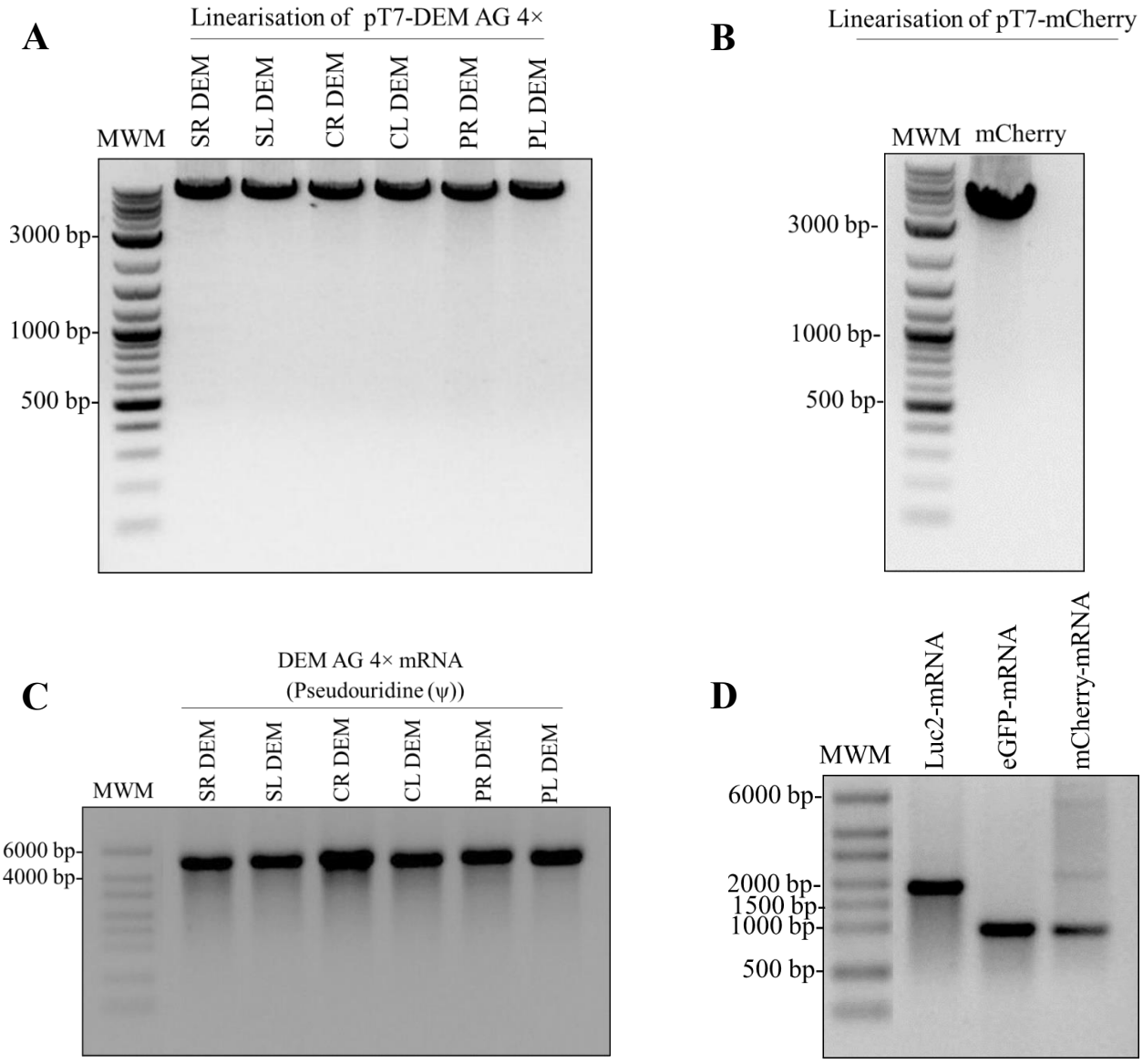

Figure 3.23:Linearisation and IVT of pT7(AG)-DEM 4×S and reporter pT7-mCherry encoding plasmids. (**A**) Active pT7(AG)-DEM 4×S plasmid DNA were linearised by *Bbs*I restriction digestion while (**B**) pT7-mCherry plasmid linearised by *Bsa*I restriction digestion. Lane 1: MWM, Molecular weight marker (O'GeneRuler DNA Ladder Mix). (C-D) IVTed RNA (**C**) pT7(AG)-DEM 4×S and (**D**) reporter DNA, pT7-Luc 2, pmRNA-GFP and pT7-mCherry. IVT reaction included complete substitution of uridine with ψ and was co-transcriptionally capped with TriLink CleanCap® AG. Transcribed RNA was cellulose-purified and recovered with LiCl precipitation. IVTed mRNAs were visualised by 1% agarose gel electrophoresis. Lane 1: MWM, RiboRuler HR RNA ladder.

3.7.4 Immunohistochemical detection of HA-tag from active DEM mRNA expressed from the pT7(AG)-DEM 4×S vector

When active anti-HBV DEMs were expressed using the pmRNA system in cultured cells, no HA-tag expression was detected (Figure 3.11 A). However, removing the KRAB domain restored HA-tag detection and enhanced expression compared to mock-transfected cells (Figure 3.13 A). Consequently, the expression of active DEMs with and without the KRAB domain (pT7(AG)-DEM 4×S and pT7(AG)-DEMΔKRAB 4×S) was analysed using immunohistochemistry.

Huh7 cells were transfected with various pT7(AG)-DEM 4×S-encoded mRNAs with (Figure 3.24 A) or without KRAB domain (Appendix, Figure 5.19). Cells transfected with mCherry mRNA served as a negative control for immunohistochemistry and for evaluating transfection efficiency. Fluorescence microscopy confirmed successful transfection evident by mCherry expression. Results showed no significant difference between the mock mCherry-transfected cells, which exhibited no detection of HA-tag, and active IVTed DEMs containing the KRAB domain (Figure 3.24 A). However, the removal of the KRAB domain in pT7(AG)-DEM 4×S restored detection of DEM-mRNA expression in liver-derived cells, showing strong expression compared to mock-transfected cells (Appendix, Figure 5.19). These findings align with observations from IVTed DEMs expressed from the pmRNA-pA backbone. Since a monoclonal primary mouse anti-HA antibody was used to detect the HA-tag and monoclonal antibodies are known for their specificity in binding a single epitope, a polyclonal anti-HA antibody, which can recognise and bind to a broader range of epitopes, was employed for the immunohistochemical detection of HA-tag. The results reveal, for the first time, the detection of the HA-tag in all active DEMs containing the KRAB domain. Strong expression was observed in all DEMs except for the CR DEM, with the majority of the expression localised in the nucleus, as expected for DEMs to perform their functions (Figure 3.24 B). These results support the theory that some HA-tag epitopes may be obscured, affecting detection with monoclonal antibodies compared to polyclonal antibodies, as monoclonal antibody was able to detect the HA-tag expression with active DEM plasmid DNA with the KRAB domain not when it is IVTed, indicating there's a distinction between folding of IVTed mRNA and *in situ* mRNA.

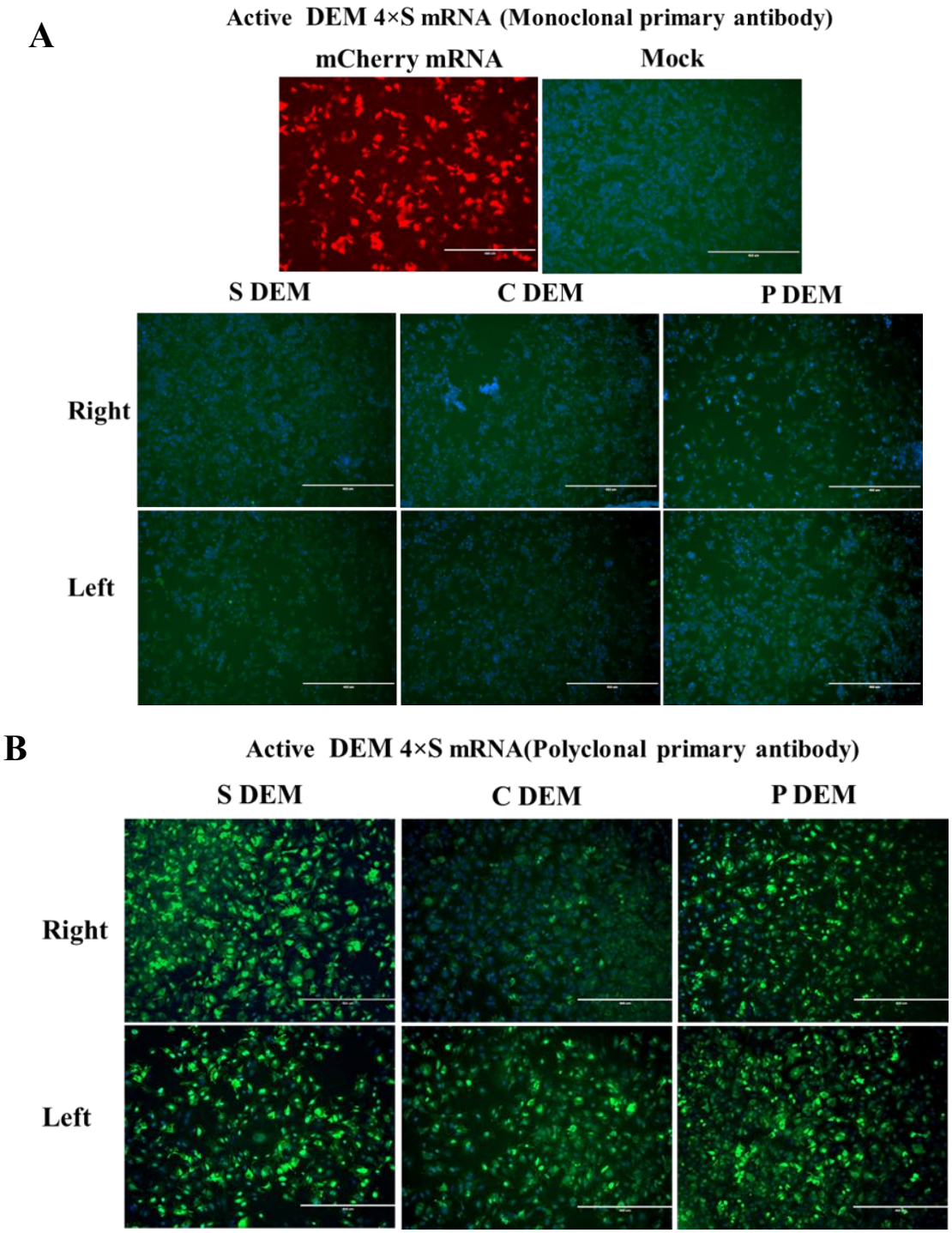

Figure 3.24: Immunofluorescence Detection of Active DEM mRNA in Huh7 Cells. Huh7 cells were transfected with either mCherry mRNA (mock) or active DEM mRNA to examine HA-epitope expression. (**A**) Monoclonal mouse anti-HA antibody with a fluorescently labelled goat anti-mouse secondary antibody; (**B**) Polyclonal rabbit anti-HA antibody with a fluorescently labelled goat anti-rabbit secondary antibody. Transfection efficiency was assessed using pT7-

mCherry. HA-tag detection (green) utilised anti-HA antibodies, and nuclei were stained with DAPI (blue). Fluorescence microscopy was performed at 20× magnification

3.8 Anti-HBV DEM mRNA expressed from the pT7(AG)-DEM 4×S vector effectively mediates transcriptional silencing of HBV

3.8.1 Active DEM mRNA mediates transcriptional silencing of HBV viral surface proteins

To assess whether incorporating anti-HBV DEMs into the new RNA expression system improved IVTed mRNA quality, efficacy of anti-HBV IVTed DEMs mRNA in cultured cells was evaluated. Several studies have shown that pseudouridine (ψ), N1-methylpseudouridine (m1ψ), and 5-methoxyuridine (5moU) enhance mRNA functionality (Karikó et al., 2008, Andries et al., 2015, Moradian et al., 2022). To optimise IVTed DEM mRNA expression, these modifications were included in IVT reactions (Appendix, Figure 5.20 A). Huh7 cells were initially transfected with the HBV replication-competent plasmid pCH-9/3091, followed by individual transfections of pT7(AG)-SR, -SL, -CR, -CL, -PR, and -PL DEM 4×S-encoding mRNA. Luc2 mRNA was used as a negative control. An ELISA was conducted twenty-four hours after transfection.

Results show transcriptional silencing of HBsAg was achieved with all IVTed anti-HBV DEM containing all the modified nucleotides (ψ, m1ψ, and 5moU). Anti-HBV DEM mRNA IVTed with ψ reduced HBsAg the greatest, reducing expression by 42%, 53%, 41%, 31%, 42%, and 60% compared to the control (Figure 3.25 A). In comparison, DEM mRNA IVTed with m1ψ achieved reductions of 49%, 56%, 24%, 13%, 45%, and 44% in HBsAg levels compared to the control (Figure 3.25 B). This contrasts with previously reported studies indicating a significant increase in mRNA functionality with m1ψ (Andries et al., 2015). DEM mRNA IVTed with 5moU achieved the lowest reduction in surface antigen compared to the other modified nucleotides, with reductions of 24%, 40%, 32%, 21%, 44%, and 26% in HBsAg levels (Figure 3.25 C). Interestingly, regardless of the modified nucleotide used to in vitro transcribe DEM plasmid DNA, PL DEM showed the greatest reduction in viral surface protein, followed by SL DEM. Furthermore, CL DEM mRNA, when IVTed with m1ψ and 5moU modifications, showed no significant reduction in surface antigen levels. This lack of reduction observed with CL DEM mRNA could be due to errors that occurred during the IVT process for this specific DEM.

Overall, the results demonstrate that ψ was more effective at reducing HBsAg levels compared to m1ψ, which differs from previously published results (Andries et al., 2015) that reported m1ψ-containing mRNA outperformed ψ and 5moU-containing mRNA.

Additionally, to further improve the transcriptional silencing effect on surface antigen, double transfection of DEM mRNA was performed. DEM mRNA was IVTed with complete substitution of uridine with ψ, as this modification achieved the greatest silencing of viral surface protein. Huh7 cells were first transfected with the replication-competent pCH-9/3091 plasmid, followed by two rounds of transfection with DEM mRNA approximately 6 hours apart. HBsAg was assessed twenty-four hours after transfection. An enhanced reduction of HBsAg of 78%, 81%, 74%, 70%, 79%, and 84% was achieved by SR, SL, CR, CL, PR, and PL DEM compared to the mock-transfected mRNA (Figure 3.25 D). The double transfection of DEM improved the reduction of surface antigen across all DEMs. Evaluating the therapeutic activity of DEM mRNA in this model has been challenging due to the high levels of surface antigen expressed by the HBV replication-competent pCH-9/3091 plasmid. Assessing HBsAg beyond twenty-four hours was problematic because the plasmid continuously expresses high levels of surface antigen, well reduction of 5%, 10%, 4%, 4%, 2%, and 8% was achieved by SR, SL, CR, CL, PR, and PL DEM at forty-eight hours, results demonstrated diminished transcriptional silencing (Appendix, Figure 5.20 B).

Overall, the results suggest that all DEMs influence protein production, likely by affecting the pre-S1, pre-S2 promoters, and enhancer I, as previously mentioned. Additionally, expressing DEM mRNA from the pT7-(AG) expression vector allowed IVTed mRNA to achieve greater efficacy compared to its DNA equivalents following double transfection. These findings align with previous studies demonstrating the significance of the 5' and 3' UTRs of mRNA, as well as the length of the poly(A) tail, in influencing mRNA stability and translational efficiency.

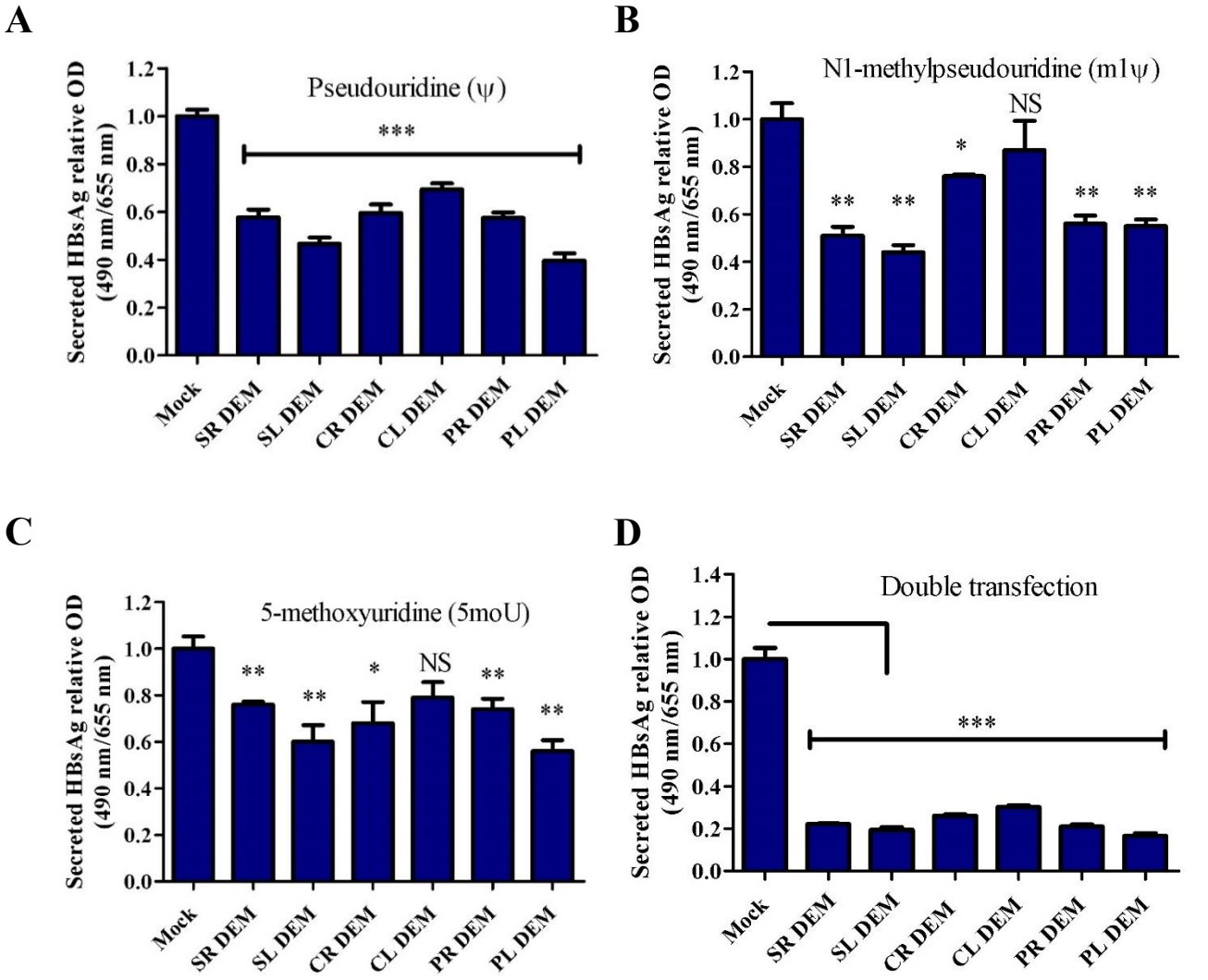

Figure 3.25: Transcriptional silencing of HBsAg by anti-HBV DEM mRNA expressed from the pT7(AG)-DEM 4×S vector. DEMs were IVTed with a complete substitution of uridine using (**A**) ψ, (**B**) m1ψ, and (**C**) 5moU. The efficacy of DEM mRNA was evaluated in Huh7 cells transfected with an HBV replication-competent pCH-9/3091 plasmid. Huh7 cells transfected with pUC118 served as a control. HBsAg levels were assessed twenty-four hours after a single mRNA transfection (**A-C**). (**D**) The efficacy of DEM mRNA, fully substituted with ψ, was evaluated after a double mRNA transfection in Huh7 cells. All transfections were performed in triplicate (n = 3) and were normalised to the mock transfection. Statistical significance is indicated as follows: * corresponds to $p < 0.05$, ** to $p < 0.01$, *** to $p < 0.001$, and NS represents non-significant results.

3.8.2 Transcriptional silencing of HBV transcription mediated by anti-HBV DEM mRNA produced from the pT7(AG)-DEM 4×S vector

HBV *surface* and pgRNA transcripts are crucial for viral replication and persistence. pgRNA serves as a template for reverse transcription, producing rcDNA, the precursor for cccDNA, while surface transcripts facilitate the expression of viral proteins needed for new virion production. To assess the effect of anti-HBV DEM-mRNA on HBV *surface* and pgRNA expression, Huh7 cells were first transfected with the HBV replication-competent pCH-9/3091 plasmid, which expresses the necessary viral subgenomic and pgRNA mRNAs. Following this, the cells were transfected twice with DEM mRNA, while Luc2-mRNA served as a mock control. Twenty-four hours post-transfection, total RNA was extracted and treated with DNase to eliminate plasmid and genomic DNA. The RNA was reverse transcribed into cDNA and amplified via real-time PCR using specific primers for HBV surface, pgRNA, and the housekeeping gene *human hypoxanthine-guanine phosphoribosyltransferase* (hHPRT). The absence of contaminating plasmid and genomic DNA was determined by evaluating the Ct values from no reverse transcriptase (no RT) control reactions using housekeeping hHPRT primers (Appendix, Table 5.7). No RT control reactions with Ct values greater than 30, or at least five cycles higher than those of the experimental samples, were considered acceptable. The levels of viral *surface* and pgRNA mRNA were normalised to hHPRT mRNA.

Strong transcriptional silencing effects on viral *surface* and pgRNA transcript levels were caused by all the anti-HBV DEMs (Figure3.26). SR, SL, CR, CL, PR, and PL DEMs reduced *surface* transcript levels by 42%, 61%, 56%, 52%, 56%, and 70% respectively, compared to the mock control (Figure 3.26 A). pgRNA transcript levels were reduced by 62%, 71%, 69%, 70%, 70%, and 72% (Figure 3.26 B). Notably, the SL and PL DEMs achieved the greatest transcriptional repression of both viral transcripts compared to the other DEMs. The reduction in *surface* and pgRNA mRNA levels demonstrates that the S, C, and P DEMs are transcriptionally silencing expression from the pre-S1, pre-S2, and basic core promoter, which are exclusively responsible for the expression of *surface* and pgRNA mRNA. Overall, these results correlate with a reduction in viral surface antigen observed and this overall suggest that anti-HBVDEM are functionally capable of suppressing or silencing viral replication at the transcriptional level.

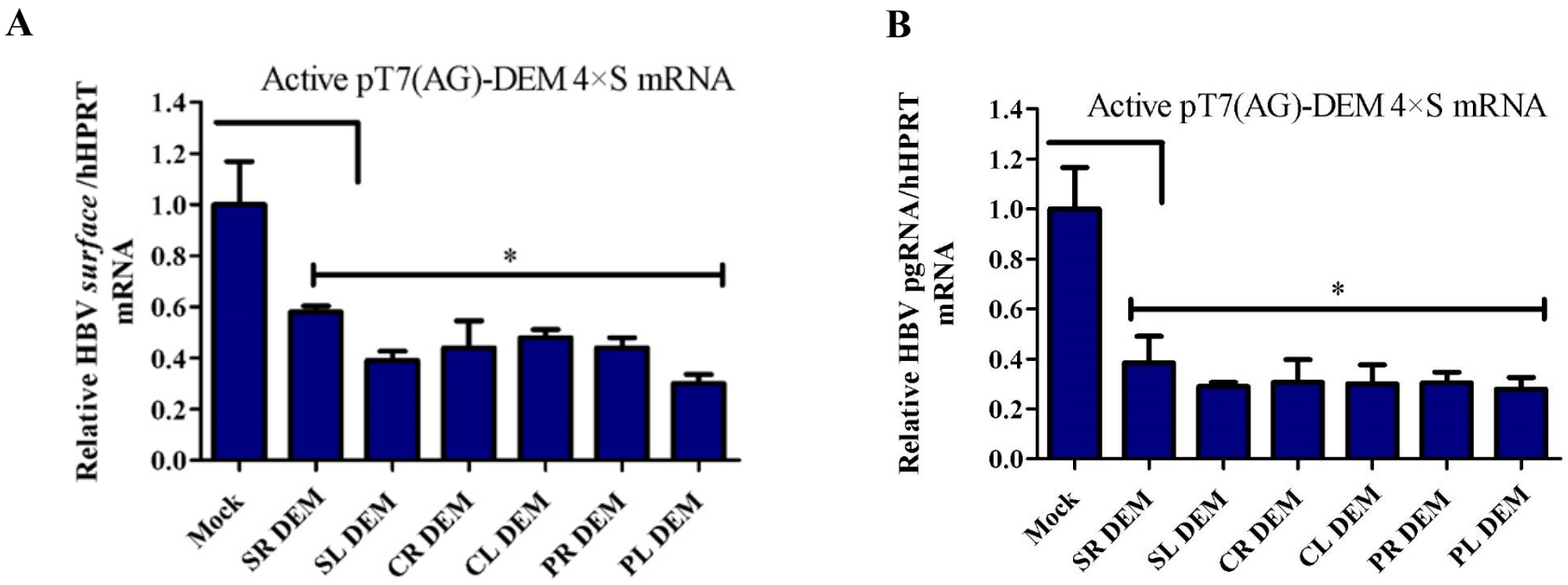

Figure 3.26: Assessment of anti-HBV DEM mRNA-mediated silencing of HBV viral transcripts *in vitro*. To assess the silencing effect of anti-HBV DEM on HBV transcripts, Huh7 cells were transfected with replication-competent pCH-9/3091 plasmid, followed by double transfection of individual DEM mRNA. Total RNA was extracted, reverse transcribed and HBV mRNA levels were measured relative to housekeeping gene hHPRT using RT-qPCR. (**A**)*Surface* mRNA and (**B**) pgRNA was measured twenty-four hours after transfection. All transfections were performed in triplicate (n = 3). Statistical significance is indicated by * corresponds to $p < 0.05$.

3.8.3 Targeted methylation of HBV CpG islands induced by DEMs

To assess whether the observed reduction in viral markers of replication was due to DNA methylation caused by anti-HBV DEMs, bisulphite sequencing of DNA was performed using Sanger sequencing. Huh7 cells were transfected with the replication-competent pCH-9/3091 plasmid, followed by double transfection with individual SL- or PL- DEM mRNA. Total DNA was then extracted, bisulphite-treated, and sequenced using bisulphite-specific primers designed for the three CpG islands. Sodium bisulphite treatment converts unmethylated cytosine to uracil, while methylated cytosine is preserved. During PCR amplification, the uracil (derived from unmethylated cytosine) is converted to thymine, whereas methylated cytosine (5mC) remains unchanged. This allows for the distinction between methylated and unmethylated cytosines. Sequencing results yielded mixed signals for all anti-HBV DEM-treated samples as well as the mock sample, likely due to incomplete bisulphite conversion or errors during Sanger sequencing. To visualise and interpret the results, chromatograms were evaluated. Specific residues with increased methylation (indicated by the increased proportion of cytosine) compared to the mock control were identified. The surface area of mixed peaks was calculated, and stacked histograms were generated to represent the distribution of peaks representing the ratio of cytosine to thymine at specific residues/sites in both control and DEM-treated samples.

The bisulphite sequencing results showed a clear trend in the proportion of cytosine to thymine in the SL and PL DEM-treated DNA compared to the mock (Figure 3.27). Schematic representation of the HBV genome with predicted CpG and DEM target sites (Figure 3.27 A). These trends suggest potential methylation at these residues and were observed with all three CpG islands I, II, and III (Figure 3.27 B-G). Notably, the increased proportion of cytosine within all three CpG islands I, II, and III with both SL and PL DEMs, indicating that DEMs can target their cognate sites and function over a long range, although the distribution is less prominent at CpG III in both SL and PL DEM-treated DNA compared to the mock. These findings are consistent with a previous study which demonstrated DEMs targeting HIV co-receptors CCR5 and CXCR4 were able to cause significant methylation at its target sites and were maintained for the duration of the investigation (18 days) (Mlambo et al., 2018). A recent study using CRISPR-Cas9 ribonucleoprotein (RNP) achieved 65% to 91% methylation of rcccDNA, a plasmid with HBV genotype D sequence cloned into a minicircle (Kostyushev et al., 2023).

SL DEM and PL DEM showed increased methylation at CpG II and CpG III (Figures 3.27 B - G). SL DEM exhibited higher cytosine proportions at residues 205, 207, and 304 in CpG I, while residues 1273, 1281, 1283, and 1284 had the highest proportions in CpG II (Figures 3.27 B - D). In CpG III, residues 2281, 2285, 2295, and 2304 were prominent for SL DEM (Figures 3.27 F). For PL DEM, the highest cytosine proportions in CpG I were found at residues 205, 243, and 264 (Figures 3.27 C), and in CpG II at residues 1252, 1258, 1263, 1273, and 1281 (Figures 3.27 E). Notably, residues 2281, 2291, 2294, and 2324 showed increased cytosine distribution in CpG III for PL DEM (Figures 3.27 G). These findings indicate a significant increase in cytosine distribution at CpG II, consistent with previous studies (Vivekanandan et al., 2008, Jain et al., 2015, Zhang et al., 2014). This assay was repeated with similar results (unpublished data, this research).

Despite the limitations of this assay, the results suggest that DEM-mediated methylation is occurring at specific CpG islands, potentially explaining the targeted epigenetic silencing of viral gene expression. However, improved methods for characterising and detecting DNA methylation are necessary to more accurately determine the extent of DNA methylation induced by anti-HBV DEMs.

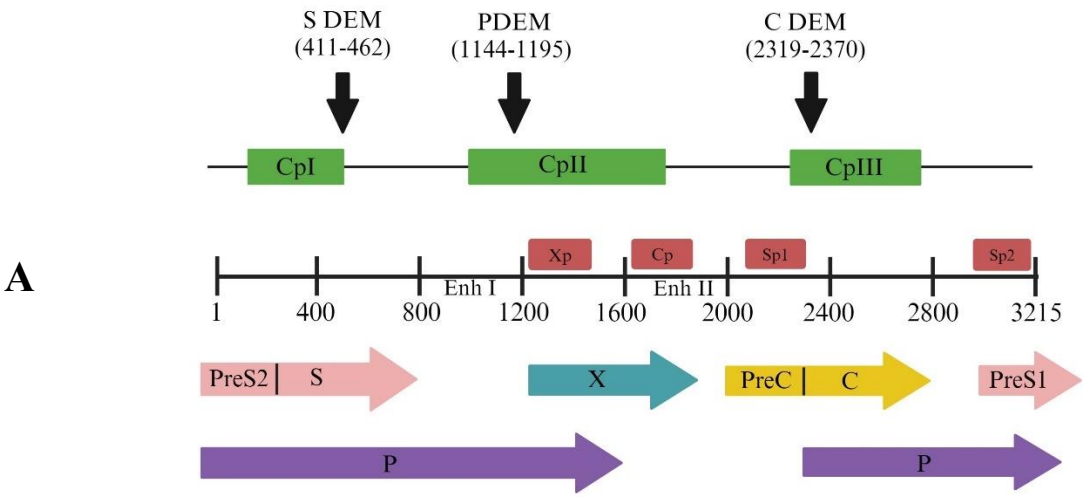
A
S DEM
(411-462)
PDEM
(1144-1195)
C DEM
(2319-2370)
CpI
CpII
CpIII
Xp
Cp
Sp1
Sp2
Enh I
Enh II
1
400
800
1200
1600
2000
2400
2800
3215
PreS2
S
X
PreC
C
PreS1
P
P

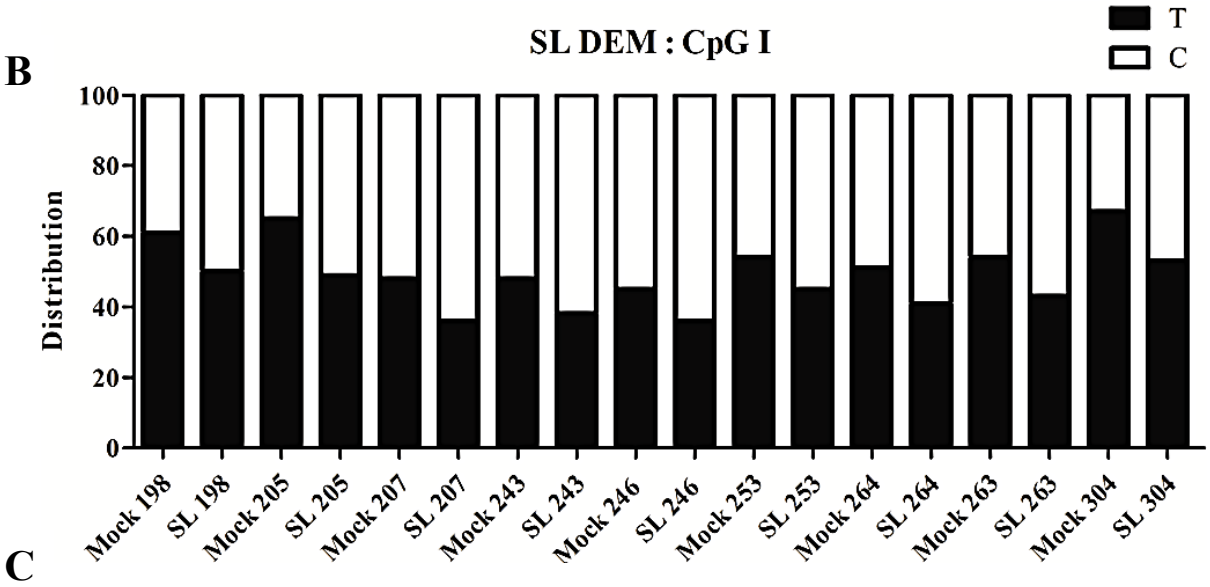
B
SL DEM : CpG I
T
C
Distribution
100
80
60
40
20
0
Mock 198
SL 198
Mock 205
SL 205
Mock 207
SL 207
Mock 243
SL 243
Mock 246
SL 246
Mock 253
SL 253
Mock 264
SL 264
Mock 263
SL 263
Mock 304
SL 304

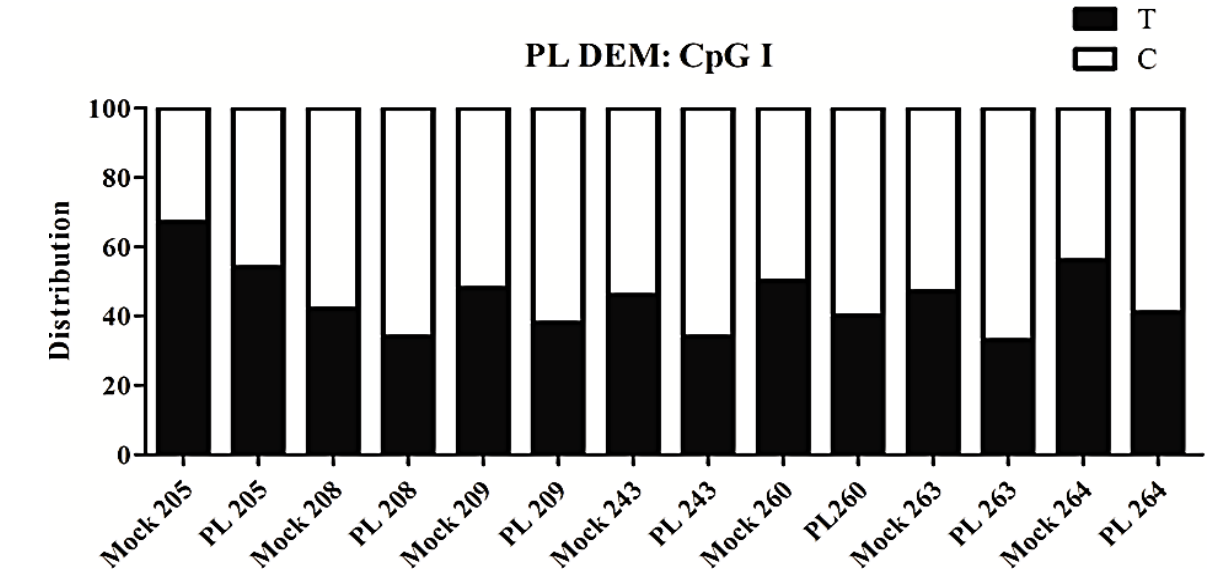
C
PL DEM: CpG I
T
C
Distribution
100
80
60
40
20
0
Mock 205
PL 205
Mock 208
PL 208
Mock 209
PL 209
Mock 243
PL 243
Mock 260
PL260
Mock 263
PL 263
Mock 264
PL 264

D

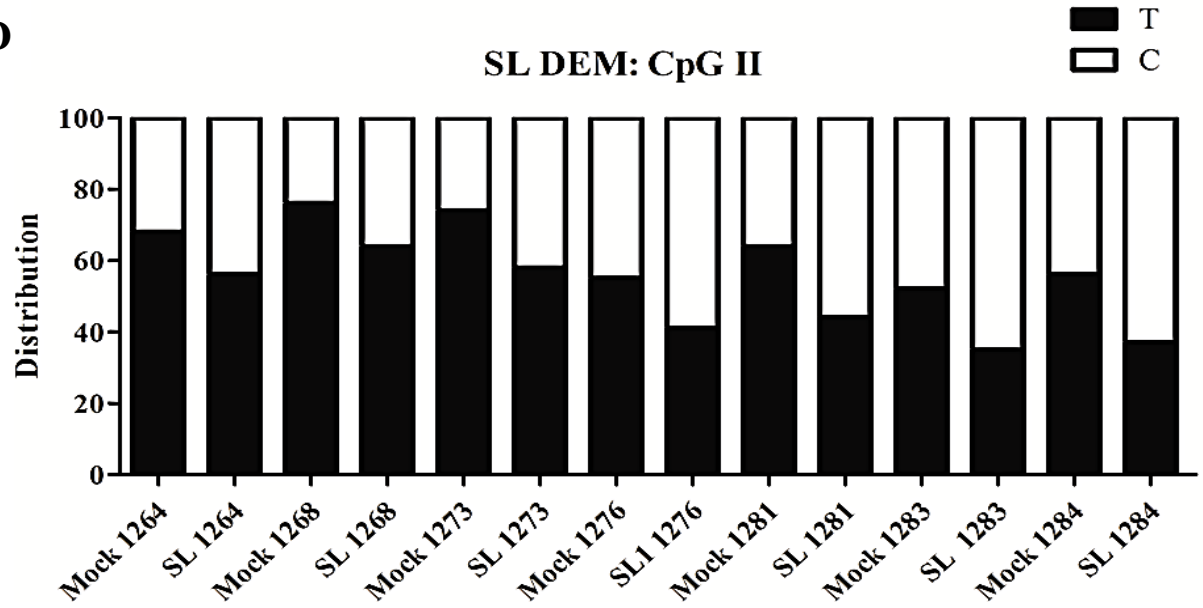
SL DEM: CpG II
T
C
Distribution
100
80
60
40
20
0
Mock 1264
SL 1264
Mock 1268
SL 1268
Mock 1273
SL 1273
Mock 1276
SL1 1276
Mock 1281
SL 1281
Mock 1283
SL 1283
Mock 1284
SL 1284

E

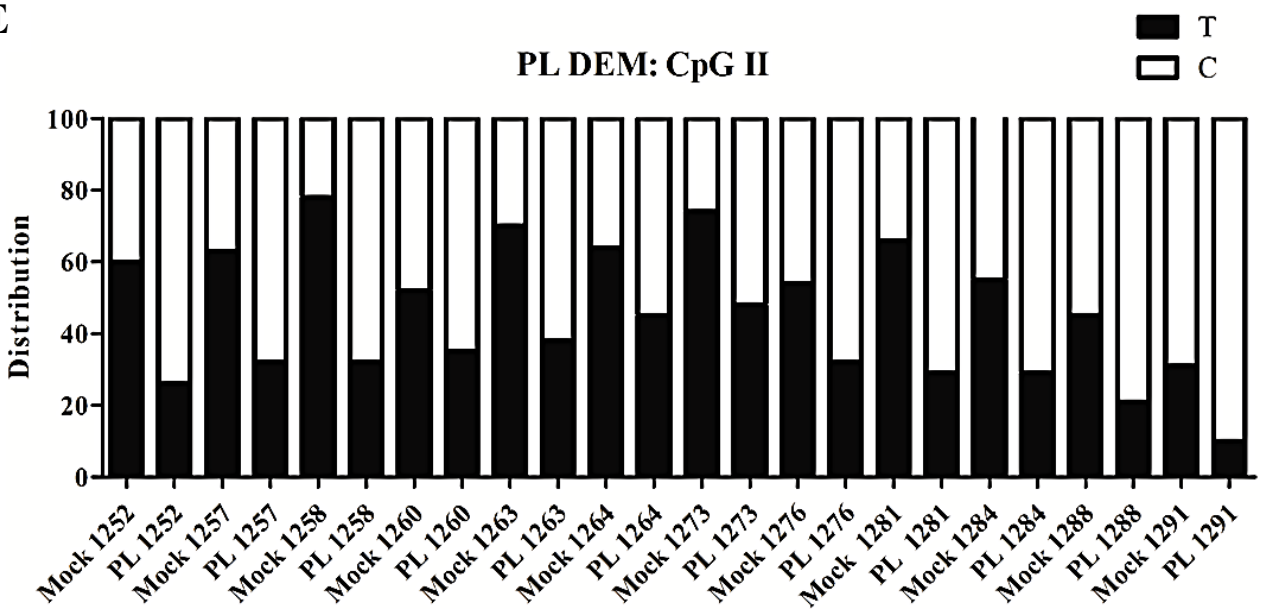
PL DEM: CpG II
T
C
Distribution
100
80
60
40
20
0
Mock 1252
PL 1252
Mock 1257
PL 1257
Mock 1258
PL 1258
Mock 1260
PL 1260
Mock 1263
PL 1263
Mock 1264
PL 1264
Mock 1273
PL 1273
Mock 1276
PL 1276
Mock 1281
PL 1281
Mock 1284
PL 1284
Mock 1288
PL 1288
Mock 1291
PL 1291

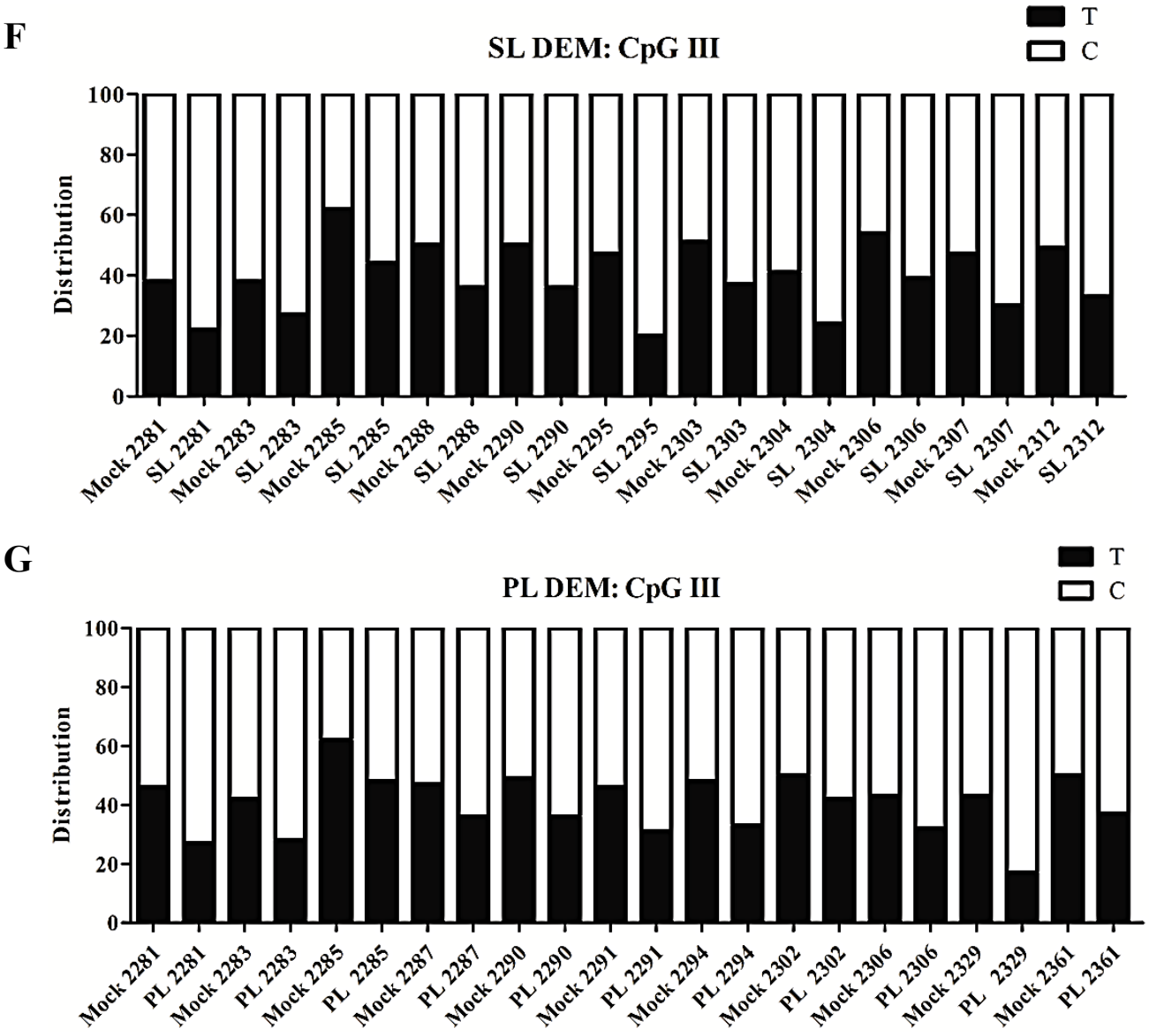

Figure 3.27: Potential methylation patterns in HBV CpG Islands I-III following DEM transfection in cultured cells. (**A**) Schematic representation of the HBV genome Highlighting CpG Islands and Anti-HBV DEM target sites (**B-F**) Huh7 cells were transfected with replication-competent pCH-9/3091 plasmid, followed by double transfection of individual DEM mRNA .Total DNA was extracted, subjected to sodium bisulphite treatment and sequenced using bisulphite-specific primers designed for the CpG I-III island The stacked histograms represent the proportions of Cytosine:Thymine at a base positions within the HBV genome in comparison to the mock-treated sample. The first T in the *Eco*RI site designated as position 1. (**B-C**) CpG I

for (**B**) SL DEM and (**C**) PL DEM, (**D-E**) CpG II for (**D**) SL DEM and (**E**) PL DEM, (**F-G**) CpG II (**F**) SL DEM and (**G**) PL DEM.

3.8.4 Anti-HBV DEMs does not exhibit cellular-mediated cytotoxicity

To eliminate the possibility that cytotoxic effects from transfections influenced the observed repression, an MTT assay was conducted to assess cell viability. Huh7 cells were double transfected with individual anti-HBV DEM mRNAs, with transfections conducted 6 hours apart. Untransfected cells served as a negative control, while Luc2-mRNA was used as a mock transfection control and DMSO as a positive control for assessing cytotoxicity. The MTT assay results showed no significant cellular toxicity in cells transfected with any of the anti-DEM-encoding mRNAs, as viability was comparable to untransfected cells. In contrast, DMSO-treated cells exhibited statistically significant toxicity. These results suggest that the transcriptional repression observed with the anti-HBV DEM mRNA is due to the activity of the DEMs rather than cellular toxicity (Figure 3.28)

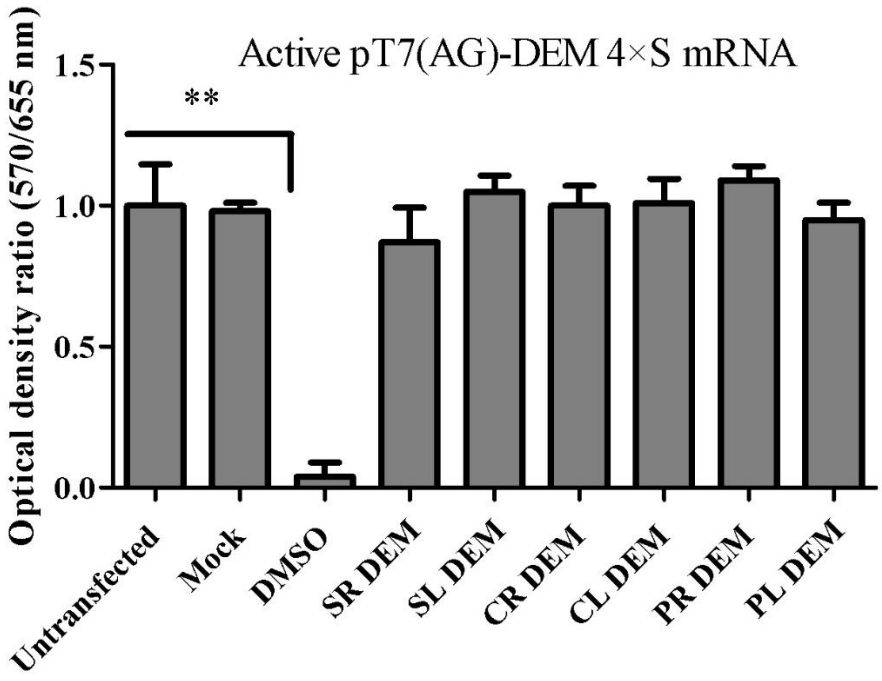

Figure 3.28: Assessment of toxicity associated with anti-HBV DEM mRNA. Huh7 cells were double transfected with anti-HBV DEM mRNA individually; the first and second transfections of IVT mRNA were 6 hours apart. A cell viability assay was conducted twenty-four hours after mRNA transfection to assess potential associated toxicity. DMSO served as the positive control, and data were normalised to the untransfected control. All transfections were performed in triplicate (n = 3). Statistical significance is indicated by ***, corresponding to $p < 0.001$

3.8.5 Lack of innate immune stimulation mediated by anti-HBV DEM mRNA expressed from the pT7(AG)-DEM 4×S vector

To determine whether DEM mRNA induces an immune response, qPCR was used to measure the mRNA levels of IFN-β and interferon-inducible genes OAS1 and IFIT1 in HEK293 cells transfected with DEM mRNA. HEK293 cells were transfected with the DEM mRNA or Luc2-mRNA, which served as a negative control. Cells transfected with poly I:C served as positive controls for the induction of IFN stimulated genes. Twenty-four hours after transfection, total RNA was extracted and treated with DNase to remove any contaminating DNA. The RNA was then reverse transcribed into cDNA and amplified with real-time PCR using specific primers for *IFN-β*, *OAS1*, *IFIT1*, and the housekeeping gene *HRPT*. The results showed no significant increase in *IFN-β*, *OAS1*, or *IFIT1* mRNA levels in HEK293 cells transfected with the anti-HBV DEM mRNA. In contrast, poly (I:C) transfections led to a statistically significant increase in *IFN-β* and other IFN-related genes (Figure 3.29 A-C). These findings suggest that DEM-encoding mRNA does not trigger an immunostimulatory response, indicating its safety for therapeutic application. Furthermore, the results indicate that the observed silencing effects are due to transcriptional repression of DEM mRNA and are independent of immune stimulation.

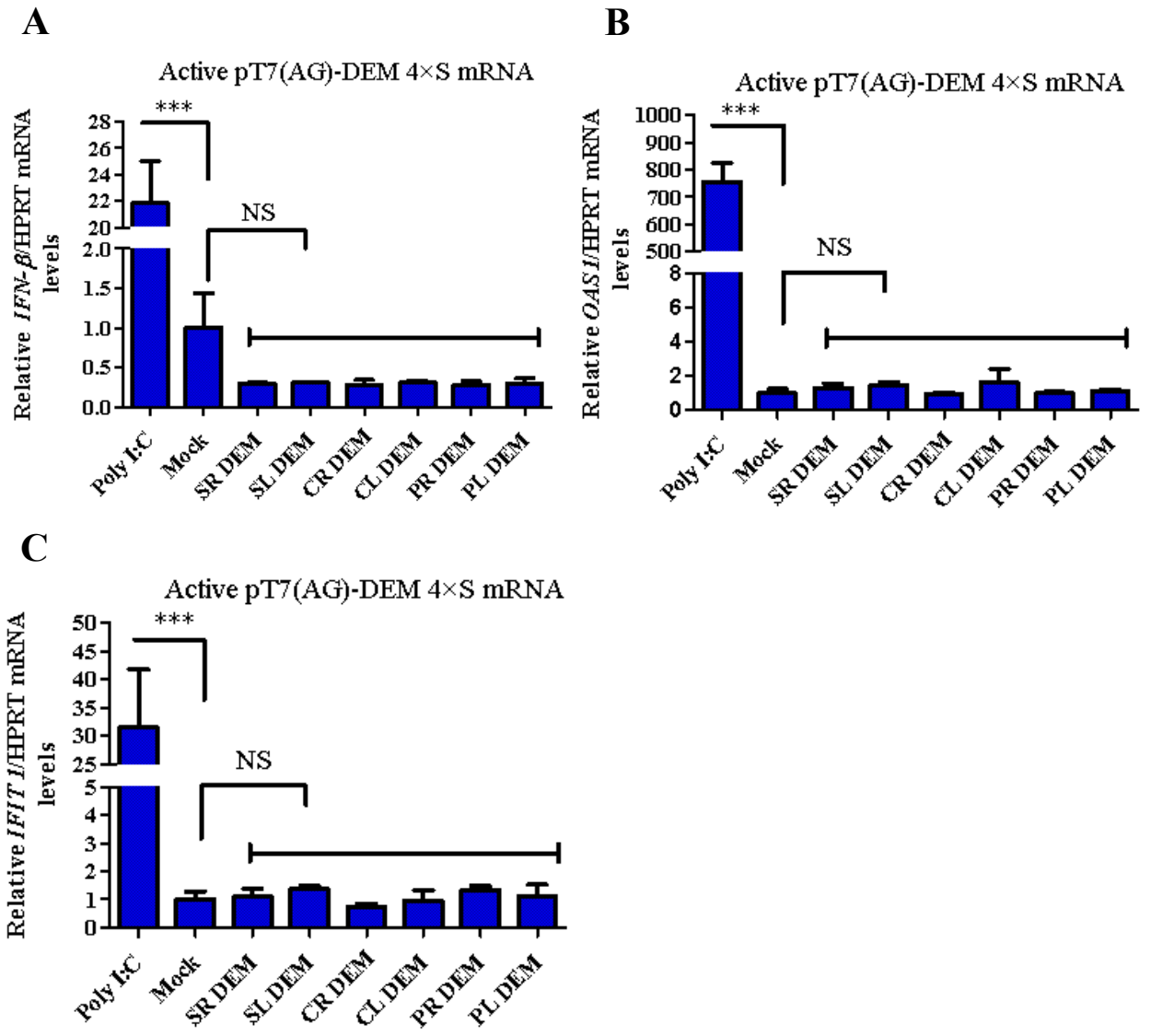

Figure 3.29: Assessment of interferon response stimulation by anti-HBV DEM-encoding mRNA in cultured cells. RNA extracted from HEK293T cells transfected with DEM-encoding mRNA or Poly I:C was subjected to RT-qPCR to evaluate mRNA transcripts encoding interferon-β and interferon-inducible genes.(**A**)*IFN-β* (**B**) *OAS1* and (**C**) *IFIT1* mRNA levels were asses and were normalised to hHPRT, and changes in expression between the mock and DEM-mRNA-transfected cells were assessed using the delta-delta Ct method. All transfections were performed in triplicate (n = 3). Statistical significance is indicated by ***, corresponding to $p < 0.001$. Poly I:C served as the positive control. Abbreviations: IFN-β = Interferon beta, OAS1 = 2'-5'-oligoadenylate synthetase 1, IFIT1 = interferon-induced proteins with tetratricopeptide repeats.

Chapter 4

4. Discussion

The current problem with chronic HBV infections is that, despite numerous novel drugs and combination therapies capable of targeting nearly every step of the viral replication cycle, there is still no cure (Lee et al., 2020). This is because the virus has evolved mechanisms to maintain the episomal cccDNA, providing a permanent template for the continuous supply of viral pgRNA and mRNA (Köck et al., 2010, Nassal, 2015). This stability allows cccDNA to persist for years, enabling viral reactivation upon cessation of treatment, which represents a major barrier to developing an effective cure.

4.1 Epigenome editing as an alternative to current therapeutic approaches for HBV

Genome-editing technologies can directly target or degrade cccDNA. The therapeutic use of anti-HBV designer nucleases has been well-documented since the first ZFN targeting HBV was reported in 2010 (Cradick et al., 2010). Nucleases induce double-strand breaks (DSBs) at specific sites, facilitating targeted mutagenesis (Bloom et al., 2013, Smith et al., 2021). However, their potential for off-target cleavage, particularly with CRISPR/Cas, poses a significant risk (Kuscu et al., 2014). This off-target mutagenesis, combined with the reliance of *Hepadnaviruses* on DSBs and cellular repair mechanisms, raises the likelihood of chromosomal translocations and genotoxicity (Feitelson and Lee, 2007, Kosicki et al., 2018). To mitigate these risks, epigenome editing is proposed as a less genotoxic alternative to designer nucleases.

Epigenetic strategies, including epigenome editing, show promise for treating CHB (Singh et al., 2021). Some approaches target specific processes regulating cccDNA (Cheng et al., 2020), while others enhance natural defences to inhibit infection (Cheng et al., 2021) or use DNA-binding domains (DBDs) to direct epigenetic effectors for transcriptional silencing (Zhao et al., 2013). A solid foundation exists for applying epigenome editors as novel antiviral gene therapies targeting HBV (Zhao et al., 2013, Luo et al., 2018, Xirong et al., 2014). Therefore, one of the aims of the study was to evaluate the therapeutic potential of IVTed anti-HBV DEM mRNA in silencing viral gene expression.

The HBV genome contains several CpG islands that regulate its gene expression (Zhang et al., 2014, Jain et al., 2015), allowing the virus to control its replication within the host(Vivekanandan et al., 2010). Silencing cccDNA through epigenetic mechanisms offers a practical approach to curing CHB (Zhang et al., 2014). This is supported by several in vivo (Vivekanandan et al., 2008, Guo et al., 2009, Kim et al., 2011, Zhang et al., 2014) as well as in vitro (Vivekanandan et al., 2009, Vivekanandan et al., 2010) studies which have reported a significant association between increased HBV CpG methylation and reduced levels of viral antigens and mRNA across various stages of infection. These findings establish a foundation for targeted transcriptional inhibition of HBV through use of the epigenome modifiers. Since the description of the first epigenome editor targeting HBV in 2013 (Zhao et al., 2013), studies in this field have been limited compared to other therapeutic approaches. Nonetheless, existing research demonstrates the promising therapeutic potential of epigenome editors.

4.2 Application of RNA expression platforms for the expression of anti-HBV epigenome modifiers

Eukaryotic mRNA contains several regulatory sequences that influence stability, translation efficiency, and degradation by exonucleases. These features consist of the 5′ and 3′ untranslated regions (UTRs), 5’ cap structure and poly(A) tail, ensuring the stability of the mRNA and enhancing translational efficiency for the production of the desired protein (Gao et al., 2000, Asrani et al., 2018, Adibzadeh et al., 2019). In this study, IVTed mRNA expressing DEMs targeting the *S*, *C* and *P* ORFs of HBV were synthesised and evaluated for the first time. To achieve this, two mRNA-based platforms consisting of pmRNA-pA and pT7-(AG) vectors were used for the IVT of DEM therapeutic sequences. Initially, the pmRNA-pA expression platform was used to clone in the anti-HBV DEM and eGFP reporter transgene sequences separately. This plasmid was designed with a single stop codon after the transgene sequence and a stretch of 52 adenine residues (poly A). The pT7-AG vector has highly stable UTR sequences, four continuous termination codons and a poly(A) track of 120 thymidine residues.

4.3 Expression of DEM mRNA from the pmRNA platform

Within the cytoplasm of a cell, the 5'-cap structure of mRNA participates in cap-dependent translation initiation, which is critical for protein synthesis (Borden and Volpon, 2020).

Additionally, the 5′ cap is responsible for regulating the stability and translational efficacy of mRNAs (Henderson et al., 2021). In this study, the initial experiments using Cap 0 for mRNA synthesis resulted in non-functional mRNA, evident from the lack of GFP expression and transcriptional silencing of HBsAg by anti-HBV DEMs. This finding corroborates previous reports indicating that Cap 0 is not ideal due to the low stability of synthesised mRNA. Incorporation of the ARCA cap showed some improvement in expression of GFP, but significant improvement was observed with using the Vaccinia Capping System, while the greatest improvement in GFP and anti-HBV DEM expression was achieved with TriLink CleanCap® AG Cap1. These findings further supports studies have demonstrated enhanced capping efficiency and translation (Henderson et al., 2021, Vlatkovic et al., 2022). Improved expression using this capping strategy is likely attributed to the reduced immunogenicity of IVT mRNA, as the Cap 1 structure diminishes RIG-I recognition, thereby reducing the cellular immune response (Devarkar et al., 2016).

This study demonstrates that the method of IVT significantly influences mRNA functionality. For instance, using the RiboMAX™ Large Scale RNA Production System to transcribe an IRES-FLuc plasmid resulted in minimal expression, indicating ineffective translation of transcripts produced with this system. This is because IRES-FLuc plasmid relies on cap-independent synthesis, an alternative mechanism that does not require a 5’ cap for mRNA synthesis. In contrast, the TranscriptAid T7 High Yield Transcription Kit produced GFP mRNA, which had improved expression, while the NEB IVT components yielded an even greater improvement in transcribed mRNA, despite the overall RNA synthesis efficiency remaining low. Notably, LiCl purification improved mRNA expression (e.g., GFP expression) by likely removing small RNAs and DNA contaminants from the IVT process, supporting previous studies that highlights the importance of mRNA purification (Nagalakshmi et al., 2008, Baiersdörfer et al., 2019).

Despite the improvements seen with the TranscriptAid T7 High Yield Transcription Kit and NEB IVT components, factors such as the short half-life of mRNA and immune stimulation which can be detrimental for gene therapy applications as it hinders mRNA stability and protein translation (Tatematsu et al., 2018). Presence of unmodified nucleotides and dsRNA byproducts produced during IVT (Karikó et al., 2008, Dousis et al., 2023), poses a significant limitation for mRNA-based therapies, because of their high immunogenicity and can trigger a strong immune

response by inducing type I interferons subsequently reducing protein expression (Milligan et al., 1987, Karikó et al., 2011, Baiersdörfer et al., 2019). Various methods exist to reduce the formation of dsRNA during IVT (e.g., inclusion of modified nucleotides) as well as after IVT to purify the mRNA of dsRNA contaminants (e.g., cellulose purification)(Karikó et al., 2008, Baiersdörfer et al., 2019). To enhance transcription and minimise immune responses, IVTs were performed using NEB nucleotides, TriLink buffers, the modified nucleotide ψ, co-transcriptional capping with TriLink AG, and cellulose purification. These modifications significantly improved the transcribed anti-HBV DEMs resulting in transcriptional repression of HBV surface antigen. The CR, CL, and PL DEMs achieved reductions of 8%, 11%, and 23% in HBsAg, respectively, suggesting that the C and P DEMs influenced the transcription of PreS1 and PreS2 promoters, which encode L, M, and S surface proteins (Hyams, 1995). These optimisations overall increased the efficacy of IVT mRNA produced.

While some silencing of the viral surface protein was achieved using this pmRNA expression platform, the efficacy of the DEMs was notably lower than those expressed from the pmRNA plasmid itself. Unpublished work by Dr Kristie Bloom showed that S DEMs from the pCMV-DEM plasmids resulted in a 90% decrease in serum HBsAg concentration and an eight-fold increase in methylation of CpG island II in vivo. Given that DEMs contain both DNMTs and KRAB domains, they can induce transcriptional silencing through CpG island methylation and chromatin remodelling (Bloom et al., 2019, Xirong et al., 2014). However, the lack of efficient silencing of viral replication by DEMs was unexpected, as the poly(A) tail in mRNA remains intact post-transcription. Additionally, the transgene sequence was shown to be functional, resulting in reduction of HBsAg when expressed from the pmRNA DEM plasmid DNA. These findings suggest that the pmRNA expression platform may not be optimal for DEM transgene sequences, despite successful GFP production using modified nucleotides, TriLink CleanCap® AG, and cellulose purification. Luc2 mRNA transcribed with an alternative RNA expression vector using the same optimised IVT protocol resulted in good luciferase expression compared to the TriLink FLuc controls. This further supported the notion that the pmRNA expression platform may not be ideal for longer and more complex sequences, such as DEM transgenes. However, smaller and less complex sequences, such as GFP reporter transgenes sequences can be effectively synthesised with this platform.

4.4 Functional DEM mRNA expressed from pT7 (AG) RNA expression platform

Translation efficiency is not only significantly improved and influenced by cap structures, chemically modified nucleotides and decreased immunogenicity of synthesised mRNA as demonstrated by this study but is also strongly influenced by the regulatory UTRs. Due to the inefficient silencing achieved from DEM mRNA expressed from pmRNA platform despite the various optimisations, this study employed a second RNA expression platform, that incorporated more stable UTRs which are known to increase translation efficiency and stability to further explore the potential of anti-HBV DEM transcribed mRNA.

The regulatory 5' and 3' UTR sequences are critical for the recruitment of ribosome and translation factors to the RNA (Sonenberg and Hinnebusch, 2009). Current findings indicate that the 5′ UTR is the main regulator of protein synthesis as modification of 5′ UTR has been shown to have the greatest influence on translation (Asrani et al., 2018). In addition to modifying the UTR sequences, the pT7(AG) RNA expression vector included a 120 poly(A) track compared to the 52 poly(A) track used in pmRNA expression vector. A longer poly (A) was included because evidence shows that the poly (A) tail not only regulates enzymatic stability and half-life of mRNA, but also facilitates the circularisation of mRNA (Leppek et al., 2018) forming a cap/PABP/eIF4E-eIF4G-PABP-poly(A) complex along with the cap structure of mRNA (Jalkanen et al., 2014). This closed loop structure improves binding, recycling of ribosomes and protects mRNA from degradation and a sufficiently long poly (A) tail is necessary to allow for the physical interactions between the poly (A) tail and the cap in mRNA to cooperatively maintain the mRNA stability (Newbury, 2006, Wells et al., 1998). During IVT, a common source of contaminants is dsRNA. When RNA polymerase fails to terminate transcription at the end of the coding sequence, it can lead to read-through transcription into the 3' UTR of the mRNA. To address this issue, the pT7-(AG) platform includes four stop codons in succession, ensuring efficient transcription termination and reducing the likelihood of run-off transcripts. Additionally, having multiple stop codons in succession enhances translation termination by increasing the likelihood that the ribosome will recognise the end of the mRNA.(Triana-Alonso et al., 1995, Gholamalipour et al., 2018, Cridge et al., 2018).

4.4.1 Expression of active anti-HBV DEMs mRNA in vitro

Initial investigations using dDEM mRNA expressed from pmRNA showed detectable HA-tag expression in both the nucleus and cytoplasm, indicating successful translation and nuclear transport. In contrast, active DEMs expressed from the pmRNA vector did not display HA-tag expression, despite achieving transcriptional repression of viral surface HBsAg. However, removing the KRAB domain from the active DEMs allowed for HA-tag detection. This suggests that the KRAB domain at the 5' end of the DEM TALE-DBD may hinder HA-epitope recognition by the anti-HA monoclonal antibody. Notably, DEMs expressed from DNA showed HA-tag expression, albeit at lower levels than inactive controls from pmRNA and pT7-(AG) vectors. This indicates that while the KRAB domain obscures the HA-tag, it remains detectable.

The absence of detectable expression of the HA-tag was hypothesised to be the result of KRAB domain and the inability of the pmRNA construct to produce functional mRNA even after the optimised IVT process was implemented. However, detectable HA-tag expression was observed with active DEMs expressed from pT7-(AG) platform using a primary monoclonal anti-HA antibody. Rather, detection of the HA-tag from active DEMs mRNA synthesised from the pT7-(AG) platform was achieved, demonstrating enhanced nuclear expression when a primary anti-HA polyclonal antibody was used. These results suggest that the monoclonal antibody used, which targets a specific epitope could be obscured in the native conformation of the active DEMs, which struggled to bind effectively. This limitation was overcome by the polyclonal antibody, which recognised and bound to alternative epitopes that remained accessible in the native conformation, thereby enabling more effective detection of the active DEMs (Lipman et al., 2005). This increase in specificity and recognition of the polyclonal antibody allowed for the detection of the HA-tag. These findings further suggest that folding of the protein could be hampering the detection of the HA-tag when the KRAB domain is present regardless of the RNA expression system. This is validated by the fact that detection and recognition of the HA-tag was achievable using primary monoclonal anti-HA antibody with active DEM DNA. This indicates a difference between *in situ* and IVTed mRNA and its influence on translation and thereby protein folding (von der Haar et al., 2023).

4.4.2 Transcriptional silencing of HBV surface protein and viral transcripts

The HBV genome is compact, comprising four ORFs: C, S, P, and X, with transcription regulated by four promoters (pre-S1, pre-S2, X, and BCP) and cis-elements like Enhancer I and II (Seeger and Mason, 2000). This study found that all six anti-HBV DEMs achieved transcriptional silencing of HBV surface protein levels, as well as surface and pgRNA transcripts, with SL and PL DEMs showing enhanced repression. Using the pCH-9/3091 replication-competent plasmid, which expresses the HBV surface protein and necessary subgenomic and pgRNA mRNAs, initial reductions of 42%-60% in viral replication were observed with anti-HBV DEMs, respectively, after a single mRNA transfection. This effect was achieved using IVTed mRNA with all uridine substituted by ψ, confirming its enhanced stability and increased protein expression (Karikó et al., 2008, Anderson et al., 2011). However, the silencing effect diminished after forty-eight hours, likely due to the plasmid's ability to replicate within host cells using the host cell's machinery, which results in high copy numbers. Copy numbers can range from 1 to 14 for low-copy plasmids and up to 200 for high-copy plasmids (Projan et al., 1987), with further increases observed with modified plasmids (Rosano and Ceccarelli, 2014). Use of the pCH-9/3091 plasmid may explain the diminished effects of anti-HBV DEMs over time. Additionally, possible delayed endosomal escape of IVTed mRNA (Jain et al., 2015) and IVTed mRNA transient expression compared to the stability of plasmid DNA could further exacerbate the diminished repression. Similar challenges with high expression of HBV are observed in HBV-integrated cell lines like HepG2.2.15 (Bloom et al., 2013).

To address this issue, double transfections of DEM mRNA were performed, leading to significant reductions in HBsAg (78%-84%), *surface* transcripts (42%-70%), and pgRNA transcripts (62%-72%) using the various DEMs. This enhanced silencing of markers of replication resulted from increased availability of therapeutic mRNA. This correlated with improved antiviral efficacy and reduced viral protein production. This suggests that DEM-mediated transcriptional silencing depends on quantity of target DNA, with efficiency declining at higher amounts. This was also observed in HepG2.2.15 cell models,. However, these two models are different. In this study plasmid DNA is used to initiate viral replication, while the other model uses an integrated HBV genome to initiate replication (Bloom et al., 2013). Use of models like the one used in this study significantly limits the adequate assessment of IVTed anti-

HBV DEM *in vitro*. Nevertheless, the anti-HBV DEMs achieved greater transcriptional repression than their DNA counterparts.

The significant reduction in HBV replication markers achieved by the DEMs aligns with studies showing a strong link between increased HBV CpG methylation and decreased levels of HBsAg, HBeAg, and mRNA. For example, occult CHB patients show higher CpG II methylation than non-occult patients (Vivekanandan et al., 2008). Individuals categorised with active infection (HBeAg-positive) exhibit approximately 48% methylation, while those with low replication (HBeAg-negative) exhibit 14% methylation (Guo et al., 2009). Additionally, methylation of CpG III has been linked to lower HBsAg levels (Zhang et al., 2014). Although no correlation was found between cccDNA methylation and HBsAg in cirrhosis patients, high methylation density correlated with reduced virion productivity and viral load (Kim et al., 2011).

In this study, bisulphite sequencing was performed to assess methylation. Results showed a clear increase in cytosine compared to thymine in cells transfected with SL and PL DEM mRNA, indicating methylation across all three CpG islands. The DEMs exhibited a long-range effect, targeting not only their respective CpG islands (CpG I for SL DEM and CpG II for PL DEM) but also CpG III albeit at lower levels compared to their cognate target sites. SL DEM primarily has an increased number of bases/residues that demonstrated greater proportion of Cytosine:Thymine at CpG II, with fewer methylation residues observed at CpG III. In contrast, PL DEM resulted in increased proportion of Cytosine:Thymine at both CpG II and CpG III. These findings align with previous studies showing higher methylation at CpG II and III, and lower at CpG I (Vivekanandan et al., 2008, Jain et al., 2015, Zhang et al., 2014) correlating with significant reductions in viral surface protein expression and transcript levels observed in this study. While the long-range targeting of DEMs may be advantageous for targeting viral sequences, it raises concerns about potential off-target effects. While Sanger sequencing is commonly used, it is a less ideal assay for targeted bisulphite sequencing because amplicons are too small (150-300 bp) and requires approximately 20-30 cycles to achieve clean peaks, which can be challenging (Leontiou et al., 2015, Crossley et al., 2020). Cloning PCR amplicons into a plasmid before sequencing can improve results, but it may introduce biased amplification (Leontiou et al., 2015). Therefore, next-generation bisulphite sequencing technologies are preferred due to their reliability, accuracy, and ability to produce quantitative results with statistical significance.

Despite mixed signals in bisulphite -converted DNA, repeated assays consistently showed increased cytosine at many of the same residues compared to mock controls. This suggests the observed methylation is likely to be genuine, although levels may be underestimated or overestimated due to mixed signals at non-target CpG islands. Therefore, further characterisation is needed to confirm DEM activity and assess on- and off-target effects.

Transcription from the pre-S1 and pre-S2 ORFs produces subgenomic mRNAs encoding the L, M, and S surface proteins of HBV, regulated by their respective promoters. A reduction in HBsAg levels was anticipated with S DEMs as they target the *S* ORF, which is near CpG I, overlapping its start site of the *S* gene. Although the C and P DEMs do not directly target the *S* ORF, the C DEM affects the *C* ORF which encompasses CpG III, overlapping the polymerase start codon and the Sp1 promoter. The P DEM targets the *P* ORF and includes CpG II, overlapping enhancer regions and the HBx and core promoters (Vivekanandan et al., 2008, Kaur et al., 2010). Given the strategic placement of CpG islands, the HBV genome is an ideal target for DNA methylation. Results suggests that all six anti-HBV DEMs could likely silence the pre-S1 and pre-S2 promoters responsible for translating the L, M, and S viral proteins that comprise the surface HBsAg, possibly through methylation. Bisulphite sequencing support this, as a clear trend of increased cytosine proportions at all CpG islands were observed, suggesting that methylation of these islands contributes to the observed silencing effect. Although no bisulphite sequencing experiments were conducted with all the DEMs, suggest similar mechanisms may apply to C DEMs.

The reduction of viral transcript levels achieved by S DEMs suggests that these DEMs may act over long distances, likely targeting enhancer I, which is situated between the *S* ORF and the X promoter region. Enhancer I activates transcription by recruiting liver-specific transcription factors in a hepatocyte-dependent manner (Antonucci and Rutter, 1989, Guo et al., 1991). These results align with the bisulphite sequencing results showing an increased trend in methylation of CpG II and CpG III by S DEMs, indicating that silencing of these CpG islands could be responsible for the observed reduction of viral transcripts. Since the basic core promoter initiates transcription of pgRNA, encoded by the *C* ORF [29, 208], a reduction in pgRNA levels is also expected by C DEMs. Similar to S DEMs, P DEMs likely target enhancer I, and the overlap of CpG II with core promoter suggests that methylation of this CpG II could contribute to the

reduced viral transcript levels, corroborating the findings observed from the bisulphite sequencing results.

The reduction in *surface* mRNA and pgRNA levels demonstrates that the S, C, and P DEMs are transcriptionally silencing expression from the pre-S1, pre-S2, and basic core promoters, which are exclusively responsible for the expression of *surface* mRNA and pgRNA. Thus, the possible methylation of CpG islands, along with targeted repression of all three promoters, could be responsible for the transcriptional inhibition observed, aligning with the findings from the bisulphite sequencing results. The enhanced efficacy of PL DEM and SL DEM observed in this study is in agreement with previous studies which showed targeting the enhancer I resulted in significant repression of markers of replication in HBV transgenic mice (Zhao et al., 2013).

Overall results in this study correlate with studies that have shown hypermethylation of CpG II is associated with little to no expression of HBsAg (Vivekanandan et al., 2008, Guo et al., 2009) and reduced HBsAg, HBeAg and viral mRNA levels. Xirong *et al*., further showed targeting CpG II and HBx promoter resulted in *de novo* methylation and significant reduction in viral particle production and expression of core mRNA, HBsAg and HBx proteins (Xirong et al., 2014). Furthermore, this study highlighted the effectiveness of using DEMs encoded from mRNA, which successfully silenced protein expression and reduced transcript levels. This emphasises the important role of DNA methylation in suppressing HBV replication and protein production.

4.5 Safety of using transcriptional repressor DEMs expressed as mRNA

One of the main limitations of mRNA-based technologies is their potential to trigger an innate immune response which may be beneficial to function as an adjuvant from a vaccine context but can be detrimental from a gene therapy approach. Unlike endogenous RNA, which is predominantly associated with ribonucleoprotein (RNP) complexes (Pichon et al., 2012), IVTed mRNA enters through endosomal-mediated entry and the detection of non-self mRNA in the endosomal (Jiang et al., 2020), extracellular and cytoplasmic compartments leads to detection by PRRs (Lee et al., 2019). Induction of an immune response by IVTed mRNA is primarily due to the recognition of uncapped 5′ triphosphates and GU-rich complex secondary structures in the

IVTed mRNA. These features give exogenous RNA a signature similar to that of a virus. Stimulation of the innate immune system can result in activation of a signal cascade leading to up-regulation of type I interferon and NF-κB related genes. These ultimately lead to translation inhibition, cell cycle arrest, increased expression of PRRs and eventually apoptosis (Nallagatla and Bevilacqua, 2008, Gil et al., 1999).

In this study the capacity of IVTed anti-HBV DEMs expressed in the form mRNA and innate immunity *in vitro,* was evaluated. The presence of modified nucleotides in the mRNA prevents its recognition as a foreign molecule by endosomal sensors, such as TLR3, TLR7, and TLR8 or cytoplasmic sensors, such as RIG-I and MDA5, responsible for the induction of type I IFNs, typically associated with antiviral responses (Karikó et al., 2005, Nelson et al., 2020). The absence of detectable IFN and IFN-inducible gene upregulation indicates incorporation of cap analogue (CleanCap®), complete substitution of canonical nucleotide uridine with ψ and cellulose purification extensively abrogated any immune stimulatory feature of IVT mRNA. Additionally, the inclusion of four consecutive stop codons may have contributed to reduced run-off transcription, thereby minimizing the production of toxic or immunogenic by-products during IVT (Tate and Mannering, 1996). In addition, cell viability assay performed demonstrated no change in mitochondrial metabolic activity with either anti-HBV DEM mRNA expressed from pmRNA-pA and pT7(AG) when compared to untransfected cells. These observations suggest that reduction of viral markers of replication was specific to activity of DEMs and not as a result of interferon stimulated response mediating apoptosis.

4.6 Future work

Further assessment of DEM mRNA is required to validate its potential as a therapy for HBV. An infectable stable cell line expressing the NTCP receptor (HepG2-hNTCP) would be a better alternative to the transfection of replication-competent plasmids as they do not reflect the physiological conditions seen in natural or chronic infections. Infection of HepG2.hNTCP with HBV would allow for the characterisation of the various markers of HBV infection (HBsAg, viral RNA and cccDNA) (Hoh et al., 2015). Evaluation of transcribed anti-HBV DEM mRNA greater than forty-eight hours would provide better indication whether the transcriptional silencing effect is maintained. Ideally assessment in vivo setting would provide better indication of activity and allow for long-term assessment of anti-HBV DEMs to be determined.

Additionally, cell culture models do not fully recapitulate the immune response observed in in vitro models, therefore, to assess the safety of IVTed mRNA in vivo evaluation in mouse models is required.

4.6.1 Target specificity and safety of epigenome editors

The TALE-DBD used in this study, repurposed from anti-HBV TALEN technology, demonstrated no off-targets of concern in the context of a TALEN, highlighting its target specificity (Smith et al., 2021). However, similar to gene editing technologies, epigenome editors could also induce off-target effects, necessitating thorough preclinical evaluations of off-target activity for anti-HBV DEMs. The DEMs contain the KRAB repressor domain, which can silence genes from up to 25 kb away from their binding sites (Bloom et al., 2019), raising potential safety risks regarding unintended gene silencing. While this characteristic may be beneficial for antiviral therapies, it introduces concerns about off-target effects on host genes. Moreover, DNMT domains can lead to DNA methylation, with the possibility of *de novo* methylation affecting host CpG islands. To mitigate off-target effects, this study expressed DEMs using an mRNA expression platform, which may limit the potential for off-target activity by epigenome modifiers.

Several bioinformatics tools, such as TAL Effector Targeter, are available to predict potential off-target binding sites based on the DNA-binding domain (DBD). These tools provide valuable insights into off-target risks. To further assess functional activity, next-generation sequencing can be employed to analyse methylation patterns comprehensively, thereby covering potential off-target activities (Leontiou et al., 2015). MassArray technology offers a more targeted approach for confirming methylation activity allowing for precise assessment of targeted methylation via bisulphite sequencing(Bloom et al., 2019). Additionally, Assay for Transposase Accessible Chromatin (ATAC-seq) can be utilised to confirm on-target and off-target regions of open and closed chromatin (Buenrostro et al., 2013), which is important because of the repressor domains included in DEMs. Whole transcriptome sequencing can also evaluate transcriptional profiling of neighbouring genes, identifying potential off-target genes with reduced expression compared to control samples (Mlambo et al., 2018). Together, these methods will enable a comprehensive assessment of both on-target and off-target activity by DEMs.

4.7 Therapeutic benefit of expressing DEMs from IVTed mRNA

Two decades ago, mRNA was considered too immunogenic for human therapy, with its transient nature and fragility leading to limited interest. However, significant advancements were highlighted in 2020 when two mRNA-based vaccines were rapidly developed in response to SARS-CoV-2 at an unprecedented record (Polack et al., 2020, Baden et al., 2021), showcasing mRNA's considerable therapeutic potential. Unlike DNA therapies, the transient nature of mRNA allows for better control of protein expression and reduces the risk of off-target effects. Since mRNA does not need to enter the nucleus for expression, it avoids the risk of genome integration associated with certain viral vectors (Zhong et al., 2018). Moreover, mRNA can be translated in the cytoplasm just hours after introduction as seen in this study, making it beneficial for both slowly dividing and non-dividing cells. mRNA is manufacturable through cell-free systems, which eliminate contaminants time constraints associated with traditional cell-based and viral vector-based therapies (Maruggi et al., 2019). Its stability, half-life, immunogenicity, and translational efficiency can be optimised for therapeutic use as demonstrated in this study, making it more easily adaptable than DNA or viral vector systems.

4.8 Targeted epigenome editing of HBV: therapeutic prospects and obstacles

Epigenome modifiers offer promising strategies for silencing cccDNA transcription as an alternative anti-HBV therapy. However, only four targeted epigenome editors have been explored to date, showing activity against HBV replication, but their impact on the cccDNA minichromosome remains unconfirmed. Liver-specific delivery of these epigenome modifiers, remain a significant challenge, as with other gene editors (Ates et al., 2020). For clinical application, several issues need to be addressed, including evaluating the efficacy and safety of DEM-mediated repression in reliable preclinical models and demonstrating effective cccDNA silencing. While models like HBV-transgenic mice, woodchucks, and uPA-SCID mice have provided insights, most fail to establish cccDNA, except for the uPA-SCID model, which lacks a functional immune system (Guidotti et al., 1994, Paronetto and Tennant, 1990, Meuleman and Leroux-Roels, 2008). Recent advances, such as the AAV8-A1 murine model, enable cccDNA production with a functional immune system, providing a more comprehensive platform for evaluating HBV biomarkers((HBsAg, HBcAg, different forms of intrahepatic HBV DNA,

including cccDNA, and viral transcripts) and long-term suppression(Limani et al., 2021). Expressing anti-HBV DEMs as mRNA offers several advantages over DNA, including avoiding viral vector constraints (Ely et al., 2021). Liposomes, with their low toxicity, immunogenicity, and biodegradability, are a promising delivery system for mRNA-based therapies (Belhadj et al., 2023), with successful applications in cell culture, animal models, and clinical trials (Kairuz et al., 2023, Polack et al., 2020, Strieth et al., 2014). These characteristics make liposomes an attractive option for delivering DEM mRNA in vivo. Given the potential of epigenome modifiers to silence HBV at the transcriptional level, combining this approach with other therapies could enhance its efficacy. Combination therapies have shown promise in previous studies (Liver, 2017, Lim et al., 2023) and could help address the persistent challenges of HBV replication and immune evasion. Overcoming delivery challenges and demonstrating sustained efficacy are key steps toward translating epigenome editing into a viable HBV treatment.

4.9 Conclusion

HBV infections represent a significant public health challenge, and the WHO has set a goal for the elimination of HBV by 2030. A major obstacle to achieving this goal is the need to eliminate or permanently silence the stable cccDNA reservoir. Epigenome editing has been proposed as a less genotoxic alternative to designer nucleases, offering a way to directly target and silence HBV for lasting therapeutic benefit. This approach aims to suppress HBV replication and transcription in infected cells, enabling gradual silencing of viral cccDNA during cell division, which substantially reduces the risk of chromosomal translocations. This study is the first to utilise DEMs expressed from RNA expression vectors (pmRNA-pA and pT7-(AG)) to silence HBV viral replication. Given the complex nature of mRNA, IVT was optimised using two RNA expression platforms. Significant efforts were dedicated to optimising IVT for anti-DEM mRNA, resulting in successful silencing of HBV HBsAg, *surface* and pgRNA transcript levels, without adversely affecting cell viability or triggering an innate immune response. While in vivo delivery of anti-HBV DEM mRNA and its characterisation could not be performed the results produced align well with previous studies indicating this technology potential. However, it warrants further in-depth preclinical evaluations to fully ascertain the therapeutic potential of anti-HBV DEM mRNA and its effects on HBV replication

This study makes a significant original contribution by being the first to demonstrate the potential of expressing epigenome modifiers as IVTed mRNA for therapeutic use. It is also the first to use dual repressors (DNMTs and KRAB) to silence HBV, showing promising results despite the inability to conduct a thorough in vitro and in vivo evaluation. The findings indicate the potential effectiveness of this approach. Furthermore, this study highlights the versatility of the mRNA platform, demonstrating its adaptability as a therapeutic tool. The IVT process and platform can be further optimized to enhance expression and reduce immune stimulation, which are critical factors for therapeutic applications.

5. Appendix

Table 5.1: Description of plasmids used in this study

Plasmid name	Function	Source or reference
pCH-9/3091	HBV target plasmid, contains a greater- than-genome length HBV genotype D sequence.	Nassal et al., 1992
pCMV-1696_ DEM (SR, SL, CR, CL, PR and PL)	Plasmids that were cloned to contain TALE and mutant DNMT (DNMT 3A and DNMT 3L) targeting the surface, core and polymerase ORFs of HBV under the expression of CMV promoter	Generously provided by Dr Kristie Bloom
pCMV- 697_ DEM (SR, SL, CR, CL, PR and PL)	Plasmids that were cloned to contain TALE, KRAB and active DNMT (DNMT 3A and DNMT 3L) targeting the surface, core and polymerase ORFs of HBV under the expression of CMV promoter	Generously provided by Dr Kristie Bloom
pCMV-TALENs (SR, SL, CR, PL TALENs)	Plasmids designed to target four conserved sites within the S, C and P ORFs of HBV. right and left TALE arrays cloned upstream of a *Fok*I nuclease domain sequence. This entire sequence is under the transcriptional control of a CMV promoter/enhancer.	Bloom et al., 2013
pmRNA-CMV-pA	Plasmid specifically designed to contain functional elements required for IVT.	Unpublished work (Danielle Gast)
pmRNA-CMV-eGFP	Reporter plasmid. Plasmid was generated by cloning the eGFP sequence into the mRNA backbone (pmRNA-pA)	This study (in conjunction with Ms Tiffany Smith)
pT7-Luc 2	Reporter plasmid used for the expression of luciferase mRNA from a mRNA expression system containing the functional elements required for IVT.	Unpublished work (Dylan Kairuz)
pT7-mCherry	Reporter plasmid used for expression of mCherry mRNA from the pT7-mRNA expression system that contains the functional elements required for IVT.	Unpublished work (Prof. Abdullah Ely)
T7-VEE-FLuc IRES	IRES FLuc mRNA reporter plasmid that functions by a Cap-independent manner and was used for the expression of luciferase mRNA	Prof. Patrick Arbuthnot

5.1 Gel electrophoresis

Agarose Gel

Materials

- 50× Tris Acetate EDTA (TAE) gel electrophoresis running buffer (242 g Tris HCL, 100 ml of 0.5 M EDTA pH 8, 57.1 ml glacial acetic acid in 1L double distilled water (ddH_2O)
- Ethidium Bromide (10 mg/ml) (Sigma-Aldrich, MO, USA)
- 6× Loading dye (Thermo Scientific, CA, USA)

Protocol

To prepare a 1% agarose gel, 1g of agarose was mixed with 100 ml of 1× TAE buffer and heated in a microwave for 5 minutes at half power until dissolved. After cooling, 2 µl of ethidium bromide was added. The mixture was poured into a gel chamber with a comb to create wells and allowed to solidify at room temperature. Once solid, the gel was placed in an electrophoresis chamber with 1× TAE buffer and run at 100 volts for 45 minutes. DNA was then visualized using the Omega Fluor™ Gel Documentation System (Gel Company Inc., CA, USA).

Formaldehyde agarose Gel

Materials

- 10× 3-(N-morpholino) propanesulfonic acid (MOPS), (0.2M MOPS, pH7.0, 20mM Sodium Acetate (NaOAc), 10mM Ethylenediaminetetraacetic acid (EDTA), pH 8.0)
- 2X RNA Loading dye (Thermo-Scientific, MA, USA)

Protocol

To prepare a denaturing 1% agarose gel, 1g of agarose was weighed and mixed with 72 ml of DEPC-treated H_2O and heated in a microwave. The melted agarose was cooled to approximately 60 °C thereafter 18 ml 32% Formaldehyde solution (Sigma-Aldrich, MO, USA) and 10 ml 10× MOPS Buffer (final concentration of 1×) added, mixed, poured into a casting tray and a gel comb.

5.2 Extraction of DNA fragments from agarose gel

Materials

MinElute Gel Extraction kit (Qiagen, Hilden, Germany)

Isopropanol

Protocol

The DNA fragment of interest was visualised using a UV transilluminator while wearing personal protective gear. The band of interest was excised from the agarose gel using a scalpel blade and each gel slice was placed in a microcentrifuge tube and weighed. To each tube, 3 volumes of guanidine thiocyanate Buffer (QG buffer) was added to 1 volume of gel (300 µl per 100 mg gel). The gel slices were melted by incubating the tubes at 50 °C for 10 minutes and periodically mixed by inverting the tubes. One gel volume of isopropanol was added to the samples, mixed, and briefly centrifuged. Samples were transferred to a QIAquick spin column with 2 ml collection tube and centrifuged for 1 minute at maximum speed (10 000 ×g) in a standard bench-top microcentrifuge to bind the DNA. The flow-through was discarded and the QIAquick spin column was placed back into the collection tube. Five hundred microlitres of Buffer QG was added to the column and centrifuged at maximum speed (10 000 ×g) for 1 minute. The flow-through was discarded and to wash the DNA 750 µl of Buffer PE of was added to the column and centrifuged at 10 000 ×g for 1 minute. To elute the DNA, the QIAquick spin column was transferred into a clean microcentrifuge tube and 30 µl of ddH_2O was added to the QIAquick spin column and incubated for 5 minutes at room temperature. After incubation the samples were centrifuged at 10 000 ×g and the eluted DNA was stored at -20 °C.

5.3 Preparation and transformation of chemically competent *E. coli*

Materials

- Luria-Bertani (LB) media (5 g Yeast extract, 10 g of Bacto-tryptone, 5 g NaCl, to 1 L ddH_2O)
- Transformation buffer (100 mM $CaCl_2$, 10 mM PIPES-HCl, 15% glycerol)
- 1000× ampicillin (Roche Applied Science, Mannheim, Germany): (1g of ampicillin in 10 ml ethanol)

- Luria-Agar (LA) (Oxoid, UK) plates: (10 g agar, 5 g Yeast extract, 10 g of Bacto-tryptone, 5 g NaCl, to 1 L ddH_2O)

Protocols

Transforming chemically competent *E. coli*

For ligation reactions, 10 µl of plasmid DNA was mixed with 100 µl of competent E. coli and incubated on ice for 30 minutes. The cells underwent a heat shock at 42°C for 90 seconds, followed by a 5-minute incubation on ice. The transformed E. coli was then plated on LB plates with selective antibiotics.

5.4 Large-scale plasmid preparation

Materials

- Plasmid Maxi Kit (Qiagen, Hilden, Germany)
- P 1 buffer: (3.72g EDTA, 6.06 g Tris-HCl RNaseA (100 µg/mL), pH 8.0 in 1 L ddH_2O)
- P 2 buffer: (10 g SDS, 8 g NaOH in 1 L)
- P 3 buffer: (380 g guanidine HCl ,49 g potassium acetate, pH 4.5 in 1 L ddH_2O)
- QBT buffer (30.3 g Tris-HCl, 0.372 g EDTA, 12 g NaCL, pH 7.5 in 1 L ddH_2O)
- QC buffer: (1.2 g Tris-HCl, 80% ethanol, pH 7.56 in 1 L)
- QF buffer: (30.3 g Tris-HCl, 0.372 g EDTA, 12 g NaCL, 50% isopropanol pH 7.5 in 1 L ddH_2O)

Protocol

A single colony containing the plasmid DNA of interest was used to inoculate 200 ml of LB media supplemented with ampicillin (100 µg/ml) and the bacterial culture was incubated overnight at 37 °C in a shaking incubator. The next day, the bacterial culture was centrifuged at 6000 ×g for 30 minutes. Ten millilitres of P1 were used to re-suspend the pellet and the solution was transferred to a 50 ml tube. Thereafter 10 ml of buffer P2 was added, and gently mixed by inverting the tube 4-6 times and allowed to incubate for 5 minutes at room temperature. Ten millilitres of chilled buffer P3 was added and gently mixed by inverting the tube 4-6 times and then incubated on ice for 20 minutes. After the incubation, the samples were centrifuged at 6000 ×g for 45 minutes. Ten millilitres of buffer QBT was added to A Qiagen-tip 500 column to equilibrate the column and allowed to empty by gravity flow. Supernatant was added to the column and allowed to enter the resin by gravity flow. The column was washed twice with 30 ml

of buffer QC. Thirty millilitres of buffer QC was used to wash the column twice. Qiagen-tip 500 column was transferred to a sterile 50 ml collection tube and 15 ml of buffer QF was added to elute the DNA. DNA was precipitated by adding 10.5 ml of isopropanol, mixed and centrifuged at 15 000 ×g for 30 minutes at 4 °C. Isopropanol was discarded and the DNA pellet was washed by adding 5 ml of 70% ethanol, and centrifuged at 15 000 ×g for 20 minutes at 4 °C. Ethanol was discarded, the DNA pellet was left to air dry for 5 minutes and then re-suspended in 100 µl of distilled water and stored at -20 °C.

5.5 In vitro transcription protocols

Material

- Formaldehyde agarose Gel
- 0.5 M EDTA Stock Solution (7.3 g EDTA in 50 ml NF.H_2O, pH 8.0 with NaOH)
- LiCl Solution (3.2 g LiCl + 1 ml 0.5 M EDTA in 10 ml NF.H_2O)
- Cellulose chromatography buffer: (1.2 g of HEPES (10 Mm), 0.01 g of ETDA (0.1 Mm), 3.7 g of NaCl (125 mM), 16% (v/v) ethanol).

Protocols

5.5.1 RiboMAX™ Large Scale RNA Production System (Promega, WI, USA)Table

Table 5.2 : IVT reaction setup with RiboMAX™ Large Scale RNA Production System reaction set up

T7 Reaction Components	Sample Reaction	Control Reaction
RiboMAX™ Express T7 2× Buffer*	50 µl	50 µl
Linear DNA template (5 µg total)	5–40 µl	-
pGEM® Express Positive Control Template (1 µg)	-	5 µl
Nuclease-Free Water	5–35 µl	35 µl
Enzyme Mix, T7 Express	10 µl	10 µl
Final volume	**100 µl**	**100 µl**

5.5.2 Transcript T7 High Yield Transcription Kit (ThermoScientific, CA, USA)

Table 5.3 : IVT reaction setup with Transcript T7 High Yield Transcription Kit

T7 Reaction Components	Sample Reaction (100 µl reaction)
DEPC-treated water	to 100 µl
5× TranscriptAid Reaction Buffer	20µl
ATP/CTP/GTP/UTP mix	40 µl
Template DNA	5 µg
TranscriptAid Enzyme Mix	10 µl
Final volume	**100 µl**

5.5.3 New England Biolabs (NEB) individual IVT components (New England Biolabs, NJ, USA)

Table 5.4: IVT reaction setup with NEB IVT components, TriLink Buffer and CleanCap AG

Component	100 µL Reaction
DNase/RNase-Free Water	Made up to 100
ATP (100 mM)	5 µL
CTP (100 mM)	5 µL
GTP (100 mM)	5 µL
UTP1 (100 mM)	5 µL
CleanCap® AG (100 mM)	5 µL
10× Transcription Buffer	10 µL
DNA template	5 µg
Murine RNase Inhibitor (40 units/µL)	2.5 µL
Yeast Inorganic Pyrophosphatase (0.1 units/µL)	2 µg
T7 RNA Polymerase (50 units/µL)	16 µg
Total Volume	**100 µL**

TriLink Buffer Composition

Table 5.5: Composition of 10× TriLink CleanCap® AG IVT buffer

Component	Stock concentration (mM)	Volume of stock (µl)	Final concentration (mM)
Magnesium acetate	1000	270	165
DTT	1000	100	100
Spermidine	200	100	20
Tris HCl, pH 8	1000	400	400
Triton X-100	0.2% v/v	2	0.02 % v/v
Nuclease free water	-	128	-
Total Volume		**1000**	

5.6 Nucleic acid extraction protocols

5.6.1 RNA extraction from monolayer cells

Materials

- TRIzol® Reagent (Thermo Scientific, CA, USA)

Protocol

Cells were washed twice with cold PBS. One millilitre of TRIzol® Reagent (Thermo Scientific, CA, USA) was added per well (per 10 cm^2 of culture plate surface area), the cells were re-suspended and transferred to a clean 1.5 ml microcentrifuge tube. To allow complete dissociation of nucleoprotein complexes, samples were allowed to incubate for 5 minutes at room temperature. Two hundred microlitres of chloroform was added to the sample and mixed vigorously for 15 seconds. Samples were incubated at room temperature for 5 minutes and centrifuged at 1 000 ×g for 15 minutes at 4 °C. Approximately 300 µl of the upper aqueous phase was transferred to a new 1.5 ml microcentrifuge tube and 500 µl of isopropanol was added, mixed by inverting the microcentrifuge tube and incubated at room temperature for 5 minutes. Following incubation, RNA was precipitated by centrifuging the samples at 12 000 ×g for 10 minutes at 4 °C. The supernatant was discarded, and the pellet was washed in 1 ml of 75% ethanol followed by centrifugation at 7 500 ×g for 5 minutes. The supernatant was removed, and

pellet briefly centrifuged to remove residual ethanol. The pellet was left to air dry for approximately 5 minutes and re-suspended in 85 µl of RNase free H_2O. To remove contaminating DNA, extracted RNA samples were treated with 5 U of DNase I and 1× DNase buffer and incubated at 37°C for an hour. Following incubation, RNA was precipitated using 500 µl chilled 100% ethanol and incubated at -20 ℃ for one hour. RNA was centrifuged at 12 000 ×g for 15 minutes at 4 ℃ and supernatant was discarded. RNA pellets were washed 500 µl 70% ethanol and centrifuged again at 12 000 ×g for 10 minutes at 4 ℃. Total RNA was resuspended in RNase free H_2O and concentration and purify of the RNA samples were measured by spectrophotometry using the N80 Nanophotometer Spectrophotometer (Implen, CA, USA) and stored at -80 °C.

5.6.2 DNA extraction from monolayer cells

Materials

- QIAamp® DNA Blood Mini Kit (Qiagen, Hilden, Germany)

Protocol

Two hundred microliters of Huh7 cells, harvested from transfections in a 48-well plate, were used for DNA extraction. This is equivalent to approximately 0.12×10^6 cells, based on the cell density of the wells used. To this, 20 µl of proteinase K was added, and the solution was mixed by pulse vortexing for 15 seconds vigorously. Following this, 200 µl of AL buffer was added and mixed again by pulse vortexing for 15 seconds and samples were incubated at 56 ℃ for 10 minutes. After incubation, the samples were centrifuged briefly, and 200 µl of ethanol (98-100%) was added to each sample and mixed by pulse vortexing for 15 seconds. The solution was then transferred to a spin column and centrifuged at 6000 × g for 1 minute, discarding the flow-through. To the column, 500 µl of AW1 buffer was added, and the column was centrifuged at 6000 × g for 1 minute; the flow-through was discarded. Next, 500 µl of AW2 buffer was added to the column, which was then centrifuged at 20,000 × g for 3 minutes, with the flow-through discarded. The column was transferred to a new collection tube and centrifuged at 20,000 × g for an additional minute to remove residual buffer. The column was then placed into a clean 1.5 ml microcentrifuge tube, and 200 µL of ddH_2O was added. After incubation at room temperature for

5 minutes, the sample was centrifuged at 6000 × g for 1 minute. The DNA concentrations were confirmed using N80 Nanophotometer Spectrophotometer (Implen, CA, USA)

5.7 Cell culture: maintenance and propagation of mammalian cells

Materials

- High glucose DMEM: (5 sachets of DMEM high glucose powder (Gibco™, Thermo Scientific, CA, USA), 18.5 g of $NaHCO_3$, pH was adjusted to 6.7 -6.8, 5L ddH_2O)
- Low glucose DMEM: (5 sachets of DMEM low glucose powder (Gibco™, Thermo Scientific, CA, USA), 18.5 g of $NaHCO_3$, pH was adjusted to 6.7 -6.8, 5L ddH_2O)
- 1000× penicillin/streptomycin (100 000 U/ml; 100 000 ug/ml): (0.9 g penicillin G sodium salt, 1.5 g streptomycin sulphate, 15 ml ddH_2O)
- 200× 4-(2-hydroxyethyl)-1-piperazineethanesulfonic acid (HEPES) (1 M): (11.91506 g HEPES in 25 ml)
- 1000× hydrocortisone (50 mM): (0.18123 g hydrocortisone in 10 ml of methanol)
- 1000× insulin (5 mg/ml): (25 mg insulin in 5 ml diluted HCl (5 mM))
- 1000× G418 (Geneticin) (400 mg/ml): (5 g of G418 in 8.9875 ml of PBS)
- Saline/0.01% EDTA solution (1 ml 10% EDTA in 1 L of saline solution)
- Complete high glucose DMEM and low glucose DMEM (Thermo Scientific, CA, USA): (450 ml of DMEM, 50 ml of 10% foetal bovine serum (FBS), 500 µl penicillin/streptomycin)
- Complete DMEM/F12, GlutaMAX^{tm} supplement (Life Technologies): (450 ml of DMEM/F12, 50 ml of 10% foetal bovine serum (FBS), 1 ml penicillin/streptomycin, 2.5 ml HEPES, 500 µl hydrocortisone, 500 µl insulin, 500 µl G418)
- Collagen coating: A concentration of 50 µg of rat tail collagen I (Gibco™, Thermo Fisher Scientific, CA, USA) was used to coat a surface area of approximately 10 cm²

Protocols

Maintenance of cultured cells

In this study, Huh7, HepG2.hNTCP, and HEK293T cells were used. Cells were grown in CellStar® cell culture flasks (Greiner Bio-One, Frickenhausen, Germany). Huh7 cells were maintained in complete low-glucose DMEM, while HEK293T cells were maintained in complete high-glucose DMEM. HepG2.hNTCP cells were cultured in complete DMEM/F12 with GlutaMAX™. All cells were incubated in a humidified incubator at 37 °C and 5% CO2. The Olympus CKX31 light microscope (Olympus, Tokyo, Japan) was used to monitor the cells.

General procedure used for propagation of cells

The cells were subcultured upon reaching a density of 90-100% by washing once with saline and EDTA and subsequently incubated for 10 minutes at 37°C in saline containing 0.01% EDTA. Following the 10-minute incubation the saline and EDTA solution was removed, 3 ml of TrypLE™ Express (Thermo Scientific, CA, USA) was added and the cells incubated for an additional 3 minutes TrypLE™ Express was omitted for HEK293 cells. The cells were then gently lifted from the culture dish by gentle aspiration. Seven milliliters of culture medium was added to inactivate TrypLE™ Express. The cell suspension was transferred into in sterile 15 mL tube and centrifuged for 3 minutes at 800 rpm. The supernatant was discarded, and 1 ml of complete growth medium was used to re-suspend the pellet. Cells were resuspended at the desired density and added to culture flasks or plate with the appropriate volume of growth media added. Cells were incubated at 37 °C (5% CO_2) in a humidified incubator.

5.8 Assessment of HBsAg using ELISA

Materials

- Monolisa™ HBs Ag ULTRA kit (Bio-Rad, CA, USA)

Protocol

The Monolisa™ HBs Ag ULTRA kit (Bio-Rad, CA, USA) was used according to the manufacturer's instructions to measure HBsAg levels. One hundred microlitres of supernatant along with the negative and positive controls were added to a well of the microplate and 50 µl of conjugate working solution was added to each well, mixed, covered with adhesive film and incubated at 37 °C for 1 hour and 30 minutes. Following the incubation, the plate was washed using the APW-200 microplate washer (Allsheng, Instruments, Co., HA, CN). One hundred microlitres of the development solution containing the substrate was added to each well and incubated in the dark for 30 minutes at room temperature. Thereafter the reaction was terminated using 100 µl of stopping solution and incubated at room temperature for 4 minutes. The OD of the samples were measured at 490/655 nm using the iMark™ Microplate Reader (Bio-Rad, CA, USA).

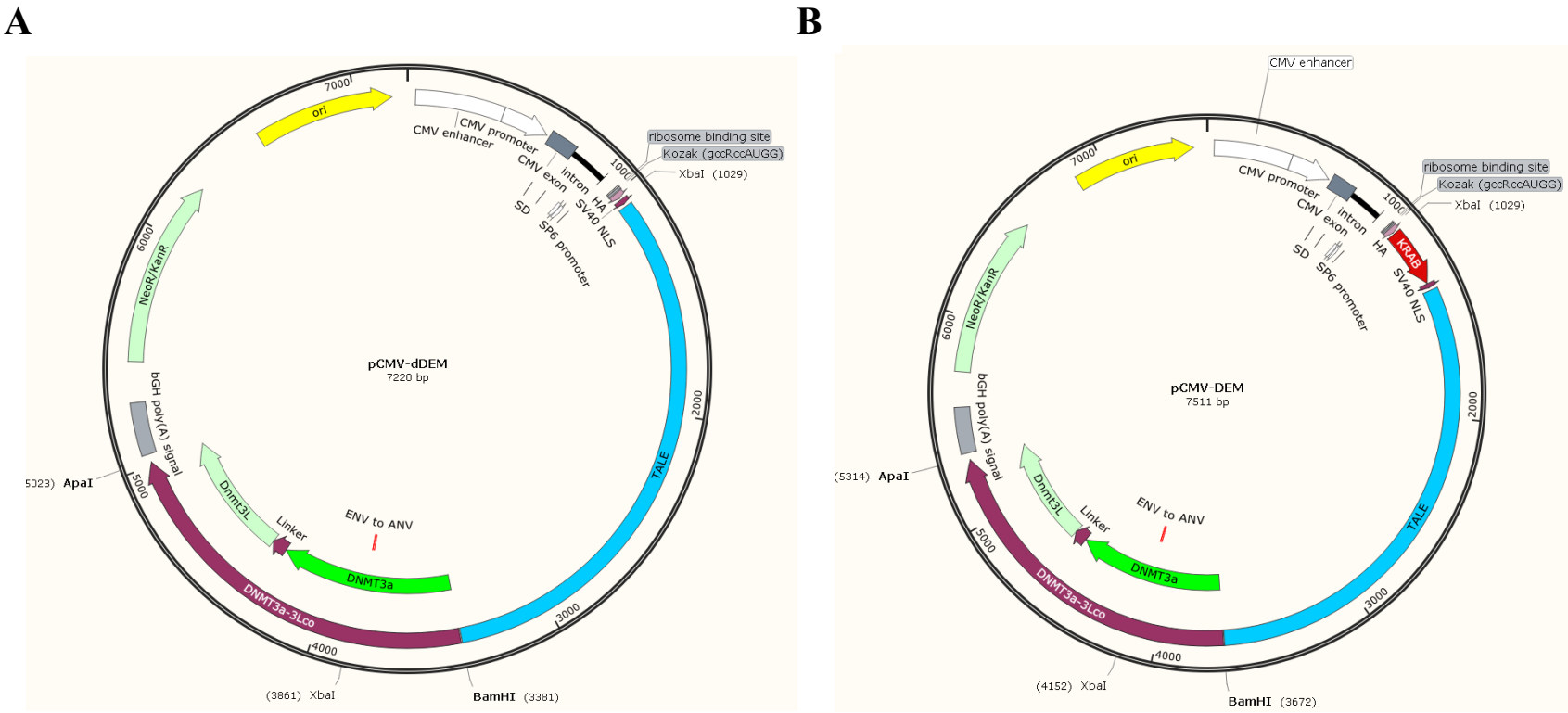

Figure 5.1: Plasmids maps of pCMV-dDEM and pCMV-DEM under the control of a CMV promoter. (**A**) An active DEM consists of TALE-DBDs targeting the *S*, *C*, and *P* ORFs within the HBV genome, combined with key effector domains, including KRAB and DNMT (DNMT3A in conjunction with DNMT3L) domains. (**B**) An inactive DEM comprises the same TALE-DBD as the active DEM and is combined with a dDNMT (mutant DNMT3A in conjunction with DNMT3L) and lacks the KRAB domain. SnapGene® software (from GSL Biotech; available at snapgene.com) was used to generate the plasmid maps.

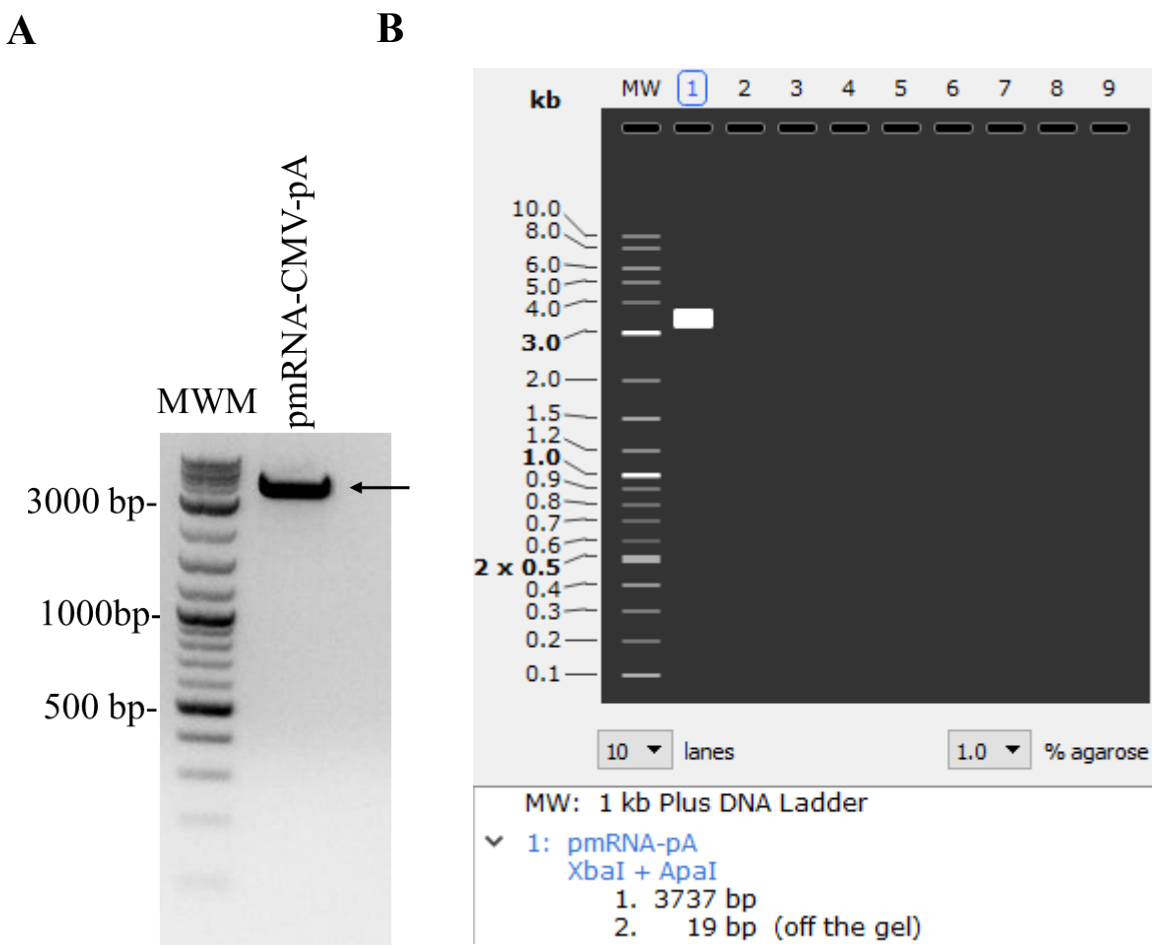

Figure 5.2: Restriction enzyme digestion of pmRNA-pA backbone. **(A)** The pmRNA-pA plasmid was double digested with *Xba*I and *Apa*I to extract the backbone for cloning. Lane 1: Molecular weight marker (O'GeneRuler DNA Ladder Mix). **(B)** Simulated digestion of pmRNA-pA encoding plasmids. A 1% agarose gel generated showing the expected fragment sizes for the digestion of pmRNA-pA with *Xba*I and *Apa*I (Lane 1). Fragment sizes for each band are indicated below, and the molecular weight marker (MW) is the O'GeneRuler DNA Ladder Mix. The simulated gel was generated using SnapGene® software (GSL Biotech; available at snapgene.co

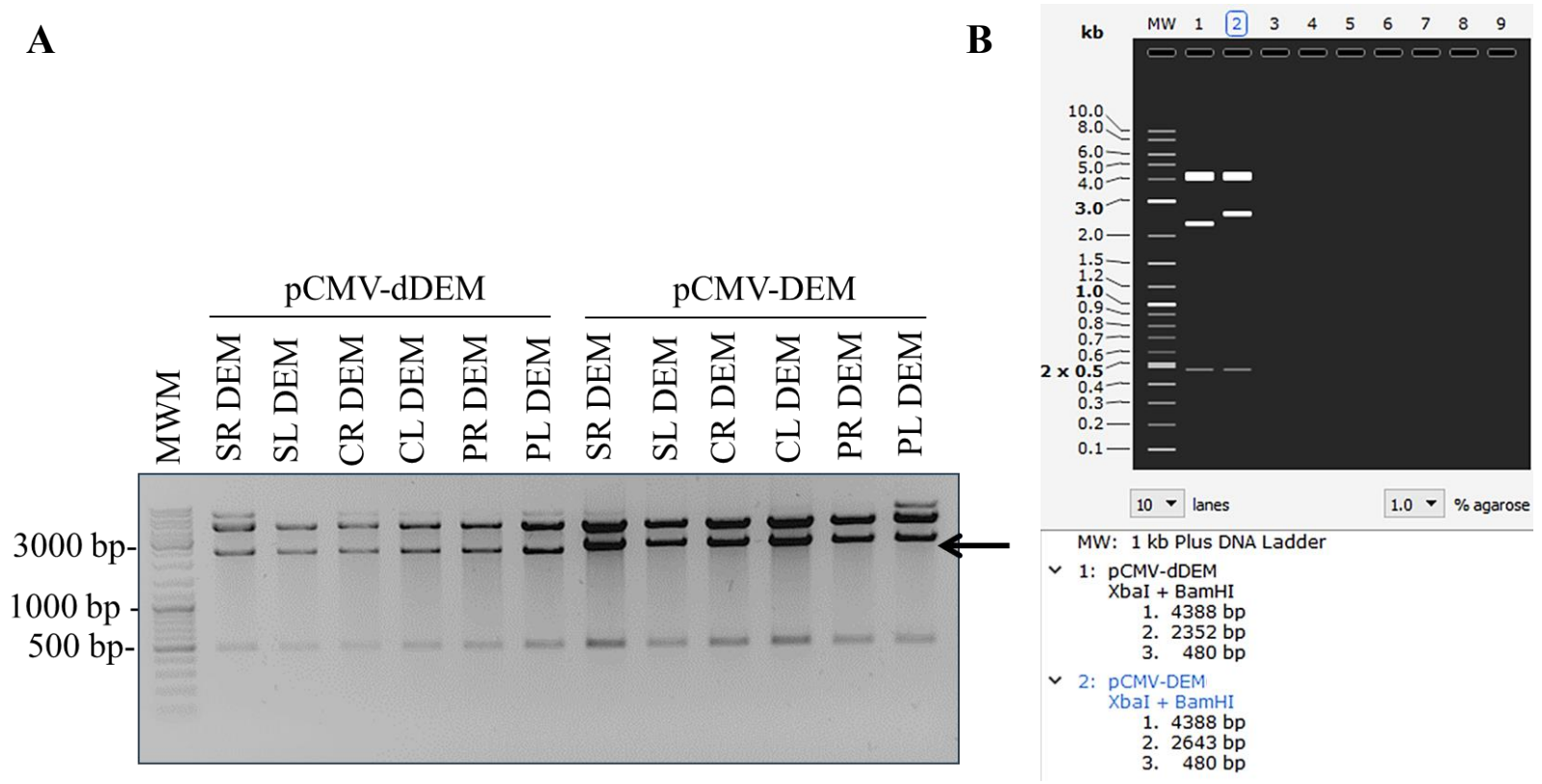

Figure 5.3: Restriction enzyme digestion of CMV inactive and active DEMs to excise the TALE-encoding domain. (**A**) The pCMV-dDEM and pCMV-DEM-encoding plasmids were double digested with *Xba*I and *Bam*HI to excise the TALE-encoding DBDs targeting the *S, C* and *P* ORFs of HBV indicated by the arrow. Lane 1: Molecular weight marker (O'GeneRuler DNA Ladder Mix). (B) Simulated digestion of pCMV-dDEM in Lane 1 and pCMV-DEM in Lane 2. A 1% simulated agarose gel generated showing the expected fragment sizes for the digest of CMV inactive and active DEMs. Fragments sizes for each band are indicated below, and the molecular weight marker (MW) is the O'GeneRuler DNA Ladder Mix. SnapGene® software (from GSL Biotech; available at snapgene.com) was used to generate the simulated gel.

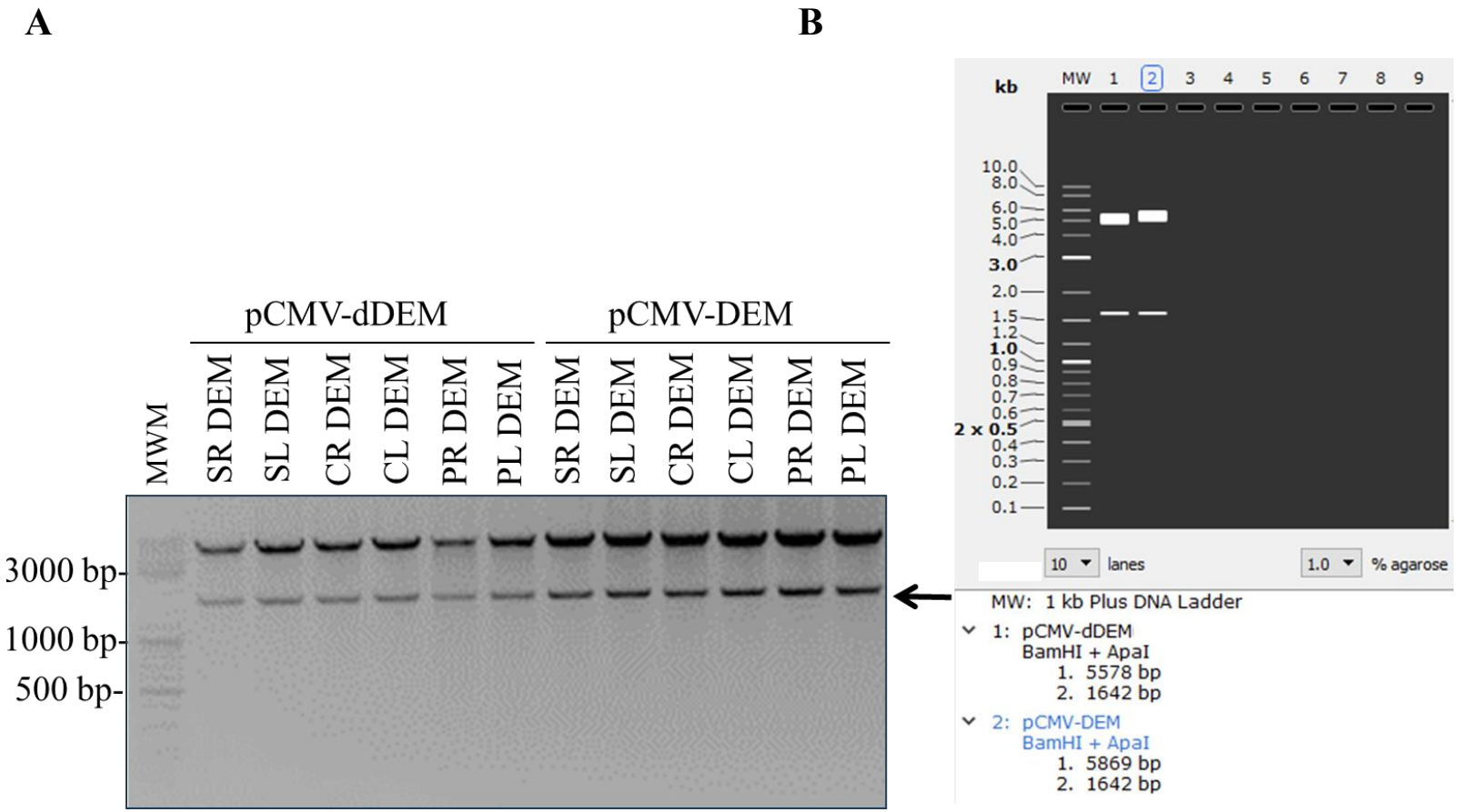

Figure 5.4: Restriction enzyme digestion of CMV inactive and active DEMs to excise the effector-encoding domains. (**A**) The pCMV-dDEM and pCMV-DEM plasmids were double digested with *Bam*HI and *Apa*I to excise the dDNMT from the inactive DEM and the KRAB and DNMT domains from the active DEM, as indicated by the arrow. Lane 1: Molecular weight marker (O'GeneRuler DNA Ladder Mix). (**B**) Simulated digestion of pCMV-dDEM in Lane 1 and pCMV-DEM in Lane 2. A 1% simulated agarose gel was generated indicating the expected fragment sizes for the digest of CMV inactive and active DEMs with *Bam*Hl and *Apa*I. Fragments sizes for each band are indicated below, and the molecular weight marker (MW) is the O'GeneRuler DNA Ladder Mix. SnapGene® software (from GSL Biotech; available at snapgene.com) was used to generate the simulated gel.

5.9 mRNA Platforms for Expressing Transgene Sequences

5.9.1 GFP reporter mRNA expression vector

The pCMV-eGFP double digested with *Xba*I and *Apa*I excised a 727 bp backbone band corresponding to eGFP encoding sequence (Figure 5.5). In separate reaction the pmRNA-pA backbone double digested with *Xba*I and *Apa*I yielded 3737 bp backbone fragment used to for insertion of eGFP transgenes (Figure 5.2). The eGFP-encoding sequence was ligated into the pmRNA-pA vector produced pmRNA-GFP and screening with *Alw*44I and *Ava*II produced the expected banding patterns (Figure 5.6). The constructed plasmids are shown schematically in Chapter 2, Figure 2.2.

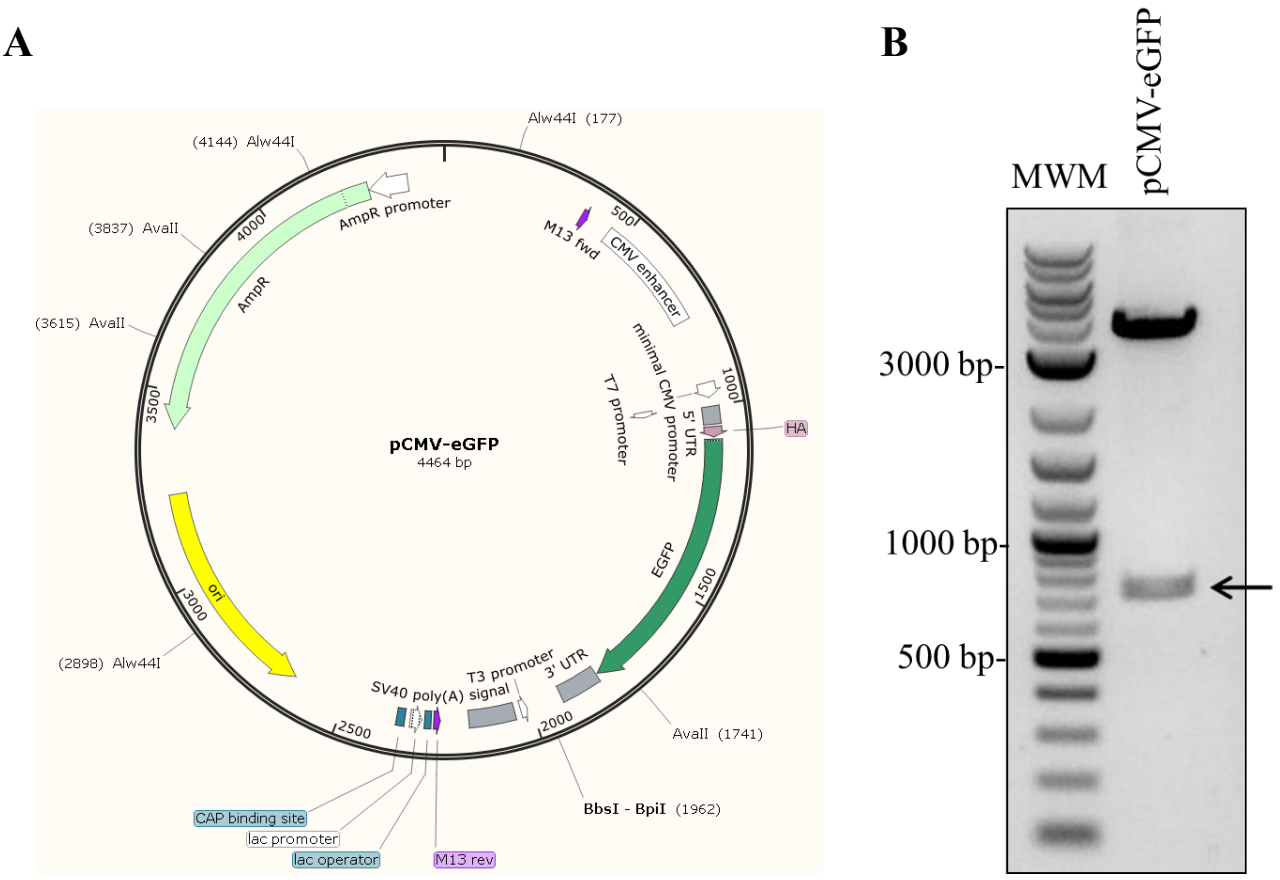

Figure 5.5: Restriction enzyme digestion of pCMV-eGFP -encoding plasmid. (**A**) Plasmid map of pCMV-eGFP showing the two *Bsa*I restriction sites. (**B**) The pCMV-eGFP encoding plasmid was double digested with *Xba*I and *Apa*I to excise the eGFP-sequence. The expected 727 bp band representing eGFP is indicated by the arrow. Lane 1: Molecular weight marker (O'GeneRuler DNA Ladder Mix).

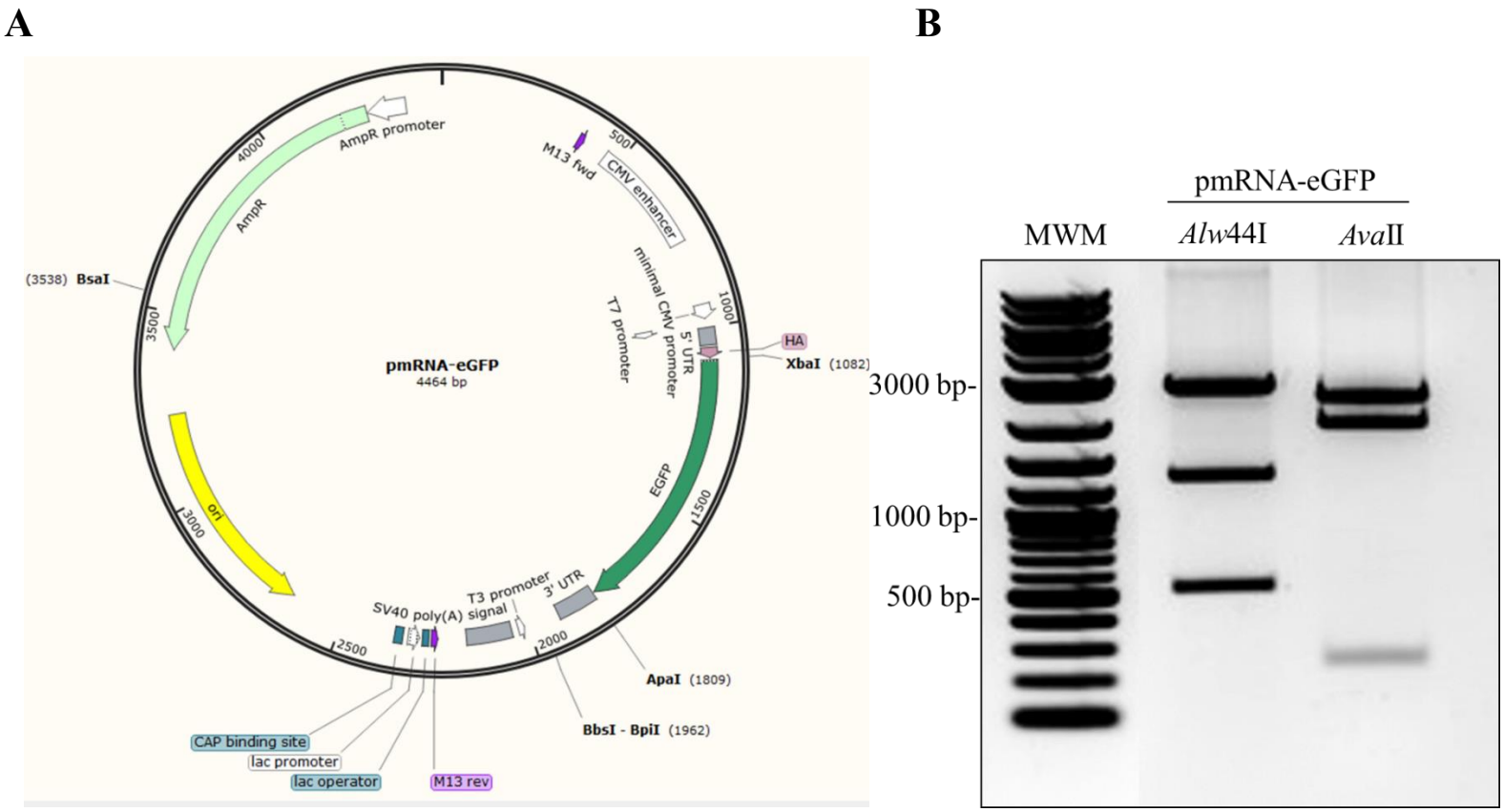

Figure 5.6: Confirmation of GFP reporter mRNA expression vector by enzymatic digestion. (**A**) Plasmid map showing pmRNA-GFP generated by ligation of eGFP-encoding sequence into pmRNA-pA backbone. The pmRNA-GFP contains a single *BbsI/Bpi*I restriction site suitable for linearisation of the plasmid DNA and consists of a total size of 4464 bp containing the essential elements required for IVT. (**B**) The pmRNA-GFP plasmid was digested with *Alw*44I produces fragments sizes of 2721 bp, 1246 bp and 497 bp and *Ava*II produces fragments sizes of 2368 bp, 1874 bp and 222 bp confirming the expected banding pattern Lane 1: MWM, Molecular weight marker (O'GeneRuler DNA Ladder Mix).

5.9.2 Active pmRNA-DEMΔKRAB plasmids

pmRNA-pA backbone double digested with *Xba*I and *Apa*I yielded 3737 bp backbone fragment (Figure 5.2). In separate reactions pCMV-DEM plasmids double digested *Xba*I and *Bam*HI yielded 1642 bp DNMT domain-encoding sequences (Figure 5.4). While double digested pVAX-CMV TALEN plasmids excised 2346 bp band corresponding to remaining TALE domain-encoding sequences (Figure 5.7) which were ligated into the the pmRNA-pA plasmid. This produced pmRNA- DEMΔKRAB plasmids (pmRNA-S, -C and -P DEMΔKRAB) (Figure 5.8). Screening with *Bam*HI and *Apa*I verified the presence of DNMT domain sequences, while *Xba*I and *Bam*HI confirmed the KRAB and TALE domains in active DEMs. *Xba*I and *Nhe*I screening further confirmed absence of KRAB domain in these constructs. All clones exhibited the expected banding patterns (Figure 5.8). The constructed plasmids are shown schematically in Chapter 2, Figure 2.3.

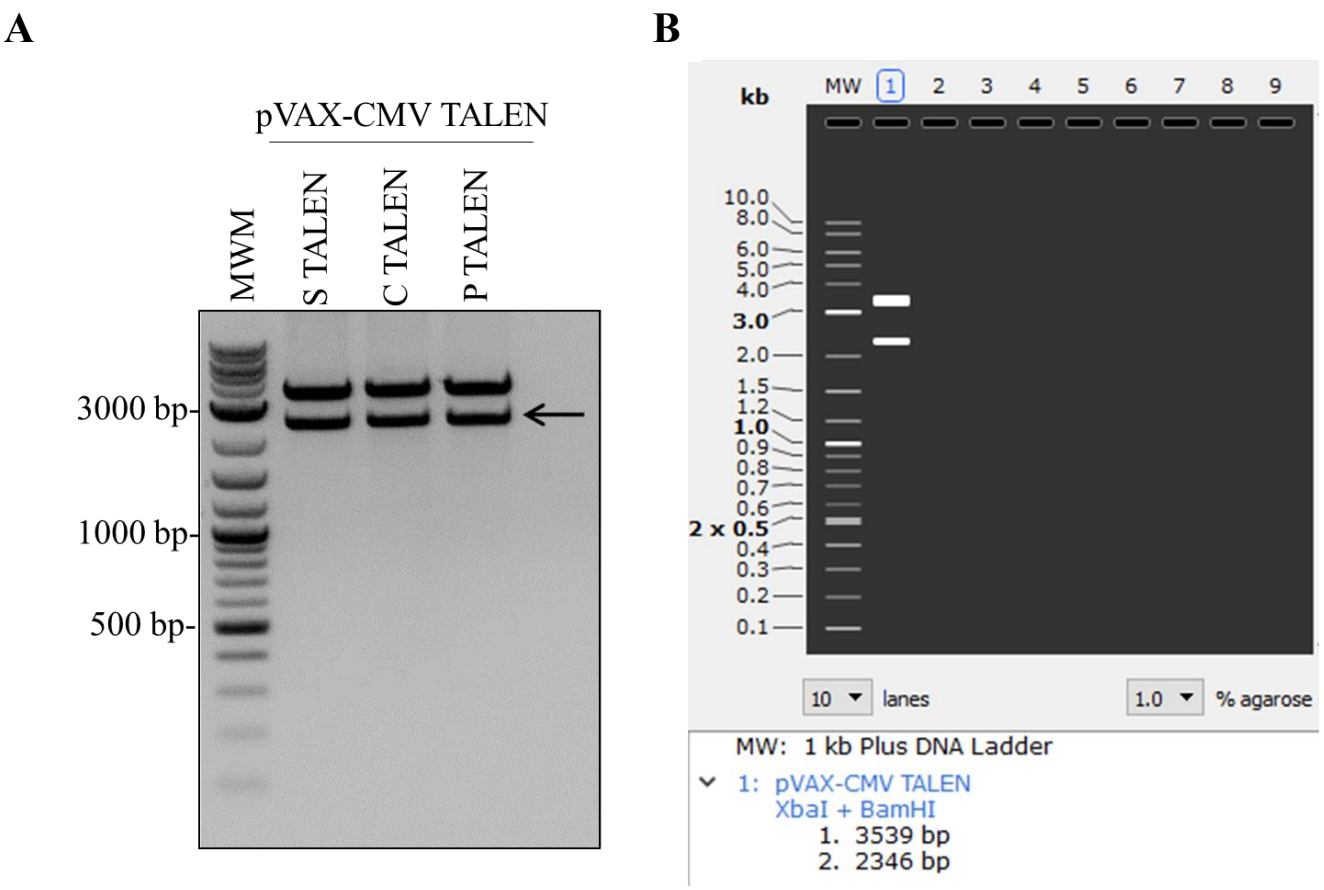

Figure 5.7: Restriction enzyme digestion of pVAX-CMV TALEN-encoding plasmids. (**A**)The pVAX-CMV-S, C and P TALEN-encoding plasmids were double digested with *Xba*I and *Bam*HI to excise the TALE-encoding domain without the KRAB-encoding domain indicated by the arrow. Lane 1: Molecular weight marker (O'GeneRuler DNA Ladder Mix). (**B**) Simulated digestion of pVAX-CMV-S, C and P TALEN encoding plasmids. A 1% simulated agarose gel generated showing the expected fragment sizes for the digest of pVAX-CMVTALENs with *XbaI* and *Bam*Hl. (Lane 1). The fragments sizes for each band are indicated below and the molecular weight marker (MW) is the O'GeneRuler DNA Ladder Mix. SnapGene® software (from GSL Biotech; available at snapgene.com) was used to generate the simulated gel.

A

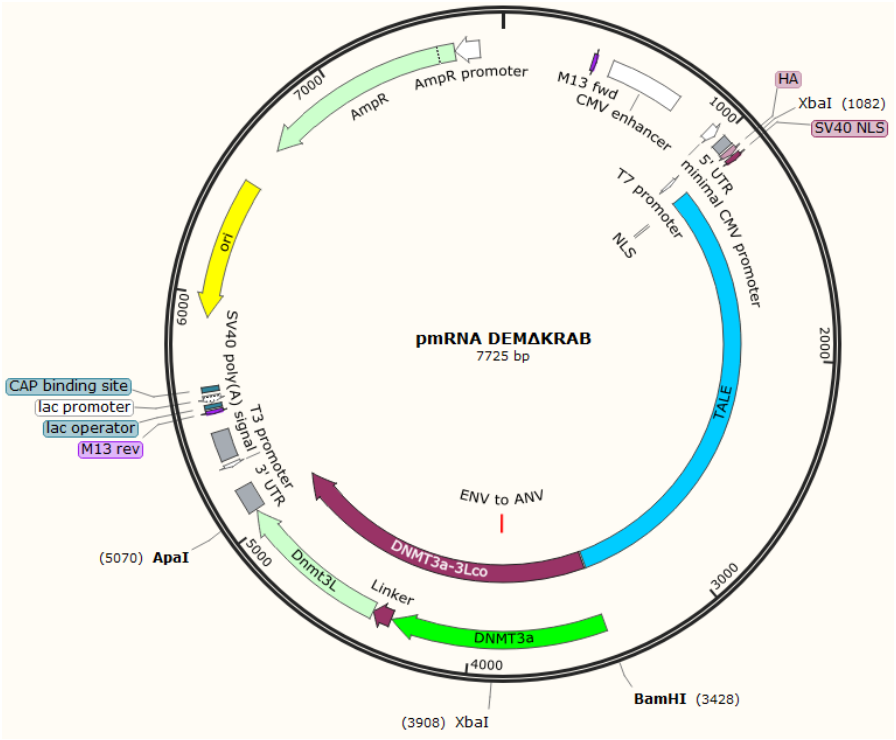

B

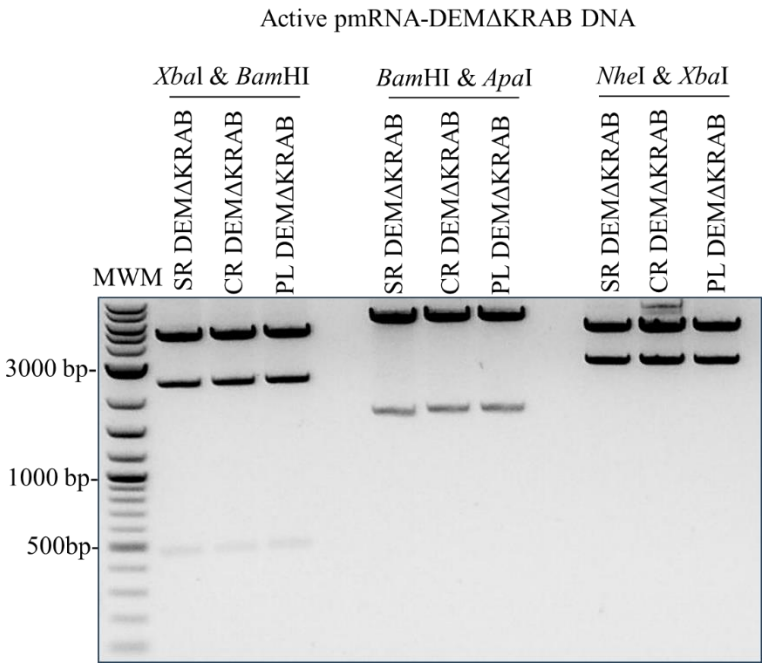

Figure 5.8: Confirmation of active pmRNA-DEMΔKRAB DNA by enzymatic digestion. (**A**) Plasmid map representing active pmRNA-S, C and P DEMΔKRAB plasmids were generated by cloning TALE with active DNMT domain-encoding sequences into an RNA expression vector (pmRNA-pA). (**B**) Restriction digestion of active pmRNA-DEMΔKRAB. Digestion with *Xba*I and *Bam*HI produced 4899 bp, 2352 bp, and 480 bp bands, confirming the presence of the TALE domain-encoding sequence. Digestion with *Bam*HI and *Apa*I produced 6089 bp and 1642 bp bands, confirming the presence of the inactive DNMT domain-encoding sequence. Digestion with *Nhe*I and *Xba*I produced in 4899 bp, 2790 bp, and a 36 bp band (off-agarose gel), confirming the absence of the KRAB domain-encoding sequence. Lane 1: MWM, Molecular weight marker (O'GeneRuler DNA Ladder Mix).

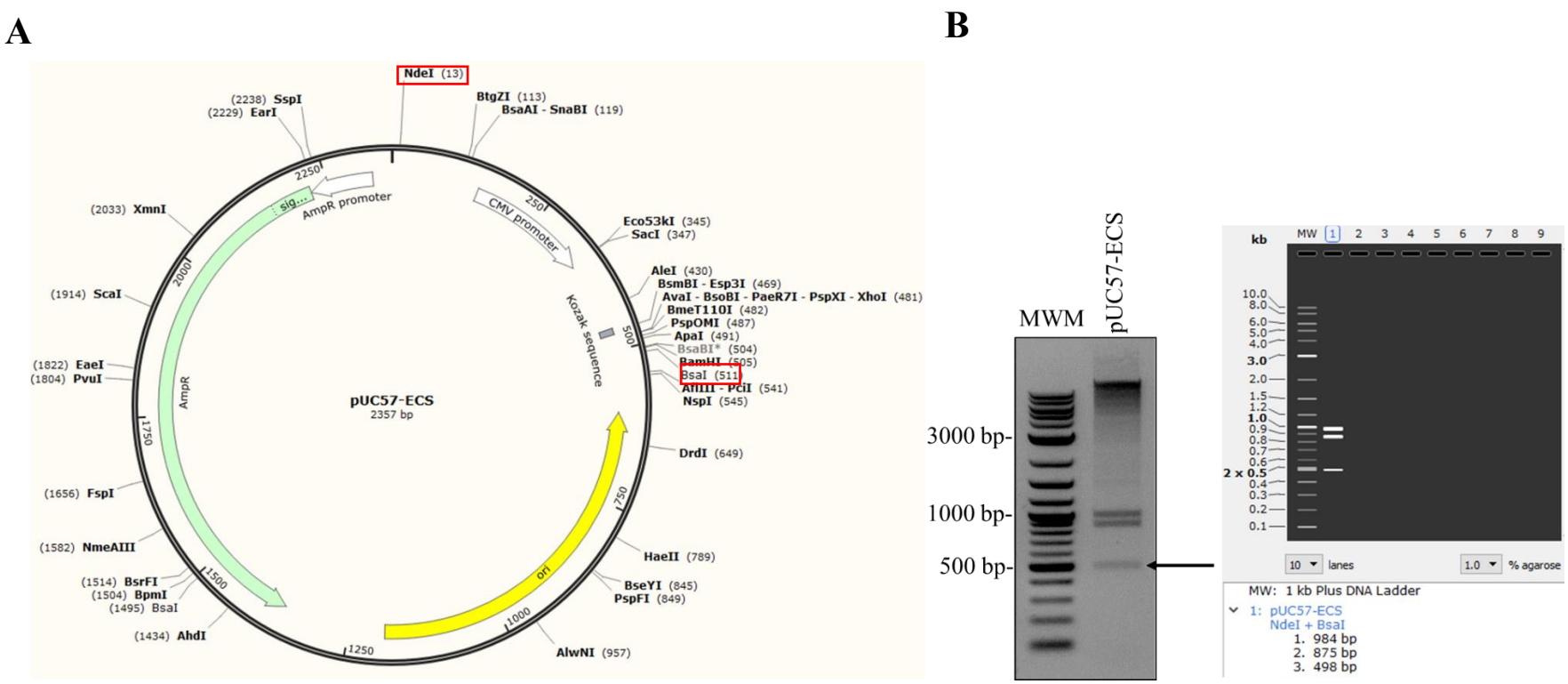

Figure 5.9: Restriction enzyme digestion of pUC57-ECS -encoding plasmid with *Nde*I and *Esp*3I. (**A**) Plasmid map representing pUC-57 mini plasmid containing the ECS insert flanked by *Nde*I and *Bsa*I restriction sites indicated in red. (**B**) The pUC57-ECS plasmid was double digested with *Nde*I and *Bsa*I excising the ECS insert at the expected fragment size of 498 bp indicated by the arrow. On the right is a 1% simulated agarose gel generated showing the expected fragment sizes for the digest of pUC57-ECS with *Nde*l and *Bsa*I. (Lane 1). The fragments sizes for each band are indicated below and the molecular weight marker (MW) is the O'GeneRuler DNA Ladder Mix. SnapGene® software (from GSL Biotech; available at snapgene.com) was used to generate the simulated gel.

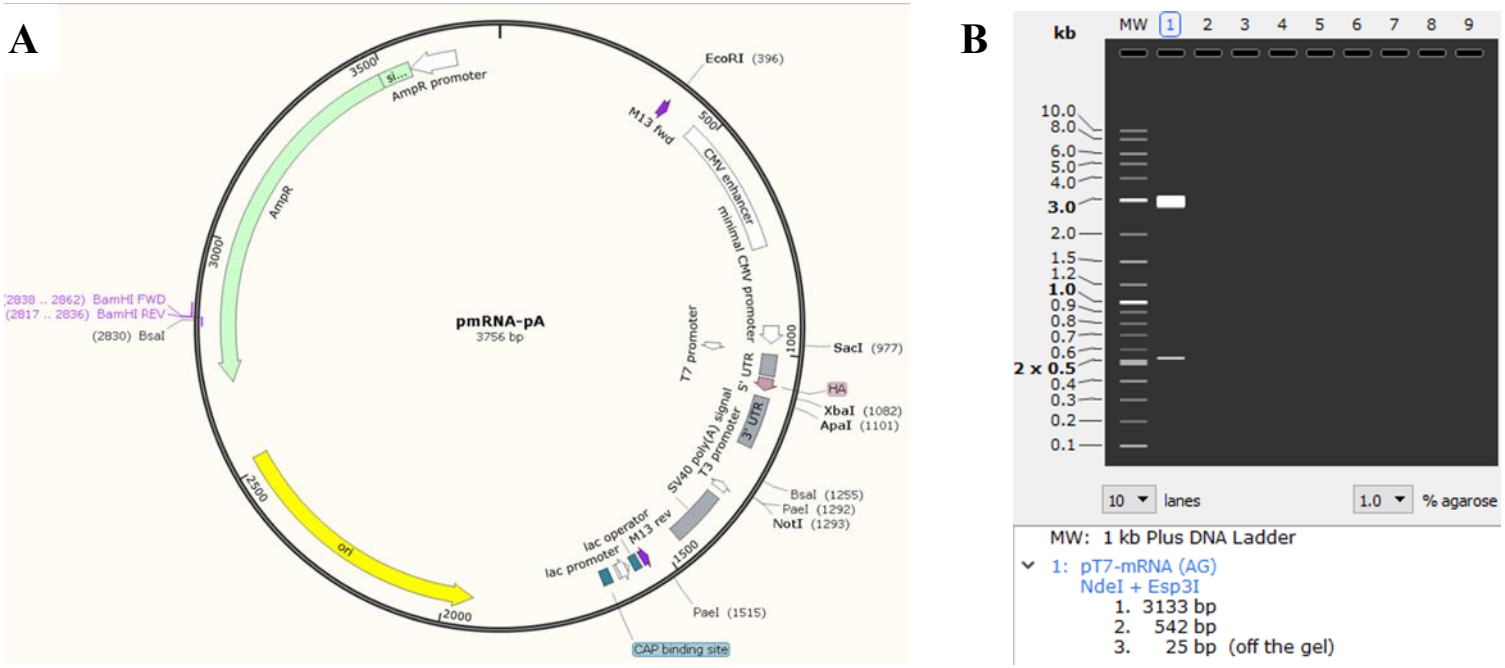

Figure 5.10: Restriction enzyme digestion of pUC57-ECS -encoding plasmid with *Nde*I and *Esp*3I. (**A**) Plasmid map representing pT7(AG) RNA expression vector with essential elements required for IVT. (**B**) A 1% simulated agarose gel generated showing the and expected fragment sizes for the digest of pT7(AG) with *Nde*I and *Esp*3I. (Lane 1). The fragments sizes for each band are indicated below.

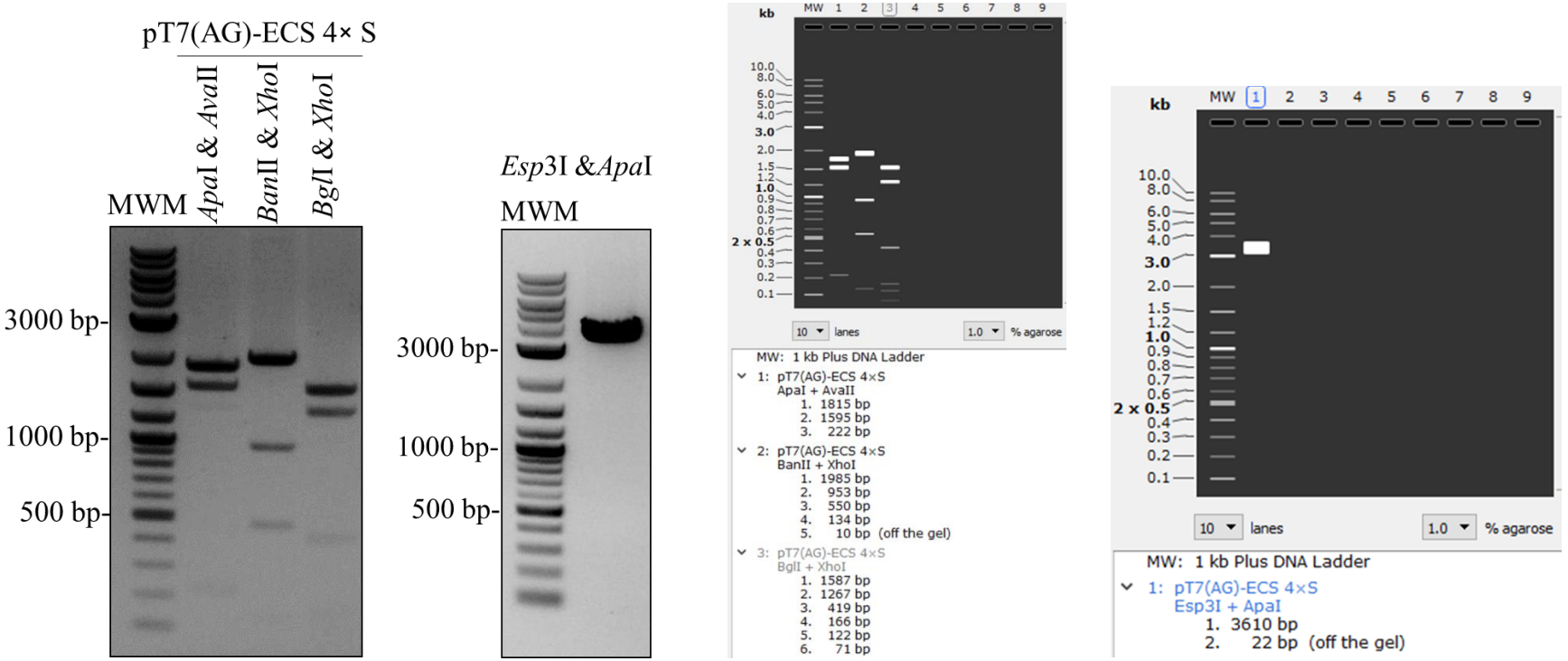

Figure 5.11: Restriction enzyme digestion of pT7(AG)-ECS 4×S-encoding plasmid. (**A**) Restriction digestion of pT7(AG)-ECS 4×S plasmid by *Apa*I and *Ava*II, *Ban*II and *Xho*I and *Bgl*I and *Xho*I confirming the correct ligation of ECS insert into pT7(AG) plasmid. (**B**) Double digestion of pT7(AG)-ECS 4×S plasmid with *Esp*3I and *Apa*I to allow for the ligation of transgene sequences. (C-D) 1% simulated agarose gel generated showing the expected fragment sizes for the digest of pT7(AG)-ECS 4×S with (**C**) *Apa*I and *Ava*II, *Ban*II and *Xho*I and *Bgl*I and *Xho*I and (**D**) *Esp*3I and *Apa*I. All expected fragments were obtained. The fragments sizes for each band are indicated below and the molecular weight marker (MW) is the O'GeneRuler DNA Ladder Mix. SnapGene® software (from GSBotech; available at snapgene.com) was used to generate the simulated gel.

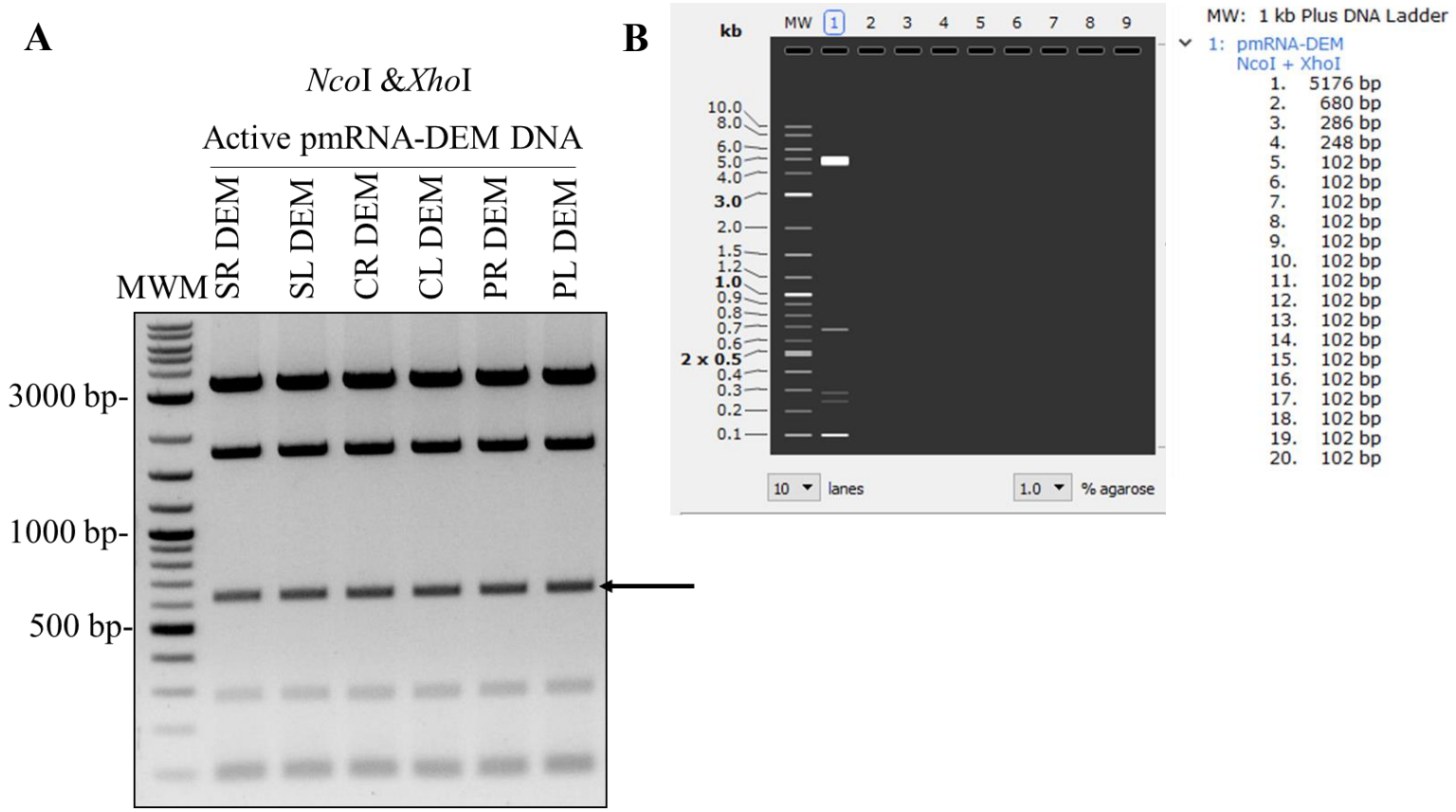

Figure 5.12: Restriction enzyme digestion of active pmRNA-DEMs. (**A**) Active pmRNA-DEM plasmids were double digested with *Nco*I and *Xho*I to excise the TALE HA-KRAB-TALE (TALE 362 bp) fragments at 680 bp as indicated by the arrow. Lane 1: Molecular weight marker (O'GeneRuler DNA Ladder Mix). (**B**) Simulated digestion of Active pmRNA-DEM plasmids in Lane 1. A 1% simulated agarose gel was generated indicating the expected fragment sizes for the digest of active pmRNA-DEM with *Nco*I and *Xho*I. Fragments sizes for each band are indicated on the right, and the molecular weight marker (MW) is the O'GeneRuler DNA Ladder Mix. SnapGene® software (from GSL Biotech; available at snapgene.com) was used to generate the simulated gel.

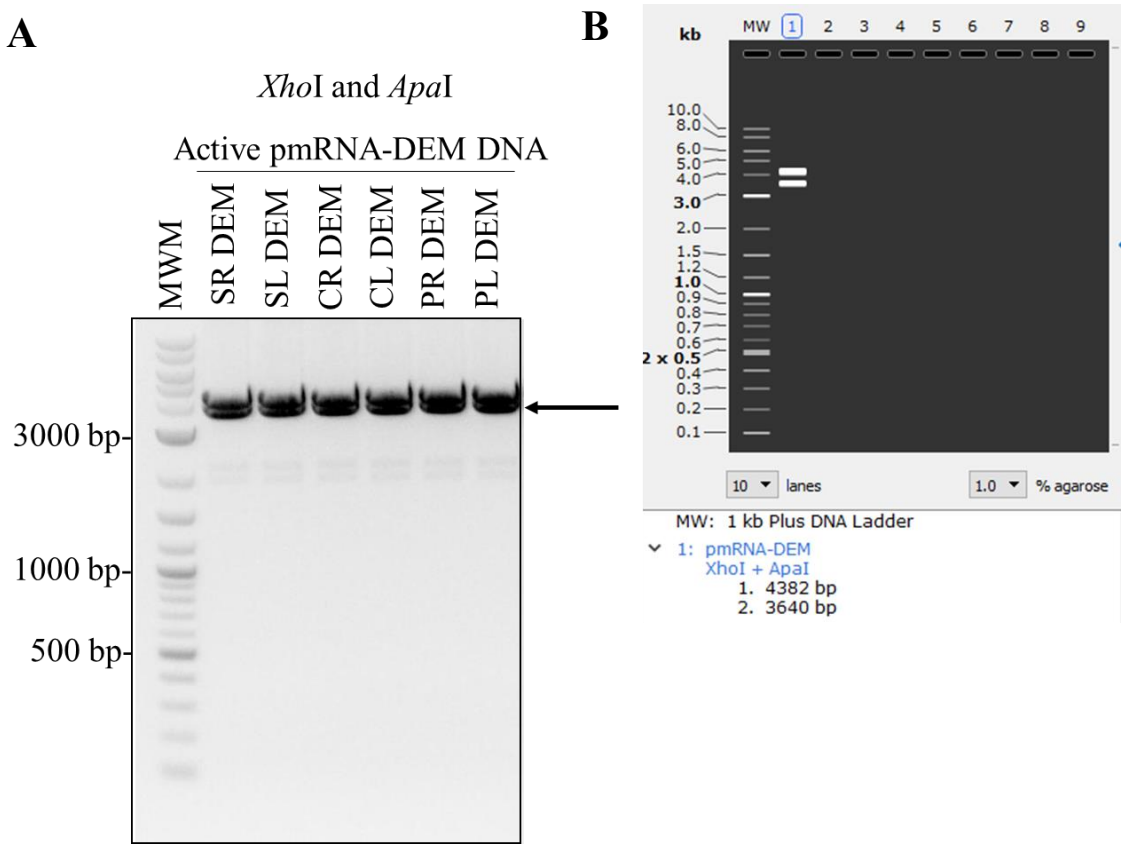

Figure 5.13: Restriction enzyme digestion of active pmRNA-DEMs to excise the TALE-DNMT-encoding sequences. (**A**) Active pmRNA-DEM plasmids were double digested with *Xho*I and *Apa*I to excise the TALE-DNMT-encoding fragments at 3640 bp as indicated by the arrow. Lane 1: Molecular weight marker (O'GeneRuler DNA Ladder Mix). (**B**) Simulated digestion of Active pmRNA-DEM plasmids in Lane 1. A 1% simulated agarose gel was generated indicating the expected fragment sizes for the digest of active pmRNA-DEM with *Xho*I and *Apa*I. Fragments sizes for each band are indicated below, and the molecular weight marker (MW) is O'GeneRuler DNA Ladder Mix. SnapGene® software (from GSL Biotech; available at snapgene.com) was used to generate the simulated gel

5.9.3 Active pT7(AG)-DEMΔKRAB 4×S plasmids

The pT7(AG)-ECS 4×S backbone double digested with *Esp*3I and *Apa*l yielded a 3610 bp backbone fragment (Figure 5.11 B). In separate reactions pmRNA-SR, SL, PL DEMs double digested *Nco*I and *Xho*I yielded 383 bp corresponding TALE 362 bp (Figure 5.14 A). While double digested pmRNA-SR, SL, PL DEMs excised 3640 bp band corresponding to remaining TALE-DNMT-encoding domains (Figure 5.14 B) which were ligated into the the pT7(AG)-ECS 4×S plasmid. This produced pT7(AG)-DEMΔKRAB 4×S plasmids (pT7(AG)-SR, -SL, and -PL DEMΔKRAB 4×S) (Figure 5.15**)**. Screening with *Ban*II, *Pvu*II and *Xba*I and *Nhe*I confirmed successful cloning with expected banding patterns achieved with all six DEMs **(**Figure 5.15**).**

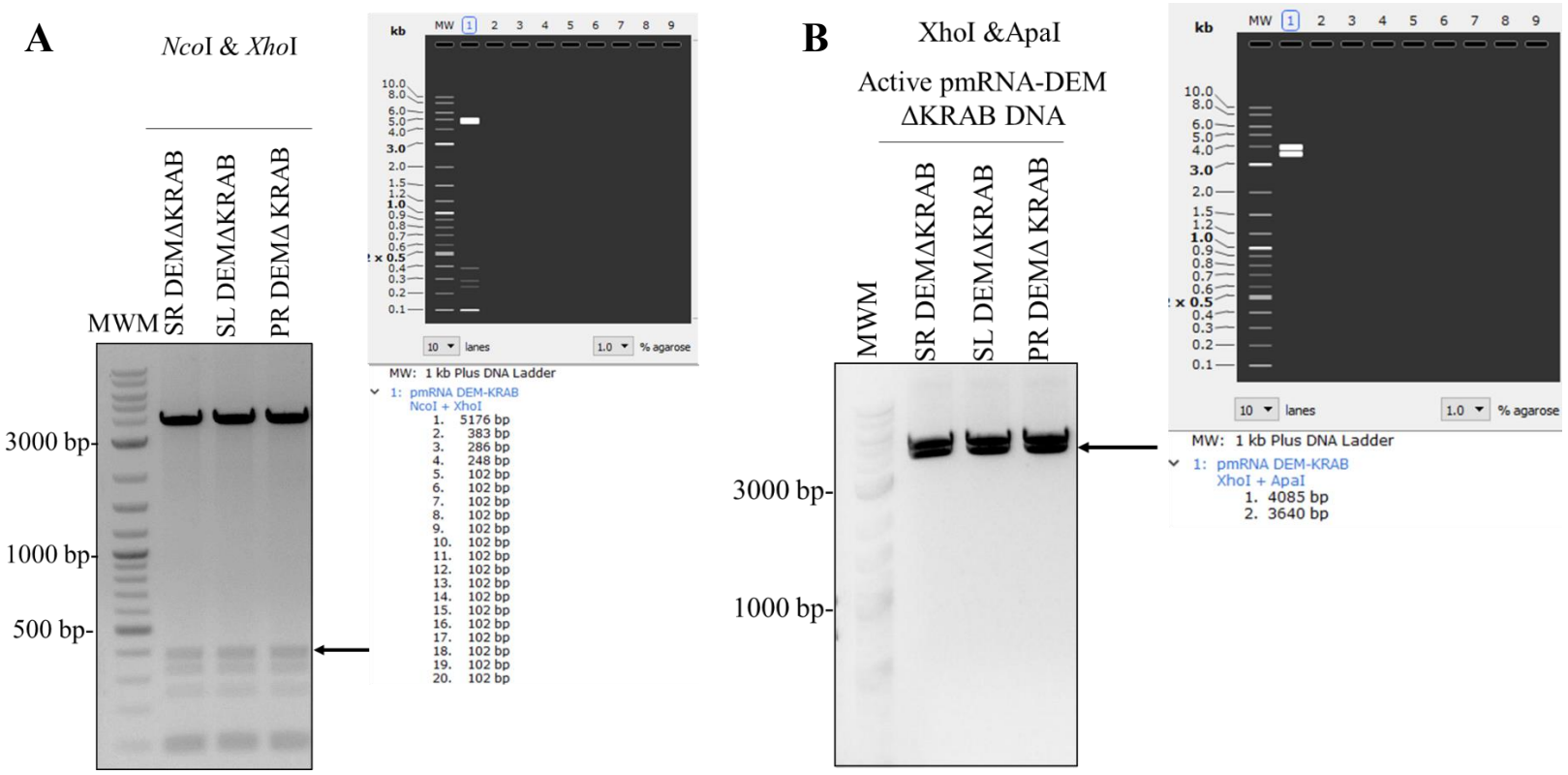

Figure 5.14: Restriction enzyme digestion of active pmRNA-DEMΔKRAB to excise transgenes. (**A**) Active pmRNA-DEMΔKRAB plasmids were double digested with *Nco*I and *Xho*I to excise the HA-TALE (TALE 362 bp)-encoding fragments at 383 bp as indicated by the arrow. Lane 1: Molecular weight marker (O'GeneRuler DNA Ladder Mix). On the right is a 1% simulated agarose gel was generated indicating the expected fragment sizes for the digest of active pmRNA-DEMΔKRAB plasmids with *Nco*I and *Xho*I. Fragments sizes for each band are indicated below. (**B**) Active pmRNA-DEMΔKRAB plasmids were double digested with *Xho*I and *Apa*I to excise the TALE-DNMT-encoding fragments at 3640 bp as indicated by the arrow. Lane 1: Molecular weight marker (O'GeneRuler DNA Ladder Mix). On the right is a 1% simulated agarose gel was generated indicating the expected fragment sizes for the digest of active pmRNA-DEMΔKRAB plasmids with *Xho*I and *Apa*I, and the molecular weight marker (MW) is the O'GeneRuler DNA Ladder Mix. SnapGene® software (from GSL Biotech; available at snapgene.com) was used to generate the simulated gel.

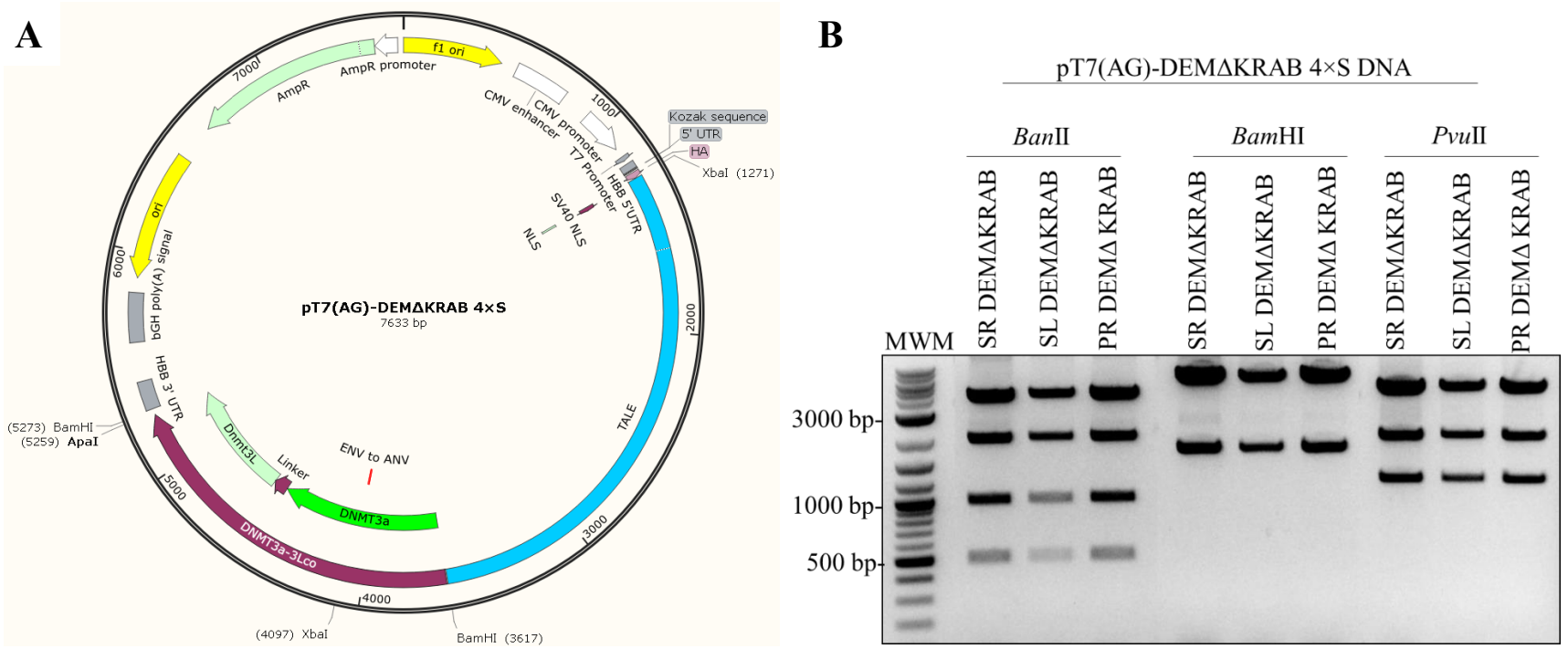

Figure 5.15: Confirmation of active pT7-DEMΔKRAB AG 4× DNA by enzymatic digestion. (**A**) Active pT7-DEMΔ AG 4× plasmids were generated by cloning TALE domain-encoding along with DNMT (DNMT3A + DNMT3L) domain-encoding sequences into an pT7(AG)-ECS 4×S RNA expression vector. (**B**) Restriction digestion of active pT7(AG)-ECS 4×S plasmids with *Ban*II, *Bam*HI and *Pvu*II. All enzymatic digestion reactions produced expected banding pattern. Lane 1: MWM, Molecular weight marker (O'GeneRuler DNA Ladder Mix).

Appendix

Table 5.6: Amino Acid Repeat-Variable Di-Residues (RVDs) of S, C, and P TALE-DBDs Responsible for Single Nucleotide Recognition (Bloom et al., 2013)

	Right TALE	**Left TALE**
Surface TALE DBD amino acid sequence	NI, HD, HD, NG, NG, NK, NI, NG, NI, NK, NG, HD, HDNI, NK, NI, NI, NK	HD, HD, NG, NK, HD, NG, NK, HD, NG, NI, NG, NK, HD, HD, NG, HD NI, NG
Core TALE DBD amino acid sequence	NI, NN, NN, NN, NN, NI, HD, HD, NG, NN, HD, HD, NG, HD, NN, NG, HD, NK	NI, NG, HD, NI, NI, HD, NI, HD, NG, NG, HD, HD, NN, NN, NI, NN, NI, HD,
Polymerase TALE DBD amino acid sequence	NN, HD, NN, NG, HD, NI, NN, HD, NI, NI, NI, HD, NI, HD, NG, NG, NN, NK	NI, HD, HD, HD, HD, NN, NG, NG, NN, HD, HD, HD, NN, NN, HD, NI, NI, HD

Key:

Amino acid RVD: Nucleotide target

HD: C

NI: A

NG: T

NK: G

NN: G

A

Sequencing results from S, C and P DEMs

Aligned using Clustal Omega and then edited

Consensus
1. pT7(AG)-SR DEM 4× STALE Forward
2. pT7(AG)-SL DEM 4× STALE Forward
3. pT7(AG)-CR DEM 4× STALE Forward
4. pT7(AG)-CL DEM 4× STALE Forward
5. pT7(AG)-PR DEM 4× STALE Forward
6. pT7(AG)-PL DEM 4× STALE Forward

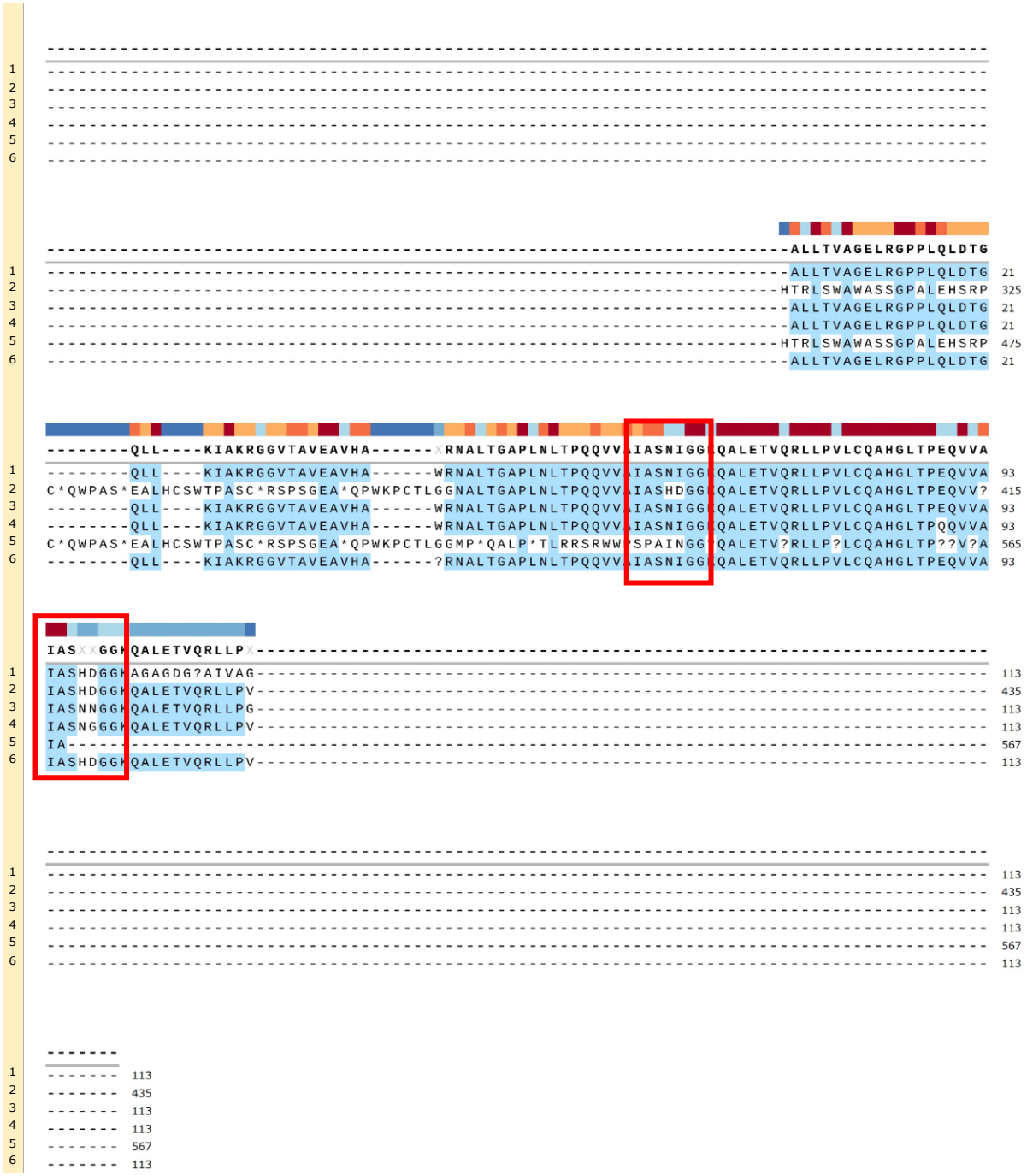

B

Aligned using Clustal Omega and then edited

Consensus
1. pT7(AG)-SR DEM 4× STALE Reverse
2. pT7(AG)-SL DEM 4× STALE Reverse
3. pT7(AG)-CR DEM 4× STALE Reverse
4. pT7(AG)-CL DEM 4× STALE Reverse
5. pT7(AG)-PR DEM 4× STALE Reverse
6. pT7(AG)-PL DEM 4× STALE Reverse



Figure 5.16: Sequencing confirmation of TALE-DBD sequences in Anti-HBV DEMs. Amino acid sequences of the S, C, and P TALEs were aligned, with the repeat variable diresidue (RVDs) responsible for single nucleotide recognition highlighted in the red box. Sequencing was performed in both directions using (A) forward and (B) reverse primers to obtain complete TALE-DBD sequences. Alignments were conducted using SnapGene® software (GSL Biotech; available at snapgene.com).

Aligned using MUSCLE and then edited

Consensus

1. Reference sequence, DNMT3A
2. pT7(AG)-SR DEM 4× S
3. pT7(AG)-SL DEM 4× S
4. pT7(AG)-CR DEM 4× S
5. pT7(AG)-CL DEM 4× S
6. pT7(AG)-PR DEM 4× S
7. pT7(AG)-PL DEM 4× S
8.

```
AACCATGATCAAGAGTTCGATCCTCCTAAAGTGTATCCCCCTGTCCCTGCCGAAAAGCGGAAACCGATCAGGGTTCTCAGTCTCTTCGAT
AACCATGATCAAGAGTTCGATCCTCCTAAAGTGTATCCCCCTGTCCCTGCCGAAAAGCGGAAACCGATCAGGGTTCTCAGTCTCTTCGAT 90
1 AACCATGATCAAGAGTTCGATCCTCCTAAAGTGTATCCCCCTGTCCCTGCCGAAAAGCGGAAACCGATCAGGGTTCTCAGTCTCTTCGAT 90
2 AACCATGATCAAGAGTTCGATCCTCCTAAAGTGTATCCCCCTGTCCCTGCCGAAAAGCGGAAACCGATCAGGGTTCTCAGTCTCTTCGAT 90
3 AACCATGATCAAGAGTTCGATCCTCCTAAAGTGTATCCCCCTGTCCCTGCCGAAAAGCGGAAACCGATCAGGGTTCTCAGTCTCTTCGAT 90
4 AACCATGATCAAGAGTTCGATCCTCCTAAAGTGTATCCCCCTGTCCCTGCCGAAAAGCGGAAACCGATCAGGGTTCTCAGTCTCTTCGAT 90
5 AACCATGATCAAGAGTTCGATCCTCCTAAAGTGTATCCCCCTGTCCCTGCCGAAAAGCGGAAACCGATCAGGGTTCTCAGTCTCTTCGAT 90
6 AACCATGATCAAGAGTTCGATCCTCCTAAAGTGTATCCCCCTGTCCCTGCCGAAAAGCGGAAACCGATCAGGGTTCTCAGTCTCTTCGAT 90
7

GGAATTGCCACAGGCCTCTTGGTCCTTAAGGACCTGGGCATCCAAGTGGACCGCTACATCGCCTCAGAAGTATGTGAGGACAGCATCACA
GGAATTGCCACAGGCCTCTTGGTCCTTAAGGACCTGGGCATCCAAGTGGACCGCTACATCGCCTCAGAAGTATGTGAGGACAGCATCACA 180
1 GGAATTGCCACAGGCCTCTTGGTCCTTAAGGACCTGGGCATCCAAGTGGACCGCTACATCGCCTCAGAAGTATGTGAGGACAGCATCACA 180
2 GGAATTGCCACAGGCCTCTTGGTCCTTAAGGACCTGGGCATCCAAGTGGACCGCTACATCGCCTCAGAAGTATGTGAGGACAGCATCACA 180
3 GGAATTGCCACAGGCCTCTTGGTCCTTAAGGACCTGGGCATCCAAGTGGACCGCTACATCGCCTCAGAAGTATGTGAGGACAGCATCACA 180
4 GGAATTGCCACAGGCCTCTTGGTCCTTAAGGACCTGGGCATCCAAGTGGACCGCTACATCGCCTCAGAAGTATGTGAGGACAGCATCACA 180
5 GGAATTGCCACAGGCCTCTTGGTCCTTAAGGACCTGGGCATCCAAGTGGACCGCTACATCGCCTCAGAAGTATGTGAGGACAGCATCACA 180
6 GGAATTGCCACAGGCCTCTTGGTCCTTAAGGACCTGGGCATCCAAGTGGACCGCTACATCGCCTCAGAAGTATGTGAGGACAGCATCACA 180
7

GTCGGCATGGTGCGCCACCAGGGGAAAATAATGTACGTCGGCGACGTCAGATCAGTTACTCAGAAACATATTCAGGAATGGGGGCCTTTT
GTCGGCATGGTGCGCCACCAGGGGAAAATAATGTACGTCGGCGACGTCAGATCAGTTACTCAGAAACATATTCAGGAATGGGGGCCTTTT 270
1 GTCGGCATGGTGCGCCACCAGGGGAAAATAATGTACGTCGGCGACGTCAGATCAGTTACTCAGAAACATATTCAGGAATGGGGGCCTTTT 270
2 GTCGGCATGGTGCGCCACCAGGGGAAAATAATGTACGTCGGCGACGTCAGATCAGTTACTCAGAAACATATTCAGGAATGGGGGCCTTTT 270
3 GTCGGCATGGTGCGCCACCAGGGGAAAATAATGTACGTCGGCGACGTCAGATCAGTTACTCAGAAACATATTCAGGAATGGGGGCCTTTT 270
4 GTCGGCATGGTGCGCCACCAGGGGAAAATAATGTACGTCGGCGACGTCAGATCAGTTACTCAGAAACATATTCAGGAATGGGGGCCTTTT 270
5 GTCGGCATGGTGCGCCACCAGGGGAAAATAATGTACGTCGGCGACGTCAGATCAGTTACTCAGAAACATATTCAGGAATGGGGGCCTTTT 270
6 GTCGGCATGGTGCGCCACCAGGGGAAAATAATGTACGTCGGCGACGTCAGATCAGTTACTCAGAAACATATTCAGGAATGGGGGCCTTTT 270
7

GATCTCGTAATTGGCGGCAGCCCCTGCAATGATCTGAGTATTGTGAACCCCGCCCGGAAAGGTTTGTACGAAGGTACGGGCAGACTGTTC
GATCTCGTAATTGGCGGCAGCCCCTGCAATGATCTGAGTATTGTGAACCCCGCCCGGAAAGGTTTGTACGAAGGTACGGGCAGACTGTTC 360
1 GATCTCGTAATTGGCGGCAGCCCCTGCAATGATCTGAGTATTGTGAACCCCGCCCGGAAAGGTTTGTACGAAGGTACGGGCAGACTGTTC 360
2 GATCTCGTAATTGGCGGCAGCCCCTGCAATGATCTGAGTATTGTGAACCCCGCCCGGAAAGGTTTGTACGAAGGTACGGGCAGACTGTTC 360
3 GATCTCGTAATTGGCGGCAGCCCCTGCAATGATCTGAGTATTGTGAACCCCGCCCGGAAAGGTTTGTACGAAGGTACGGGCAGACTGTTC 360
4 GATCTCGTAATTGGCGGCAGCCCCTGCAATGATCTGAGTATTGTGAACCCCGCCCGGAAAGGTTTGTACGAAGGTACGGGCAGACTGTTC 360
5 GATCTCGTAATTGGCGGCAGCCCCTGCAATGATCTGAGTATTGTGAACCCCGCCCGGAAAGGTTTGTACGAAGGTACGGGCAGACTGTTC 360
6 GATCTCGTAATTGGCGGCAGCCCCTGCAATGATCTGAGTATTGTGAACCCCGCCCGGAAAGGTTTGTACGAAGGTACGGGCAGACTGTTC 360
7

TTCGAGTTTTACAGACTGTTGCACGACGCACGACCAAAGGAGGGTGACGATCGACCCTTCTTCTGGCTGTTCGAGAACGTGGTCGCTATG
TTCGAGTTTTACAGACTGTTGCACGACGCACGACCAAAGGAGGGTGACGATCGACCCTTCTTCTGGCTGTTCGAGAACGTGGTCGCTATG 450
1 TTCGAGTTTTACAGACTGTTGCACGACGCACGACCAAAGGAGGGTGACGATCGACCCTTCTTCTGGCTGTTCGAGAACGTGGTCGCTATG 450
2 TTCGAGTTTTACAGACTGTTGCACGACGCACGACCAAAGGAGGGTGACGATCGACCCTTCTTCTGGCTGTTCGAGAACGTGGTCGCTATG 450
3 TTCGAGTTTTACAGACTGTTGCACGACGCACGACCAAAGGAGGGTGACGATCGACCCTTCTTCTGGCTGTTCGAGAACGTGGTCGCTATG 450
4 TTCGAGTTTTACAGACTGTTGCACGACGCACGACCAAAGGAGGGTGACGATCGACCCTTCTTCTGGCTGTTCGAGAACGTGGTCGCTATG 450
5 TTCGAGTTTTACAGACTGTTGCACGACGCACGACCAAAGGAGGGTGACGATCGACCCTTCTTCTGGCTGTTCGAGAACGTGGTCGCTATG 450
6 TTCGAGTTTTACAGACTGTTGCACGACGCACGACCAAAGGAGGGTGACGATCGACCCTTCTTCTGGCTGTTCGAGAACGTGGTCGCTATG 450
7

GGCGTGTCTGACAAGCGGGACATTTCTAGATTCCTGGAGAGCAATCCAGTGATGATTGATGCAAAGGAAGTATCCGCTGCCCACCGCGCC
GGCGTGTCTGACAAGCGGGACATTTCTAGATTCCTGGAGAGCAATCCAGTGATGATTGATGCAAAGGAAGTATCCGCTGCCCACCGCGCC 540
1 GGCGTGTCTGACWMGCGGGACATTTCTAGATTCCTGGAGAGCAATCCAGTGATGATTGATGCAAAGGAAGTATCCGCTGCCCACCGCGCC 540
2 GGCGTGTCTGACWMGCGGGACATTTCTAGATTCCTGGAGAGCAATCCAGTGATGATTGATGCAAAGGAAGTATCCGCTGCCCACCGCGCC 540
3 GGCGTGTCTGACAAGCGGGACATTTCTAGATTCCTGGAGAGCAATCCAGTGATGATTGATGCAAAGGAAGTATCCGCTGCCCACCGCGCC 540
4 GGCGTGTCTGACAAGCGGGACATTTCTAGATTCCTGGAGAGCAATCCAGTGATGATTGATGCAAAGGAAGTATCCGCTGCCCACCGCGCC 540
5 GGCGTGTCTGACWMGCGGGACATTTCTAGATTCCTGGAGAGCAATCCAGTGATGATTGATGCAAAGGAAGTATCCGCTGCCCACCGCGCC 540
6 GGCGTGTCTGACAAGCGGGACATTTCTAGATTCCTGGAGAGCAATCCAGTGATGATTGATGCAAAGGAAGTATCCGCTGCCCACCGCGCC 540
7

AGATACTTCTGGGGCAATCTGCCCGGCATGAATCGACCCTTGGCAAGCACCGTGAATGATAAGTTGGAGTTGCAGGAGTGTCTGGAGCAT
1 AGATACTTCTGGGGCAATCTGCCCGGCATGAATCGACCCTTGGCAAGCACCGTGAATGATAAGTTGGAGTTGCAGGAGTGTCTGGAGCAT 630
2 AGATACTTCTGGGGCAATCTGCCCGGCATGAATCGACCCTTGGCAAGCACCGTGAATGATAAGTTGGAGTTGCAGGAGTGTCTGGAGCAT 630
3 AGATACTTCTGGGGCAATCTGCCCGGCATGAATCGACCCTTGGCAAGCACCGTGAATGATAAGTTGGAGTTGCAGGAGTGTCTGGAGCAT 630
4 AGATACTTCTGGGGCAATCTGCCCGGCATGAATCGACCCTTGGCAAGCACCGTGAATGATAAGTTGGAGTTGCAGGAGTGTCTGGAGCAT 630
5 AGATACTTCTGGGGCAATCTGCCCGGCATGAATCGACCCTTGGCAAGCACCGTGAATGATAAGTTGGAGTTGCAGGAGTGTCTGGAGCAT 630
6 AGATACTTCTGGGGCAATCTGCCCGGCATGAATCGACCCTTGGCAAGCACCGTGAATGATAAGTTGGAGTTGCAGGAGTGTCTGGAGCAT 630
7 AGATACTTCTGGGGCAATCTGCCCGGCATGAATCGACCCTTGGCAAGCACCGTGAATGATAAGTTGGAGTTGCAGGAGTGTCTGGAGCAT 630
```

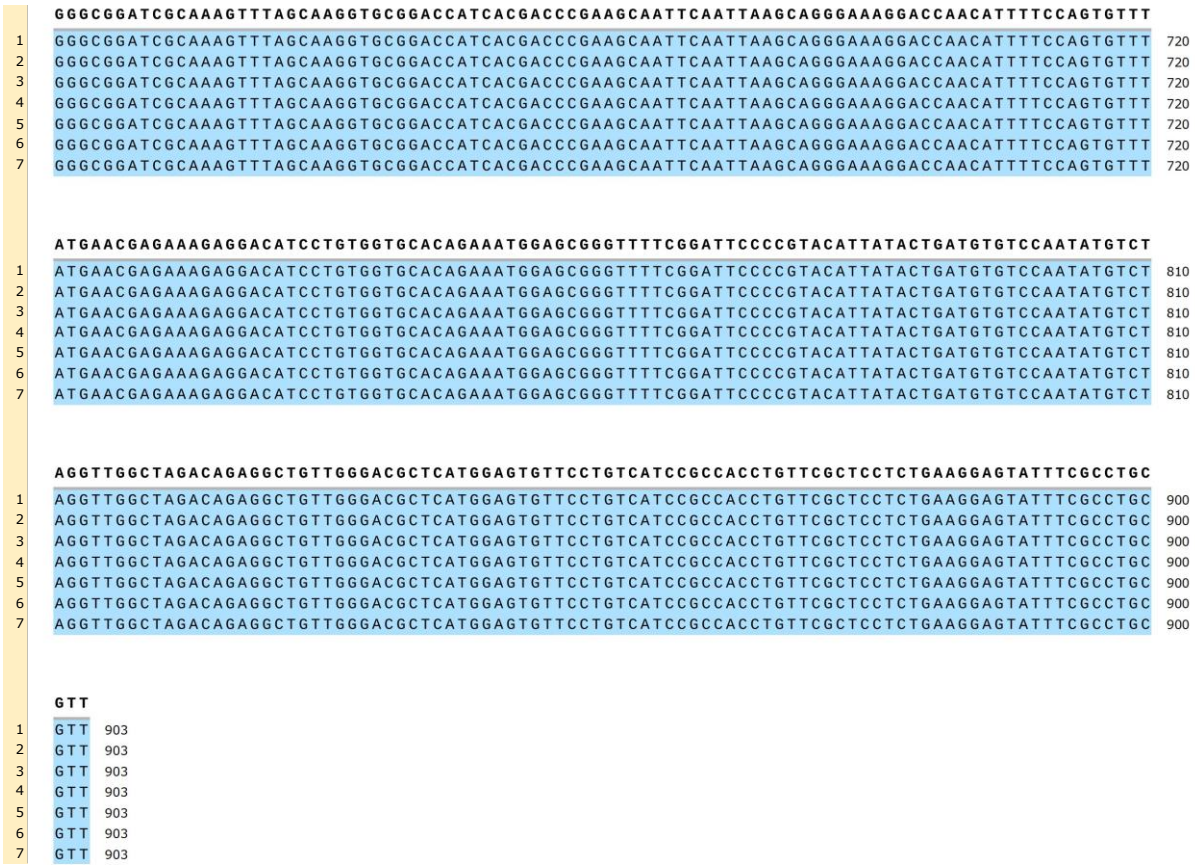

Figure 5.17: Sequencing confirmation of DNMT3A sequences in anti-HBV DEMs. Alignment of DNMT3A nucleotide sequences from S, C, and P DEMs DNA shows 100% identity with the reference plasmid DNMT3A sequence. SL, CR, and PL DEMs, nucleotides (WM) observed in the sequencing data represent artifacts rather than true mutations, are highlighted in red box. Alignment was performed using SnapGene® software (GSL Biotech; available at snapgene.com).

Appendix

Aligned using an external algorithm

Consensus

1. Reference seqeunce DNM3L
2. pT7(AG)-SR DEM 4x S
3. pT7(AG)-SL DEM 4x S
4. pT7(AG)-CR DEM 4x S
5. pT7(AG)-CL DEM 4x S
6. pT7(AG)-PR DEM 4x S
7. pT7(AG)-PL DEM 4x S

```
  AACCATGATCAAGAGTTCGATCCTCCTAAAGTGTATCCCCCTGTCCCTGCCGAAAAGCGGAAACCGATCAGGGTTCTCAGTCTCTTCGAT
1 AACCATGATCAAGAGTTCGATCCTCCTAAAGTGTATCCCCCTGTCCCTGCCGAAAAGCGGAAACCGATCAGGGTTCTCAGTCTCTTCGAT 90
2 AACCATGATCAAGAGTTCGATCCTCCTAAAGTGTATCCCCCTGTCCCTGCCGAAAAGCGGAAACCGATCAGGGTTCTCAGTCTCTTCGAT 90
3 AACCATGATCAAGAGTTCGATCCTCCTAAAGTGTATCCCCCTGTCCCTGCCGAAAAGCGGAAACCGATCAGGGTTCTCAGTCTCTTCGAT 90
4 AACCATGATCAAGAGTTCGATCCTCCTAAAGTGTATCCCCCTGTCCCTGCCGAAAAGCGGAAACCGATCAGGGTTCTCAGTCTCTTCGAT 90
5 AACCATGATCAAGAGTTCGATCCTCCTAAAGTGTATCCCCCTGTCCCTGCCGAAAAGCGGAAACCGATCAGGGTTCTCAGTCTCTTCGAT 90
6 AACCATGATCAAGAGTTCGATCCTCCTAAAGTGTATCCCCCTGTCCCTGCCGAAAAGCGGAAACCGATCAGGGTTCTCAGTCTCTTCGAT 90
7 AACCATGATCAAGAGTTCGATCCTCCTAAAGTGTATCCCCCTGTCCCTGCCGAAAAGCGGAAACCGATCAGGGTTCTCAGTCTCTTCGAT 90

  GGAATTGCCACAGGCCTCTTGGTCCTTAAGGACCTGGGCATCCAAGTGGACCGCTACATCGCCTCAGAAGTATGTGAGGACAGCATCACA
1 GGAATTGCCACAGGCCTCTTGGTCCTTAAGGACCTGGGCATCCAAGTGGACCGCTACATCGCCTCAGAAGTATGTGAGGACAGCATCACA 180
2 GGAATTGCCACAGGCCTCTTGGTCCTTAAGGACCTGGGCATCCAAGTGGACCGCTACATCGCCTCAGAAGTATGTGAGGACAGCATCACA 180
3 GGAATTGCCACAGGCCTCTTGGTCCTTAAGGACCTGGGCATCCAAGTGGACCGCTACATCGCCTCAGAAGTATGTGAGGACAGCATCACA 180
4 GGAATTGCCACAGGCCTCTTGGTCCTTAAGGACCTGGGCATCCAAGTGGACCGCTACATCGCCTCAGAAGTATGTGAGGACAGCATCACA 180
5 GGAATTGCCACAGGCCTCTTGGTCCTTAAGGACCTGGGCATCCAAGTGGACCGCTACATCGCCTCAGAAGTATGTGAGGACAGCATCACA 180
6 GGAATTGCCACAGGCCTCTTGGTCCTTAAGGACCTGGGCATCCAAGTGGACCGCTACATCGCCTCAGAAGTATGTGAGGACAGCATCACA 180
7 GGAATTGCCACAGGCCTCTTGGTCCTTAAGGACCTGGGCATCCAAGTGGACCGCTACATCGCCTCAGAAGTATGTGAGGACAGCATCACA 180

  GTCGGCATGGTGCGCCACCAGGGGAAAATAATGTACGTCGGCGACGTCAGATCAGTTACTCAGAAACATATTCAGGAATGGGGGCCTTTT
1 GTCGGCATGGTGCGCCACCAGGGGAAAATAATGTACGTCGGCGACGTCAGATCAGTTACTCAGAAACATATTCAGGAATGGGGGCCTTTT 270
2 GTCGGCATGGTGCGCCACCAGGGGAAAATAATGTACGTCGGCGACGTCAGATCAGTTACTCAGAAACATATTCAGGAATGGGGGCCTTTT 270
3 GTCGGCATGGTGCGCCACCAGGGGAAAATAATGTACGTCGGCGACGTCAGATCAGTTACTCAGAAACATATTCAGGAATGGGGGCCTTTT 270
4 GTCGGCATGGTGCGCCACCAGGGGAAAATAATGTACGTCGGCGACGTCAGATCAGTTACTCAGAAACATATTCAGGAATGGGGGCCTTTT 270
5 GTCGGCATGGTGCGCCACCAGGGGAAAATAATGTACGTCGGCGACGTCAGATCAGTTACTCAGAAACATATTCAGGAATGGGGGCCTTTT 270
6 GTCGGCATGGTGCGCCACCAGGGGAAAATAATGTACGTCGGCGACGTCAGATCAGTTACTCAGAAACATATTCAGGAATGGGGGCCTTTT 270
7 GTCGGCATGGTGCGCCACCAGGGGAAAATAATGTACGTCGGCGACGTCAGATCAGTTACTCAGAAACATATTCAGGAATGGGGGCCTTTT 270

  GATCTCGTAATTGGCGGCAGCCCCTGCAATGATCTGAGTATTGTGAACCCCGCCCGGAAAGGTTTGTACGAAGGTACGGGCAGACTGTTC
1 GATCTCGTAATTGGCGGCAGCCCCTGCAATGATCTGAGTATTGTGAACCCCGCCCGGAAAGGTTTGTACGAAGGTACGGGCAGACTGTTC 360
2 GATCTCGTAATTGGCGGCAGCCCCTGCAATGATCTGAGTATTGTGAACCCCGCCCGGAAAGGTTTGTACGAAGGTACGGGCAGACTGTTC 360
3 GATCTCGTAATTGGCGGCAGCCCCTGCAATGATCTGAGTATTGTGAACCCCGCCCGGAAAGGTTTGTACGAAGGTACGGGCAGACTGTTC 360
4 GATCTCGTAATTGGCGGCAGCCCCTGCAATGATCTGAGTATTGTGAACCCCGCCCGGAAAGGTTTGTACGAAGGTACGGGCAGACTGTTC 360
5 GATCTCGTAATTGGCGGCAGCCCCTGCAATGATCTGAGTATTGTGAACCCCGCCCGGAAAGGTTTGTACGAAGGTACGGGCAGACTGTTC 360
6 GATCTCGTAATTGGCGGCAGCCCCTGCAATGATCTGAGTATTGTGAACCCCGCCCGGAAAGGTTTGTACGAAGGTACGGGCAGACTGTTC 360
7 GATCTCGTAATTGGCGGCAGCCCCTGCAATGATCTGAGTATTGTGAACCCCGCCCGGAAAGGTTTGTACGAAGGTACGGGCAGACTGTTC 360

  TTCGAGTTTTACAGACTGTTGCACGACGCACGACCAAAGGAGGGTGACGATCGACCCTTCTTCTGGCTGTTCGAGAACGTGGTCGCTATG
1 TTCGAGTTTTACAGACTGTTGCACGACGCACGACCAAAGGAGGGTGACGATCGACCCTTCTTCTGGCTGTTCGAGAACGTGGTCGCTATG 450
2 TTCGAGTTTTACAGACTGTTGCACGACGCACGACCAAAGGAGGGTGACGATCGACCCTTCTTCTGGCTGTTCGAGAACGTGGTCGCTATG 450
3 TTCGAGTTTTACAGACTGTTGCACGACGCACGACCAAAGGAGGGTGACGATCGACCCTTCTTCTGGCTGTTCGAGAACGTGGTCGCTATG 450
4 TTCGAGTTTTACAGACTGTTGCACGACGCACGACCAAAGGAGGGTGACGATCGACCCTTCTTCTGGCTGTTCGAGAACGTGGTCGCTATG 450
5 TTCGAGTTTTACAGACTGTTGCACGACGCACGACCAAAGGAGGGTGACGATCGACCCTTCTTCTGGCTGTTCGAGAACGTGGTCGCTATG 450
6 TTCGAGTTTTACAGACTGTTGCACGACGCACGACCAAAGGAGGGTGACGATCGACCCTTCTTCTGGCTGTTCGAGAACGTGGTCGCTATG 450
7 TTCGAGTTTTACAGACTGTTGCACGACGCACGACCAAAGGAGGGTGACGATCGACCCTTCTTCTGGCTGTTCGAGAACGTGGTCGCTATG 450

  GGCGTGTCTGACAAGCGGGACATTTCTAGATTCCTGGAGAGCAATCCAGTGATGATTGATGCAAAGGAAGTATCCGCTGCCCACCGCGCC
1 GGCGTGTCTGACAAGCGGGACATTTCTAGATTCCTGGAGAGCAATCCAGTGATGATTGATGCAAAGGAAGTATCCGCTGCCCACCGCGCC 540
2 GGCGTGTCTGACAAGCGGGACATTTCTAGATTCCTGGAGAGCAATCCAGTGATGATTGATGCAAAGGAAGTATCCGCTGCCCACCGCGCC 540
3 GGCGTGTCTGACAAGCGGGACATTTCTAGATTCCTGGAGAGCAATCCAGTGATGATTGATGCAAAGGAAGTATCCGCTGCCCACCGCGCC 540
4 GGCGTGTCTGACAAGCGGGACATTTCTAGATTCCTGGAGAGCAATCCAGTGATGATTGATGCAAAGGAAGTATCCGCTGCCCACCGCGCC 540
5 GGCGTGTCTGACAAGCGGGACATTTCTAGATTCCTGGAGAGCAATCCAGTGATGATTGATGCAAAGGAAGTATCCGCTGCCCACCGCGCC 540
6 GGCGTGTCTGACAAGCGGGACATTTCTAGATTCCTGGAGAGCAATCCAGTGATGATTGATGCAAAGGAAGTATCCGCTGCCCACCGCGCC 540
7 GGCGTGTCTGACAAGCGGGACATTTCTAGATTCCTGGAGAGCAATCCAGTGATGATTGATGCAAAGGAAGTATCCGCTGCCCACCGCGCC 540

  AGATACTTCTGGGGCAATCTGCCCGGCATGAATCGACCCTTGGCAAGCACCGTGAATGATAAGTTGGAGTTGCAGGAGTGTCTGGAGCAT
1 AGATACTTCTGGGGCAATCTGCCCGGCATGAATCGACCCTTGGCAAGCACCGTGAATGATAAGTTGGAGTTGCAGGAGTGTCTGGAGCAT 630
2 AGATACTTCTGGGGCAATCTGCCCGGCATGAATCGACCCTTGGCAAGCACCGTGAATGATAAGTTGGAGTTGCAGGAGTGTCTGGAGCAT 630
3 AGATACTTCTGGGGCAATCTGCCCGGCATGAATCGACCCTTGGCAAGCACCGTGAATGATAAGTTGGAGTTGCAGGAGTGTCTGGAGCAT 630
4 AGATACTTCTGGGGCAATCTGCCCGGCATGAATCGACCCTTGGCAAGCACCGTGAATGATAAGTTGGAGTTGCAGGAGTGTCTGGAGCAT 630
5 AGATACTTCTGGGGCAATCTGCCCGGCATGAATCGACCCTTGGCAAGCACCGTGAATGATAAGTTGGAGTTGCAGGAGTGTCTGGAGCAT 630
6 AGATACTTCTGGGGCAATCTGCCCGGCATGAATCGACCCTTGGCAAGCACCGTGAATGATAAGTTGGAGTTGCAGGAGTGTCTGGAGCAT 630
7 AGATACTTCTGGGGCAATCTGCCCGGCATGAATCGACCCTTGGCAAGCACCGTGAATGATAAGTTGGAGTTGCAGGAGTGTCTGGAGCAT 630
```

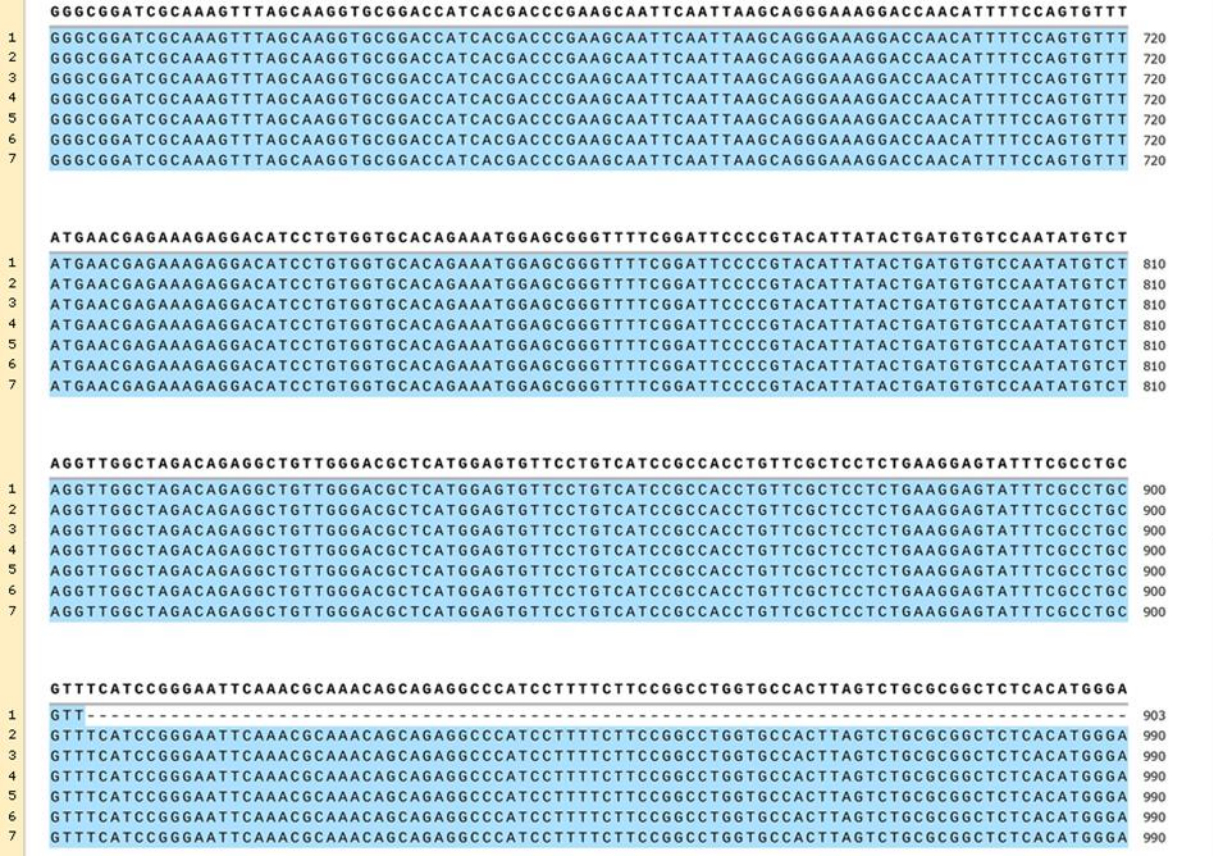

Figure 5.18: Sequencing confirmation of DNMT3L sequences in anti-HBV DEMs. Alignment of DNMT3L nucleotide sequences from S, C, and P DEM DNA shows 100% identity with the reference plasmid DNMT3L sequence. Sequence alignment was performed using SnapGene® software (GSL Biotech; available at snapgene.com).

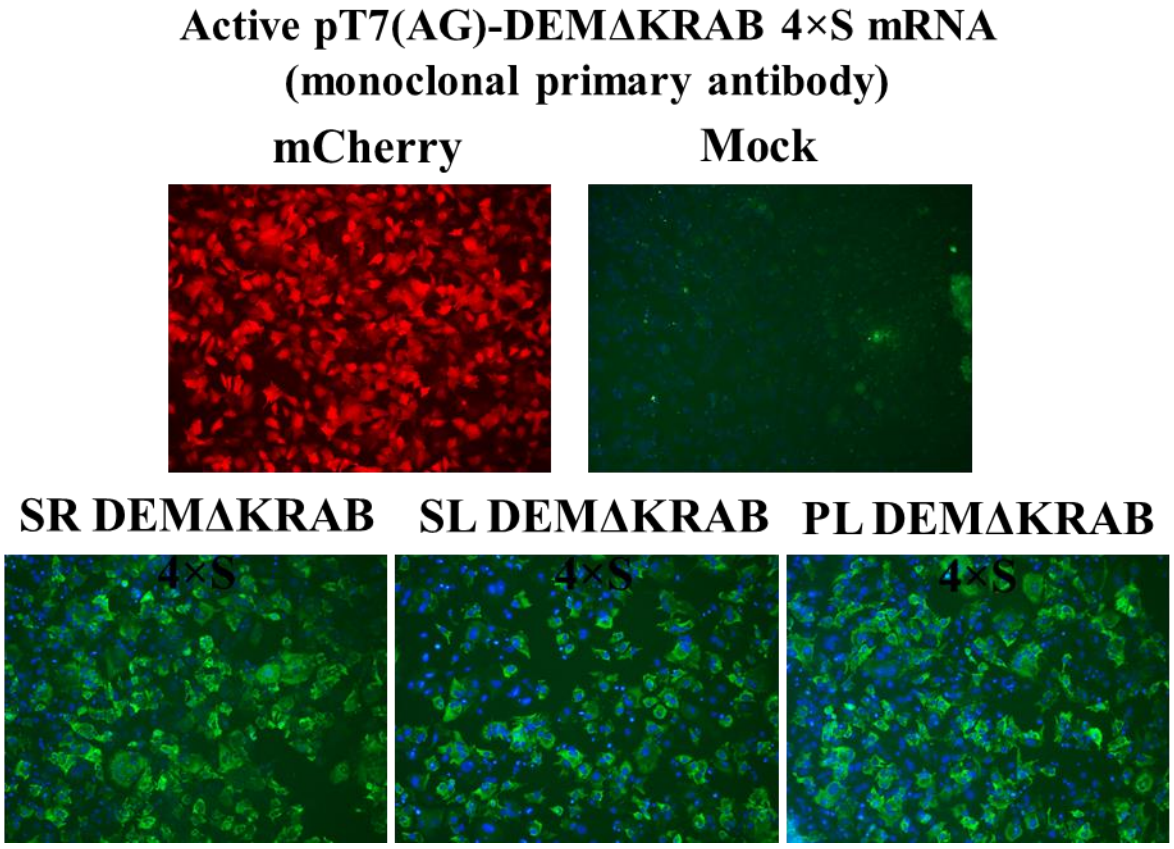

Figure 5.19: Immunofluorescence detection of pT7(AG)-DEMΔKRAB 4×S mRNA. Huh7 cells were transfected with individual active pT7(AG)-DEMΔKRAB 4×S mRNA. In parallel, cells were transfected with mCherry mRNA to assess transfection efficiency. HA-tag expression was evaluated three hours post-transfection using a monoclonal primary mouse anti-HA antibody and a fluorescently labeled goat anti-mouse secondary antibody for detection (green). Nuclei were stained with DAPI (blue). Cells were visualized by fluorescence microscopy at 20× magnification.

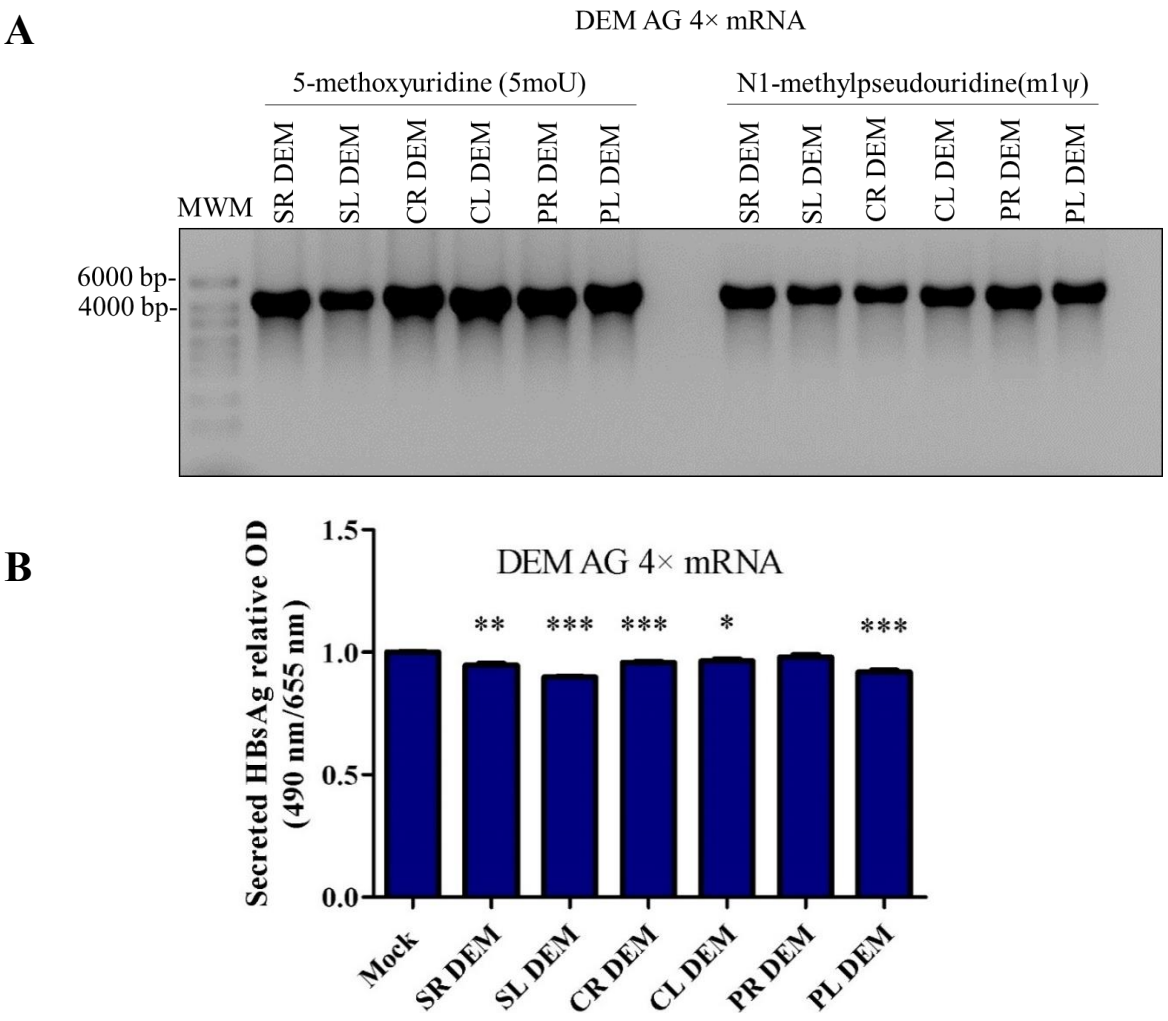

Figure 5.20: IVT of DEM produced from pT7-DEM 4× AG vector and assessment of transcriptional repression of HBsAg *in vitro*. (**A**) The IVT reaction of active DEM involved complete substitution of uridine with 5moU or m1ψ and was co-transcriptionally capped with TriLink CleanCap AG. Transcribed RNA was purified using cellulose and recovered via LiCl precipitation. IVTed mRNAs were visualized by 1% agarose gel electrophoresis. Lane 1: MWM, RiboRuler HR RNA ladder. (**B**) The efficacy of DEM mRNA was evaluated following single mRNA transfection. Huh7 cells were transfected with an HBV replication-competent plasmid, followed by transfection with individual DEM mRNA or FLuc mRNA as a mock control. HBsAg levels were assessed 48 hours post-transfection. All transfections were performed in triplicate (n = 3). Statistical significance is indicated as follows: * $p < 0.05$, ** $p < 0.01$, *** $p < 0.001$; NS indicates non-significant results.

Table 5.7: RT-qPCR results for HPRT Gene amplification in mock and DEM-transfected Huh7 cells using Luna® Universal One-Step Reagent (without reverse transcriptase)

Sample	**No Reverse Transcriptase**		
Mock	31.78	31.63	30.11
SR DEM mRNA	30.13	29.68	29.82
SL DEM mRNA	29.71	31.14	32.22
CR DEM mRNA	32.28	32.63	30.12
CL DEM mRNA	29.94	29.73	29.30
PR DEM mRNA	29.60	29.36	29.46
PL DEM mRNA	29.30	29.27	29.94

5.10 Ethic Clearance

STRICTLY CONFIDENTIAL

CLEARANCE CERTIFICATE NUMBER: 2021/03/08/C

APPLICANT: Ms P Singh
School: School of Pathology; Department: N/A; Location: WRAF

PROJECT TITLE: Pilot study investigating the safety and efficacy of the delivery of firefly luciferase mRNA by the hydrodynamic injection into NMRI mice
Category: C; Species and Numbers involved: *42X 2-3 weeks, 20g female mouse (NMRI)*

Approval is hereby given for the use of animals for the research project named above and described in the application reviewed by a quorate meeting of the AREC held on 30 Mar 2021. This approval remains valid until 27 Apr 2023 and is conditional to the following (if blank there are no special conditions):

Condition 1	Condition 2	Condition 3	Condition 4
Negative control to be shared with 2021/03/10/C			

All material changes to the approved research must be reported to the AREC before they are implemented. Failure to do so will invalidate this clearance certificate.

An annual progress report must be provided to the AREC.

The use of these animals is subject to AREC guidelines on the use and care of laboratory animals, is limited to the procedures described in the application and is subject to additional conditions listed below:

I, the Chair of the AREC (or my designated representative) am satisfied that the proposed research is ethical as judged by local law, international standards and University policy.

Signed: _____ _____ Date: __28/04/2021_____
(Chairperson of the AREC)

I am satisfied that the persons listed in this application are competent to perform the procedures described in the application, in the context of Section 23 (1) (c) of the veterinary and Para-veterinary Professions Act (19 of 1982).

ANIMALS RESEARCH ETHICS COMMITTEE (AREC) UNIVERSITY OF THE WITWATERSRAND, JOHANNESBURG

Signed: __ _____ Date: __29 April 2021_____
(Registered Veterinarian)

While animal ethics was applied and granted, in vivo characterisation of IVTed anti-DEMs could not be carried out.

References

ADDISON, W. R., WALTERS, K.-A., WONG, W. W., WILSON, J. S., MADEJ, D., JEWELL, L. D. & TYRRELL, D. L. J. 2002. Half-life of the duck hepatitis B virus covalently closed circular DNA pool in vivo following inhibition of viral replication. *Journal of virology,* 76**,** 6356-6363.

ADIBZADEH, S., FARDAEI, M., TAKHSHID, M. A., MIRI, M. R., DEHBIDI, G. R., FARHADI, A., RANJBARAN, R., ALAVI, P., NIKOUYAN, N. & SEYYEDI, N. 2019. Enhancing stability of destabilized green fluorescent protein using chimeric mRNA containing human beta-globin 5′ and 3′ untranslated regions. *Avicenna Journal of Medical Biotechnology,* 11**,** 112.

AMABILE, A., MIGLIARA, A., CAPASSO, P., BIFFI, M., CITTARO, D., NALDINI, L. & LOMBARDO, A. 2016. Inheritable silencing of endogenous genes by hit-and-run targeted epigenetic editing. *Cell,* 167**,** 219-232. e14.

AMPONSAH-DACOSTA, E. 2021. Hepatitis B virus infection and hepatocellular carcinoma in sub-Saharan Africa: Implications for elimination of viral hepatitis by 2030? *World journal of gastroenterology,* 27**,** 6025.

ANDERSON, B. R., MURAMATSU, H., JHA, B. K., SILVERMAN, R. H., WEISSMAN, D. & KARIKÓ, K. 2011. Nucleoside modifications in RNA limit activation of 2′-5′-oligoadenylate synthetase and increase resistance to cleavage by RNase L. *Nucleic acids research,* 39**,** 9329-9338.

ANDREWS, F. H., STRAHL, B. D. & KUTATELADZE, T. G. 2016. Insights into newly discovered marks and readers of epigenetic information. *Nature chemical biology,* 12**,** 662-668.

ANDRIES, O., MC CAFFERTY, S., DE SMEDT, S. C., WEISS, R., SANDERS, N. N. & KITADA, T. 2015. N1-methylpseudouridine-incorporated mRNA outperforms pseudouridine-incorporated mRNA by providing enhanced protein expression and reduced immunogenicity in mammalian cell lines and mice. *Journal of Controlled Release,* 217**,** 337-344.

ANTONUCCI, T. K. & RUTTER, W. J. 1989. Hepatitis B virus (HBV) promoters are regulated by the HBV enhancer in a tissue-specific manner. *Journal of virology,* 63**,** 579-583.

ASRANI, K. H., FARELLI, J. D., STAHLEY, M. R., MILLER, R. L., CHENG, C. J., SUBRAMANIAN, R. R. & BROWN, J. M. 2018. Optimization of mRNA untranslated regions for improved expression of therapeutic mRNA. *RNA biology,* 15**,** 756-762.

ATES, I., RATHBONE, T., STUART, C., BRIDGES, P. H. & COTTLE, R. N. 2020. Delivery approaches for therapeutic genome editing and challenges. *Genes,* 11**,** 1113.

BADEN, L. R., EL SAHLY, H. M., ESSINK, B., KOTLOFF, K., FREY, S., NOVAK, R., DIEMERT, D., SPECTOR, S. A., ROUPHAEL, N. & CREECH, C. B. 2021. Efficacy and safety of the mRNA-1273 SARS-CoV-2 vaccine. *New England journal of medicine,* 384**,** 403-416.

BAIERSDÖRFER, M., BOROS, G., MURAMATSU, H., MAHINY, A., VLATKOVIC, I., SAHIN, U. & KARIKÓ, K. 2019. A facile method for the removal of dsRNA contaminant from in vitro-transcribed mRNA. *Molecular Therapy-Nucleic Acids,* 15**,** 26-35.

BARONTI, L., KARLSSON, H., MARUŠIČ, M. & PETZOLD, K. 2018. A guide to large-scale RNA sample preparation. *Analytical and bioanalytical chemistry,* 410**,** 3239-3252.

References

BAZINET, M., PÂNTEA, V., PLACINTA, G., MOSCALU, I., CEBOTARESCU, V., COJUHARI, L., JIMBEI, P., IAROVOI, L., SMESNOI, V. & MUSTEATA, T. 2020. Safety and efficacy of 48 weeks REP 2139 or REP 2165, tenofovir disoproxil, and pegylated interferon alfa-2a in patients with chronic HBV infection naïve to nucleos (t) ide therapy. *Gastroenterology,* 158**,** 2180-2194.

BECK, J. & NASSAL, M. 2007. Hepatitis B virus replication. *World journal of gastroenterology: WJG,* 13**,** 48.

BELHADJ, Z., QIE, Y., CARNEY, R. P., LI, Y. & NIE, G. 2023. Current advances in non-viral gene delivery systems: Liposomes versus extracellular vesicles. *BMEMat,* 1**,** e12018.

BELLONI, L., ALLWEISS, L., GUERRIERI, F., PEDICONI, N., VOLZ, T., POLLICINO, T., PETERSEN, J., RAIMONDO, G., DANDRI, M. & LEVRERO, M. 2012. IFN-α inhibits HBV transcription and replication in cell culture and in humanized mice by targeting the epigenetic regulation of the nuclear cccDNA minichromosome. *The Journal of clinical investigation,* 122**,** 529-537.

BERKE, J. M., DEHERTOGH, P., VERGAUWEN, K., VAN DAMME, E., MOSTMANS, W., VANDYCK, K. & PAUWELS, F. 2017. Capsid assembly modulators have a dual mechanism of action in primary human hepatocytes infected with hepatitis B virus. *Antimicrobial agents and chemotherapy,* 61**,** e00560-17.

BIRD, A. P. 1987. CpG islands as gene markers in the vertebrate nucleus. *Trends in Genetics,* 3**,** 342-347.

BLONDOT, M.-L., BRUSS, V. & KANN, M. 2016. Intracellular transport and egress of hepatitis B virus. *Journal of hepatology,* 64**,** S49-S59.

BLOOM, K., ELY, A., MUSSOLINO, C., CATHOMEN, T. & ARBUTHNOT, P. 2013. Inactivation of hepatitis B virus replication in cultured cells and in vivo with engineered transcription activator-like effector nucleases. *Molecular therapy,* 21**,** 1889-1897.

BLOOM, K., KALDINE, H., CATHOMEN, T., MUSSOLINO, C., ELY, A. & ARBUTHNOT, P. 2019. Inhibition of replication of hepatitis B virus using transcriptional repressors that target the viral DNA. *BMC Infectious Diseases,* 19**,** 1-10.

BLUMBERG, B. S., GERSTLEY, B. J. S., HUNGERFORD, D. A., LONDON, W. T. & SUTNICK, A. I. 1967. A serum antigen (Australia antigen) in Down's syndrome, leukemia, and hepatitis. *Annals of internal medicine,* 66**,** 924-931.

BORDEN, K. L. & VOLPON, L. 2020. The diversity, plasticity, and adaptability of cap-dependent translation initiation and the associated machinery. *RNA biology,* 17**,** 1239-1251.

BORGIA, G., CARLEO, M. A., GAETA, G. B. & GENTILE, I. 2012. Hepatitis B in pregnancy. *World journal of gastroenterology: WJG,* 18**,** 4677.

BRENNER, S., JACOB, F. & MESELSON, M. 1961. An unstable intermediate carrying information from genes to ribosomes for protein synthesis. *Nature,* 190**,** 576-581.

BUENROSTRO, J. D., GIRESI, P. G., ZABA, L. C., CHANG, H. Y. & GREENLEAF, W. J. 2013. Transposition of native chromatin for fast and sensitive epigenomic profiling of open chromatin, DNA-binding proteins and nucleosome position. *Nature methods,* 10**,** 1213-1218.

CALIGIURI, P., CERRUTI, R., ICARDI, G. & BRUZZONE, B. 2016. Overview of hepatitis B virus mutations and their implications in the management of infection. *World journal of gastroenterology,* 22**,** 145.

CHAN, C.-P. & JIN, D.-Y. 2022. Cytoplasmic RNA sensors and their interplay with RNA-binding partners in innate antiviral response: theme and variations. *Rna,* 28**,** 449-477.

CHEN, C.-Y. A. & SHYU, A.-B. 1995. AU-rich elements: characterization and importance in mRNA degradation. *Trends in biochemical sciences,* 20**,** 465-470.

CHEN, L., SHI, Y., YANG, W., ZHANG, Y., XIE, Q., LI, Y., LI, X., LI, J. & ZHANG, Z. 2018. Differences in Cpg island distribution between subgenotypes of the hepatitis B virus genotype. *Medical Science Monitor: International Medical Journal of Experimental and Clinical Research,* 24**,** 6781.

CHEN, Y. & TIAN, Z. 2019. HBV-induced immune imbalance in the development of HCC. *Frontiers in immunology,* 10**,** 478201.

CHENG, J., ZHAO, Q., ZHOU, Y., TANG, L., SHERAZ, M., CHANG, J. & GUO, J.-T. 2020. Interferon alpha induces multiple cellular proteins that coordinately suppress hepadnaviral covalently closed circular DNA transcription. *Journal of virology,* 94**,** 10.1128/jvi. 00442-20.

CHENG, S.-T., HU, J.-L., REN, J.-H., YU, H.-B., ZHONG, S., WONG, V. K. W., LAW, B. Y. K., CHEN, W.-X., XU, H.-M. & ZHANG, Z.-Z. 2021. Dicoumarol, an NQO1 inhibitor, blocks cccDNA transcription by promoting degradation of HBx. *Journal of hepatology,* 74**,** 522-534.

CHUANG, Y.-C., TSAI, K.-N. & OU, J.-H. J. 2022. Pathogenicity and virulence of Hepatitis B virus. *Virulence,* 13**,** 258-296.

CRADICK, T. J., KECK, K., BRADSHAW, S., JAMIESON, A. C. & MCCAFFREY, A. P. 2010. Zinc-finger nucleases as a novel therapeutic strategy for targeting hepatitis B virus DNAs. *Molecular therapy,* 18**,** 947-954.

CRIDGE, A. G., CROWE-MCAULIFFE, C., MATHEW, S. F. & TATE, W. P. 2018. Eukaryotic translational termination efficiency is influenced by the 3′ nucleotides within the ribosomal mRNA channel. *Nucleic acids research,* 46**,** 1927-1944.

CROSSLEY, B. M., BAI, J., GLASER, A., MAES, R., PORTER, E., KILLIAN, M. L., CLEMENT, T. & TOOHEY-KURTH, K. 2020. Guidelines for Sanger sequencing and molecular assay monitoring. *Journal of Veterinary Diagnostic Investigation,* 32**,** 767-775.

DANE, D., CAMERON, C. & BRIGGS, M. 1970. Virus-like particles in serum of patients with Australia-antigen-associated hepatitis. *The lancet,* 295**,** 695-698.

DASGUPTA, P., HENSHAW, C., YOULDEN, D. R., CLARK, P. J., AITKEN, J. F. & BAADE, P. D. 2020. Global trends in incidence rates of primary adult liver cancers: a systematic review and meta-analysis. *Frontiers in Oncology,* 10**,** 171.

DE GROOTE, M. L., VERSCHURE, P. J. & ROTS, M. G. 2012. Epigenetic editing: targeted rewriting of epigenetic marks to modulate expression of selected target genes. *Nucleic acids research,* 40**,** 10596-10613.

DELIUS, H., GOUGH, N. M., CAMERON, C. H. & MURRAY, K. 1983. Structure of the hepatitis B virus genome. *Journal of virology,* 47**,** 337-343.

DEVARKAR, S. C., WANG, C., MILLER, M. T., RAMANATHAN, A., JIANG, F., KHAN, A. G., PATEL, S. S. & MARCOTRIGIANO, J. 2016. Structural basis for m7G recognition and 2′-O-methyl discrimination in capped RNAs by the innate immune receptor RIG-I. *Proceedings of the National Academy of Sciences,* 113**,** 596-601.

DOUSIS, A., RAVICHANDRAN, K., HOBERT, E. M., MOORE, M. J. & RABIDEAU, A. E. 2023. An engineered T7 RNA polymerase that produces mRNA free of immunostimulatory byproducts. *Nature biotechnology,* 41**,** 560-568.

DRAPER, A. 2020. A concise review of the changing landscape of hepatocellular carcinoma. *The American Journal of Managed Care,* 26**,** S211-S219.

DUNN, J. J., MCALLISTER, W. T. & BAUTZ, E. K. 1972. In vitro transcription of T3 DNA by Escherichia coli and T3 polymerases. *Virology,* 48**,** 112-125.

EDELMANN, F. T., NIEDNER, A. & NIESSING, D. 2014. Production of pure and functional RNA for in vitro reconstitution experiments. *Methods,* 65**,** 333-341.

ELY, A., NAIDOO, T., MUFAMADI, S., CROWTHER, C. & ARBUTHNOT, P. 2008. Expressed anti-HBV primary microRNA shuttles inhibit viral replication efficiently in vitro and in vivo. *Molecular therapy,* 16**,** 1105-1112.

ELY, A., SINGH, P., SMITH, T. S. & ARBUTHNOT, P. 2021. In vitro transcribed mRNA for expression of designer nucleases: Advantages as a novel therapeutic for the management of chronic HBV infection. *Advanced drug delivery reviews,* 168**,** 134-146.

EVDOKIMOVA, V., RUZANOV, P., IMATAKA, H., RAUGHT, B., SVITKIN, Y., OVCHINNIKOV, L. P. & SONENBERG, N. 2001. The major mRNA-associated protein YB-1 is a potent 5′ cap-dependent mRNA stabilizer. *The EMBO journal*.

FANG, E., LIU, X., LI, M., ZHANG, Z., SONG, L., ZHU, B., WU, X., LIU, J., ZHAO, D. & LI, Y. 2022. Advances in COVID-19 mRNA vaccine development. *Signal transduction and targeted therapy,* 7**,** 94.

FANNING, G. C., ZOULIM, F., HOU, J. & BERTOLETTI, A. 2019. Therapeutic strategies for hepatitis B virus infection: towards a cure. *Nature reviews Drug discovery,* 18**,** 827-844.

FEITELSON, M. A. & LEE, J. 2007. Hepatitis B virus integration, fragile sites, and hepatocarcinogenesis. *Cancer letters,* 252**,** 157-170.

FISICARO, P., VALDATTA, C., MASSARI, M., LOGGI, E., BIASINI, E., SACCHELLI, L., CAVALLO, M. C., SILINI, E. M., ANDREONE, P. & MISSALE, G. 2010. Antiviral intrahepatic T-cell responses can be restored by blocking programmed death-1 pathway in chronic hepatitis B. *Gastroenterology,* 138**,** 682-693. e4.

FORSBACH, A., NEMORIN, J.-G., MONTINO, C., MULLER, C., SAMULOWITZ, U., VICARI, A. P., JURK, M., MUTWIRI, G. K., KRIEG, A. M. & LIPFORD, G. B. 2008. Identification of RNA sequence motifs stimulating sequence-specific TLR8-dependent immune responses. *The Journal of Immunology,* 180**,** 3729-3738.

FURUICHI, Y. 2014. Caps on eukaryotic mRNAs. *eLS*.

GALLIE, D. R. 1998. A tale of two termini:: A functional interaction between the termini of an mRNA is a prerequisite for efficient translation initiation. *Gene,* 216**,** 1-11.

GALLUCCI, L. & KANN, M. 2017. Nuclear import of hepatitis B virus capsids and genome. *Viruses,* 9**,** 21.

GAO, M., FRITZ, D. T., FORD, L. P. & WILUSZ, J. 2000. Interaction between a poly (A)-specific ribonuclease and the 5′ cap influences mRNA deadenylation rates in vitro. *Molecular cell,* 5**,** 479-488.

GASPAR, P., MOURA, G., SANTOS, M. A. & OLIVEIRA, J. L. 2013. mRNA secondary structure optimization using a correlated stem–loop prediction. *Nucleic acids research,* 41**,** e73-e73.

GHOLAMALIPOUR, Y., KARUNANAYAKE MUDIYANSELAGE, A. & MARTIN, C. T. 2018. 3′ end additions by T7 RNA polymerase are RNA self-templated, distributive and diverse in character—RNA-Seq analyses. *Nucleic acids research,* 46**,** 9253-9263.

GIL, J., ALCAMÍ, J. & ESTEBAN, M. 1999. Induction of apoptosis by double-stranded-RNA-dependent protein kinase (PKR) involves the α subunit of eukaryotic translation initiation factor 2 and NF-κB. *Molecular and cellular biology,* 19**,** 4653-4663.

GILBERT, L. A., HORLBECK, M. A., ADAMSON, B., VILLALTA, J. E., CHEN, Y., WHITEHEAD, E. H., GUIMARAES, C., PANNING, B., PLOEGH, H. L. & BASSIK, M. C. 2014. Genome-scale CRISPR-mediated control of gene repression and activation. *Cell,* 159**,** 647-661.

GINGRAS, A.-C., RAUGHT, B. & SONENBERG, N. 1999. eIF4 initiation factors: effectors of mRNA recruitment to ribosomes and regulators of translation. *Annual review of biochemistry,* 68**,** 913-963.

GISH, R. G., GIVEN, B. D., LAI, C.-L., LOCARNINI, S. A., LAU, J. Y., LEWIS, D. L. & SCHLUEP, T. 2015. Chronic hepatitis B: virology, natural history, current management and a glimpse at future opportunities. *Antiviral research,* 121**,** 47-58.

GNYAWALI, B., PUSATERI, A., NICKERSON, A., JALIL, S. & MUMTAZ, K. 2022. Epidemiologic and socioeconomic factors impacting hepatitis B virus and related hepatocellular carcinoma. *World journal of gastroenterology,* 28**,** 3793.

GODET, A.-C., DAVID, F., HANTELYS, F., TATIN, F., LACAZETTE, E., GARMY-SUSINI, B. & PRATS, A.-C. 2019. IRES trans-acting factors, key actors of the stress response. *International journal of molecular sciences,* 20**,** 924.

GOELL, J. H. & HILTON, I. B. 2021. CRISPR/Cas-based epigenome editing: advances, applications, and clinical utility. *Trends in Biotechnology,* 39**,** 678-691.

GONATOPOULOS-POURNATZIS, T. & COWLING, V. H. 2014. Cap-binding complex (CBC). *Biochemical Journal,* 457**,** 231-242.

GRIER, A. E., BURLEIGH, S., SAHNI, J., CLOUGH, C. A., CARDOT, V., CHOE, D. C., KRUTEIN, M. C., RAWLINGS, D. J., JENSEN, M. C. & SCHARENBERG, A. M. 2016. pEVL: a linear plasmid for generating mRNA IVT templates with extended encoded poly (A) sequences. *Molecular Therapy-Nucleic Acids,* 5.

GRIMM, D., STREETZ, K. L., JOPLING, C. L., STORM, T. A., PANDEY, K., DAVIS, C. R., MARION, P., SALAZAR, F. & KAY, M. A. 2006. Fatality in mice due to oversaturation of cellular microRNA/short hairpin RNA pathways. *Nature,* 441**,** 537-541.

GUIDOTTI, L. G., MARTINEZ, V., LOH, Y.-T., ROGLER, C. E. & CHISARI, F. V. 1994. Hepatitis B virus nucleocapsid particles do not cross the hepatocyte nuclear membrane in transgenic mice. *Journal of virology,* 68**,** 5469-5475.

GUO, D., LI, J., ZHAO, P., MEI, T., LI, K. & ZHANG, Y. 2024. The hepatocellular carcinoma risk in patients with HBV-related cirrhosis: a competing risk nomogram based on a 4-year retrospective cohort study. *Frontiers in Oncology,* 14.

GUO, H., URBAN, S. & WANG, W. 2023. In vitro cell culture models to study hepatitis B and D virus infection. *Frontiers in Microbiology,* 14**,** 1169770.

GUO, W., BELL, K. D. & OU, J.-H. 1991. Characterization of the hepatitis B virus EnhI enhancer and X promoter complex. *Journal of virology,* 65**,** 6686-6692.

GUO, Y., LI, Y., MU, S., ZHANG, J. & YAN, Z. 2009. Evidence that methylation of hepatitis B virus covalently closed circular DNA in liver tissues of patients with chronic hepatitis B modulates HBV replication. *Journal of medical virology,* 81**,** 1177-1183.

HALL, D. B. & STRUHL, K. 2002. The VP16 activation domain interacts with multiple transcriptional components as determined by protein-protein cross-linking in vivo. *Journal of Biological Chemistry,* 277**,** 46043-46050.

HAMERS, R. L., ZAAIJER, H. L., WALLIS, C. L., SIWALE, M., IVE, P., BOTES, M. E., SIGALOFF, K. C., HOEPELMAN, A. I., STEVENS, W. S. & DE WIT, T. F. R. 2013. HIV–HBV coinfection in southern Africa and the effect of lamivudine-versus tenofovir-containing cART on HBV outcomes. *JAIDS Journal of Acquired Immune Deficiency Syndromes,* 64**,** 174-182.

HE, S., LIANG, Y., SHAO, F. & WANG, X. 2011. Toll-like receptors activate programmed necrosis in macrophages through a receptor-interacting kinase-3–mediated pathway. *Proceedings of the National Academy of Sciences,* 108**,** 20054-20059.

HENDERSON, J. M., UJITA, A., HILL, E., YOUSIF-ROSALES, S., SMITH, C., KO, N., MCREYNOLDS, T., CABRAL, C. R., ESCAMILLA-POWERS, J. R. & HOUSTON, M. E. 2021. Cap 1 messenger RNA synthesis with co-transcriptional cleancap® analog by in vitro transcription. *Current protocols,* 1**,** e39.

HINNEBUSCH, A. G. & LORSCH, J. R. 2012. The mechanism of eukaryotic translation initiation: new insights and challenges. *Cold Spring Harbor perspectives in biology,* 4**,** a011544.

HOH, A., HEEG, M., NI, Y., SCHUCH, A., BINDER, B., HENNECKE, N., BLUM, H. E., NASSAL, M., PROTZER, U. & HOFMANN, M. 2015. Hepatitis B virus-infected HepG2hNTCP cells serve as a novel immunological tool to analyze the antiviral efficacy of CD8+ T cells in vitro. *Journal of virology,* 89**,** 7433-7438.

HOLTKAMP, S., KREITER, S., SELMI, A., SIMON, P., KOSLOWSKI, M., HUBER, C., TURECI, O. & SAHIN, U. 2006. Modification of antigen-encoding RNA increases stability, translational efficacy, and T-cell stimulatory capacity of dendritic cells. *Blood,* 108**,** 4009-17.

HONG, X., KIM, E. S. & GUO, H. 2017. Epigenetic regulation of hepatitis B virus covalently closed circular DNA: Implications for epigenetic therapy against chronic hepatitis B. *Hepatology,* 66**,** 2066-2077.

HORII, T., MORITA, S., HINO, S., KIMURA, M., HINO, Y., KOGO, H., NAKAO, M. & HATADA, I. 2020. Successful generation of epigenetic disease model mice by targeted demethylation of the epigenome. *Genome biology,* 21**,** 1-17.

HU, J., PROTZER, U. & SIDDIQUI, A. 2019. Revisiting hepatitis B virus: challenges of curative therapies. *Journal of virology,* 93**,** 10.1128/jvi. 01032-19.

HUEZ, I., CRÉANCIER, L., AUDIGIER, S., GENSAC, M.-C., PRATS, A.-C. & PRATS, H. 1998. Two independent internal ribosome entry sites are involved in translation initiation of vascular endothelial growth factor mRNA. *Molecular and cellular biology,* 18**,** 6178-6190.

HYAMS, K. C. 1995. Risks of chronicity following acute hepatitis B virus infection: a review. *Clinical Infectious Diseases,* 20**,** 992-1000.

IWAMOTO, M., SASO, W., SUGIYAMA, R., ISHII, K., OHKI, M., NAGAMORI, S., SUZUKI, R., AIZAKI, H., RYO, A. & YUN, J.-H. 2019. Epidermal growth factor receptor is a host-entry cofactor triggering hepatitis B virus internalization. *Proceedings of the National Academy of Sciences,* 116**,** 8487-8492.

JACKSON, A. L., BURCHARD, J., SCHELTER, J., CHAU, B. N., CLEARY, M., LIM, L. & LINSLEY, P. S. 2006. Widespread siRNA “off-target” transcript silencing mediated by seed region sequence complementarity. *Rna,* 12**,** 1179-1187.

JAENISCH, R. & BIRD, A. 2003. Epigenetic regulation of gene expression: how the genome integrates intrinsic and environmental signals. *Nature genetics,* 33**,** 245-254.

JAIN, S., CHANG, T.-T., CHEN, S., BOLDBAATAR, B., CLEMENS, A., LIN, S. Y., YAN, R., HU, C.-T., GUO, H. & BLOCK, T. M. 2015. Comprehensive DNA methylation analysis of hepatitis B virus genome in infected liver tissues. *Scientific reports,* 5**,** 10478.

JALKANEN, A. L., COLEMAN, S. J. & WILUSZ, J. Year. Determinants and implications of mRNA poly (A) tail size–does this protein make my tail look big? *In:* Seminars in cell & developmental biology, 2014. Elsevier, 24-32.

JAVANBAKHT, H., MUELLER, H., WALTHER, J., ZHOU, X., LOPEZ, A., PATTUPARA, T., BLAISING, J., PEDERSEN, L., ALBÆK, N. & JACKEROTT, M. 2018. Liver-targeted anti-HBV single-stranded oligonucleotides with locked nucleic acid potently reduce HBV gene expression in vivo. *Molecular Therapy-Nucleic Acids,* 11**,** 441-454.

JELTSCH, A. & JURKOWSKA, R. Z. 2014. New concepts in DNA methylation. *Trends in biochemical sciences,* 39**,** 310-318.

JIANG, Y., LU, Q., WANG, Y., XU, E., HO, A., SINGH, P., WANG, Y., JIANG, Z., YANG, F. & TIETJEN, G. T. 2020. Quantitating endosomal escape of a library of polymers for mRNA delivery. *Nano letters,* 20**,** 1117-1123.

JIRIKOWSKI, G. F., SANNA, P. P., MACIEJEWSKI-LENOIR, D. & BLOOM, F. E. 1992. Reversal of diabetes insipidus in Brattleboro rats: intrahypothalamic injection of vasopressin mRNA. *Science,* 255**,** 996-998.

JONES, P. A. 2012. Functions of DNA methylation: islands, start sites, gene bodies and beyond. *Nature reviews genetics,* 13**,** 484-492.

KAIRUZ, D., SAMUDH, N., ELY, A., ARBUTHNOT, P. & BLOOM, K. 2023. Production, Characterization, and Assessment of Permanently Cationic and Ionizable Lipid Nanoparticles for Use in the Delivery of Self-Amplifying RNA Vaccines. *Pharmaceutics,* 15**,** 1173.

KANNEGANTI, T.-D., BODY-MALAPEL, M., AMER, A., PARK, J.-H., WHITFIELD, J., FRANCHI, L., TARAPOREWALA, Z. F., MILLER, D., PATTON, J. T. & INOHARA, N. 2006. Critical role for Cryopyrin/Nalp3 in activation of caspase-1 in response to viral infection and double-stranded RNA. *Journal of Biological Chemistry,* 281**,** 36560-36568.

KARIKÓ, K., BUCKSTEIN, M., NI, H. & WEISSMAN, D. 2005. Suppression of RNA recognition by Toll-like receptors: the impact of nucleoside modification and the evolutionary origin of RNA. *Immunity,* 23**,** 165-175.

KARIKÓ, K., MURAMATSU, H., LUDWIG, J. & WEISSMAN, D. 2011. Generating the optimal mRNA for therapy: HPLC purification eliminates immune activation and improves translation of nucleoside-modified, protein-encoding mRNA. *Nucleic acids research,* 39**,** e142-e142.

KARIKÓ, K., MURAMATSU, H., WELSH, F. A., LUDWIG, J., KATO, H., AKIRA, S. & WEISSMAN, D. 2008. Incorporation of pseudouridine into mRNA yields superior nonimmunogenic vector with increased translational capacity and biological stability. *Molecular therapy,* 16**,** 1833-1840.

KASIANCHUK, N., DOBROWOLSKA, K., HARKAVA, S., BRETCAN, A., ZARĘBSKA-MICHALUK, D., JAROSZEWICZ, J., FLISIAK, R. & RZYMSKI, P. 2023. Gene-Editing and RNA Interference in Treating Hepatitis B: A Review. *Viruses,* 15**,** 2395.

KATO, H., TAKEUCHI, O., MIKAMO-SATOH, E., HIRAI, R., KAWAI, T., MATSUSHITA, K., HIIRAGI, A., DERMODY, T. S., FUJITA, T. & AKIRA, S. 2008. Length-dependent recognition of double-stranded ribonucleic acids by retinoic acid–inducible gene-I and

melanoma differentiation–associated gene 5. *The Journal of experimental medicine,* 205**,** 1601-1610.

KAUR, P., PALIWAL, A., DURANTEL, D., HAINAUT, P., SCOAZEC, J.-Y., ZOULIM, F., CHEMIN, I. & HERCEG, Z. 2010. DNA methylation of hepatitis B virus (HBV) genome associated with the development of hepatocellular carcinoma and occult HBV infection. *The Journal of infectious diseases,* 202**,** 700-704.

KEANE, E., FUNK, A. L. & SHIMAKAWA, Y. 2016. Systematic review with meta-analysis: the risk of mother-to-child transmission of hepatitis B virus infection in sub-Saharan Africa. *Alimentary pharmacology & therapeutics,* 44**,** 1005-1017.

KIM, J.-W., LEE, S. H., PARK, Y. S., HWANG, J.-H., JEONG, S.-H., KIM, N. & LEE, D. H. 2011. Replicative activity of hepatitis B virus is negatively associated with methylation of covalently closed circular DNA in advanced hepatitis B virus infection. *Intervirology,* 54**,** 316-325.

KLAUSNER, R. D., ROUAULT, T. A. & HARFORD, J. B. 1993. Regulating the fate of mRNA: the control of cellular iron metabolism. *Cell,* 72**,** 19-28.

KLOSE, R. J. & BIRD, A. P. 2006. Genomic DNA methylation: the mark and its mediators. *Trends in biochemical sciences,* 31**,** 89-97.

KO, C., CHAKRABORTY, A., CHOU, W.-M., HASREITER, J., WETTENGEL, J. M., STADLER, D., BESTER, R., ASEN, T., ZHANG, K. & WISSKIRCHEN, K. 2018. Hepatitis B virus genome recycling and de novo secondary infection events maintain stable cccDNA levels. *Journal of hepatology,* 69**,** 1231-1241.

KÖCK, J., RÖSLER, C., ZHANG, J.-J., BLUM, H. E., NASSAL, M. & THOMA, C. 2010. Generation of covalently closed circular DNA of hepatitis B viruses via intracellular recycling is regulated in a virus specific manner. *PLoS pathogens,* 6**,** e1001082.

KOCMIK, I., PIECYK, K., RUDZINSKA, M., NIEDZWIECKA, A., DARZYNKIEWICZ, E., GRZELA, R. & JANKOWSKA-ANYSZKA, M. 2018. Modified ARCA analogs providing enhanced translational properties of capped mRNAs. *Cell Cycle,* 17**,** 1624-1636.

KOSICKI, M., TOMBERG, K. & BRADLEY, A. 2018. Repair of double-strand breaks induced by CRISPR–Cas9 leads to large deletions and complex rearrangements. *Nature biotechnology,* 36**,** 765-771.

KOSTYUSHEV, D., KOSTYUSHEVA, A., BREZGIN, S., PONOMAREVA, N., ZAKIROVA, N. F., EGORSHINA, A., YANVAREV, D. V., BAYUROVA, E., SUDINA, A. & GOPTAR, I. 2023. Depleting hepatitis B virus relaxed circular DNA is necessary for resolution of infection by CRISPR-Cas9. *Molecular Therapy-Nucleic Acids,* 31**,** 482-493.

KOZAK, M. 1986. Point mutations define a sequence flanking the AUG initiator codon that modulates translation by eukaryotic ribosomes. *Cell,* 44**,** 283-292.

KRAMVIS, A. 2014. Genotypes and genetic variability of hepatitis B virus. *Intervirology,* 57**,** 141-150.

KUMAR, A., KUMAR, S. I., PANDEY, R., NAIK, S. & AGGARWAL, R. 2005. Hepatitis B virus genotype A is more often associated with severe liver disease in northern India than is genotype D. *Indian J Gastroenterol,* 24**,** 19-22.

KUNGULOVSKI, G. & JELTSCH, A. 2016. Epigenome editing: state of the art, concepts, and perspectives. *Trends in Genetics,* 32**,** 101-113.

KUNGULOVSKI, G., NUNNA, S., THOMAS, M., ZANGER, U. M., REINHARDT, R. & JELTSCH, A. 2015. Targeted epigenome editing of an endogenous locus with chromatin modifiers is not stably maintained. *Epigenetics & chromatin,* 8**,** 1-11.

KUSCU, C., ARSLAN, S., SINGH, R., THORPE, J. & ADLI, M. 2014. Genome-wide analysis reveals characteristics of off-target sites bound by the Cas9 endonuclease. *Nature biotechnology,* 32**,** 677-683.

KYRIELEIS, O. J., CHANG, J., DE LA PEÑA, M., SHUMAN, S. & CUSACK, S. 2014. Crystal structure of vaccinia virus mRNA capping enzyme provides insights into the mechanism and evolution of the capping apparatus. *Structure,* 22**,** 452-465.

LAI, C.-L., WONG, D., IP, P., KOPANISZEN, M., SETO, W.-K., FUNG, J., HUANG, F.-Y., LEE, B., CULLARO, G. & CHONG, C. K. 2017. Reduction of covalently closed circular DNA with long-term nucleos (t) ide analogue treatment in chronic hepatitis B. *Journal of hepatology,* 66**,** 275-281.

LAMONTAGNE, R. J., BAGGA, S. & BOUCHARD, M. J. 2016. Hepatitis B virus molecular biology and pathogenesis. *Hepatoma research,* 2**,** 163.

LARAS, A., KOSKINAS, J., DIMOU, E., KOSTAMENA, A. & HADZIYANNIS, S. J. 2006. Intrahepatic levels and replicative activity of covalently closed circular hepatitis B virus DNA in chronically infected patients. *Hepatology,* 44**,** 694-702.

LARSON, M. H., GILBERT, L. A., WANG, X., LIM, W. A., WEISSMAN, J. S. & QI, L. S. 2013. CRISPR interference (CRISPRi) for sequence-specific control of gene expression. *Nature protocols,* 8**,** 2180-2196.

LEE, H.-C., CHATHURANGA, K. & LEE, J.-S. 2019. Intracellular sensing of viral genomes and viral evasion. *Experimental & molecular medicine,* 51**,** 1-13.

LEE, H. W., LEE, J. S. & AHN, S. H. 2020. Hepatitis B virus cure: targets and future therapies. *International journal of molecular sciences,* 22**,** 213.

LEONTIOU, C. A., HADJIDANIEL, M. D., MINA, P., ANTONIOU, P., IOANNIDES, M. & PATSALIS, P. C. 2015. Bisulfite conversion of DNA: performance comparison of different kits and methylation quantitation of epigenetic biomarkers that have the potential to be used in non-invasive prenatal testing. *PloS one,* 10**,** e0135058.

LEPPEK, K., DAS, R. & BARNA, M. 2018. Functional 5′ UTR mRNA structures in eukaryotic translation regulation and how to find them. *Nature reviews Molecular cell biology,* 19**,** 158-174.

LEVRERO, M., POLLICINO, T., PETERSEN, J., BELLONI, L., RAIMONDO, G. & DANDRI, M. 2009. Control of cccDNA function in hepatitis B virus infection. *Journal of hepatology,* 51**,** 581-592.

LEWIS, M. 1996. Response: DNA looping and Lac repressor—CAP interaction. *Science,* 274**,** 1931-1932.

LIM, S. G., BAUMERT, T. F., BONI, C., GANE, E., LEVRERO, M., LOK, A. S., MAINI, M. K., TERRAULT, N. A. & ZOULIM, F. 2023. The scientific basis of combination therapy for chronic hepatitis B functional cure. *Nature Reviews Gastroenterology & Hepatology,* 20**,** 238-253.

LIMA, S. A., CHIPMAN, L. B., NICHOLSON, A. L., CHEN, Y.-H., YEE, B. A., YEO, G. W., COLLER, J. & PASQUINELLI, A. E. 2017. Short poly (A) tails are a conserved feature of highly expressed genes. *Nature structural & molecular biology,* 24**,** 1057-1063.

LIMANI, S. W., MNYANDU, N., ELY, A., WADEE, R., KRAMVIS, A., ARBUTHNOT, P. & MAEPA, M. B. 2021. In Vivo Modelling of Hepatitis B Virus Subgenotype A1 Replication Using Adeno-Associated Viral Vectors. *Viruses,* 13**,** 2247.

LIPMAN, N. S., JACKSON, L. R., TRUDEL, L. J. & WEIS-GARCIA, F. 2005. Monoclonal versus polyclonal antibodies: distinguishing characteristics, applications, and information resources. *ILAR journal,* 46**,** 258-268.

LIU, P.-Q., REBAR, E. J., ZHANG, L., LIU, Q., JAMIESON, A. C., LIANG, Y., QI, H., LI, P.-X., CHEN, B. & MENDEL, M. C. 2001. Regulation of an endogenous locus using a panel of designed zinc finger proteins targeted to accessible chromatin regions: activation of vascular endothelial growth factor A. *Journal of Biological Chemistry,* 276**,** 11323-11334.

LIVAK, K. J. & SCHMITTGEN, T. D. 2001. Analysis of relative gene expression data using real-time quantitative PCR and the 2− ΔΔCT method. *Methods,* 25**,** 402-408.

LIVER, E. A. F. T. S. O. T. 2017. EASL 2017 Clinical Practice Guidelines on the management of hepatitis B virus infection. *Journal of hepatology,* 67**,** 370-398.

LLOVET, J., ZUCMAN-ROSSI, J., PIKARSKY, E., SANGRO, B., SCHWARTZ, M., SHERMAN, M. & GORES, G. 2016. Hepatocellular carcinoma Nat Rev Dis Primers 2: 16018.

LOK, A. S., ZOULIM, F., DUSHEIKO, G. & GHANY, M. G. 2017. Hepatitis B cure: from discovery to regulatory approval. *Hepatology,* 66**,** 1296-1313.

LONG, S. S., PROBER, C. G., FISCHER, M. & KIMBERLIN, D. 2022. *Principles and practice of pediatric infectious diseases E-Book*, Elsevier Health Sciences.

LUCIFORA, J. & PROTZER, U. 2016. Attacking hepatitis B virus cccDNA–The holy grail to hepatitis B cure. *Journal of hepatology,* 64**,** S41-S48.

LUCIFORA, J., XIA, Y., REISINGER, F., ZHANG, K., STADLER, D., CHENG, X., SPRINZL, M. F., KOPPENSTEINER, H., MAKOWSKA, Z. & VOLZ, T. 2014. Specific and nonhepatotoxic degradation of nuclear hepatitis B virus cccDNA. *Science,* 343**,** 1221-1228.

LUO, W., WANG, J., XU, D., BAI, H., ZHANG, Y., ZHANG, Y. & LI, X. 2018. Engineered zinc-finger transcription factors inhibit the replication and transcription of HBV in vitro and in vivo. *International Journal of Molecular Medicine,* 41**,** 2169-2176.

MA, Z., CAO, Q., XIONG, Y., ZHANG, E. & LU, M. 2018. Interaction between hepatitis B virus and toll-like receptors: current status and potential therapeutic use for chronic hepatitis B. *Vaccines,* 6**,** 6.

MAEPA, M. B., ROELOFSE, I., ELY, A. & ARBUTHNOT, P. 2015. Progress and prospects of anti-HBV gene therapy development. *International journal of molecular sciences,* 16**,** 17589-17610.

MAKUZA, J. D., JEONG, D., WONG, S., BINKA, M., ADU, P. A., GARCÍA, H. A. V., MORROW, R. L., CUA, G., YU, A. & ALVAREZ, M. 2024. Association of hepatitis B virus treatment with all-cause and liver-related mortality among individuals with HBV and cirrhosis: a population-based cohort study. *The Lancet Regional Health–Americas,* 36.

MANI, S. K. K. & ANDRISANI, O. 2019. Interferon signaling during Hepatitis B Virus (HBV) infection and HBV-associated hepatocellular carcinoma. *Cytokine,* 124**,** 154518.

MAPONGA, T. G., GLASHOFF, R. H., VERMEULEN, H., ROBERTSON, B., BURMEISTER, S., BERNON, M., OMOSHORO-JONES, J., RUFF, P., NEUGUT, A. I. & JACOBSON,

J. S. 2020. Hepatitis B virus-associated hepatocellular carcinoma in South Africa in the era of HIV. *BMC gastroenterology,* 20**,** 1-9.

MARION, P. L. & ROBINSON, W. S. 1983. Hepadna viruses: hepatitis B and related viruses. *Current Topics in Microbiology and Immunology: Volume 105***,** 99-121.

MARTIN, S. & MOSS, B. 1975. Modification of RNA by mRNA guanylyltransferase and mRNA (guanine-7-) methyltransferase from vaccinia virions. *Journal of Biological Chemistry,* 250**,** 9330-9335.

MARUGGI, G., ZHANG, C., LI, J., ULMER, J. B. & YU, D. 2019. mRNA as a transformative technology for vaccine development to control infectious diseases. *Molecular therapy,* 27**,** 757-772.

MCNAUGHTON, A. L., D'ARIENZO, V., ANSARI, M. A., LUMLEY, S. F., LITTLEJOHN, M., REVILL, P., MCKEATING, J. A. & MATTHEWS, P. C. 2019. Insights from deep sequencing of the HBV genome—unique, tiny, and misunderstood. *Gastroenterology,* 156**,** 384-399.

MELTON, D., KRIEG, P., REBAGLIATI, M., MANIATIS, T., ZINN, K. & GREEN, M. 1984. Efficient in vitro synthesis of biologically active RNA and RNA hybridization probes from plasmids containing a bacteriophage SP6 promoter. *Nucleic acids research,* 12**,** 7035-7056.

MENG, Z., O'KEEFFE-AHERN, J., LYU, J., PIERUCCI, L., ZHOU, D. & WANG, W. 2017. A new developing class of gene delivery: messenger RNA-based therapeutics. *Biomaterials science,* 5**,** 2381-2392.

MEULEMAN, P. & LEROUX-ROELS, G. 2008. The human liver-uPA-SCID mouse: a model for the evaluation of antiviral compounds against HBV and HCV. *Antiviral research,* 80**,** 231-238.

MILLIGAN, J. F., GROEBE, D. R., WITHERELL, G. W. & UHLENBECK, O. C. 1987. Oligoribonucleotide synthesis using T7 RNA polymerase and synthetic DNA templates. *Nucleic acids research,* 15**,** 8783-8798.

MILLIGAN, J. F. & UHLENBECK, O. C. 1989. [5] Synthesis of small RNAs using T7 RNA polymerase. *Methods in enzymology.* Elsevier.

MIMMS, L. 1995. Hepatitis B virus escape mutants:"pushing the envelope" of chronic hepatitis B virus infection. *Hepatology,* 21**,** 884-887.

MLAMBO, T., NITSCH, S., HILDENBEUTEL, M., ROMITO, M., MÜLLER, M., BOSSEN, C., DIEDERICHS, S., CORNU, T. I., CATHOMEN, T. & MUSSOLINO, C. 2018. Designer epigenome modifiers enable robust and sustained gene silencing in clinically relevant human cells. *Nucleic acids research,* 46**,** 4456-4468.

MOHAMUD, A. K., INCHON, P., SUWANNAPORN, S., PRASERT, K. & DIRIE, N. I. 2024. Assessment of prevalence and risk factors associated with Hepatitis B virus infection among blood donors in Mogadishu Somalia. *BMC Public Health,* 24**,** 690.

MORADIAN, H., ROCH, T., ANTHOFER, L., LENDLEIN, A. & GOSSEN, M. 2022. Chemical modification of uridine modulates mRNA-mediated proinflammatory and antiviral response in primary human macrophages. *Molecular Therapy-Nucleic Acids,* 27**,** 854-869.

MORRISON, O. & THAKUR, J. 2021. Molecular complexes at euchromatin, heterochromatin and centromeric chromatin. *International journal of molecular sciences,* 22**,** 6922.

MORRISSEY, D. V., LOCKRIDGE, J. A., SHAW, L., BLANCHARD, K., JENSEN, K., BREEN, W., HARTSOUGH, K., MACHEMER, L., RADKA, S. & JADHAV, V. 2005.

Potent and persistent in vivo anti-HBV activity of chemically modified siRNAs. *Nature biotechnology,* 23**,** 1002-1007.

MU, X., GREENWALD, E., AHMAD, S. & HUR, S. 2018. An origin of the immunogenicity of in vitro transcribed RNA. *Nucleic acids research,* 46**,** 5239-5249.

MURPHY, K. E., SHYLO, N. A., ALEXANDER, K. A., CHURCHILL, A. J., COPPERMAN, C. & GARCÍA-GARCÍA, M. J. 2016. The transcriptional repressive activity of KRAB zinc finger proteins does not correlate with their ability to recruit TRIM28. *PloS one,* 11**,** e0163555.

NAGALAKSHMI, U., WANG, Z., WAERN, K., SHOU, C., RAHA, D., GERSTEIN, M. & SNYDER, M. 2008. The transcriptional landscape of the yeast genome defined by RNA sequencing. *Science,* 320**,** 1344-1349.

NALLAGATLA, S. R. & BEVILACQUA, P. C. 2008. Nucleoside modifications modulate activation of the protein kinase PKR in an RNA structure-specific manner. *Rna,* 14**,** 1201-1213.

NASSAL, M. 1992. The arginine-rich domain of the hepatitis B virus core protein is required for pregenome encapsidation and productive viral positive-strand DNA synthesis but not for virus assembly. *Journal of virology,* 66**,** 4107-4116.

NASSAL, M. 2015. HBV cccDNA: viral persistence reservoir and key obstacle for a cure of chronic hepatitis B. *Gut,* 64**,** 1972-1984.

NAULLY, P. G., TAN, M. I., AGUSTININGSIH, A., SUKOWATI, C. & GIRI-RACHMAN, E. A. 2024. cccDNA epigenetic regulator as target for therapeutical vaccine development against hepatitis B. *Annals of Hepatology***,** 101533.

NELSON, J., SORENSEN, E. W., MINTRI, S., RABIDEAU, A. E., ZHENG, W., BESIN, G., KHATWANI, N., SU, S. V., MIRACCO, E. J. & ISSA, W. J. 2020. Impact of mRNA chemistry and manufacturing process on innate immune activation. *Science advances,* 6**,** eaaz6893.

NEWBURY, S. 2006. Control of mRNA stability in eukaryotes. *Biochemical Society Transactions,* 34**,** 30-34.

NGUYEN, M. H., WONG, G., GANE, E., KAO, J.-H. & DUSHEIKO, G. 2020. Hepatitis B virus: advances in prevention, diagnosis, and therapy. *Clinical microbiology reviews,* 33**,** 10.1128/cmr. 00046-19.

NUÑEZ, J. K., CHEN, J., POMMIER, G. C., COGAN, J. Z., REPLOGLE, J. M., ADRIAENS, C., RAMADOSS, G. N., SHI, Q., HUNG, K. L. & SAMELSON, A. J. 2021. Genome-wide programmable transcriptional memory by CRISPR-based epigenome editing. *Cell,* 184**,** 2503-2519. e17.

OKANO, M., BELL, D. W., HABER, D. A. & LI, E. 1999. DNA methyltransferases Dnmt3a and Dnmt3b are essential for de novo methylation and mammalian development. *Cell,* 99**,** 247-257.

PALMORE, T. N., SHAH, N. L., LOOMBA, R., BORG, B. B., LOPATIN, U., FELD, J. J., KHOKHAR, F., LUTCHMAN, G., KLEINER, D. E. & YOUNG, N. S. 2009. Reactivation of hepatitis B with reappearance of hepatitis B surface antigen after chemotherapy and immunosuppression. *Clinical Gastroenterology and Hepatology,* 7**,** 1130-1137.

PARIKH, P. K., PARIKH, N. H., MAHALAKSHMI, B., RANCH, K. M., BODDU, S. H. & TIWARI, A. K. 2023. Developments in small molecule antiviral drugs against hepatitis B

and C viruses: FDA approved therapies and new drugs in clinical trials. *Arabian Journal of Chemistry,* 16**,** 105013.

PARK, J.-E., YI, H., KIM, Y., CHANG, H. & KIM, V. N. 2016. Regulation of poly (A) tail and translation during the somatic cell cycle. *Molecular cell,* 62**,** 462-471.

PARONETTO, F. & TENNANT, B. 1990. Woodchuck hepatitis virus infection: a model of human hepatic diseases and hepatocellular carcinoma. *Progress in liver diseases,* 9**,** 463-483.

PAYANKAULAM, S., LI, L. M. & ARNOSTI, D. N. 2010. Transcriptional repression: conserved and evolved features. *Current biology,* 20**,** R764-R771.

PÉNEAU, C., IMBEAUD, S., LA BELLA, T., HIRSCH, T. Z., CARUSO, S., CALDERARO, J., PARADIS, V., BLANC, J.-F., LETOUZÉ, E. & NAULT, J.-C. 2022. Hepatitis B virus integrations promote local and distant oncogenic driver alterations in hepatocellular carcinoma. *Gut,* 71**,** 616-626.

PHILLIPS, S., CHOKSHI, S., RIVA, A., EVANS, A., WILLIAMS, R. & NAOUMOV, N. V. 2010. CD8+ T cell control of hepatitis B virus replication: direct comparison between cytolytic and noncytolytic functions. *The Journal of Immunology,* 184**,** 287-295.

PICARD-JEAN, F., BRAND, C., TREMBLAY-LÉTOURNEAU, M., ALLAIRE, A., BEAUDOIN, M. C., BOUDREAULT, S., DUVAL, C., RAINVILLE-SIROIS, J., ROBERT, F. & PELLETIER, J. 2018. 2'-O-methylation of the mRNA cap protects RNAs from decapping and degradation by DXO. *PloS one,* 13**,** e0193804.

PICHON, X., A WILSON, L., STONELEY, M., BASTIDE, A., A KING, H., SOMERS, J. & E WILLIS, A. 2012. RNA binding protein/RNA element interactions and the control of translation. *Current Protein and Peptide Science,* 13**,** 294-304.

POLACK, F. P., THOMAS, S. J., KITCHIN, N., ABSALON, J., GURTMAN, A., LOCKHART, S., PEREZ, J. L., PÉREZ MARC, G., MOREIRA, E. D. & ZERBINI, C. 2020. Safety and efficacy of the BNT162b2 mRNA Covid-19 vaccine. *New England journal of medicine,* 383**,** 2603-2615.

POP, C., ROUSKIN, S., INGOLIA, N. T., HAN, L., PHIZICKY, E. M., WEISSMAN, J. S. & KOLLER, D. 2014. Causal signals between codon bias, mRNA structure, and the efficiency of translation and elongation. *Molecular systems biology,* 10**,** 770.

POPOVA, P. G., LAGACE, M. A., TANG, G. & BLAKNEY, A. K. 2024. Effect of in vitro transcription conditions on yield of high quality messenger and self-amplifying RNA. *European Journal of Pharmaceutics and Biopharmaceutics,* 198**,** 114247.

PROJAN, S., MONOD, M., NARAYANAN, C. & DUBNAU, D. 1987. Replication properties of pIM13, a naturally occurring plasmid found in Bacillus subtilis, and of its close relative pE5, a plasmid native to Staphylococcus aureus. *Journal of bacteriology,* 169**,** 5131-5139.

QIN, S., TANG, X., CHEN, Y., CHEN, K., FAN, N., XIAO, W., ZHENG, Q., LI, G., TENG, Y. & WU, M. 2022. mRNA-based therapeutics: powerful and versatile tools to combat diseases. *Signal transduction and targeted therapy,* 7**,** 166.

QUASDORFF, M. & PROTZER, U. 2010. Control of hepatitis B virus at the level of transcription. *Journal of viral hepatitis,* 17**,** 527-536.

RAJORIYA, N., COMBET, C., ZOULIM, F. & JANSSEN, H. L. 2017. How viral genetic variants and genotypes influence disease and treatment outcome of chronic hepatitis B. Time for an individualised approach? *Journal of hepatology,* 67**,** 1281-1297.

REHERMANN, B., FERRARI, C., PASQUINELLI, C. & CHISARI, F. V. 1996. The hepatitis B virus persists for decades after patients' recovery from acute viral hepatitis despite active maintenance of a cytotoxic T–lymphocyte response. *Nature medicine,* 2**,** 1104-1108.

ROMANO', L. & ZANETTI, A. R. 2022. Hepatitis B vaccination: A historical overview with a focus on the Italian achievements. *Viruses,* 14**,** 1515.

ROSANO, G. L. & CECCARELLI, E. A. 2014. Recombinant protein expression in Escherichia coli: advances and challenges. *Frontiers in Microbiology,* 5**,** 172.

RYAN, B. C., LOWE, K., HANSON, L., GIL, T., BRAUN, L., HOWARD, P. L. & CHOW, R. L. 2018. Mapping the Pax6 3'untranslated region microRNA regulatory landscape. *BMC genomics,* 19**,** 1-17.

SAHIN, U., KARIKÓ, K. & TÜRECI, Ö. 2014. mRNA-based therapeutics—developing a new class of drugs. *Nature reviews Drug discovery,* 13**,** 759-780.

SAUERBREI, A. 2014. Is hepatitis B-virucidal validation of biocides possible with the use of surrogates? *World journal of gastroenterology: WJG,* 20**,** 436.

SCHILLIE, S. F. & MURPHY, T. V. 2013. Seroprotection after recombinant hepatitis B vaccination among newborn infants: a review. *Vaccine,* 31**,** 2506-2516.

SCHINAZI, R. F., EHTESHAMI, M., BASSIT, L. & ASSELAH, T. 2018. Towards HBV curative therapies. *Liver International,* 38**,** 102-114.

SCHIWON, M., EHRKE-SCHULZ, E., OSWALD, A., BERGMANN, T., MICHLER, T., PROTZER, U. & EHRHARDT, A. 2018. One-vector system for multiplexed CRISPR/Cas9 against hepatitis B virus cccDNA utilizing high-capacity adenoviral vectors. *Molecular Therapy-Nucleic Acids,* 12**,** 242-253.

SCHLAEGER, T. M., DAHERON, L., BRICKLER, T. R., ENTWISLE, S., CHAN, K., CIANCI, A., DEVINE, A., ETTENGER, A., FITZGERALD, K. & GODFREY, M. 2015. A comparison of non-integrating reprogramming methods. *Nature biotechnology,* 33**,** 58-63.

SCHOENBERG, D. R. 2011. Mechanisms of endonuclease-mediated mRNA decay. *Wiley Interdisciplinary Reviews: RNA,* 2**,** 582-600.

SCHREINER, S. & NASSAL, M. 2017. A role for the host DNA damage response in hepatitis B virus cccDNA formation—and beyond? *Viruses,* 9**,** 125.

SEEGER, C. & MASON, W. S. 2000. Hepatitis B virus biology. *Microbiology and molecular biology reviews,* 64**,** 51-68.

SEEGER, C. & MASON, W. S. 2015. Molecular biology of hepatitis B virus infection. *Virology,* 479**,** 672-686.

SELABE, S. G., LUKHWARENI, A., SONG, E., LEEUW, Y. G., BURNETT, R. J. & MPHAHLELE, M. J. 2007. Mutations associated with lamivudine-resistance in therapy-naïve hepatitis B virus (HBV) infected patients with and without HIV co-infection: Implications for antiretroviral therapy in HBV and HIV co-infected South African patients. *Journal of medical virology,* 79**,** 1650-1654.

SERGEEVA, O., KOTELIANSKY, V. & ZATSEPIN, T. 2016. mRNA-based therapeutics–Advances and perspectives. *Biochemistry (Moscow),* 81**,** 709-722.

SHEENA, B. S., HIEBERT, L., HAN, H., IPPOLITO, H., ABBASI-KANGEVARI, M., ABBASI-KANGEVARI, Z., ABBASTABAR, H., ABDOLI, A., ALI, H. A. & ADANE, M. M. 2022. Global, regional, and national burden of hepatitis B, 1990–2019: a systematic analysis for the Global Burden of Disease Study 2019. *The Lancet Gastroenterology & Hepatology,* 7**,** 796-829.

SIEBER, P., PLATZER, M. & SCHUSTER, S. 2018. The definition of open reading frame revisited. *Trends in Genetics,* 34**,** 167-170.

SIKORSKI, P. J., WARMINSKI, M., KUBACKA, D., RATAJCZAK, T., NOWIS, D., KOWALSKA, J. & JEMIELITY, J. 2020. The identity and methylation status of the first transcribed nucleotide in eukaryotic mRNA 5′ cap modulates protein expression in living cells. *Nucleic acids research,* 48**,** 1607-1626.

SINGH, P., KAIRUZ, D., ARBUTHNOT, P. & BLOOM, K. 2021. Silencing hepatitis B virus covalently closed circular DNA: The potential of an epigenetic therapy approach. *World journal of gastroenterology,* 27**,** 3182.

SINGH, P., SMITH, T., ARBUTHNOT, P. & ELY, A. 2024. 14 In Vitro RNA Transcription. *Handbook of Molecular Biotechnology***,** 137.

SMEKALOVA, E. M., MARTINEZ, M. G., COMBE, E., KUMAR, A., DEJENE, S., LEBOEUF, D., CHEN, C.-Y., DORKIN, J. R., SHUANG, L. S. & KIEFT, S. 2024. Cytosine base editing inhibits hepatitis B virus replication and reduces HBsAg expression in vitro and in vivo. *Molecular Therapy-Nucleic Acids,* 35.

SMITH, T., SINGH, P., CHMIELEWSKI, K. O., BLOOM, K., CATHOMEN, T., ARBUTHNOT, P. & ELY, A. 2021. Improved Specificity and Safety of Anti-Hepatitis B Virus TALENs Using Obligate Heterodimeric FokI Nuclease Domains. *Viruses,* 13**,** 1344.

SONDERUP, M. W., DUSHEIKO, G., DESALEGN, H., LEMOINE, M., TZEUTON, C., TAYLOR-ROBINSON, S. D. & SPEARMAN, C. W. 2020. Hepatitis B in sub-Saharan Africa—How many patients need therapy? *Journal of viral hepatitis,* 27**,** 560-567.

SONENBERG, N. & HINNEBUSCH, A. G. 2009. Regulation of translation initiation in eukaryotes: mechanisms and biological targets. *Cell,* 136**,** 731-745.

SOUSSAN, P., GARREAU, F., ZYLBERBERG, H., FERRAY, C., BRECHOT, C. & KREMSDORF, D. 2000. In vivo expression of a new hepatitis B virus protein encoded by a spliced RNA. *The Journal of clinical investigation,* 105**,** 55-60.

STEPINSKI, J., WADDELL, C., STOLARSKI, R., DARZYNKIEWICZ, E. & RHOADS, R. E. 2001. Synthesis and properties of mRNAs containing the novel "anti-reverse" cap analogs 7-methyl(3'-O-methyl)GpppG and 7-methyl (3'-deoxy)GpppG. *RNA,* 7**,** 1486-95.

STOLZENBURG, S., GOUBERT, D. & ROTS, M. G. 2016. Rewriting DNA methylation signatures at will: the curable genome within reach? *DNA Methyltransferases-Role and Function***,** 475-490.

STRIETH, S., DUNAU, C., MICHAELIS, U., JÄGER, L., GELLRICH, D., WOLLENBERG, B. & DELLIAN, M. 2014. Phase I/II clinical study on safety and antivascular effects of paclitaxel encapsulated in cationic liposomes for targeted therapy in advanced head and neck cancer. *Head & neck,* 36**,** 976-984.

SUKNUNTHA, K., TAO, L., BROK-VOLCHANSKAYA, V., D'SOUZA, S. S., KUMAR, A. & SLUKVIN, I. 2018. Optimization of synthetic mRNA for highly efficient translation and its application in the generation of endothelial and hematopoietic cells from human and primate pluripotent stem cells. *Stem cell reviews and reports,* 14**,** 525-534.

SUNG, H., FERLAY, J., SIEGEL, R. L., LAVERSANNE, M., SOERJOMATARAM, I., JEMAL, A. & BRAY, F. 2021. Global cancer statistics 2020: GLOBOCAN estimates of incidence and mortality worldwide for 36 cancers in 185 countries. *CA: a cancer journal for clinicians,* 71**,** 209-249.

SUNG, W.-K., ZHENG, H., LI, S., CHEN, R., LIU, X., LI, Y., LEE, N. P., LEE, W. H., ARIYARATNE, P. N. & TENNAKOON, C. 2012. Genome-wide survey of recurrent HBV integration in hepatocellular carcinoma. *Nature genetics,* 44**,** 765-769.

TATE, W. P. & MANNERING, S. A. 1996. Three, four or more: the translational stop signal at length. *Molecular microbiology,* 21**,** 213-219.

TATEMATSU, M., FUNAMI, K., SEYA, T. & MATSUMOTO, M. 2018. Extracellular RNA sensing by pattern recognition receptors. *Journal of innate immunity,* 10**,** 398-406.

TRÉPO, C., CHAN, H. L. & LOK, A. 2014. Hepatitis B virus infection. *The lancet,* 384**,** 2053-2063.

TREPOTEC, Z., GEIGER, J., PLANK, C., ANEJA, M. K. & RUDOLPH, C. 2019. Segmented poly (A) tails significantly reduce recombination of plasmid DNA without affecting mRNA translation efficiency or half-life. *Rna,* 25**,** 507-518.

TRIANA-ALONSO, F. J., DABROWSKI, M., WADZACK, J. & NIERHAUS, K. H. 1995. Self-coded 3′-Extension of Run-off Transcripts Produces Aberrant Products during in Vitro Transcription with T7 RNA Polymerase (∗). *Journal of Biological Chemistry,* 270**,** 6298-6307.

VAN DEN ENDE, C., MARANO, C., VAN AHEE, A., BUNGE, E. M. & DE MOERLOOZE, L. 2017. The immunogenicity and safety of GSK's recombinant hepatitis B vaccine in adults: a systematic review of 30 years of experience. *Expert review of vaccines,* 16**,** 811-832.

VAN DER GUN, B., HUISMAN, C., STOLZENBURG, S., KAZEMIER, H., RUITERS, M., BLANCAFORT, P. & ROTS, M. 2013. Bidirectional modulation of endogenous EpCAM expression to unravel its function in ovarian cancer. *British journal of cancer,* 108**,** 881-886.

VANDIVER, A. R., IDRIZI, A., RIZZARDI, L., FEINBERG, A. P. & HANSEN, K. D. 2015. DNA methylation is stable during replication and cell cycle arrest. *Scientific reports,* 5**,** 17911.

VERRIER, E. R., COLPITTS, C. C., BACH, C., HEYDMANN, L., WEISS, A., RENAUD, M., DURAND, S. C., HABERSETZER, F., DURANTEL, D. & ABOU-JAOUDÉ, G. 2016. A targeted functional RNA interference screen uncovers glypican 5 as an entry factor for hepatitis B and D viruses. *Hepatology,* 63**,** 35-48.

VIVEKANANDAN, P., DANIEL, H. D.-J., KANNANGAI, R., MARTINEZ-MURILLO, F. & TORBENSON, M. 2010. Hepatitis B virus replication induces methylation of both host and viral DNA. *Journal of virology,* 84**,** 4321-4329.

VIVEKANANDAN, P., THOMAS, D. & TORBENSON, M. 2008. Hepatitis B viral DNA is methylated in liver tissues. *Journal of viral hepatitis,* 15**,** 103-107.

VIVEKANANDAN, P., THOMAS, D. & TORBENSON, M. 2009. Methylation regulates hepatitis B viral protein expression. *The Journal of infectious diseases,* 199**,** 1286-1291.

VLATKOVIC, I., LUDWIG, J., BOROS, G., SZABÓ, G. T., REICHERT, J., BUFF, M., BAIERSDÖRFER, M., REINHOLZ, J., MAHINY, A. J. & ŞAHIN, U. 2022. Ribozyme assays to quantify the capping efficiency of in vitro-transcribed mRNA. *Pharmaceutics,* 14**,** 328.

VON DER HAAR, T., MULRONEY, T. E., HEDAYIOGLU, F., KURUSAMY, S., RUST, M., LILLEY, K. S., THAVENTHIRAN, J. E., WILLIS, A. E. & SMALES, C. M. 2023. Translation of in vitro-transcribed RNA therapeutics. *Frontiers in Molecular Biosciences,* 10**,** 1128067.

WADDINGTON, C. H. 1942. Canalization of development and the inheritance of acquired characters. *Nature,* 150**,** 563-565.

WEI, L. & PLOSS, A. 2020. Core components of DNA lagging strand synthesis machinery are essential for hepatitis B virus cccDNA formation. *Nature microbiology,* 5**,** 715-726.

WELLS, S. E., HILLNER, P. E., VALE, R. D. & SACHS, A. B. 1998. Circularization of mRNA by eukaryotic translation initiation factors. *Molecular cell,* 2**,** 135-140.

WHITTAKER, M. N., TESTA, L. C., QUIGLEY, A., JINDAL, I., CORTEZ-ALVARADO, S. V., QU, P., YANG, Y., ALAMEH, M.-G., MUSUNURU, K. & WANG, X. 2023. Epigenome Editing Durability Varies Widely Across Cardiovascular Disease Target Genes. *Arteriosclerosis, Thrombosis, and Vascular Biology,* 43**,** 2075-2077.

WHO. 2022. *Hepatitis B Fact sheets* [Online]. World Health Organisation Available: https://www.who.int/news-room/fact-sheets/detail/hepatitis-b [Accessed Accessed on 14 Febuary 2024].

WU, C.-T. & MORRIS, J. R. 2001. Genes, genetics, and epigenetics: a correspondence. *Science,* 293**,** 1103-1105.

WU, C., DUAN, Y., GONG, S., OSTERHOFF, G., KALLENDRUSCH, S. & SCHOPOW, N. 2022. Identification of tumor antigens and immune subtypes for the development of mRNA vaccines and individualized immunotherapy in soft tissue sarcoma. *Cancers,* 14**,** 448.

XIA, X. 2021. Detailed dissection and critical evaluation of the Pfizer/BioNTech and Moderna mRNA vaccines. *Vaccines,* 9**,** 734.

XIRONG, L., RUI, L., XIAOLI, Y., QIUYAN, H., BIKUI, T., SIBO, Z. & NAISHUO, Z. 2014. Hepatitis B virus can be inhibited by DNA methyltransferase 3a via specific zinc-finger-induced methylation of the X promoter. *Biochemistry (Moscow),* 79**,** 111-123.

XU, S., YANG, K., LI, R. & ZHANG, L. 2020. mRNA vaccine era—mechanisms, drug platform and clinical prospection. *International journal of molecular sciences,* 21**,** 6582.

YAN, H., ZHONG, G., XU, G., HE, W., JING, Z., GAO, Z., HUANG, Y., QI, Y., PENG, B. & WANG, H. 2012. Sodium taurocholate cotransporting polypeptide is a functional receptor for human hepatitis B and D virus. *elife,* 1**,** e00049.

YU, C.-H., DANG, Y., ZHOU, Z., WU, C., ZHAO, F., SACHS, M. S. & LIU, Y. 2015. Codon usage influences the local rate of translation elongation to regulate co-translational protein folding. *Molecular cell,* 59**,** 744-754.

YUEN, M.-F., TANAKA, Y., SHINKAI, N., POON, R. T., BUT, D. Y.-K., FONG, D. Y., FUNG, J., WONG, D. K.-H., YUEN, J. C.-H. & MIZOKAMI, M. 2008. Risk for hepatocellular carcinoma with respect to hepatitis B virus genotypes B/C, specific mutations of enhancer II/core promoter/precore regions and HBV DNA levels. *Gut,* 57**,** 98-102.

ZEISEL, M. B., LUCIFORA, J., MASON, W. S., SUREAU, C., BECK, J., LEVRERO, M., KANN, M., KNOLLE, P. A., BENKIRANE, M. & DURANTEL, D. 2015. Towards an HBV cure: state-of-the-art and unresolved questions—report of the ANRS workshop on HBV cure. *Gut,* 64**,** 1314-1326.

ZHANG, J., LIU, Y., LI, C., XIAO, Q., ZHANG, D., CHEN, Y., ROSENECKER, J., DING, X. & GUAN, S. 2023. Recent advances and innovations in the preparation and purification of in Vitro-Transcribed-mRNA-Based molecules. *Pharmaceutics,* 15**,** 2182.

ZHANG, Y., LI, C., ZHANG, Y., ZHU, H., KANG, Y., LIU, H., WANG, J., QIN, Y., MAO, R. & XIE, Y. 2013. Comparative analysis of CpG islands among HBV genotypes. *PloS one,* 8**,** e56711.

ZHANG, Y., MAO, R., YAN, R., CAI, D., ZHANG, Y., ZHU, H., KANG, Y., LIU, H., WANG, J. & QIN, Y. 2014. Transcription of hepatitis B virus covalently closed circular DNA is regulated by CpG methylation during chronic infection. *PloS one,* 9**,** e110442.

ZHAO, X., ZHAO, Z., GUO, J., HUANG, P., ZHU, X., ZHOU, X., YANG, Z., ZHAO, L., XU, L. & XU, J. 2013. Creation of a six-fingered artificial transcription factor that represses the hepatitis B virus HBx gene integrated into a human hepatocellular carcinoma cell line. *Journal of Biomolecular Screening,* 18**,** 378-387.

ZHONG, Z., MC CAFFERTY, S., COMBES, F., HUYSMANS, H., DE TEMMERMAN, J., GITSELS, A., VANROMPAY, D., CATANI, J. P. & SANDERS, N. N. 2018. mRNA therapeutics deliver a hopeful message. *Nano today,* 23**,** 16-39.

ZHOU, Y. & HOLMES, E. C. 2007. Bayesian estimates of the evolutionary rate and age of hepatitis B virus. *Journal of molecular evolution,* 65**,** 197-205.

ZOULIM, F. 2011. Hepatitis B virus resistance to antiviral drugs: where are we going? *Liver International,* 31**,** 111-116.